Numerical modelling of Constructed Wetlands for wastewater treatment

PhD. Thesis
Doctoral Programme: Environmental Engineering

Author: Roger Samsó Campà
Supervisor: Joan García Serrano

February 19, 2014

UNIVERSITAT POLITÈCNICA DE CATALUNYA
BARCELONATECH
Escola de Doctorat

Acta de qualificació de tesi doctoral

Curs acadèmic:

Nom i cognoms

Programa de doctorat

Unitat estructural responsable del programa

Resolució del Tribunal

Reunit el Tribunal designat a l'efecte, el doctorand / la doctoranda exposa el tema de la seva tesi doctoral titulada

_____

_____.

Acabada la lectura i després de donar resposta a les qüestions formulades pels membres titulars del tribunal, aquest atorga la qualificació:

☐ NO APTE ☐ APROVAT ☐ NOTABLE ☐ EXCEL·LENT

(Nom, cognoms i signatura) President/a	(Nom, cognoms i signatura) Secretari/ària	
(Nom, cognoms i signatura) Vocal	(Nom, cognoms i signatura) Vocal	(Nom, cognoms i signatura) Vocal

_____, _____ d'/de _____ de _____

El resultat de l'escrutini dels vots emesos pels membres titulars del tribunal, efectuat per l'Escola de Doctorat, a instància de la Comissió de Doctorat de la UPC, atorga la MENCIÓ CUM LAUDE:

☐ SÍ ☐ NO

(Nom, cognoms i signatura) Presidenta de la Comissió de Doctorat	(Nom, cognoms i signatura) Secretària de la Comissió de Doctorat

Barcelona, _____ d'/de _____ de _____

People think computers will keep them from making mistakes. They're wrong. With computers you make mistakes faster.

Adam Osborne

Preface

The research presented in this document was financed through participation in three research projects: grant agreements n°308502 and n°308336 from the European Union Seventh Framework Programme (FP7/2013-2015) and the NEWWET2008 (CTM2008-06676-C05-01) project, granted by the Spanish Ministry of Science and Innovation. Roger Samsó also acknowledges the scholarship co-financed by the Universitat Politècnica de Catalunya-BarcelonaTech (UPC) and by the Group of Environmental Engineering and Microbiology (GEMMA) of the Hydraulic, Maritime and Environmental Engineering Department of UPC.

Abstract

Constructed Wetlands (Cws) are a wastewater treatment technology that benefits from the inherent water-purification potential of natural wetlands and optimizes their performance to comply with regulations for treated discharges. These systems have evolved to become a real and equally performing alternative to conventional wastewater treatment technologies for small communities (up to 2000PE) with significantly lower energy and maintenance costs. Despite their great potential, CWs still lack reliability, which holds back their full deployment in the territory. This fact results from the lack of understanding on their internal functioning and also because they are prone to clogging.

The enormous diversity of CWs typologies and operation strategies, and the fact that they operate at the mercy of the environmental conditions, makes each CW unique on its kind, and experimental studies are usually only representative of the studied system. This fact makes mathematical models an essential tool to evaluate the relative impact of each parameter on the internal functioning of CWs. Several mathematical models for CWs have proliferated in the last dozen years to simulate the behaviour of these systems and to provide supporting tools for their design and operation as well as more insight into the treatment processes. However, until the begining of this research, and compared to models utilized in similar disciplines, CWs models development was still in an embrionary stage.

Accordingly, the main objectives of the current work were, on the one hand, to develop a CWs mathematical model able to describe the most common processes taking place within these systems. And, on the other hand, to use this model to shed some light on the internal functioning of these systems in the long-term.

The model, named BIO_PORE, was built in COMSOL Multiphysics™ and includes equations to simulate subsurface flow and pollutants transport in porous media. It also implements the biokinetic model Constructed Wetlands Model number 1 (CWM1) to describe the fate of organic matter, nitrogen and sulphur and the growth of the most common functional bacterial groups found within these systems. The model was calibrated with experimental data for an entire year of operation of a pilot system.

Two empirical parameters (M_{cap} and M_{bio_max}) were used to improve the description of bacterial growth obtained with the original formulation of CWM1 and to include the effects of solids accumulation on bacterial communities. The effect of these two parameters was evaluated by means of a local sensitivity analysis. The model was later used to unveil the dynamics of bacterial communities within CWs. In addition, a theory was derived from simulation results, which aimed at describing the most basic functioning patterns of horizontal subsuface flow CWs based on the interaction between bacterial communities and accumulated solids. At the end of the document a mathematical formulation is presented to describe bioclogging in CWs and a numerical experiment is carried out to showcase its impact on simulation results.

The main outcome of the current work was the BIO_PORE model. This model was able to reproduce effluent pollutant concentrations measured during an entire year of operation of the pilot system. Empirical parameters M_{cap} and M_{bio_max} proved essential to prevent unlimited bacterial growth predicted by the original Monod equations of CWM1 near the inlet section of CWs. These two parameters were in great part responsible for the good fitting with experimental data. This was confirmed with the results from the sensitivity analysis, which helped demonstrate that they have a major impact on the model predictions for effluent COD and ammonia and ammonium nitrogen. The theory derived from simulation results, named *The Cartridge Theory*, indicated that bacterial communities are not static, but move towards the outlet with time, following the progressive accumulation of inert solids from inlet to outlet. This result may prove that CWs have a limited life-span, corresponding to the time after which bacterial communities are pushed as much towards the outlet that their total biomass is not sufficient to provide effluents with acceptable quality. The inclusion of bioclogging effects on the hydrodynamics of the granular media was seen to be a requisite in order to properly reproduce the bacterial distribution, fluid flow and pollutants transport within CWs.

Finally, results of this work also showed that more work on the BIO_PORE model is required and more experimental data is necessary to calibrate its results.

Keywords: Constructed Wetlands, modelling, finite elements, porous media, flow, reactive transport, biokinetic reactions, bacterial growth, clogging.

Resum

Els aiguamolls construïts (AC) són sistemes de tractament d'aigües residuals que aprofiten la capacitat de purificació d'aigua dels aiguamolls naturals i n'optimitzen el rendiment per tal de complir regulacions aplicables als abocaments tractats. Aquests sistemes han evolucionat per esdevenir una alternativa real i d'eficiència equiparable a les tecnologies de tractament convencionals per a petites comunitats (fins a 2000PE), amb costos energètics i de manteniment significativament menors. Malgrat el seu gran potencial, els AC tenen encara una baixa fiabilitat, deguda entre altres coses, a la manca de coneixement sobre el seu funcionament intern i al fenomen de la colmatació, que en redueix considerablement la vida útil.

L'enorme diversitat de tipologies i estratègies d'operació dels AC, i el fet que operen a mercè de les condicions ambientals, fa que cada aiguamoll sigui únic en el seu gènere. En conseqüència, en força ocasions, els resultats d'estudis experimentals en AC no són extrapolables. Aquest fet converteix els models numèrics en una eina clau per estudiar el funcionament intern dels aiguamolls.

Així, en la darrera dècada diversos models han proliferat com a eines de suport per al disseny i operació dels AC, així com per comprendre millor els processos que s'hi donen. No obstant, fins a l'inici daquesta investigació, el desenvolupament de models d'AC encara es trobava en una etapa embrionària. D'acord amb això, els principals objectius del present treball han estat, d'una banda, desenvolupar un model matemàtic capaç de descriure els principals processos que tenen lloc dins els AC i de l'altra, aplicar el model per millorar el coneixement sobre el seu funcionament intern a llarg termini.

En aquest treball s'ha desenvolupat un model d'AC en COMSOL Multiphysics™ que s'ha anomenat BIO_PORE. Inclou equacions per simular flux subterrani i transport de contaminants en medis porosos. També implementa el model biocinètic Con-

structed Wetlands Model numero 1 (CWM1) per descriure l'eliminació de matèria orgànica, nitrogen i sofre així com el creixement dels grups bacterians més habituals en AC. A més, BIO_PORE inclou dos paràmetres empírics (M_{cap} i M_{bio_max}) que permeten millorar la descripció del creixement bacterià obtinguda amb la formulació original del CWM1.

El model es va calibrar amb dades experimentals d'un any de funcionament d'un sistema pilot i l'efecte dels dos paràmetres introduïts es va avaluar mitjançant un anàlisi de sensibilitat. Posteriorment el model va ser utilitzat per simular la dinàmica de les comunitats bacterianes dins els AC. Al final del document es presenta una formulació matemàtica per descriure la colmatació d'origen biològic en medi porós i es duu a terme un experiment numèric per demostrar l'impacte d'aquest fenomen en la dinàmica dels AC.

El principal resultat d'aquest treball és el propi model BIO_PORE. Aquest model va permetre reproduir les concentracions efluents de contaminants mesurats durant tot un any de funcionament del sistema pilot. Els paràmetres M_{cap} i M_{bio_max} van demostrar ser essencials per prevenir el creixement bacterià il.limitat predits per les equacions originals del CWM1. A la vegada, aquests dos paràmetres van ser en gran mesura responsables del bon ajust dels efluents simulats amb els mesurats experimentalment, fet que es va confirmar amb els resultats de l'anàlisi de sensibilitat posterior. Els resultats obtinguts amb el model es van utilitzar per construir un marc teòric conceptual, que s'ha anomenat the Cartridge Theory, i que descriu els patrons més bàsics de funcionament dels AC de flux subsuperficial horitzontal. La teoria indica que les comunitats bacterianes no són estàtiques, sinó que es desplacen cap a la secció de sortida amb el temps, seguint l'acumulació progressiva de sòlids inerts en la mateixa direcció. Segons aquest resultat els AC tenen una vida limitada, que correspon al temps després del qual les comunitats bacterianes es concentren tan aprop de la secció de sortida que la seva biomassa total no és capaç de proporcionar efluents de qualitat acceptable.

Per altra banda, la inclusió dels efectes de la colmatació biològica sobre la hidrodinàmica del medi granular va demostrar ser un requisit indispensable per poder reproduir correctament la distribució de bacteris i el flux i transport de contaminants dins els AC.

Finalment, de resultes d'aquest treball també es fa evident que és necessari concentrar més esforços en el desenvolupament del model BIO_PORE i que calen més dades experimentals per tal de calibrar-ne els resultats.

Paraules clau: Aiguamolls construïts , modelització, elements finits, medi porós, flux subterrani, transport reactiu, reaccions biocinètiques, creixement bacterià, colmatació.

Contents

Acronyms and Abreviations

Acronym	Definition
ADM	Anaerobic Digestion Model
AOLR	Areal Organic Loading Rate
ASM	Activated Sludge Model
BOD	Biochemical Oxygen Demand
COD	Chemical Oxygen Demand
CPU	Central Processing Unit
CSTR	Constantly Stirred Tank Reactor
CWM1	Constructed Wetlands Model number 1
CWs	Constructed Wetlands
CW2D	Constructed Wetlands two dimensional
DOM	Dissolved Organic Mater
FEM	Finite Elements Method
HLR	Hydraulic Loading Rate
HSSF CWs	Horizontal Subsurface Flow Constructed Wetlands
IWA	International Water Association
KBr	Potassium Bromide
MDG	Millenium Development Goals
MZ	Mixing Zone sub-domain
$NH_4^+ - N$	Ammonium nitrogen
OLR	Organic Loading Rate
OM	Organic Matter
OTR	Oxygen Transfer Rate
PCR	Polymerase Chain Reaction

Continues on the next page

Continued

Acronym	**Definition**
PE	Population Equivalent
PFR	Plug Flow Reactor
POM	Particulate Organic Mater
PPCPs	Pharmaceuticals and Personal Care Products
RAM	Random Access Memory
RCB	RetrasoCodeBright
RL	Runoff Layer sub-domain
$S1$	Simulation one in Chapter 7
$S2$	Simulation two in Chapter 7
$S3$	Simulation three in Chapter 7
SF CWs	CWs Surface Flow Constructed Wetlands
SSE	Sum of Squared Errors
SSF CWs	Subsurface Flow Constructed Wetlands
TSS	Total Suspended Solids
VFAs	Volatile Fatty Acids
VS	Volatile Solids
VSSF CWs	Vertical Subsurface Flow Constructed Wetlands
WB	Wetland Body sub-domain
WHO	World Health Organisation
WWTPs	Wastewater Treatment Plants

List of Symbols

Symbol	Description
A	Surface area of the wetland
b_A	Rate constant for lysis of X_A
b_{AMB}	Rate constant for lysis of X_{AMB}
b_{ASRB}	Rate constant for lysis of X_{ASRB}
b_{FB}	Rate constant for lysis of X_{FB}
b_H	Rate constant for lysis of X_H
b_{SOB}	Rate constant for lysis of X_{SOB}
C	Substrate concentration in Chapter 8
C_k	Concentration of aqueous component k
$\check{C}_l$	Concentration of solid component l
C_u	Coefficient of uniformity $\left(\frac{D_{60}}{D_{10}}\right)$
$D_{i,j}$	Hydrodynamic dispersion tensor
D_{10}	Particle size in mm of which 10% of a material is finer
D_{60}	Particle size in mm of which 60% of a material is finer
D_{WB}	Depth of the wetland body
$f_{BM,SF}$	Fraction of S_F generated in biomass lysis
$f_{BM,XI}$	Fraction of X_I generated in biomass lysis
$f_{Hyd,SI}$	Production of S_I in hydrolysis
f_{GL}	Product of the logistic functions including parameters M_{cap} and M_{bio_max}
h	Hydraulic head
H'	Shannon diversity index
$i_{N,SF}$	N content of S_F

Continues on the next page

Continued

Symbol	Description
$i_{N,SI}$	N content of S_I
$i_{N,XS}$	N content of X_S
$i_{N,XI}$	N content of X_I
$i_{N,BM}$	N content of biomass
$K(h)$	Hydraulic conductivity
k_b	Relative hydraulic conductivity in the presence of biofilm
k_r	Relative hydraulic conductivity in the absence of biofilm
K_h	Hydrolysis rate constant
$K_{i,j}$	Saturated hydraulic conductivity tensor
K_{La,S_O}	Oxygen mass transfer coefficient
K_{SAH}	Saturation/inhibition coefficient of S_A for X_H
K_{sat}	Saturated hydraulic conductivity
$K_{sat_{RL}}$	Saturated hydraulic conductivity of the Runoff Layer
K_{SFAMB}	Saturation/inhibition coefficient of S_F for X_{AMB}
K_{SFASRB}	Saturation/inhibition coefficient of S_F for X_{ASRB}
K_{SFFB}	Saturation/inhibition coefficient of S_F for X_{FB}
K_{SFH}	Saturation/inhibition coefficient of S_F for X_H
K_{SH2SA}	Saturation/inhibition coefficient of S_{H2S} for X_A
$K_{SH2SAMB}$	Saturation/inhibition coefficient of S_{H2S} for X_{AMB}
$K_{SH2SASRB}$	Saturation/inhibition coefficient of S_{H2S} for X_{ASRB}
K_{SH2SFB}	Saturation/inhibition coefficient of S_{H2S} for X_{FB}
K_{SH2SH}	Saturation/inhibition coefficient of S_{H2S} for X_H
$K_{SH2SSOB}$	Saturation/inhibition coefficient of S_{H2S} for X_{SOB}
K_{SNHA}	Saturation/inhibition coefficient of S_{NH} for X_A
K_{SNHAMB}	Saturation/inhibition coefficient of S_{NH} for X_{AMB}
$K_{SNHASRB}$	Saturation/inhibition coefficient of S_{NH} for X_{ASRB}
K_{SNHFB}	Saturation/inhibition coefficient of S_{NH} for X_{FB}
K_{SNHH}	Saturation/inhibition coefficient of S_{NH} for X_H
K_{SNHSOB}	Saturation/inhibition coefficient of S_{NH} for X_{SOB}
K_{SNOAMB}	Saturation/inhibition coefficient of S_{NO} for X_{AMB}
$K_{SNOASRB}$	Saturation/inhibition coefficient of S_{NO} for X_{ASRB}
K_{SNOFB}	Saturation/inhibition coefficient of S_{NO} for X_{FB}
K_{SNOH}	Saturation/inhibition coefficient of S_{NO} for X_H
K_{SNOSOB}	Saturation/inhibition coefficient of S_{NO} for X_{SOB}
K_{SOA}	Saturation/inhibition coefficient of S_O for X_A
K_{SOAMB}	Saturation/inhibition coefficient of S_O for X_{AMB}
K_{SOASRB}	Saturation/inhibition coefficient of S_O for X_{ASRB}
K_{SOFB}	Saturation/inhibition coefficient of S_O for X_{FB}
K_{SOH}	Saturation/inhibition coefficient of S_O for X_H
K_{SOSOB}	Saturation/inhibition coefficient of S_O for X_{SOB}

Continues on the next page

Continued

Symbol	Description
$K_{SO4ASRB}$	Saturation/inhibition coefficient of S_{SO4} for X_{ASRB}
k_X	Decay rate of X (Chapter 8)
K_X	Saturation/inhibition coefficient for hydrolysis
$K_{X,C}$	Saturation/inhibition coefficient of C for X (Chapter 8)
L_{WB}	Length of the wetland body
$M_{0.1}$	Mesh with maximum element size of 0.1 m
$M_{0.04}$	Mesh with maximum element size of 0.04 m
$M_{0.03}$	Mesh with maximum element size of 0.03 m
$M_{0.025}$	Mesh with maximum element size of 0.025 m
M_{cap}	Solids capacity of a representative volume of granular material
M_{bio_max}	Carrying capacity of the granular media for bacteria
$M_{BIO-PORE}$	Mesh used in Chapter 4
M_T	Mass of accumulated solids
M_{bio}	Total microbial biomass of a representative volume of granular material
M_{bio_max}	Carrying capacity of the granular media expressed in mass
n	van Genuchten parameter
N	Nitrogen
$N_{b,i}$	Density number of the pores of radius $r_{b,i}$
l	van Genuchten parameter
O_2	Molecular Oxygen
q_i	Specific discharge
r_{att}	Attachment rate of aqueous particulate components
$r_{b,i}$	Effective radius of the largest water-filled capillary pore in the presence of biofilm
r_{C_k}	Reaction rate of C_k
$r_{\check{C}_l}$	Reaction rate of solid components
r_{det}	Detachment rate of solid particulate components
$r_{f,i}$	Effective radius of the largest water-filled capillary pore
r_i	Reaction rate for component i
r_r	Reaction rate in the solute transport equation
S	Sulphur
s_{C_k}	Source/sink term of aqueous phase components
S_A	Fermentation products as acetate
S_e	Effective water saturation
S_{em}	Effective bacteria saturation
$S_{ew,j}$	Effective water saturation in the presence of biofilm/biomat
S_F	Soluble fermentable COD
S_{H2S}	Dihydrogen sulphide sulphur

Continues on the next page

Continued

Symbol	Description
S_I	Soluble inert COD
S_i	Dissolved components
S_{NH}	Ammonia and ammonium nitrogen
S_{NO}	Nitrite and nitrate nitrogen
S_O	Dissolved Oxygen
$S_{O_{sat}}$	Dissolved oxygen concentration at saturation
S_{SO4}	Sulphate sulphur
s_s	Source/sink term in the Richards and transport equations
t	Time
V	Volume of pore water
$v_{i,j}$	Stoichiometric factor for component i and process j
V_m	Volume of biomass in the representative volume of granular material V_{total}
V_{total}	Representative volume of granular material
v_x	Horizontal component of the flow velocity
v_y	Vertical component of the flow velocity
W_{WB}	Width of the wetland body
X	Generic bacteria group (Chapter 8)
X_A	Autotrophic nitrifying bacteria
X_{AMB}	Acetotrophic methanogenic bacteria
X_{ASRB}	Acetotrophic sulphate reducing bacteria
X_{FB}	Fermenting bacteria
X_{FB_0}	Initial concentration of fermenting bacteria
X_H	Heterotrophic bacteria
X_i	Particulate components
X_I	Inert particulate COD
X_{If}	Solid inert particulate COD
X_{Im}	Aqueous inert particulate COD
X_S	Slowly biodegradable particulate COD
X_{Sf}	Solid slowly biodegradable particulate COD
X_{Sm}	Aqueous slowly biodegradable particulate COD
X_{SOB}	Sulphide oxidising bacteria
Y_A	Yield coefficient for autotrophic nitrifying bacteria
Y_{AMB}	Yield coefficient for acetotrophic methanogenic bacteria
Y_{ASRB}	Yield coefficient for acetotrophic sulphate reducing bacteria
Y_{FB}	Yield coefficient for fermenting bacteria
Y_H	Yield coefficient for heterotrophic bacteria
Y_{SOB}	Yield coefficient for sulphide oxidising bacteria
$Y_{X,C}$	Yield coefficient for X (Chapter 8)
α	van Genuchten parameter

Continues on the next page

Continued

Symbol	Description
α_L	Longitudinal dispersivity
α_T	Transverse dispersivity
η_g	Correction factor for denitrification by X_H
η_H	Correction factor for hydrolysis by heterotrophic bacteria
η_{SOB}	Correction factor for denitrification by X_{SOB}
$\theta(h)$	Volumetric water content
θ_m	Volume fraction of the soil occupied by bacteria
θ_r	Residual liquid volume fraction
θ_s	Saturated liquid volume fraction
$\theta_{w,j}$	Water content in the presence of biofilm
λ_{att}	Attachment coefficient
λ_{det}	Detachment coefficient
μ_A	Maximum aerobic growth rate of X_A on S_{NH}
μ_{AMB}	Maximum growth rate of X_{AMB}
μ_{ASRB}	Maximum growth rate of X_{ASRB}
μ_{FB}	Maximum growth rate of X_{FB}
μ_H	Maximum aerobic growth rate of X_H on S_F and S_A
μ_{SOB}	Maximum growth rate of X_{SOB}
μ_X	Maximum growth rate of X (Chapter 8)
ρ_{biomat}	Biomat density
ρ_j	Reaction rate for process j
ρ_X	Density of bacteria X (Chapter 8)
$\sigma(h)$	Specific volumetric storability
ϕ	Porosity

CHAPTER 1

Introduction

1.1 Global water context

Water is indispensable for all forms of life on Earth. According to the World Health Organization (WHO) a single human being requires between 50 and 100 litres of water to ensure that its most basic needs are met. This fact was officially recognised by the United Nations General Assembly on July 28^{th} 2010, which declared the human right to water and sanitation through Resolution 64/292 (UN-OHCH-UNHabitat-WHO, 2010). This resolution acknowledges the importance of equitable access to safe and clean drinking water and sanitation as an integral component of the realization of all human rights.

Moreover, among The Millennium Development Goals (MDG), established in year 2000 following the Millennium Summit of the United Nations, goal number seven was dedicated to *Ensure environmental sustainability.* Section three of goal number seven was dedicated to *Halve, by 2015, the proportion of the population without sustainable access to safe drinking water and basic sanitation.*

Although this goal was achieved 5 years before schedule, there are still lots of challenges ahead regarding sanitation and water accessibility and quality. In fact, at current time approximately 884 million people still lack access to safe drinking water and more than 2.6 billion do not have access to basic sanitation. It is also estimated that approximately 1.5 million children under 5 years of age die each year as a result of water and sanitation-related diseases (UN-OHCH-UNHabitat-WHO, 2010) and according to WHO, 88% of the diarrhoeal deaths are due to unsafe

water, inappropriate sanitation and lack of hygiene. In fact, an estimated 1 billion people (15% of the world population) still practice open defecation. This is of special concern, since just a small number of people practicing open defecation can threaten the quality of water resources, which will in turn infringe the right to water and the right to health (Alburquerque, 2013). Moreover the majority (71%) of those without sanitation live in rural areas and 90% of all open defecation takes place in rural areas.

Adding to all that, water is a limited resource and, most importantly, it is badly distributed geographically. This fact combined with the ever increasing population living on Earth is expected to be the cause of many conflicts in the future.

Figure 1.1 helps the purpose of showing how water is a scarce resource. In this figure, the largest sphere represents all of Earth's water (estimated diameter of 1384.0 km), the intermediate corresponds to Earth's liquid fresh water (i.e. groundwater, lakes, swamp water and rivers) and the smallest one is the water in lakes and rivers.

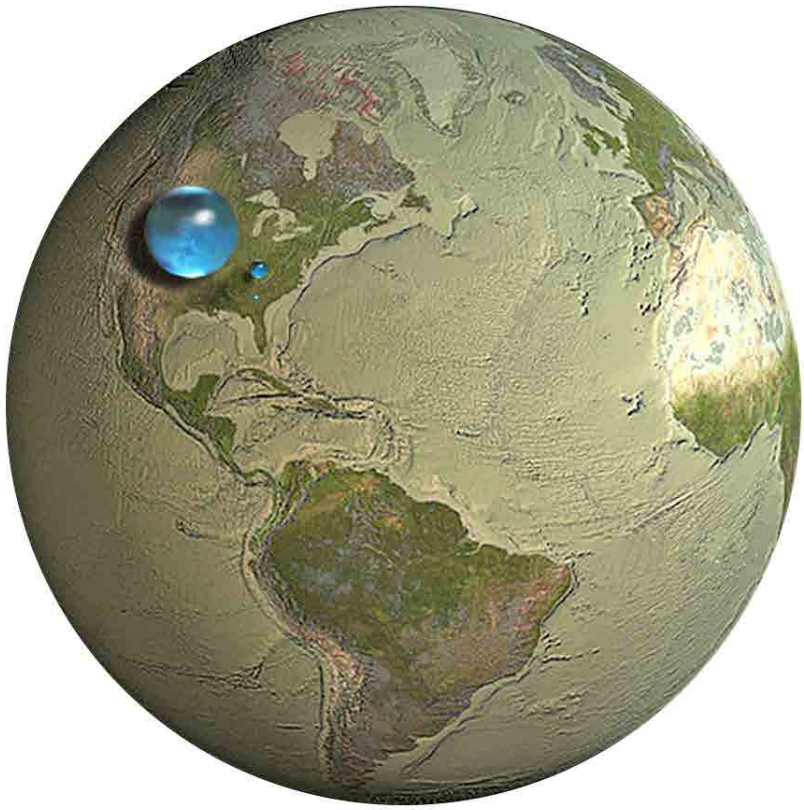

Figure 1.1: Spheres representing all of Earth's water, Earth's liquid fresh water and water in lakes and rivers (Credit: Howard Perlman, USGS; globe illustration by Jack Cook, Woods Hole Oceanographic Institution).

In 2010, nearly all megacities (>10 million inhabitants) were facing water scarcity and as the world population continues to grow, so has the demand for water (Alburquerque, 2013). In 2011 world population hit the 7 billion figure, which is twofold the population on the earth on the 1970. This pace of growth is expected to continue at least for the next 40 years, and predictions indicate that the population in 2050 will reach 9.6 billion (United Nations, 2013). Accordingly water withdrawals tripled over the last 50 years and demand for water for food production is projected to double by 2050 (Alburquerque, 2013). Moreover, global warming is expected to put water resources even more at stake.

Moreover, the increasing world population also contributes to the deterioration of water quality (UNEP-UNWATER-FAOWATER, 2010). Deterioration of water quality occurs when existing water treatment and/or sanitation infrastructures are overloaded or when there are no water treatment facilities at all. In those cases wastewater is discharged directly into the environment and the receiving water body, and possibly subsurface water are contaminated (UNEP-UNWATER-FAOWATER, 2010).

Enhancing and expanding infrastructure can be very costly and therefore in general is not keeping up with rapid development. Wastewater management therefore is emerging as a major global challenge (Alburquerque, 2013). According to the World Water Development Report of 2012, over 80% of wastewater worldwide is not collected or treated, and urban settlements are the main source of pollution. And in developing countries up to 90 % of wastewater is released untreated into the receiving bodies, which in many cases pollute potable water sources.

However, this is not only a problem concerning developing countries. For instance, and according to the World factbook from the Central Intelligence Agency of the USA, among the main environmental issues affecting Spain are the pollution of the Mediterranean Sea from different sources and the water quality and quantity nationwide.

To this regard Alburquerque (2013) states that in times of financial and economic crisis, retrogressive measures are more common and their impacts often exacerbated by austerity measures. Indeed, in the current context of economical crisis, the treatment of wastewater is less of a priority for administrations. For the sake of example, in Catalonia the lack of financial resources is letting the water management at the hands of private companies. Nowadays c.a. 80% of wastewater treatment plants in Catalonia are run by private capital (Garriga Riu, 2013), which may condition the treatment of water to net profit.

For all the reasons stated before, it is clear that among many other things, the world needs sustainable, economical and reliable wastewater treatment technologies to tackle the challenges of the future regarding water quality and accessibility.

According to Alburquerque (2013), choosing the right technology is essential to achieving sustainability of water and sanitation services. To this regard, in this work we focus on Constructed Wetlands technology; these systems are cheap, low in energy requirements and thus, a sustainable treatment technology. However, as we will expose in following sections of this work, they suffer from certain issues, derived from the combined effect of their internal complexity and our lack of understanding of their functioning, which can hinder their full deployment in the territory.

1.2 Constructed Wetlands for wastewater treatment

1.2.1 General background

Constructed Wetlands (CWs) are engineered systems, based on the principles of natural wetlands, that are used to treat wastewater originated from different sources (urban runoff, municipal, industrial, agricultural and acid mine drainage) (Figure 1.2). The most common application of these systems is for the treatment of municipal wastewater. CWs are designed to simulate the conditions that allow the development of the processes occurring in natural wetlands, but in a controlled environment (García et al., 2010).

Figure 1.2: Treatment plant based on Constructed Wetlands technology (Verdú, Catalonia). The treatment line consisted on three septic tanks in parallel followed by four parallel horizontal subsurface flow Constructed Wetlands and two surface flow wetlands.

This technology is recognized to have low energy and maintenance requirements and to be easy to operate. These facts make it suitable for wastewater treatment

where land availability and land prices are not limiting factors (García et al., 2001; Puigagut et al., 2007).

CWs have been actively used around the world since the early 70's as an alternative to intensive treatment technologies for the sanitation of small communities (Puigagut et al., 2007).

1.2.2 Constructed Wetlands typologies

CWs consist of impermeable excavated basins, which use engineered structures to control the flow direction, liquid retention time and water level (USEPA, 2000). Water is fed and retained during a specified time in these systems, which depends on the inflow rate and the volume of the basin. CWs are planted with aquatic macrophytes, typical from natural wetland areas. According to the way water circulates through the basins, they can be classified as either Subsurface Flow Wetlands (SSF CWs) or Surface Flow Wetlands (SF CWs). In the first case, water circulates underground through the porosity of a granular medium, whereas in SF CWs water circulates in contact with the atmosphere (Kadlec and Wallace, 2008).

SSF CWs can also be subdivided in horizontal flow or vertical flow systems (Kadlec and Wallace, 2008). In horizontal flow wetlands (HSSF CWs) (Figure 1.3), wastewater is maintained at a constant depth and flows horizontally below the surface of the granular medium.

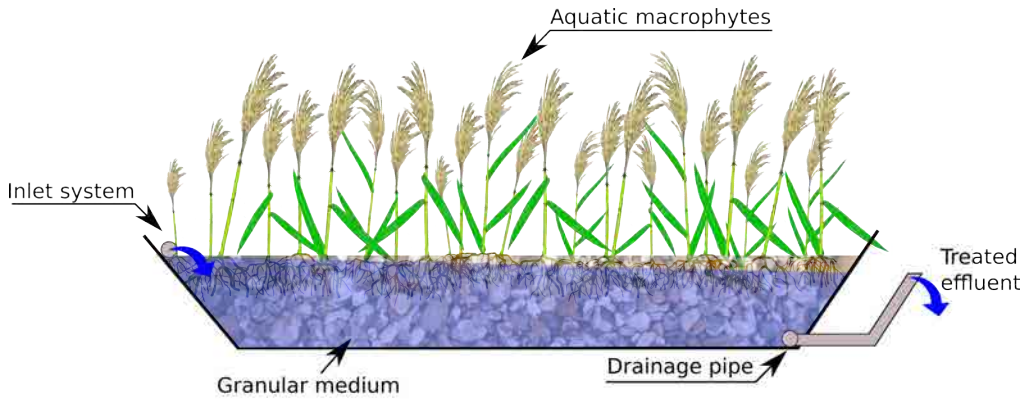

Figure 1.3: Schematic representation of a horizontal subsurface flow CW. Flow circulates from left to right.

In vertical flow systems (VSSF CWs) (Figure 1.4), wastewater is distributed over the surface of the wetland and trickles downward through the granular medium (Brix and Arias, 2005).

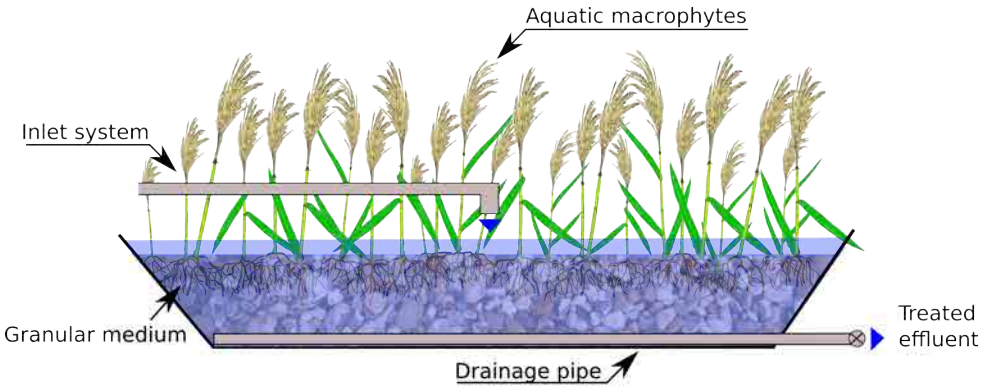

Figure 1.4: Schematic representation of a vertical subsurface flow CW. Flow circulates from top to bottom.

Combinations of these two types of systems can be used in certain cases, benefiting from the advantages of the two. However, from now onwards, only HSSF CWs will be considered, although most of the criteria that applies for HSSF CWs does also apply for VSSF CWs and any combination of the two.

1.2.3 Applications

CWs are designed to eliminate pollutants from wastewater such as: suspended solids, organic matter, nutrients and faecal bacteria indicators. Other pollutants that are also removed but that are not commonly targeted when designing municipal wastewater treatment systems are heavy metals, surfactants, pharmaceuticals and personal care products (PPCPs) as well as other emerging pollutants.

In particular, SSF CWs are one of the most common types of extensive wastewater systems used throughout the world (García et al., 2010). Traditionally, wastewater treatment plants (WWTPs) based on HSSF CWs consist of several in-series treatment stages. First, the pre-treatment and primary treatment are combined to eliminate solids, while subsequent stages consist of CWs sometimes combined with other extensive technologies (Rousseau et al., 2004; Vera et al., 2011; Vymazal, 2005).

Thus, SSF CWs are mainly designed to treat primary settled wastewater, although they are also used to improve the quality of secondary treated effluents (García et al., 2010).

1.2.4 Design criteria

In engineering practice, the design of SSF CWs is often carried out using the black box concept. Hence, important design factors such as areal organic loading rate (AOLR), hydraulic loading rate (HLR), aspect ratio, granular medium size and water depth are defined mostly from previous experience (García et al., 2005). Other equally important parameters are the selection of the pretreatment, inflow and collection systems, as well as the plant species to be planted.

Several experimental studies have focused on studying different systems under different hydraulic loading rates (HLR) (García et al., 2004a), organic loading rates (OLR) and other design parameters. Results of these studies have been used to propose recommended ranges for the different factors.

The main operational problem associated with SSF CWs is the clogging of the granular media (Knowles et al., 2011; Pedescoll et al., 2011; Rousseau et al., 2005). Clogging development reduces the infiltration capacity (Caselles-Osorio et al., 2007; Ruiz et al., 2010) thus causing the hydraulic malfunctioning of wetlands and, in some cases, the decrease of treatment efficiency (Rousseau et al., 2005). Among the most important factors contributing to clogging are the retention and accumulation of wastewater solids, biofilm and plant growth and the accumulation of plant litter and chemical precipitates (Knowles et al., 2011). Several authors (Langergraber, 2003; Nguyen, 2000; Pedescoll et al., 2011) have reported that correct operation and maintenance is of great importance to avoid rapid clogging of SSF CWs.

The organic and suspended solids loads are the main operation factors affecting clogging development (Álvarez et al., 2008; Chazarenc et al., 2007; Winter and Goetz, 2003). In this regard, some authors have suggested that the OLR in horizontal SSF CWs should not exceed 6 $gBOD \cdot m^{-2}d^{-1}$ (García et al., 2005; USEPA, 2000). Organic loads between 8 and 12 $gBOD \cdot m^{-2}d^{-1}$ are generally associated with a total suspended solids loading of 110 $gTSS \cdot m^{-2}d^{-1}$ (Kadlec and Wallace, 2008). However, as reported by Álvarez et al. (2008), little information is available on the maximum acceptable total suspended solid (TSS) loading rates and only some recommendations are prescribed for vertical SSF CWs.

It is well known that the reduction of suspended solids and organic content in wastewater achieved by using a good previous treatment, is essential to delay clogging development and thus to extend life-span of SSF CWs (Álvarez et al., 2008; Caselles-Osorio et al., 2007; Pedescoll et al., 2011; Winter and Goetz, 2003). The life-span of CWs depends directly on solids retention (organic and inorganic) and on the intrinsic organic matter turn-over rate (decomposition and cycling) (Nguyen, 2000). If the accumulation rate is higher than the turn-over rate then it is likely that clogging will develop at a rapid peace.

The HLR applied to these systems is dependent on the allowed OLR, but it is also considered in the hydraulic design of a wetland.

1.2.5 Contaminant removal processes

The two major mechanisms at work in most treatment systems are liquid/solid separations and constituent degradations and transformations (USEPA, 2000). SSF CWs are essentially fixed-biofilm reactors in which organic matter is removed through interactions between complex physical, chemical, and biochemical processes. Many studies have shown that organic matter removal rates are not clearly related to changes in water temperature, which suggests that the principal removal mechanisms are physic-chemical and subsequently biological (McNevin et al., 2000). The relative importance of the different biochemical pathways for removing organic matter depends primarily on the redox conditions (García et al., 2010).

The main mechanisms for influent particulate organic mater (POM) (and in general TSS) retention in SSF CWs are those of physic-chemical nature, and include impact and retention encouraged by path variations of water flow owing to the grains of the medium, settling due to low speed movement, and adhesion owing to superficial interaction forces.

Retained POM either accumulates or disintegrates and undergoes hydrolysis, which generates dissolved organic compounds that can be degraded by different pathways that occur simultaneously in a given wetland (García et al., 2010). POM accumulation in the granular medium is a typical feature of SSF CWs (Nguyen, 2001). Most of the POM is removed close to the inlet, and the remaining dissolved organic matter is removed more slowly along the entire length of the beds (García et al., 2010). The removal rates of influent TSS in SSF CWs are usually very high (>90%).

During the hydrolysis step, which occurs after disintegration, a defined particulate or macromolecular substrate is degraded into its soluble compounds. Disintegration and hydrolysis are processes that occur either under aerobic, anoxic, or anaerobic conditions. The hydrolysis reaction is one of the processes that most restricts the removal of organic matter in wastewater treatment plants (García et al., 2010).

Inflow dissolved organic matter (DOM) and that produced after disintegration and hydrolysis processes can be removed by aerobic respiration through the metabolism of a large number of heterotrophic bacteria that use oxygen as a final electron acceptor. Aerobic respiration requires oxygen, which can be the most limiting substrate for this reaction in SSF CWs, as the amount of oxygen transported from air to water in a horizontal SSF CW is insignificant in comparison to the oxygen demand of standard urban wastewater (García et al., 2010).

Studies carried out in the last 10 years have shown that aerobic respiration is not the only reaction to exert a significant influence on organic matter removal in horizontal SSF CWs (Aguirre et al., 2005; Baptista et al., 2003). In fact, aerobic respiration is not the most important reaction involved in organic matter removal. In the next few lines, a description of other reactions occurring in constructed wetlands that also lead to the removal of organic matter is made.

Denitrification is the biochemical reduction of nitrate and nitrite to nitrogen gas. This process links the C and N cycles in CWs because it enables denitrifying bacteria to obtain energy from organic compounds at the same time that nitrate is used as an electron acceptor. Denitrification is conducted by a wide range of heterotrophic aerobic facultative bacteria that are able to use nitrate as electron acceptor under anoxic conditions. These bacteria groups use oxygen preferentially over nitrate as electron acceptor when it is available in the surrounding environment. Consequently, significant denitrification rates are only observed in depleted oxygen environments (García et al., 2010).

Fermentation is a multi-stage biochemical process in which the soluble organic monomers present in wastewater and those generated through hydrolysis are converted into volatile short-chain fatty acids (VFAs). A large number of heterotrophic bacteria groups are involved in fermentation reactions. Fermentation occurs under anaerobic conditions and is therefore an important reaction in horizontal SSF CWs.

Interest in sulphate reduction in SSF CWs has grown in recent years because research has shown that it can contribute significantly to the removal of organic matter in horizontal SSF CWs (Aguirre et al., 2005). Sulphate is a normal constituent of many types of wastewater and can be used as an electron acceptor in the absence of oxygen by a large group of strictly anaerobic heterotrophic microorganisms called sulphate-reducing bacteria. These microorganisms can grow by using a wide range of fermentation products as electron donors (e.g., acetate, lactate, butyrate) (Lloyd et al., 2004; Stein et al., 2007). Reduced sulphur compounds such as sulphide are released by the activity of sulphate-reducing bacteria which are known to be potent inhibitors of plant growth and certain microbial activities (Gonzalias et al., 2007; Wiessner et al., 2005).

Methanogens are strictly anaerobic bacteria that produce methane as an end product of metabolism. Methanogens and sulphate-reducing bacteria require environments with similar redox potential levels and use the same types of electron donors (i.e., hydrogen, acetic acid). When these two groups of bacteria grow together and the COD:sulfate ratio (expressed as COD:S) is lower than 1.5, sulfate-reducing bacteria are able to outcompete methanogens. When the ratio is greater than 6, methanogens predominate over sulfate-reducing bacteria (Stein et al., 2007). Methanogenesis can remove significant quantities of organic matter from wastewater and has been studied more extensively in recent years (García et al., 2010).

Despite the extensive literature available on CWs, and all the efforts dedicated over the years to improve their understanding, there are still some knowledge gaps which prevent us from being able to optimize their functioning and reduce their known weaknesses (i.e. clogging development). Over recent decades, several mathematical and numerical models have been developed to help improve the understanding of these systems. The following section is dedicated to update the state of the art regarding these models.

1.3 Constructed Wetland models

This section is based on the book chapter:

- Samsó, R., Meyer, D., García, J., 2014. Subsurface flow constructed wetlands models: review and prospects, in: Vymazal, J. (Ed.), The Role of Natural and Constructed Wetlands in Nutrient Cycling and Retention on the Landscape. Springer, Dordrecht, The Netherlands (in press).

A mathematical model can be simply described as an attempt to translate the conceptual understanding of a real-world system or process (conceptual model) into mathematical terms (Eberl et al., 2006). Therefore, mathematical models for Constructed Wetlands are a set of mathematical expressions (algebraic or differential equations), each describing a process that is known to take place within them. Among the many processes taking place within wetlands, those originated from microbial metabolism are key to describe their global functioning (Samsó and García, 2013b). The mathematical models describing the rates at which microbial processes take place are called biokinetic models.

On the other hand, numerical models involve the use of some sort of spacial and/or temporal discretization techniques to obtain approximate solutions to mathematical equations. Numerical modelling is an interesting tool as it allows to observe the outcome of complex conceptual models in various experimental conditions and to test their validity and how they enable a better understanding of the involved processes (Oberkampf and Trucano, 2002).

For several years now, numerical models for CWs have been considered a promising tool to increase the understanding of the simultaneous physic-chemical and biological processes involved in the treatment of wastewater with this technology.

This belief has translated in an increase on the number of publications on the development and utilization of these models over time. In fact, there exist arguably as many numerical models for CWs as there are types of wetlands, water pollutants and processes that take place within these systems. Indeed, a general search for the words *constructed wetland model* on common databases of scientific papers brings a limitless number of publications on this topic.

Among them, a very general distinction can be made: those focusing on the simulation of the hydraulics (Arias et al., 2014; Dittmer et al., 2005; Fan et al., 2008; Galvão et al., 2010; Korkusuz et al., 2007; Kotti et al., 2013),the hydrodynamics and clogging (or any of them individually) (Brovelli et al., 2009b; Giraldi et al., 2009, 2010; Hua et al., 2013; Knowles et al., 2011; Suliman et al., 2006) and those focusing on the removal of a specific pollutant or a set of pollutants (which generally also include hydraulic and hydrodynamic models of diverse complexity). Among the latter, the most commonly targeted pollutants are organic compounds (Akratos et al., 2008; Henrichs et al., 2007; Liolios et al., 2012; Toscano et al., 2009), nitrogen (Akratos et al., 2009; Henrichs et al., 2009; Mayo and Bigambo, 2005; Mcbride and Tanner, 2000; Meyer et al., 2006; Meyer, 2011; Moutsopoulos et al., 2011; Toscano et al., 2009) sulphur (Lloyd et al., 2004), phosphorous (Hafner and Jewell, 2006), heavy metals and mine drainage (Goulet, 2001; Lee et al., 2006; Mitsch and Wise, 1998), arsenic (Llorens et al., 2013) pesticides (Krone-Davis et al., 2013) and emerging pollutants (Hijosa-Valsero et al., 2011).

At least 7 review papers have been published in recent times to summarize the state of the art of CWs numerical models (García et al., 2010; Kumar and Zhao, 2011; Langergraber et al., 2009b; Langergraber, 2010, 2008; Meyer et al., 2014; Rousseau et al., 2004). These reviews mostly consist of descriptions of the models features and no critical in-depth comparison is made between them (Samsó et al., 2014b).

In this section only the most recent numerical codes, applied to simulate the treatment of urban wastewater and those able to provide new insight into the functioning of CWs are reviewed. The 5 models selected for review are: *PHWAT* (Brovelli et al., 2009a,b,c, 2007), *FITOVERT* (Giraldi et al., 2009, 2010), *HYDRUS-2D-CW2D* (Langergraber, 2005), *HYDRUS-2D-CWM1* (Langergraber and Simunek, 2012), *CWM1-RETRASO* (Llorens et al., 2011a,b) and *AQUASIM-CWM1* (Mburu et al., 2012).

From the selected numerical codes, the only one that does not use either the biokinetics models CW2D or CWM1 is *FITOVERT* model. Provided the importance of the biokinetic equations within CWs models, the description of the selected models will be preceded by a brief description of CW2D and CWM1.

CW2D

Constructed Wetlands 2D (CW2D) (Langergraber, 2001) is a biokinetic model, based on the mathematical formulation of the Activated Sludge Model series (ASM) (Henze et al., 2000). This model was specifically conceived to simulate the most common biokinetic processes taking place in VF CWs.

The components defined in CW2D include dissolved oxygen ($O2$), three fractions of organic matter (CR, CS, and CI), four nitrogen compounds ($NH4$, $NO2$,

$NO3$ and $N2N$), inorganic phosphorus (IP), and heterotrophic and autotrophic microorganisms. Organic nitrogen and organic phosphorous are modelled as part of the COD. Heterotrophic bacteria (XH) are assumed to be responsible for hydrolysis, mineralization of organic matter (aerobic growth) and denitrification (anoxic growth). On the other hand, autotrophic bacteria ($XANs$ and $XANb$) are assumed to be responsible for nitrification, which is modelled as a two-step process. Microorganisms are assumed to be immobile. Lysis is considered to be the sum of all decay and loss processes. The temperature dependence of all process rates and diffusion coefficients is described using the Arrhenius equation.

CWM1

The biokinetic model Constructed Wetland Model number 1 (CWM1) (Langergraber et al., 2009a) is another general model based on the ASM series (Henze et al., 2000) and the Anaerobic Digestion Model (ADM) (Batstone et al., 2002) for anaerobic processes, to describe biochemical transformation and degradation of organic matter, nitrogen and sulphur in SSF CWs. The main objective of CWM1 is to predict effluent concentrations from either VF or HF CWs without predicting gaseous emissions (Langergraber et al., 2009a).

This model considers 17 processes and 16 components (8 soluble and 8 particulate). In terms of notation and structure, CWM1 is described in a way similar to the ASMs. As in the ASMs concentrations of dissolved components are referred to as S_i and particulate components as X_i. Among the dissolved components there are: dissolved oxygen (S_O), ammonia and nitrate nitrogen (S_{NH} and S_{NO}), sulphate and dihydrogensulphide sulphur (S_{SO4} and S_{H2S}), soluble fermentable COD (S_F), fermentation products as acetate (S_A) and soluble inert COD (S_I). Organic nitrogen is considered as a fraction of organic matter (COD). Among the particulate components there are 6 functional bacteria groups, including heterotrophic, nitrifying, fermenting, methanogenic, sulphate reducing and sulphide oxidising bacteria (X_H, X_A, X_{FB}, X_{AMB}, X_{ASRB} and X_{SOB}, respectively) and two particulate fractions of COD (X_I and X_S). Such as in the IWA ASMs, the kinetic expressions of CWM1 are based on switching functions (hyperbolic of saturation terms and Monod equations (Monod, 1949)).

Figure 1.5 presents a graphical representation of the cycles of carbon, nitrogen and silphur as described in CWM1.

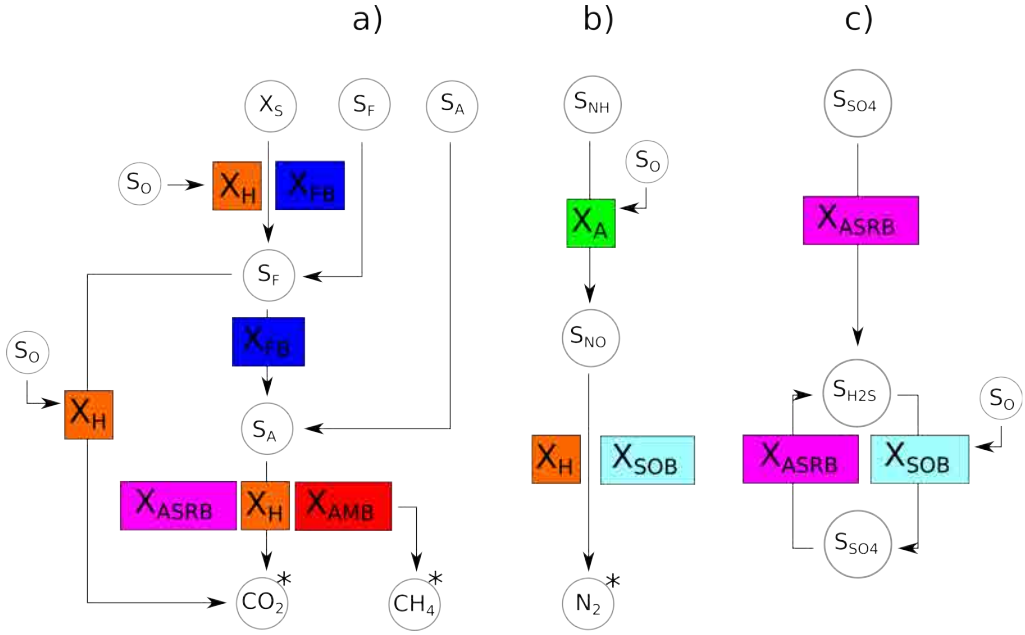

Figure 1.5: Main interactions between bacteria groups (coloured boxes) and substrates (circles) in the a) carbon, b) nitrogen and c) sulphur cycles. The substrates at the top of the image enter the wetland with the influent wastewater. Inert particulate COD (X_I) and soluble intert COD (S_I) are not included in the Figure since they are neither degraded nor transformed. Note, though, that the decay of all bacteria groups and hydrolysis produce inert particulate COD. The components marked with an asterisk are not considered in CWM1.

The stoichiometric matrix of CWM1 is presented in Table 1.1 and the rate of each individual process is described in Table 1.2.

Table 1.1: Stoichiometric matrix of CWM1 (Langergraber et al., 2009a).

	i	1	2	3	4	5	6	7	8	9	10	11	12	13	14	15	16
	Process component	S_O	S_F	S_A	S_I	S_{NH}	S_{NO}	S_{SO4}	S_{H2S}	X_S	X_I	X_H	X_A	X_{FB}	X_{AMB}	X_{ASRB}	X_{SOB}
j	*expressed as*	O_2	COD	COD	COD	N	N	S	S	COD	COD	COD	COD	COD	COD	COD	COD
1	Hydrolysis		$1-f_{Hyd,SI}$		$f_{Hyd,SI}$	$v_{5,1}$											
2	Aerobic growth of X_H on S_F	$1-\frac{1}{Y_H}$	$\frac{-1}{Y_H}$			$v_{5,2}$						1					
3	Anoxic growth of X_H on S_F		$\frac{-1}{Y_H}$			$v_{5,3}$	$\frac{-1-Y_H}{2.86\cdot Y_H}$					1					
4	Aerobic growth of X_H on S_A	$1-\frac{1}{Y_H}$		$-\frac{1}{Y_H}$		$v_{5,4}$						1					
5	Anoxic growth of X_H on S_A			$-\frac{1}{Y_H}$		$v_{5,5}$	$-\frac{1-Y_H}{2.86\cdot Y_H}$					1					
6	Lysis of X_H		$f_{BM,SF}$			$v_{5,6}$				$v_{9,Lysis}$	$f_{BM,XI}$	-1					
7	Aerobic growth of X_A on S_{NH}	$-\frac{4.57-Y_A}{Y_A}$				$v_{5,7}$							1				
8	Lysis of X_A		$f_{BM,SF}$			$v_{5,8}$				$v_{9,Lysis}$	$f_{BM,XI}$		-1				
9	Growth of X_{FB}		$\frac{-1}{Y_{FB}}$	$\frac{1-Y_{FB}}{Y_{FB}}$		$v_{5,9}$								1			
10	Lysis of X_{FB}		$f_{BM,SF}$			$v_{5,10}$				$v_{9,Lysis}$	$f_{BM,XI}$			-1			
11	Growth of X_{AMB}			$\frac{-1}{Y_{AMB}}$		$v_{5,11}$									1		
12	Lysis of X_{AMB}		$f_{BM,SF}$			$v_{5,12}$				$v_{9,Lysis}$	$f_{BM,XI}$				-1		
13	Growth of X_{ASRB}			$\frac{-1}{Y_{ASRB}}$		$v_{5,13}$		$-\frac{1-Y_{ASRB}}{2\cdot Y_{ASRB}}$	$\frac{1-Y_{ASRB}}{2\cdot Y_{ASRB}}$							1	
14	Lysis of X_{XASRB}		$f_{BM,SF}$			$v_{5,14}$				$v_{9,Lysis}$	$f_{BM,XI}$					-1	
15	Aerobic growth of X_{SOB} on S_{H2S}	$-\frac{2-Y_{SOB}}{Y_{SOB}}$				$v_{5,15}$		$\frac{-1-Y_{SOB}}{0.875-Y_{SOB}}$	$\frac{1}{Y_{SOB}}$								1
16	Anoxic growth of X_{SOB} on S_{H2S}					$v_{5,16}$	$\frac{-1-Y_{SOB}}{0.875-Y_{SOB}}$	$\frac{1}{Y_{SOB}}$	$\frac{-1}{Y_{SOB}}$								1
17	Lysis of X_{SOB}		$f_{BM,SF}$			$v_{5,17}$				$v_{9,Lysis}$	$f_{BM,XI}$						-1

$v_{9,Lysis}=1-f_{BM,SF}-f_{BM,XI}$

Table 1.2: Processes rates in $mg \cdot l^{-1}d^{-1}$ (Langergraber et al., 2009a).

j	**Process**	**Process rate** ρ_j
1	Hydrolysis	$k_h \left[\frac{\frac{X_S}{X_H+X_{FB}}}{K_X\left(\frac{X_S}{X_H+X_{FB}}\right)} \right] (X_H+\eta_h X_{FB})$
2	Aerobic growth of X_H on S_F	$\mu_H \left(\frac{S_F}{K_{SFH}+S_F}\right)\left(\frac{S_F}{S_F+S_A}\right)\left(\frac{S_O}{K_{SOH}+S_O}\right)\left(\frac{S_{NH}}{K_{SNHH}+S_{NH}}\right)\left(\frac{K_{SH2SH}}{K_{SH2SH}+S_{H2S}}\right)X_H$
3	Anoxic growth of X_H on S_F	$\eta_g \cdot \mu_H \left(\frac{S_F}{K_{SFH}+S_F}\right)\left(\frac{S_F}{S_F+S_A}\right)\left(\frac{K_{SOH}}{K_{SOH}+S_O}\right)\left(\frac{S_{NO}}{K_{SNOH}+S_{NO}}\right)\left(\frac{S_{NH}}{K_{SNHH}+S_{NH}}\right)\left(\frac{K_{SH2SH}}{K_{SH2SH}+S_{H2S}}\right)X_H$
4	Aerobic growth of X_H on S_A	$\mu_H \left(\frac{S_A}{K_{SAH}+S_A}\right)\left(\frac{S_A}{S_F+S_A}\right)\left(\frac{S_O}{K_{SOH}+S_O}\right)\left(\frac{S_{NH}}{K_{SNHH}+S_{NH}}\right)\left(\frac{K_{SH2SH}}{K_{SH2SH}+S_{H2S}}\right)X_H$
5	Anoxic growth of X_H on S_A	$\eta_g \mu_H \left(\frac{S_A}{K_{SAH}+S_A}\right)\left(\frac{S_A}{S_F+S_A}\right)\left(\frac{K_{SOH}}{K_{SOH}+S_O}\right)\left(\frac{S_{NO}}{K_{SNOH}+S_{NO}}\right)\left(\frac{S_{NH}}{K_{SNHH}+S_{NH}}\right)\left(\frac{K_{SH2SH}}{K_{SH2SH}+S_{H2S}}\right)X_H$
6	Lysis of X_H	$b_X X_H$
7	Aerobic growth of X_A on S_{NH}	$\mu_A \left(\frac{S_{NH}}{K_{SNHA}+S_{NH}}\right)\left(\frac{S_O}{K_{SOA}+S_O}\right)\left(\frac{K_{SH2SA}}{K_{SH2SA}+S_{H2S}}\right)X_A$
8	Lysis of X_A	$b_A X_A$
9	Growth of X_{FB}	$\mu_{FB} \left(\frac{S_F}{K_{SFFB}+S_F}\right)\left(\frac{K_{SH2SFB}}{K_{SH2SFB}+S_{H2S}}\right)\left(\frac{K_{SOFB}}{K_{SOFB}+S_O}\right)\left(\frac{K_{SNOFB}}{K_{SNOFB}+S_{NO}}\right)\left(\frac{S_{NH}}{K_{SNHFB}+S_{NH}}\right)X_{FB}$
10	Lysis of X_{FB}	$b_{FB} X_{FB}$
11	Growth of X_{AMB}	$\mu_{AMB} \left(\frac{S_A}{K_{SAMB}+S_A}\right)\left(\frac{K_{SH2SAMB}}{K_{SH2SAMB}+S_{H2S}}\right)\left(\frac{K_{SOAMB}}{K_{SOAMB}+S_O}\right)\left(\frac{K_{SNOAMB}}{K_{SNOAMB}+S_{NO}}\right)\left(\frac{S_{NH}}{K_{SNHAMB}+S_{NH}}\right)X_{AMB}$
12	Lysis of X_{AMB}	$b_{AMB} X_{AMB}$
13	Growth of X_{ASRB}	$\mu_{ASRB} \left(\frac{SA}{K_{SAASRB}+S_A}\right)\left(\frac{S_{SO4}}{K_{SO4ASRB}+S_{SO4}}\right)\left(\frac{K_{SH2SASRB}}{K_{SH2SASRB}+S_{H2S}}\right)\left(\frac{K_{SOASRB}}{K_{SOASRB}+S_O}\right)\left(\frac{K_{SNOASRB}}{K_{SNOASRB}+S_{NO}}\right)$ $\left(\frac{S_{NH}}{K_{SNHASRB}+S_{NH}}\right)X_{ASRB}$
14	Lysis of X_{XASRB}	$b_{ASRB} X_{ASRB}$
15	Aerobic growth of X_{SOB} on S_{H2S}	$\mu_{SOB} \left(\frac{S_{H2S}}{K_{SH2SSOB}+S_{H2S}}\right)\left(\frac{S_O}{K_{SOSOB}+S_O}\right)\left(\frac{S_{NH}}{K_{SNHSOB}+S_{NH}}\right)X_{SOB}$
16	Anoxic growth of X_{SOB} on S_{H2S}	$\mu_{SOB} \cdot \eta_{SOB} \left(\frac{S_{H2S}}{K_{SH2SSOB}+S_{H2S}}\right)\left(\frac{S_{NO}}{K_{SNOSOB}+S_{NO}}\right)\left(\frac{K_{SOSOB}}{K_{SOSOB}+S_O}\right)\left(\frac{S_{NH}}{K_{SNHSOB}+S_{NH}}\right)X_{SOB}$
17	Lysis of X_{SOB}	$b_{SOB} X_{SOB}$

The stoichiometric parameters for ammonia (see Table 1.1) are obtained from mass balances over each process as follows:

$$v_{5,1} = i_{N,XS} - (1 - f_{HYD,SI}) \cdot i_{N,SF} - f_{HYD,SI} \cdot i_{N,SI} \tag{1.1}$$

$$v_{5,2} = v_{5,3} = \frac{i_{N,SF}}{Y_H} - i_{N,BM} \tag{1.2}$$

$$v_{5,4} = v_{5,5} = v_{5,11} = v_{5,13} = v_{5,15} = v_{5,16} = -i_{N,BM} \tag{1.3}$$

$$\begin{aligned} v_{5,6} = v_{5,8} = v_{5,10} = v_{5,12} = v_{5,14} = v_{5,17} = i_{N,BM} - f_{BM,SF} \cdot i_{N,SF} - \\ -(1 - f_{BM,SF} - f_{BM,XI}) \cdot i_{N,XS} - f_{BM,XI} \cdot i_{N,XI} \end{aligned} \tag{1.4}$$

$$v_{5,7} = -i_{N,BM} - \frac{1}{Y_A} \tag{1.5}$$

$$v_{5,9} = \frac{i_{N,SF}}{Y_{FB}} - i_{N,BM} \tag{1.6}$$

Using Tables 1.1 and 1.2, the reaction rate for each component (r_i) is obtained with Equation 1.7:

$$r_i = \sum_{j=1}^{R} v_{i,j} \cdot \rho_j \tag{1.7}$$

where $i = 1, \ldots, N$ and N being the number of components, and $j = 1, \ldots, R$ and R is the number of processes. $v_{i,j}$ is the stoichiometric factor for component i and process j from Table 1.1 and ρ_j is the reaction rate of process j as described in Table 1.2.

For a list and a description of the parameters in Tables 1.1 and 1.2, the reader is referred to the original source (Langergraber et al., 2009a).

1.3.1 Numerical models for Constructed Wetlands

FITOVERT

FITOVERT (Giraldi et al., 2009, 2010) is a 1D code developed in MATLAB® and expressly designed to simulate subsurface VF CWs. This software is able to describe the water flow through unsaturated porous media as well as evapotranspiration and surface ponding. It is also able to simulate transport of dissolved and particulate components and clogging produced by bacterial growth and solids filtration.

The vertical water flow through porous media in unsaturated conditions is described using the volumetric water content form of the Richards equation. The

constitutive relationships between pressure head, hydraulic conductivity, and water content are handled using van Genuchten-Mualem functions, the parameters of which were obtained from a previous experimental study (Giraldi et al., 2009).

To describe the root water uptake a sink term was added to the Richards equation. The model is also able to automatically handle the ponding on the surface of the vertical bed by changing the hydraulic boundary conditions.

The biochemical module, based on the ASM1 (Henze et al., 2000), describes the degradation of both organic matter and transformation of nitrogen. Thirteen components are taken into account, seven of which are dissolved and six are particulate. Neither the features of the biochemical module nor the components and processes considered are described in the original paper.

The advection-dispersion transport in the liquid phase for dissolved components is described according to Bresler's equation (Bresler, 1973). Neither the uptake of nutrients and metals by the plants nor adsorption is considered in the existing version of *FITOVERT*. On the other hand, the transport and filtration of particulate components is described with a scheme based on the work of Iwasaki (1937) for the numerical analysis of the sand filtration process in saturated conditions.

FITOVERT is also able to handle the porosity reduction due to bacteria growth and filtration of particulate components. The effect of pore size reduction on the hydraulic conductivity is considered using a modified version of the Carman-Kozeny's equation (Boller and Kavanaugh, 1995).

The oxygen transport is modelled using the same equations as for the rest of the dissolved components, and the diffusive exchange of oxygen with the gas phase is included in the reaction term and described using Fick's law. Oxygen transfer by plants from the atmosphere to their roots is not implemented.

The hydraulic model was calibrated by comparing model outputs for inert components with experimental breakthrough curves of a pilot plant. Unfortunately, the biochemical and transport modules were not calibrated (Giraldi et al., 2009).

HYDRUS-2D-CW2D

The multi-component reactive transport module CW2D (Constructed Wetlands 2D), (Langergraber, 2001, 2005, 2008; Langergraber and Simunek, 2012), was developed as an extension of the HYDRUS-2D variably-saturated flow and solute transport program (Simunek et al., 1999). The variable saturated flow is described using the Richards equation. The constitutive relationships between pressure head, hydraulic conductivity, and water content are handled using van Genuchten-Mualem functions. Two additional boundary conditions are implemented to represent surface ponding in the vertical bed during wastewater loadings that exceed the infiltration capacity.

The transport of solutes is described using the advection-dispersion-diffusion equation which includes several sources and sinks to simulate adsorption/desorption and nutrients uptake by plant roots. The exchange of O_2 from the gas phase into the aqueous phase is described using the equation of Gujer and Boller (1990).

The effect of plants uptake on the removal of organic matter and nutrients in subsurface flow constructed wetlands was tested in Langergraber (2005). The model for plant uptake implemented describes nutrient uptake coupled to water uptake, which is an intrinsic capability of HYDRUS-2D. Literature values were used to calculate potential water and nutrient uptake rates.

Nowadays *HYDRUS-2D-CW2D* only considers dissolved wastewater compounds and therefore is currently unsuitable for investigating clogging phenomena (García et al., 2010).

PHWAT

PHWAT (Brovelli et al., 2009a,b,c, 2007; Mao et al., 2006) is a 3D macro-scale code that uses MODFLOW (McDonald and Harbaugh, 1988) to solve saturated/variably saturated water flow, MT3DMS (Zheng and Wang, 1998) to simulate transport processes, and PHREEQC-2 (Parkhurst and Appelo, 1999) to describe biochemical reactions. Aerobic processes are based on CW2D, while anaerobic processes are based on the model formulation by Maurer and Rittmann (2004). Aside from the biokinetic reactions, full water chemistry and sediment-water interactions can be modelled using PHREEQC. *PHWAT* is also able to simulate bioclogging, bacteria attachment and flow-induced biofilm detachment. This model includes a growth-limiting expression to account for the reduction of porosity caused by bacterial-growth.

HYDRUS-2D-CWM1

In Langergraber and Simunek (2012), a new version of the wetland module for HYDRUS-2D was presented. This new version adds the possibility to choose between the already implemented CW2D and the newly implemented CWM1 biokinetic models. The only change of *HYDRUS-2D-CWM1* with respect to *HYDRUS-2D-CW2D* is thus the biokinetic model.

In Langergraber and Simunek (2012) simulations were run to make a numerical verification of the implementation of the two biokinetic models in HYDRUS. The authors compared results with simplified versions of the two biokinetic models in a 20 by 20 *cm* vertical domain. The results demonstrated that the two biokinetic models were implemented correctly in HYDRUS-2D. *HYDRUS-2D-CWM1* was also used to recreate the simulations performed by Llorens et al. (2011a,b), obtaining different results.

AQUASIM-CWM1

Mburu et al. (2012) implemented the biokinetic model CWM1 into AQUASIM software (Reichert, 1998) to simulate the fate of organic matter, nitrogen and sulphur within 16 batch-operated subsurface-flow wetland mesocosms planted with three different plant species (for a detailed description of the mesocosms the reader is referred to Allen et al. (2002) and Stein et al. (2006)). The mixed reactor compartment configuration in AQUASIM was used and the mesocosms were described as constantly stirred tank reactors (CSTR). In addition to the biokinetic reactions of CWM1, this model considers physical reaeration, adsorption and desorption of COD and ammonium as well as a complex description of plant related processes. Indeed, the plant model includes 5 processes, namely growth, decay/senescence, physical degradation, oxygen leaching and nutrients uptake. The growth rate of microorganisms and plants are made temperature dependent by means of Arrhenius relationships. In this model, the growth of bacterial communities is only limited by substrates.

The model was calibrated and validated with different sets of experimental data from the mesocosms and sensitivity analysis, parameter estimation and uncertainty analysis were carried out.

CWM1-RETRASO

The *CWM1-RETRASO* model (Llorens et al., 2011a,b) is a 2D simulation model obtained from the implementation of CWM1 (Langergraber et al., 2009a) in RetrasoCodeBright (RCB) code (Saaltink et al., 2004) to simulate the hydraulics and hydrodynamics as well as the main biodegradation and transformation processes in horizontal SSF CWs.

RCB enables the simulation of the reactive transport of inorganic dissolved and gaseous species in non-isothermal saturated and unsaturated problems by finite elements. The transport of solutes in water is modelled by means of advection, dispersion and diffusion, together with chemical reactions. This model considers the wetland as a saturated porous media, and thus, the advective flux and dispersive and diffusive fluxes are computed by means of Darcys and Ficks laws, respectively.

The implementation of the biochemical processes within RCB code consisted on adding the rates relevant to CWM1 to the reaction term of the RCB transport equations. The reactive transport model of the present study basically consists of 19 reactions or processes instead of the 17 described by CWM1.

Physical oxygen transfer from the atmosphere to the water was included in the model. Oxygen leaking from macrophytes, plant uptake, biofilm development and processes linked to clogging were not considered.

A multiplicative exponential function similar to that used by Ojeda et al. (2008) for the hydrolysis process, was added to avoid total COD overestimations. In the paper by Llorens et al. (2011b), some changes to CWM1 formulation and to its parameters were proposed and both the hydraulic and biochemical models were calibrated and validated comparing it experimental data.

In *CWM1-RETRASO* bacterial concentrations are defined as inflow concentrations and travel through the wetland just as dissolved components do. Therefore, with this model, only stationary simulations can be performed, as the growth of bacterial populations cannot be simulated.

CHAPTER 2

Objectives and outline of the Thesis

From the bibliographical review carried out, four major issues stood out:

- Constructed Wetlands (CWs) functioning is still not well understood. Moreover, the enormous diversity of wetland typologies and operation strategies, and the fact that they operate at the mercy of the environmental conditions, makes each wetland unique on its kind, and so experimental studies are most of the time representative of only the studied system. Therefore it is extremely complicated to distinguish the most basic functioning patterns that apply to all horizontal subsurface flow CWs from experimental studies.
- Mathematical models can be of great help to improve the understanding of CWs internal processes since, with them, each individual factor affecting the functioning of this water treatment technology can be studied individually and at reasonable time and economic costs.
- Despite their great potential, before starting the current work, most available models for CWs had been used to match effluent pollutant concentrations measured in field experiments and, in general, less attention had been dedicated to understanding their internal functioning. Moreover the available results were presented for short simulation periods which masked the fact that the dynamics of bacteria were not properly described using the available biokinetic models. Finally, the impact of accumulated solids on the dynamics of bacterial communities was not studied in any of the cases.

- At the time of starting this research, there were virtually no models able to simulate clogging in CWs. Thus, the effects of this phenomenon on the hydraulics, hydrodynamics and on the dynamics of bacterial communities within CWs could not be numerically evaluated.

2.1 Objectives

Following these main issues of the state of the art of Constructed Wetlands science, the main objectives of the current PhD work were:

1. To develop a mathematical model able to describe the main processes taking place within horizontal subsurface flow CWs and in the long-term.
2. To improve the understanding of the dynamics of bacterial communities within CWs from simulating results.
3. To build a theory, based on modelling results, to describe the most basic functioning patterns of horizontal subsurface flow CWs, paying special attention to bacterial communities and their interaction with accumulated solids.
4. To present a mathematical formulation to simulate bioclogging in CWs. This formulation should also be able to describe the effect of bioclogging in the hydraulics and hydrodynamics of these systems.

2.2 Outline of the thesis

This document is structured in 10 chapters, each focusing on a specific topic. Note that the order of the chapters does not correspond to the chronological order of the works performed but to a more logical and easy to follow structure. Moreover, the following chapters do not cover a separate objective each, since the objectives of this work are very wide, and thus they are covered through several chapters.

In Chapter 3, the pilot system from where all the experimental data used in this work was gathered is described, and the available data is also detailed.

The equations of the proposed model and the required changes to the original formulation of the biokinetic model CWM1 are detailed in Chapter 4. As outlined in all chapters of this thesis, the most significant change applied to CWM1 is the inclusion of two logistic functions to the growth rate expressions of all bacteria groups which include two empirical parameters (M_{bio_max} and M_{cap}). Finally, Chapter 4 also includes the calibration of the model using experimental data from the pilot system, both in terms of the hydrodynamics and effluent pollutant concentrations.

Parameters M_{bio_max} and M_{cap}, which are introduced to the original formulation of CWM1 in Chapter 4, come with an underlying degree of uncertainty. For this reason, in Chapter 5 a local sensitivity analysis of these two parameters is carried out. Moreover, in this chapter a mesh optimization procedure is also carried out to reduce computational cost of further simulations.

Chapters 6 and 7 are dedicated to the second objective of the current work, which is to improve the understanding of the internal functioning of CWs based on the results obtained with the model. Chapter 6 is a case study, in which we focus our attention on evaluating the distribution of each bacterial group within the wetland individually and determine the time it takes for bacterial communities to get a stable population. This is done using 3 indicators: effluent pollutant concentrations, total bacterial biomass and Shannon's diversity index. On the other hand, Chapter 7 aims at developing a high-end theory, that we call *The Cartridge Theory*. This theory aims at explaining the internal functioning of horizontal flow Constructed Wetlands based on the interaction between accumulated solids and bacterial communities.

In chapter 8, a mathematical formulation is presented to simulate bioclogging in horizontal subsurface flow CWs. Equations are also presented to describe variably saturated subsurface flow and overland flow of wastewater resulting from severe bioclogging of the granular media. Moreover, results of a numerical experiment, in which several model outputs are compared for the same model running with and without considering bioclogging, are presented.

Chapter 9 consists of a general discussion that summarizes and extends all the knowledge generated over the whole study. Finally, in Chapter 10 the main conclusions that can be extracted from this work are presented.

CHAPTER 3

Pilot plant and experimental data

3.1 The pilot plant

The experimental data used in this work comes from previous studies in a CW pilot plant located in Les Franqueses del Vallès (Catalonia), that was set up in March 2001 and consisted on 8 horizontal SSF CWs planted with common reed (*Phragmites australis*) (Figure 3.1).

Figure 3.1: Image of the pilot plant at the Can Suquet housing scheme, Les Franqueses del Vallès, Barcelona, Catalonia.

Each bed was designed with different features in order to evaluate the effects of the aspect ratio, depth, type of granular media and HLR on the efficiency of CWs. All 8 beds were fed with urban wastewater previously treated in an Imhoff tank (Figure 3.2).

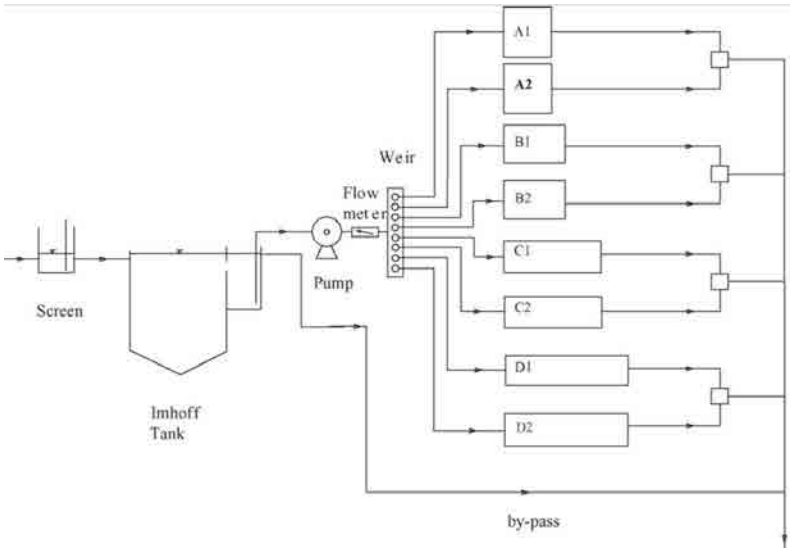

Figure 3.2: Schematic diagram of the pilot plant at the Can Suquet housing scheme, Les Franqueses del Vallès, Barcelona, Catalonia (García et al., 2004b).

The experimental data used in this work comes only from bed *C2* in Figure 3.2. This particular bed was designed with an aspect ratio of 2 : 1 (with a length and width of approximately 10.3 m and 5.3 m, respectively) and fine granitic gravel as a granular medium (D_{60} = 3.5 mm, C_u = 1.7, initial porosity = 40%). The first 0.3 m of the bed were composed of coarser gravel, the properties of which were not specified. During the experiments carried out in this bed, the water level was adjusted at 0.05 m below the surface, giving as a result an average water depth of approximately 0.5 m (García et al., 2004b).

3.2 Experimental data used in this work

Although the construction of the pilot plant ended in March 2001, it was not until May of the same year that it started operating normally. Monitoring was carried out until December 2003.

In this work, only data of the first year of operation of the pilot CW is used. During that period, the system was operated with HLR of approximately 20, 27, 36 and 45 $mm \cdot d^{-1}$ (Llorens et al., 2011b; García et al., 2004a,b).

Available experimental data come from grab samples of the influent and effluent, taken two to four times per month. These samples were analysed for COD and $NH_4{}^+$. The flow rate at the inlet and the water temperature were also measured. This way, the available experimental data during the first year of operation consists of: 39 values of flow rate, 32 values of water temperature, 31 values of inflow COD and 33 values of inflow $NH_4 - N$. Influent concentrations of other components which were measured much less frequently were obtained from García et al. (2005).

Moreover, a tracer test experiment was carried out in the experimental treatment plant by García et al. (2004a) between June and July 2001. Tracer tests are usually employed to determine the hydraulic and hydrodynamic properties of CWs, such as the hydraulic retention time and the dispersion coefficients. In this experiment, the flow was set to 2 $m^3 \cdot d^{-1}$ and a single-shot injection of 1.5 L of a dissolution of 200 $gKBr \cdot L^{-1}$ was made into the inlet tubes. Tracer solution was added in 10 minutes mixed with wastewater in order to reduce sinking effects related to density differences. Effluent grab samples of the bed were taken every 12 hours during the first 10 days and every 24 hours from that point and until a total sampling period of approximately 330 hours, and analysed for bromide. The mass tracer recovery was of 105% (García et al., 2004a).

The resulting tracer curves for all beds are shown in Figure 3.3:

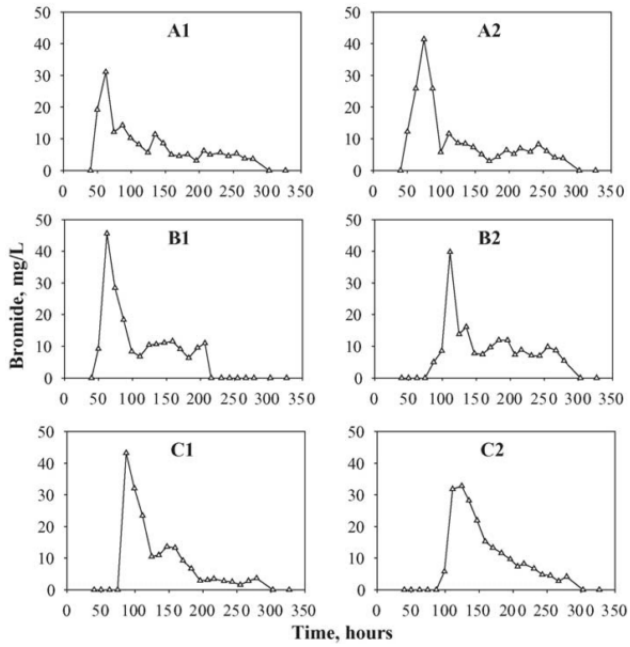

Figure 3.3: Tracer test curves obtained by García et al. (2004a).

The treatment plant in Les Franqueses del Vallès was dismantled in 2007. For a

more detailed description of the pilot, the reader is referred to Aguirre et al. (2005), García et al. (2007, 2004a,b) and Huang et al. (2005).

CHAPTER 4

Formulation and calibration of the BIO_PORE model

This chapter is based on the article:

- Samsó, R., García, J., 2013a. BIO_PORE, a mathematical model to simulate biofilm growth and water quality improvement in porous media: application and calibration for constructed wetlands. Ecological Engineering 54, 116127. doi:10.1016/j.ecoleng.2013. 01.021

4.1 Introduction

The potential of microbial biofilms growing in subsurface environments to remove pollutants from water has long been exploited in many forms. Horizontal subsurface-flow (HSSF) constructed wetlands (CWs) are one of such type of engineered bioremediation techniques aimed at treating wastewater.

Despite CWs are now ubiquitous in practice, their performance is still difficult to predict due to the diversity and simultaneousness of the physical, chemical, and biological processes involved, of which some are yet to be understood. Provided that good engineering design and operation of CWs demands a detailed insight of the processes taking place (Fan et al., 2008), fundamental and applied research must be encouraged so as to improve the comprehension of their functioning. It is only this way that CWs shall become more efficient, reliable, and easier to control and operate in the long-term. This in turn will increase their acceptance as an alternative to conventional wastewater treatment techniques.

During the last decade several mathematical models aiming at describing the functioning of CWs have proliferated (Llorens et al., 2011a). Nowadays, most efforts in this specific field are being put on the development of mechanistic or process-based models, which not only predict effluent pollutant concentrations but can also shed light on the treatment processes involved. For this reason, mechanistic models are gaining relevance over simple black box or first-order decay models (Kadlec and Wallace, 2008; Rousseau et al., 2004).

One notable limitation of the mechanistic models developed so far resides in their static or quasi-static nature. Hence, these models are only able to provide pictures of the state of a wetland at specific points in time or during very short time-scales. However, CWs are known to be complex systems, the behaviour of which depends on both external (e.g. flow-rate, wastewater composition and temperature) and internal (e.g. bacteria growth and development) factors (García et al., 2010). To understand the effect of all these factors on the functioning of CWs and to capture their evolution through time, long-term simulations are required.

The aim of the present work is to present and calibrate a new 2D mechanistic model that includes a wide range of physical and biological processes to reproduce the general functioning of CWs during long-term scenarios. This model implements fluid flow and transport equations together with the biokinetic model Constructed Wetland Model number 1 (CWM1) (Langergraber et al., 2009a; Llorens et al., 2011a,b) into COMSOL Multiphysics™, which solves the problem equations using the finite elements method (FEM). CWM1 is mostly based on ASM and ADM formulations (Batstone et al., 2002; Henze et al., 2000), and is seen as the most advanced biokinetic model developed for CWs. As such, it has been implemented by several authors in similar modelling attempts (Langergraber and Simunek, 2012; Llorens et al., 2011a,b; Mburu et al., 2012). In the present work, modifications have been made to its original formulation to include attachment and detachment of influent particulate components.

The most relevant innovation of the presented model, from which the name BIO_PORE was inspired, is the biofilm sub-model. This sub-model prevents unlimited and unrealistic growth of BIOmass in areas with high substrate concentrations and also accounts for the effects of PORE volume reduction resulting from inert solids accumulation. In this chapter we show and discuss why the inclusion of these functions represent a very significant advance with respect to previous implementations of CWM1. Finally, the complete model is calibrated using experimental data of a period of 1 year obtained from the pilot SSF CW (Chapter 3). The most relevant outputs of the model, which provide some clues on the general functioning of CWs, are also discussed.

4.2 Methods

4.2.1 Model domain

The model domain represents the wetted depth of a 2D longitudinal section of the pilot CW (Figure 4.1).

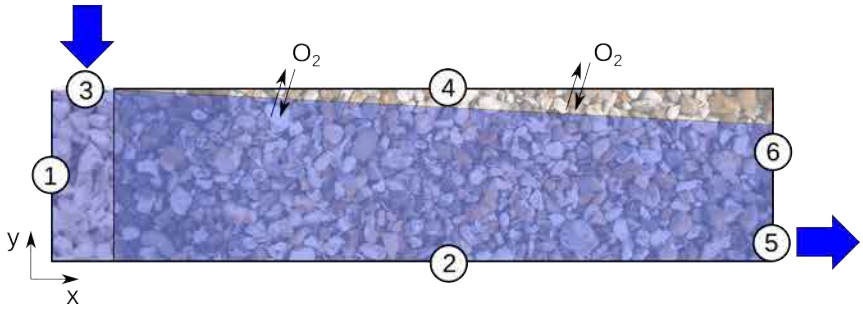

Figure 4.1: Schematic representation of the model domain. Numbers 1 to 6 identify the domain boundaries which are described in text.

Wastewater enters the domain through boundary 3 (a length of 0.3 m in the x^{th} direction representing the mixing zone) and the effluent leaves through boundary 5 (a length of 0.1 m in the y^{th} direction), where a constant hydraulic head of 0.45 m is defined. Boundary 4 represents the water table level within the bed, through which oxygen is transported from the atmosphere to the water body. Boundaries 1, 2 and 6 correspond to impervious walls.

4.2.2 Model equations

Hydraulic, reactive-transport, biofilm and plants sub-models compose the basic structure of the BIO_PORE model (Figure 4.2).

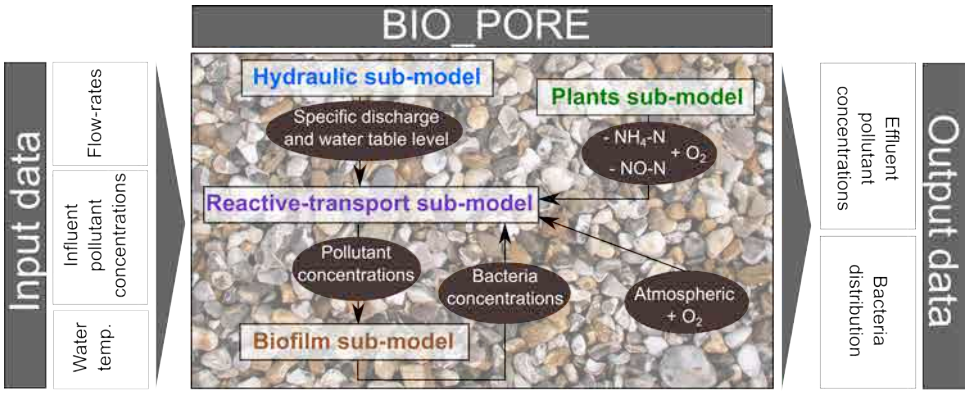

Figure 4.2: Schematic representation of the data flux (in the arrows) between the 4 sub-models (represented in boxes). Input and output data are also shown.

Hydraulic sub-model

The saturated flow through a multidimensional heterogeneous and anisotropic porous media is described using Darcy's equation as follows:

$$q_i = -K_{ij}\frac{\partial h}{\partial x_j} \tag{4.1}$$

Where, q_i is the specific discharge $[LT^{-1}]$, K_{ij} is the saturated hydraulic conductivity tensor $[LT^{-1}]$, and $\frac{\partial h}{\partial x_j}$ the hydraulic gradient vector (unitless).

In this model, using the *Deformed Geometry* node found in COMSOL Multiphysics™, the domain deforms dynamically to adjust boundary 4 to the calculated water table level at every time step. Changes in the water table level within the system obey exclusively to variations of the inflow-rate, as neither evapotranspiration nor precipitation is considered in the current version of the model and the hydraulic conductivity remains constant through time.

Reactive-transport sub-model

This sub-model describes the fate and transport of the components of CWM1 listed in Table 4.1. Dissolved species are only present in the aqueous phase. On the other hand, particulate species (X_S and X_I in CWM1) are defined both in the aqueous and solid phases. This strategy was adopted to be able to simulate attachment and detachment processes of particulate components, and required an important modification of CWM1's formulation (which considers X_S and X_I as single-phase components).

Table 4.1: Components adapted from CWM1 (Langergraber et al., 2009a). S_i are dissolved components (all in the aqueous phase) and X_i are particulate components (either in aqueous or solid phase).

Componenet	**Description**	**Unit**	**Phase**
S_O	Dissolved oxygen	$mgCOD \cdot L^{-1}$	Aqueous
S_F	Soluble fermentable COD	$mgCOD \cdot L^{-1}$	Aqueous
S_A	Fermentation products as acetate as COD	$mgCOD \cdot L^{-1}$	Aqueous
S_I	Inert soluble COD	$mgCOD \cdot L^{-1}$	Aqueous
X_{Sm}	Aqueous slowly biodegradable particulate COD	$mgCOD \cdot L^{-1}$	Aqueous
X_{Sf}	Solid slowly biodegradable particulate COD	$mgCOD \cdot L^{-1}$	Solid
X_{Im}	Aqueous inert particulate COD	$mgCOD \cdot L^{-1}$	Aqueous
X_{If}	Solid inert particulate COD	$mgCOD \cdot L^{-1}$	Solid
S_{NO}	Nitrite and nitrate nitrogen	$mgN \cdot L^{-1}$	Aqueous
S_{NH}	Anmonium and ammonia nitrogen	$mgN \cdot L^{-1}$	Aqueous
S_{SO4}	Sulphate sulphur	$mgS \cdot L^{-1}$	Aqueous
S_{H2S}	Dihydrogensulphide sulphur	$mgS \cdot L^{-1}$	Aqueous

The fate and transport of the aqueous (mobile) phase components in a multidimensional saturated porous media is described with Eq. 4.2 (Clement et al., 1998):

$$\frac{\partial C_k}{\partial t} = \frac{\partial}{\partial x_i}\left(D_{ij}\frac{\partial C_k}{\partial x_j}\right) - \frac{\partial}{\partial x_i}(q_i C_k) + r_{C_k} - r_{att} + r_{det} + s_{C_k} \tag{4.2}$$

Where $k = 1, 2 \ldots m$

Where, m is the total number of aqueous phase components (dissolved and particulate, see Table 4.1), C_k $[ML^{-3}]$ is the aqueous phase concentration of the k^{th} component, D_{ij} $[L^2T^{-1}]$ is the hydrodynamic dispersion tensor and q_i $[LT^{-1}]$ is the specific discharge. q_i acts as the coupling variable between the hydraulic and reactive-transport sub-models. r_{C_k} $[ML^{-3}T^{-1}]$ is the reaction rate of the k^{th} species on the aqueous phase. r_{att} $[ML^{-3}T^{-1}]$ and r_{det} $[ML^{-3}T^{-1}]$ are attachment and detachment rates, respectively; the former describes the rate of exchange from the aqueous to the solid phase and the latter accounts for the opposite process. s_{C_k} $[ML^{-3}T^{-1}]$ is the source/sink term, which represents external sources or sinks of component C_k. This last term is only used to simulate oxygen release through plant roots (see Section 4.2.2).

On the other hand, Eq. 4.3 (Clement et al., 1998) describes the fate of the solid phase (immobile) components (Table 4.1):

$$\frac{d\check{C}_l}{dt} = r_{\check{C}_l} + r_{att} - r_{det} \tag{4.3}$$

Where $l = 1, 2, ..n$

Where, n is the total number of solid phase components (particulate only), $\check{C}_l[ML^{-3}]$ is the concentration of the l^{th} component and $r_{\check{C}_l}[ML^{-3}T^{-1}]$ is the reaction rate of the l^{th} component on the solid phase.

Attachment rates of X_{Sm} and X_{Im} are described using Eq. 4.4, while detachment rates of X_{Sf} and X_{If} are defined using Eq. 4.6 (adapted from Bradford et al. (2004)):

$$r_{att} = \begin{cases} \lambda_{att} C_k & \text{for } (M_T < M_{cap}) \\ 0 & \text{for } (M_T = M_{cap}) \end{cases} \tag{4.4}$$

$$r_{det} = \lambda_{det} \check{C}_l \tag{4.5}$$

Where λ_{att} $[T^{-1}]$ and λ_{det} $[T^{-1}]$ are first-order attachment and detachment coefficients, respectively, obtained during the calibration step. The new reaction rates of particulate components resulting from their division into aqueous and solid phases and the inclusion of attachment and detachment processes, represent a significant modification from CWM1, and are shown in Table 4.2.

Table 4.2: Reaction rates of the components present both in the aqueous and solid phases (X_{Sm}, X_{Sf}, X_{Im} and X_{If}).

[a]	X_{Sm}	$-k_h \frac{\frac{X_{Sm}}{X_H+X_{FB}}}{K_x+\frac{X_{Sm}}{X_H+X_{FB}}}(X_H+\eta_h X_{FB}) - \lambda_{att} X_{Sm} + \lambda_{det} X_{Sf}$
	X_{Sf}	$-k_h \frac{\frac{X_{Sf}}{X_H+X_{FB}}}{K_x+\frac{X_{Sf}}{X_H+X_{FB}}}(X_H+\eta_h X_{FB}) + v_{9,Lysis}(b_H X_H + b_A X_A + b_{FB} X_{FB} + b_{AMB} X_{AMB} + b_{ASRB} X_{ASRB} + b_{SOB} X_{SOB}) + \lambda_{att} X_{Sm} - \lambda_{det} X_{Sf}$
	X_{Im}	$-\lambda_{att} X_{Im} + \lambda_{det} X_{If}$
	X_{If}	$f_{BM,X_I}(b_H X_H + b_A X_A + b_{FB} X_{FB} + b_{AMB} X_{AMB} + b_{ASRB} X_{ASRB} + b_{SOB} X_{SOB}) + \lambda_{att} X_{Im} - \lambda_{det} X_{If}$

[a] K_h is the hydrolysis rate constant $[d^{-1}]$, K_X is the saturation/inhibition coefficient for hydrolysis $\frac{gCOD_{S_F}}{gCOD_{BM}}$, η_h is the correction factor for hydrolysis by fermenting bacteria [-]. $v_{9,Lysis}$ $\frac{gCOD_{X_S}}{gCOD_{BM}}$ and f_{BM,X_I} $\frac{gCOD_{X_I}}{gCOD_{BM}}$ are respectively the fractions of X_{Sf} and X_{If} generated in biomass lysis. b_H, b_A, b_{FB}, b_{AMB}, b_{ASRB}, b_{SOB} are rate constants for lysis of X_H, X_A, X_{FB}, X_{AMB}, X_{ASRB} and X_{SOB} $[d^{-1}]$. See Chapter 1 for details on the formulation of CWM1.

In Eq. 4.4, the rate of attachment becomes zero when the mass of accumulated solids (M_T) equals the maximum capacity of the representative volume (M_{cap}). The value of M_{cap} is obtained by multiplying the pore volume by the density of accumulated solids (ρ_{biomat}). Accumulated solids are a mixture of biomass (mostly in the form of biofilms) and inert particulate solids. Therefore its average density is

difficult to predict, as it depends on the proportion of each fraction. In the current model, ρ_{biomat} was found to be 15 $kgVS \cdot m^{-3}$ during the calibration step (see Section 4.4.1). This value is an average value between biofilm density and accumulated solids densities, and thus it is lower than the reported values for biofilm denisities.

The description of the fate and transport of dissolved oxygen (S_O in Table 4.1) differs from that of the other aqueous components in the fact that external sources of oxygen (transfer from the atmosphere and release from plant roots) had to be considered as well. Oxygen transfer from the atmosphere to the water body is simulated as a flux condition through boundary 4 of the domain (Figure 4.1) as proposed by Tyroller et al. (2010):

$$OTR = K_{La,S_O}(S_{O_{sat}} - S_O)\frac{V}{A} \tag{4.6}$$

Where, OTR $[ML^{-2}T^{-1}]$ is the oxygen transfer rate and K_{La,S_O} $[T^{-1}]$ is the oxygen mass transfer coefficient. The latter was set to 0.132 h^{-1}, which corresponds to the maximum value of those measured by Tyroller et al. (2010) in experimental HSSF CWs. $S_{O_{sat}}$ $[ML^{-3}]$ is the dissolved oxygen concentration at saturation (which is temperature dependent), S_O $[ML^{-3}]$ is the dissolved oxygen concentration at time t, V is the volume of pore water in the wetland $[L^3]$ and A is the surface area of the wetland $[L^2]$.

Biofilm sub-model

The macroscopic biofilm sub-model uses the expressions defined in CWM1 to simulate the growth and development of the bacteria groups presented in Table 4.3.

Table 4.3: Bacterial groups considered in CWM1 (Langergraber et al., 2009a).

Componenet	Description	Unit	Phase
X_H	Heterotrophic bacteria	$mgCOD \cdot L^{-1}$	Solid
X_A	Autotrophic nitrifying bacteria	$mgCOD \cdot L^{-1}$	Solid
X_{FB}	Fermenting bacteria	$mgCOD \cdot L^{-1}$	Solid
X_{AMB}	Acetotrophic methanogenic bacteria	$mgCOD \cdot L^{-1}$	Solid
X_{ASRB}	Acetotrophic sulphate reducing bacteria	$mgCOD \cdot L^{-1}$	Solid
X_{SOB}	Sulphide oxidising bacteria	$mgCOD \cdot L^{-1}$	Solid

Functions 4.7 and 4.8 were added to the original formulation of CWM1 to prevent unlimited and unrealistic growth of bacteria groups as well as to avoid the complexity of a dedicated micro-scale biofilm model. Function 4.7 takes into account biofilms self-exerted growth limitation due to diffusion-controlled transport of substrates through its exterior boundary (Wanner et al., 2006).

$$\left(1 - \frac{M_{bio}}{M_{bio\_max}}\right) \tag{4.7}$$

Where, $M_{bio}(= M_{X_H} + M_{X_A} + M_{X_{FB}} + M_{X_{AMB}} + M_{X_{ASRB}} + M_{X_{SOB}})$ $[M]$ is the sum of the total microbial biomass present in a representative volume of granular material and M_{bio_max} $[M]$ is an empirical parameter representing the maximum mass of microbial active biomass that can be maintained in the same volume. Function 4.8 represents the growth limitation exerted by the reduction of porosity as a consequence of inert solids (X_{If}) accumulation through time.

$$\left(1 - \frac{M_{X_{If}}}{M_{cap}}\right) \tag{4.8}$$

Where, $M_{X_{If}}$ $[M]$ is the actual mass of immobile X_I. Biodegradable particulated organic matter (X_S) is considered not to hinder the growth of microorganisms, as bacteria can feed on it and replace the occupied volume with new cells. Despite the accumulation of inert solids hinders the growth of new bacterial cells, their effect on the hydraulic and hydrodynamic parameters of the granular media is not currently considered.

The values of kinetic parameters of CWM1 are interpolated to account for water temperature variations with the expression recommended by Henze et al. (2000):

$$k_{(T)} = k_{(20°C)} e^{\theta_T (T - 20°C)} \tag{4.9}$$

$$\theta_T = \frac{\ln\left(\frac{k(T_1)}{k(T_2)}\right)}{T_1 - T_2} \tag{4.10}$$

Where $k(T)$ is the value of the kinetic parameter at a certain temperature T, $k_{(20°C)}$ is the value of the kinetic parameter at 20 °C and T_1 and T_2 are the two temperatures (in °C) at which $k_{(T)}$ is known.

Plants sub-model

Provided the knowledge gap still present in CWs plant science, this sub-model is purposely the simplest of all of them. In the current model, plants roots are defined to be homogeneously distributed only in the 30 cm top layer of the granular media (Parr, 1990; Reed et al., 1995; Rousseau et al., 2005), and after the mixing zone. Two different values (one for the cold season and one for the warm season) for oxygen release and nutrients uptake rates by plant roots are included in the source/sink

term (s_{C_k}) of Eq. 4.2 for S_O (dissolved Oxygen), S_{NH} (ammonium and ammonia nitrogen) and S_{NO} (nitrite and nitrate nitrogen). The exact values of these rates are detailed in Section 4.3.2. It is assumed that S_{NH} and S_{NO} are taken up by plants with the same preference. Note that the model does not explicitly consider the growth of plants.

4.2.3 Calibration procedure

The hydraulic and hydrodynamic properties of CWs remain only constant for relatively short periods of time (due to progressive pore volume reduction), and hence the model was calibrated using only data of the first year of operation (May 2001 to May 2002). Note that at the present stage of model development, the hydraulic and hydrodynamic properties of the domain are kept constant through time. In the considered period 39 values for flow-rate, 32 values for water temperature, 31 values for influent COD (28 for effluent COD) and 33 values for influent $NH_4 - N$ (34 for effluent $NH_4 - N$) were available, and were used as input data for the model.

The fractioning of the influent COD was made using recommended values for primary effluents in ASMs (Henze et al., 2000). Accordingly, the proportion of each fraction was defined to be: 15% S_F, 50% X_{Sm} (0% X_{Sf}), 20% S_A, 5% S_I and 10% X_{Im} (0% X_{If}). In order to reduce the impact of imposed initial conditions on bacteria distribution and to recreate the startup situation, initial concentrations of all bacterial groups and substrates were set to values very close to zero (0.001 $mgCOD \cdot L^{-1}$).

Influent concentrations of the rest of components considered in CWM1 (except for S_O) (Table 4.1), which were measured much less frequently in the field, were extracted from an experimental study carried out in the same pilot wetland by García et al. (2005). These concentrations correspond to mean values measured in all samples and are 0 $mg \cdot L^{-1}$ for S_{NO} and S_{H2S}, and 72 $mg \cdot L^{-1}$ for S_{SO4}. Influent oxygen concentration was set to zero, provided that DO concentration in primary treated wastewater is usually very small (Tyroller et al., 2010). Influent concentrations of bacteria groups are generally very small in comparison to the amount present within the granular media and were consequently neglected.

The hydraulic and hydrodynamic parameters included in the hydraulic and reactive-transport sub-models were calibrated by comparing simulated and experimental tracer curves. These parameters are the hydraulic conductivity (K) ($m \cdot d^{-1}$) and the longitudinal and transverse dispersivity coefficients (α_L and α_T respectively) (m) of the media. To reasonably match the tracer test response curve, the domain was divided at a depth of 0.3 m in two areas with different hydraulic conductivities and dispersivity values. The top layer of the domain was assumed to have lower hydraulic conductivity and higher dispersivity than the bottom layer. This approach is in agreement with studies that have observed preferential flow along the bottom

of wetlands, which are essentially a result of the higher density of belo-wground plant biomass on the top layer of the granular media (Parr, 1990; Reed et al., 1995; Rousseau et al., 2005; Knowles et al., 2011). Note that this approach was necessary because by considering homogeneous domain properties, dispersion parameters would have been overestimated (Mena et al., 2011). In fact, the trials performed considering homogeneous domain properties did not render acceptable results.

The reactive-transport, biofilm and plants sub-models were calibrated together, by comparing experimental and simulated effluent COD and $NH_4{}^+$ concentrations and using the hydraulic and hydrodynamic parameters obtained in the previous step. As the premise of calibration was to simulate the behaviour of the pilot wetland since the beginning of operation, the values of α_L, α_T and K of the deeper gravel layer, which may resemble those of the clean gravel, were applied for the entire bed.

The empirical parameter of the reactive-transport sub-model targeted during calibration was λ_{att}. λ_{det} was set to zero, as for shear detachment to occur, flow-rates must be high (Rittmann, 1982) and the pilot wetland was operated with hydraulic loadings resulting in relatively low flow velocities.

Given that only a few studies on microbial distribution in CWs exist, microbial activity in these systems is still largely based on assumption and circumstantial evidence (Krasnits et al., 2009; Mburu et al., 2012; Ojeda et al., 2008). Therefore the distribution of microbial biomass obtained with the model cannot be directly calibrated and must be considered as an output of the model. Despite that, the empirical parameters used by this sub-model (ρ_{biomat}, M_{bio_max} and the biokinetic parameters affecting the growth rates of different bacteria) directly affect its output concentrations, and therefore their values were also targeted during calibration.

Similarly, in the case of the plants sub-model, homogeneous below-ground plant roots distribution was imposed, as experimental data on this aspect was not available; hence calibration for this sub-model focused only on matching effluent concentrations of COD and $NH_4 - N$ by fine tuning nutrients uptake and oxygen leaching rates.

4.3 Results

4.3.1 Hydraulic and hydrodynamic calibration

Figure 4.3 shows how the model was able to match the experimental tracer curve with an acceptable degree of accuracy. Note that so as to reproduce the dual-shape of the experimental curve it was absolutely necessary to divide the domain in the two layers with different hydraulic properties. Calibrated values of the hydraulic and hydrodynamic parameters of the two layers are shown in Table 4.4.

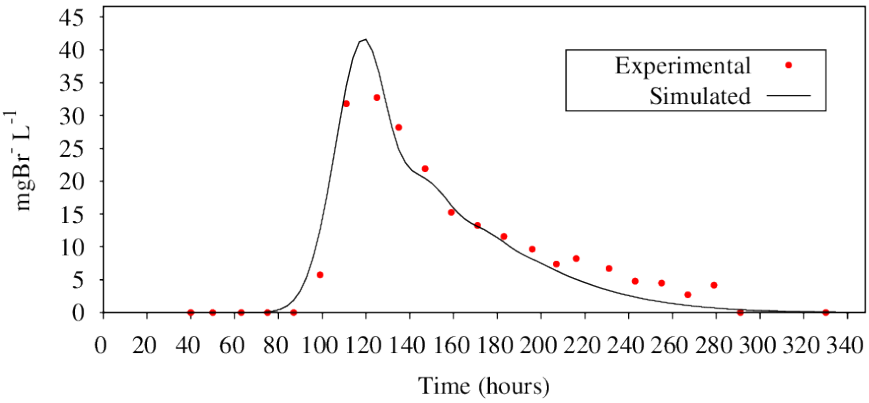

Figure 4.3: Experimental (dots) and simulated (continuous line) tracer curves.

Table 4.4: Values of the hydraulic and hydrodynamic parameters of the upper and bottom material layers after calibration.

Parameter	**Description**	**Unit**	**Upper layer**	**Bottom layer**
α_L	Longitudinal dispersivity	m	0.25	0.05
α_T	Transverse dispersivity	m	0.022	0.005
K	Hydraulic conductivity	$m \cdot d^{-1}$	22	50

4.3.2 Reactive-transport, biofilm and plants sub-models calibration

In order to fit the experimental effluent COD and $NH_4 - N$ concentrations, some biokinetic parameters at different temperatures missing in CWM1 (Langergraber et al., 2009a) had to be included, and some of the available parameters had to be adjusted (see Table 4.5).

Table 4.5: List of modified parameters from those given in original CWM1 (Langergraber et al., 2009a).

Parameter	Description	Value in CWM1	Current value	Source
b_{FB} $(10°C)$	Rate constant for lysis of X_{FB} at $10°C$ $[d^{-1}]$	-	0.07	Calibration
μ_{AMB} $(10°C)$	Maximum growth rate for X_{AMB} at $10°C$ $[d^{-1}]$	-	0.04	Batstone et al. (2002) and Langergraber et al. (2009a)
b_{AMB} $(10°C)$	Rate constant for lysis of X_{AMB} at $10°C$ $[d^{-1}]$	-	0.004	Batstone et al. (2002) and Langergraber et al. (2009a)
μ_{ASRB} $(10°C)$	Maximum growth rate for X_{ASRB} at $10°C$ $[d^{-1}]$	-	0.009	Calibration
b_{ASRB} $(10°C)$	Rate constant for lysis of X_{ASRB} at $10°C$ $[d^{-1}]$	-	0.006	Calibration
μ_{SOB} $(10°C)$	Maximum growth rate for X_{SOB} at $10°C$ $[d^{-1}]$	-	2.64	Calibration
b_{SOB} $(10°C)$	Rate constant for lysis of X_{SOB} at $10°C$ $[d^{-1}]$	-	0.075	Calibration
K_{SOASRB}	Saturation/inhibition coefficient of X_{ASRB} for S_O at $20°C$ $[mgCOD \cdot L^{-1}]$	0.0002	0.002	Calibration
K_{SOAMB}	Saturation/inhibition coefficient of X_{AMB} for S_O at $20°C$ $[mgCOD \cdot L^{-1}]$	0.0002	0.002	Calibration
K_{SOFB}	Saturation/inhibition coefficient of X_{FB} for S_O at $20°C$ $[mgCOD \cdot L^{-1}]$	0.2	0.002	Calibration
K_{SOA}	Saturation/inhibition coefficient of X_A for S_O at $20/10°C$ $[mgCOD \cdot L^{-1}]$	1/-	0.4/0.4	Henze et al. (2000)
K_{SNHA}	Saturation/inhibition coefficient of X_A for S_{NH} at $20/10°C$ $[mgN \cdot L^{-1}]$	0.5/5	1/1	Henze et al. (2000)

The values of the maximum growth and lysis rates of methanogenic bacteria (μ_{AMB} and b_{AMB}) at $10°C$ were calculated by introducing the values of these parameters at $55°C$ and $35°C$ given by Batstone et al. (2002) in Eq. 4.10 and later interpolating from the value given in CWM1 at $20°C$ using Eq. 4.9. The other missing values at $10°C$ were b_{FB}, μ_{ASRB}, b_{ASRB}, μ_{SOB} and b_{SOB} and were obtained during calibration.

Saturation/inhibition coefficients of X_{ASRB}, X_{AMB} and X_{FB} for S_O (K_{SOASRB}, K_{SOAMB}, K_{SOFB}) at $20°C$ were modified from CWM1. K_{SOASRB} and K_{SOAMB} were increased from 0.0002 $mgCOD \cdot L^{-1}$ to 0.002 $mgCOD \cdot L^{-1}$, as simulations showed that almost negligible concentrations of dissolved oxygen (in the order of 10^{-4} $mgCOD \cdot L^{-1}$) were hindering the growth of X_{ASRB} and X_{AMB}. On the other hand, K_{OFB} was decreased from 0.2 $mgCOD \cdot L^{-1}$ to 0.002 $mgCOD \cdot L^{-1}$, as by using the original value, fermenting bacteria (X_{FB}) grew even in the presence of high oxygen concentrations. The values of the saturation/inhibition coefficients of X_A for S_O and S_{NH} (K_{SOA} and K_{SNHA}) at 10 and $20°C$ were adjusted to the values

given by Henze et al. (2000), which allowed a better fitting of experimental effluent $NH_4 - N$ concentrations.

Figures 4.4 and 4.5 show that, despite the great variability of water temperatures, flow-rates and influent pollutant concentrations during the first year of operation of the pilot wetland, simulated effluent COD and $NH_4 - N$ concentrations reasonably match the general trends of field measurements. The values of the calibrated parameters that led to these results are shown in Table 4.6.

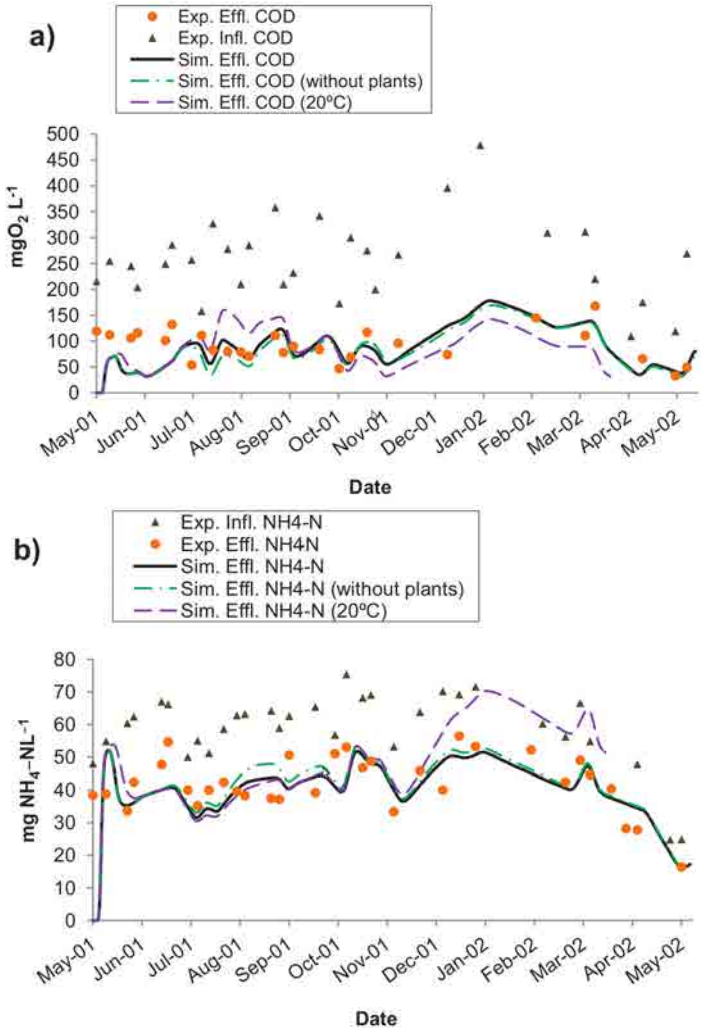

Figure 4.4: Experimental influent and effluent concentrations (triangles and dots) and simulated concentrations with plant effects and variable water temperatures (black line), without plant effects (green line) and at constant water temperature (20°C) (purple line) for a) COD ($mgCOD \cdot L^{-1}$) and b) $NH_4 - N$ ($mgNH_4 - N \cdot L^{-1}$). Note that the simulation at a constant temperature of 20°C did not reach the end of computation due to convergence issues.

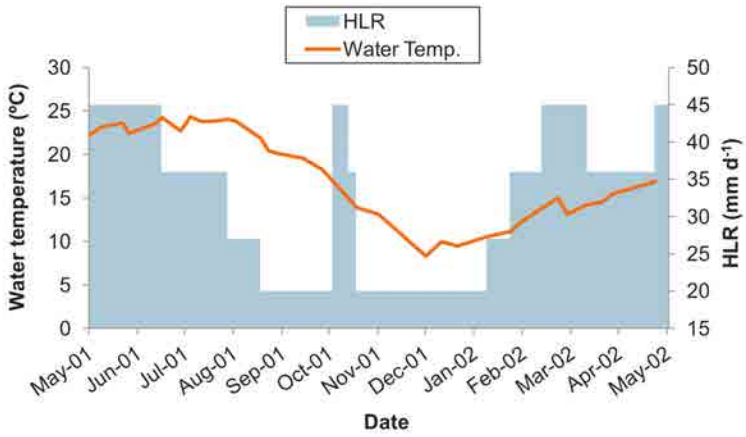

Figure 4.5: Water temperatures ($°C$) and hydraulic loading rates (HLR) ($mm \cdot d^{-1}$) during the first year of operation of the pilot wetland.

Table 4.6: Values of the parameters targeted during calibration.

Parameter	Value	Unit
M_{bio_max}	0.093	$KgVS \cdot m^{-3}$ of gravel
ρ_{biomat}	15	$KgVS \cdot m^{-3}$
λ_{att}	1.8	h^{-1}

The systematic differences observed between simulated and measured effluent COD and $NH_4 - N$ concentrations from May to July 2001 (Figure 4.4) are a consequence of the low initial concentrations of bacteria and accumulated solids (X_{Sf} and X_{If}) imposed (0.001 $mgCOD \cdot L^{-1}$, see Section 4.2.3) and also to the fact that influent bacteria concentrations were neglected. As a matter of fact, until July 2001 small amounts of slowly biodegradable solids (X_{Sf}, represented with a red line in Figure 4.6) had accumulated in the bed, and thus the internal production of COD from hydrolysis was proportionally small. With such small internal sources of COD during this period, existing bacteria communities were able to degrade most incoming COD (from wastewater) and the modelled wetland seemed to overperform the real system (Figure 4.4a). Similarly, simulated concentrations of $NH_4 - N$ fitted better the experimental data from July 2001 (Figure 4.4b). It has to be noted though, that if higher initial concentrations of bacteria and substrates had been given, the internal equilibrium of bacteria distribution (and effluent pollutant concentrations) would have taken shorter to reach.

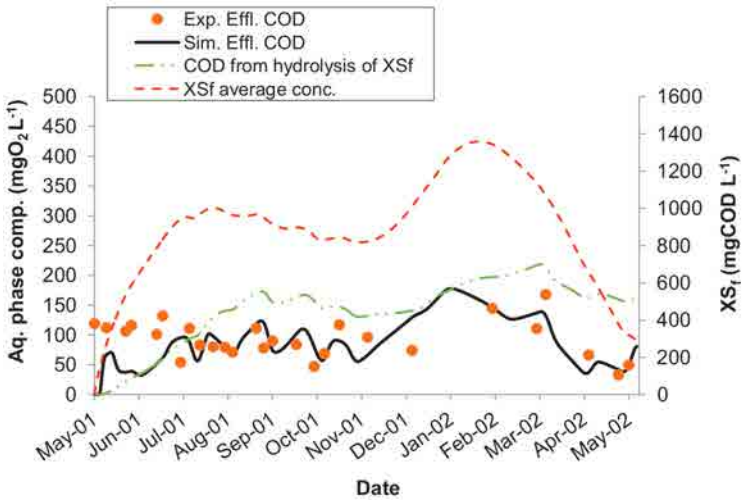

Figure 4.6: Simulated averaged concentration of accumulated X_{Sf} in the whole domain ($mgCOD \cdot L^{-1}$) (red line) and simulated concentration of the COD ($mgCOD \cdot L^{-1}$) produced strictly from hydrolysis and measured at the effluent (green line). Note that this is not the real effluent of the system, but the concentration of an intermediate product that would be present in the effluent if no further degradation occurred. Experimental (dots) and simulated total effluent COD concentrations (black line) ($mgCOD \cdot L^{-1}$) are also shown for comparison.

The model also indicates that the amount of particulate biodegradable COD accumulated within the wetland (X_{Sf}) clearly depends on water temperatures (see Figures 4.5 and 4.6), and increases during cold months, when hydrolysis rates are smaller than accumulation rates. This behaviour was already suggested by Huang et al. (2005) in the same pilot wetland, who related the decrease of the system efficiency during warm months to the internal production of acetic acid from the accumulated organic particulate matter during the cold season.

The effect of water temperature on biokinetic reactions was equally important to match effluent concentrations. When a constant water temperature of $20°C$ was considered (purple lines in Figure 4.4), simulated effluent concentrations deviated more from experimental data and especially when the difference with the real temperature was higher. When simulating at the real temperatures (black lines in Figsures 4.4a and 4.4b), a significant decrease of bacteria growth rates occurred following the water temperature drop from October 2001. Thus, from that month bacterial growth rates at $20°C$ were much higher than with the real temperatures. This fact explains why simulated effluent COD concentrations at $20°C$ were clearly lower (Figure 4.4a). The opposite occurs for effluent $NH_4 - N$ concentrations, in which case the removal efficiency of this component at 20 °C decreases, thus resulting in an increase of its effluent concentration from November 2001. This is a consequence of the competition of nitrifying and heterotrophic bacteria (X_A and X_H) for the available oxygen (S_O). At low temperatures the difference between the maximum growth rates of these two

bacteria groups is smaller than at higher temperatures. Therefore, when simulating at 20°C X_H grows much faster than X_A and consumes most of the available oxygen. This effect progressively reduces the concentration of X_A within the system, which causes the observable increase in the effluent $NH_4 - N$ concentration.

Several simulations with different rates of nitrogen uptake and oxygen release by plants roots were carried out until the best fitting between experimental and simulated effluent COD and $NH_4 - N$ concentrations was achieved. Figure 4.4 shows that only slight improvements on the fitting of the two curves were obtained when considering plant effects. The obtained oxygen release rate was 3 $gO_2 \cdot m^{-2}d^{-1}$, which falls between the values reported by Mburu et al. (2012) ($0.45-1.9$ $gO_2 \cdot m^{-2}d^{-1}$) and those of Langergraber and Simunek (2012) (5 $gO_2 \cdot m^{-2}d^{-1}$). Ammonium and nitrate nitrogen (S_{NH} and S_{NO} respectively) uptake rates were found to be 0.2 $gN_2 \cdot m^{-2}d^{-1}$ for each component. This value is again higher than that reported by Mcbride and Tanner (2000) ($0.005 gN_2 m^{-2}d^{-1}$) and in the range of those reported by Tanner (2001) (0.20.3 $gN_2 \cdot m^{-2}d^{-1}$). To better fit the experimental data, both the oxygen release and nitrogen uptake rates were intentionally decreased by 40% when water temperatures fell below 15°C (from October 2001 to March 2002). This way, during this period the oxygen release and nutrient uptake rates were 1.2 $gO_2 \cdot m^{-2}d^{-1}$ and 0.08 $gN_2 \cdot m^{-2}d^{-1}$, respectively, which still fall among the values reported in literature. This approach is in agreement with the common understanding that plant metabolism varies through the annual growth/senescence cycle (USEPA, 2000).

Figure 4.7 shows simulated effluent concentrations of the different fractions of COD. Neither X_{Im} nor X_{Sm} was seen in the effluent as they were filtered and retained within the system. It can be observed that most of the effluent COD (around 80%) were fermentation products as acetate (S_A), while soluble fermentable COD (S_F) was only detected during the maturation period of the system. The rest of the effluent COD was composed by S_I, which remained at the same concentration as in the inflow.

In an experimental study in the same wetland, Huang et al. (2005) measured effluent concentrations of volatile fatty acids (VFA) and concluded that acetic acid was the major effluent intermediate component making up a third of the total effluent BOD. Thus, despite in CWM1 S_A is not only acetate, but a sum of all fermentation products, our model overestimates the effluent concentrations of this component. This discrepancy may have its origin on the uncertainty on the fractioning of the influent COD. However, it was not possible to calibrate the effluent concentrations of the different fractions of COD, as only the organic matter degradation intermediates were measured in the field.

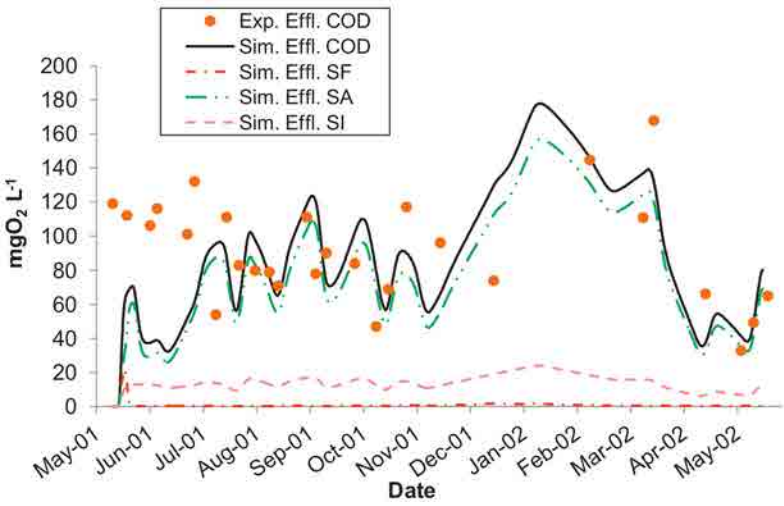

Figure 4.7: Simulated effluent concentrations of the different fractions of COD: soluble fermentable COD (SF), fermentation products as acetate (S_A) and inert soluble COD (S_I) (all expressed in $mgCOD \cdot L^{-1}$)

Figure 4.8 shows the distribution and concentrations (in $mgCOD \cdot L^{-1}$) of the different bacteria groups after 1 year of operation. The bacteria concentrations at this time are in the lower range of those reported by Llorens et al. (2011b), Mburu et al. (2012) and Langergraber and Simunek (2012) at different times. This Figure also shows that X_H, X_{FB} and X_{ASRB} were the dominant bacteria groups within the system, while X_A, X_{AMB} and X_{SOB} were found in lower concentrations.

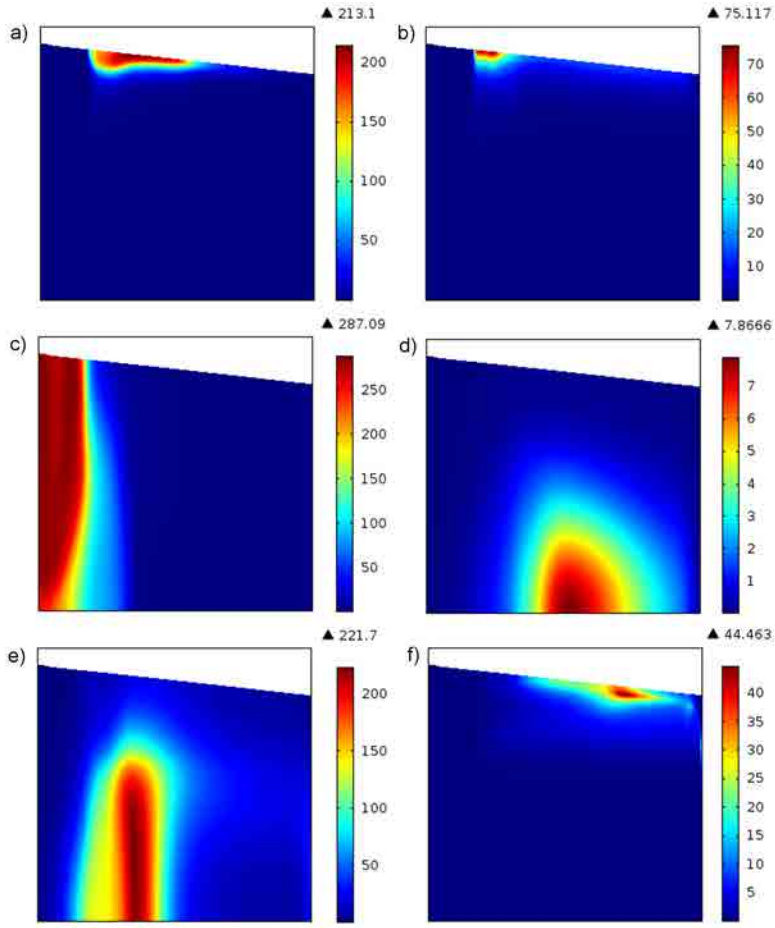

Figure 4.8: Longitudinal cross sections of the wetland (as in Figure 4.1) were the distribution of a) Heterotrophic (X_H), b) Autotrophic nitrifying (X_A), c) Fermenting (X_{FB}), d) Acetotrophic methanogenic (X_{AMB}), e) Acetotrophic sulphate reducing (X_{ASRB}), and f) Sulphide oxidising (X_{SOB}) bacteria are shown after 1 year of operation. The key at the right of each image indicate the concentration in $mgCOD \cdot L^{-1}$of each bacteria group, and the values besides the black triangles represent the maximum concentration shown in each image. Note that the images have been deformed to fit a reasonable size. The x-axis of each image represents the longitudinal direction of the bed (from 0 to 10.3 m) and the y-axis the depth of the bed (from 0 to 0.7 m). Also note that the coloured areas of each image correspond to wetted areas, while the white areas correspond to areas without water. Note that water level decreases from inlet to outlet.

4.4 Discussion

4.4.1 Innovative features of the model

In the following lines the main innovative features of the model and their contribution to modelling bacteria-induced water quality improvement in porous media, and more specifically in CWs, are outlined.

Growth-limiting functions for biofilm

Based on the accepted idea that the treatment efficiency of CWs (and other groundwater remediation techniques) is vastly dependant on bacterial communities (Krasnits et al., 2009), in the present model special attention was put into properly simulating reactive-transport and biofilm sub-models. Moreover, long-term simulations were pursued to be able to observe the effect of changes in bacteria concentrations within the wetland through time on the effluent pollutant concentrations.

During the initial implementations of CWM1 into COMSOL Multiphysics™, at the beginning of this research, we observed that unrealistically high bacteria concentrations were reached near the inlet section for very short simulation times. This behaviour resulted from the fact that near the inlet section, all wastewater constituents are at their maximum concentrations at all times; under such favourable conditions bacteria thrive and their growth-rate rapidly becomes exponential. In this situation, all influent COD is consumed close to the inlet section and no effluent COD is detected.

This, in fact, is a mathematical artifact that does not occur in real wetlands (as several growth-limitations apply). Despite this issue is inherent of CWM1's formulation, none of the published works based on this model (Langergraber and Simunek, 2012; Llorens et al., 2011a,b; Mburu et al., 2012) referred to it in their respective discussions.

In the model by Llorens et al. (2011a,b) bacteria growth was not considered and their simulations were of quasi-static nature, which explains why they did not encounter this issue. On the other hand, the experimental data used by Mburu et al. (2012) to calibrate their model came from 16 batch-operated mesocosms with an incubation period of 20 days after each loading. Their results show that the substrates were rapidly consumed at the beginning of each incubation period, and thus the scarcity of substrates became the limiting factor for bacterial growth from approximately half of the incubation time on. Moreover, their model was zero-dimensional, which prevented the development of any bacteria gradients within the domain (inlet to outlet). Therefore, due to the intrinsic characteristics of their experimental set-up, the model could safely be applied without having to deal with unrealistic bacteria

growth. Finally, in the case of Langergraber and Simunek (2012) their experimental system was the same as the one used in the current work. However in their simulations they considered short time-frames (maximum simulation time of 50 days) and low organic matter influent concentrations ($X_S = 115\ mgCOD \cdot L^{-1}$, and $0\ mg \cdot L^{-1}$ for the other influent organic components considered in CWM1). Although under these particular conditions the unrealistic growth of bacteria was apparently avoided, they did report that in just 50 days all biodegradable COD was degraded in half of the flow distance. Only in a last simulation they did consider real influent concentrations (scenario 5 in Llorens et al. (2011b)), but unfortunately no reference was made to the simulation time used to obtain the discussed results.

To overcome the inability of CWM1 to provide realistic bacteria concentrations when substrate concentrations are high, a theoretic reformulation of the model and its corresponding mathematical description were needed. In this new formulation one can imagine every pore of the granular media of a SSF CWs as a micro-reactor in which bacterial growth is limited by both substrate and space availability. Moreover, in the pores, bacteria form biofilms, which have their own specific growth limitations in addition to those of direct availability (Zysset et al., 1994). To mathematically describe these growth limitations, two functions were utilized: one for the self-exerted growth limitation of biofilm (Eq. 4.7) and another for the space limitation (Eq. 4.8). These functions, not only prevent unrealistic growth of microorganisms, but also enable to account for the effects of the accumulation of inert solids in the porosity on bacteria distribution.

Eq. 4.7 represents the self-exerted growth limitation of biofilm. It is generally assumed that when the concentration of microbial biomass (M_{bio}) reaches a certain value (M_{bio_max}), the availability of substrates is thereafter limited by the diffusivity of the biofilm exterior boundary (Chen-Charpentier, 1999; Wanner et al., 2006). Indeed, bacteria near the surface of the granular media particles get less substrate than the bacteria near the film-water interface, and hence, the former grow slower than the latter (Tiwari et al., 2001).

The mathematical representation of this limitation, which has been used in the present model, was firstly proposed by Zysset et al. (1994) and later used by other authors (Brovelli et al., 2009b; Kildsgaard and Engesgaard, 2001; Stewart and Kim, 2004). These same authors also discuss that the value of M_{bio_max} is generally smaller than porosity's capacity. This fact suggests that Eq. 4.7 does not consider growth limitations from decreasing pore volume, and for this reason we included a specific function for pore volume reduction (Eq. 4.8).

In the current model pore volume reduction is exclusively due to inert solids (X_I) accumulation. Inorganic solids contained in wastewater and those produced from disintegration of the granular media are not taken into account at the present stage of development.

The value of the empirical parameter M_{bio_max} in Eq. 4.7 may vary for different wetlands as it depends on the biofilm characteristics (e.g. density, thickness), which in turn depend on granular media properties, wastewater composition and water flow, among others. Eq. 4.8 includes the parameter M_{cap}, the value of which is found by multiplying the pore volume (ϕ) by the density of biomat (ρ_{biomat}). In the present work, the value of ρ_{biomat} was obtained during calibration and was found to be 15 $kgVS \cdot m^{-3}$. With this density, the value of $M_{cap} = \rho_{biomat}\ \phi = 6\ kg$ of biomass for every cubic meter of granular material was obtained. ρ_{biomat} is an empirical parameter defined in this study and thus no other values are available in literature for comparison. The impact of the value of biomat density in the results is limited at the current stage of development of the model, as it only affects the maximum concentration of accumulated X_{Sf} and thus the maximum rate of hydrolysis. Lower values of biomat density will result in slower rates of hydrolysis, whereas higher values for this parameter will result (if enough hydrolysing bacteria are present) in higher concentrations of soluble COD internally produced from this process.

Eqs. 4.7 and 4.8 are multiplied by the maximum growth-rate of each bacteria group instead of being summed up, since the accumulation of X_{If} not only reduces porosity but also hinders the transport of substrates through the media. Therefore their combined effect must be stronger than when acting separately.

Unfortunately, no comparison was possible between simulation results obtained with and without Eqs. 4.7 and 4.8 since, for the second case, the high bacteria concentration gradients reached within the domain caused convergence issues after short simulation times. Therefore, the combined effect of Eqs. 4.7 and 4.8 was the key to obtain long-term results.

Other innovations

Apart from the two growth-limiting functions described in the previous section, the current model also includes innovative features in the hydraulic and in the transport sub-models. The first one is used to prevent overestimations of the extent of bacteria distribution within the domain when the unsaturated areas present within SSF CWs are omitted. Within these systems the water table level varies through time as a consequence of changes in flow rate, precipitation and evapotranspiration. The growth of bacteria in CWs requires the presence of water and if no distinction is made between wetted and dry areas, simulated bacteria colonization can be overestimated. From the available models implementing CWM1, three approaches are used to describe the hydraulics of wetlands. Langergraber and Simunek (2012) consider unsaturated flow conditions by means of the Richards equation, whereas Mburu et al. (2012) use the continuously stirred-tank reactors approach. On the other hand, the hydraulic description used by Llorens et al. (2011a,b) is similar to the one used in the current work as both consider saturated flow conditions by means of the Darcy

equation. However, the current model adds a new functionality that continuously calculates the location of the water table within the wetland, based on the applied flow-rates, and adjusts the top boundary of the domain (boundary 4 in Figure 4.1) to the wetted/dry interface at every time-step. This way, when running the model, bacteria growth is conditioned by the presence/absence of water in a similar way as if unsaturated flow equations had been used (as in Langergraber and Simunek (2012)).

The other innovative feature allows a simple description of attachment and detachment of particulate COD, although future refinement will be needed in prospective versions. So far none of the models implementing CWM1 are able to simulate these two processes. Both in Langergraber and Simunek (2012) and in Llorens et al. (2011a,b), particulate matter compounds are considered only in the aqueous phase. On the other hand, in Mburu et al. (2012) the simplistic hydraulic description prevents simulating attachment and detachment. The implementation of these two processes in the current model firstly required changes in CWM1s formulation detailed in Table 4.2 in order to divide X_S and X_I into mobile and immobile fractions each.

Analytical expressions for the attachment coefficient exist, which depend on the flow velocity, the porous media grain diameter, porosity and collector efficiency (Hornberger et al., 1992; Tien et al., 1979), and consequently are different for each wetland. For the sake of simplicity, in the current model λ_{att} (Eq. (4.4)) was obtained during calibration by imposing that all influent particulate matter had to be retained within the bed and would not be present in the outlet. In addition, the effective rate of attachment was defined to become zero once the pore space is fully occupied. Despite this strategy may appear contradictory and may not be able to reproduce the solids accumulation pattern as described by Knowles et al. (2011), it was adopted because, at present stage, changes in hydraulic conductivity caused by solids accumulation are not currently being computed. Therefore wastewater circulates through the same paths continuously and as a result, the inlet section is responsible for filtration throughout the whole simulation time. Unless this limit had been included, accumulated solids would reach unrealistically high concentrations and exceed pore capacity. Once the changes of the hydraulic and hydrodynamic properties of the media caused by the accumulation of solids can be computed, this workaround will not be required anymore.

On the other hand, shear detachment of accumulated solids is only a dominant process when high pore velocities exist. The experimental wetland operated with low flow-rates (20, 36 and 45 $mm \cdot d^{-1}$) and although the equation for describing detachment is included (Eq. 4.6), λ_{det} was set to zero during calibration.

4.4.2 Current limitations of the model and future developments

Despite the advances proposed in the current model, some issues are still to be addressed in upcoming versions.

Given that plants science and their relation to bacteria in CWs is still vaguely understood, the plants sub-model was kept deliberately simple. Consequently neither plant growth nor transpiration is considered and only oxygen release and nutrients uptake through their roots are taken into account.

Similarly, the effects of plant roots development, bacteria growth and solids accumulation on the hydrodynamics of wetlands are currently not considered in the model. This simplification may cause some disagreements between the model output and field observations, as these three processes have been reported to significantly change the hydraulic and hydrodynamic properties of the granular media (Knowles et al., 2011; Pedescoll et al., 2011; Sharp et al., 1999). However, omitting these effects at the current stage of development does not represent an oversimplification, as great changes in these factors develop slowly with a time-scale of several years. Future versions of the model will include these effects with the inclusion of a clogging sub-model (see Chapter 8).

It is also worth mentioning that neither attachment nor detachment processes affecting biomass are simulated. These two processes, as well as the transport of detached biomass may become important for simulating the total amount of biomass and its spatial distribution (Thullner, 2009). Biomass detachment has been subjected to some debate in literature. Peyton and Characklis (1993) suggested that the large number of existing methods indicates a failure of any one method to model the detachment rate over a broad range of conditions (Cooke et al., 2005). Similarly, Clement et al. (1997) attribute the difficulty to compute detachment rates to the lack of simple analytical expressions to model the underlying phenomena causing detachment. According to Rittmann (1982) detachment is controlled by fluid shear stress acting on the biomass surface. Accordingly, biofilm fragments become detached if they are exposed to shear stress higher than a critical value (Kapellos et al., 2007). Hence, the rate of biofilm shear increases as the flow rate increases and/or as porosity decreases. However, Rittmann (1982) also states that the shearing stress is not a significant detachment mechanism in a porous medium whose particles are of the size of gravel, as in the case of CWs. Moreover, using the expression from Rittmann (1982), Thullner et al. (2004) found that biomass detachment rate in their experiment was several orders of magnitude smaller than the assumed biomass decay rate, and thus detachment was neglected. Following these observations, and due to the impossibility to measure detachment rates in the pilot wetland (which was decommissioned in 2006), detachment processes were neglected in the current work.

On the other hand, influent bacteria concentrations were assumed to be negligible (see Section 4.2.3), and as detachment is not considered, attachment processes

affecting biomass will not occur and have not been included.

Neither evapotranspiration nor rainfall is currently considered in the model. Although in this work these two processes did not seem to substantially affect the results, this simplification may have a significant impact on the effluent pollutant concentrations, as they play an important role on the water balance of CWs (Chazarenc, 2003). However, these processes can be easily included in further versions of the model.

For a complete determination of the main removal mechanisms in CWs and for a more accurate calibration of the model, more continuous and specific experimental data on influent and effluent concentrations of the different components considered in CWM1 are required. Also, extensive experimental data from other systems will be needed to validate the present model. Finally, we acknowledge that the great amount of parameters used by CWM1, together with the new parameters included in its current implementation, makes the use of uncertainty and sensitivity analysis techniques a necessity. Although these type of studies can be easily performed using COMSOL Multiphysics™, the great computational power required has rendered this study impossible with the available hardware.

4.5 Conclusions

In this chapter we have presented a new model to describe the fate and transport of water pollutants in porous media. To this end, fluid flow and transport equations together with the biokinetic model Constructed Wetlands Model number 1 have been implemented in COMSOL Multiphysics™. The model has been calibrated comparing simulated and experimental effluent COD and $NH_4 - N$ concentrations for a period of 1 year.

Results indicate that the model was able to accurately reproduce the hydraulic and hydrodynamic behaviour of the pilot wetland. Simulated effluent COD and $NH_4 - N$ concentrations showed also a reasonably good fit to the measured concentrations during the first year of operation. Simulation results also show that by considering measured water temperatures, the experimental data can be better matched. On the other hand, the inclusion of plant roots oxygen release and nutrients uptake did not cause significant differences in the results.

The most notable advantage of BIO_PORE over similar models is that it can be used to predict the functioning of constructed wetlands in long-term scenarios. This was achieved by including two bacterial growth-limiting functions in the biofilm submodel. The first function prevents unrealistic growth of biomass in areas with high substrate concentrations, while the second one accounts for the effects on bacteria growth of porosity reduction due to the accumulation of inert solids. These two functions facilitate convergence of the model by preventing high bacteria concentration

gradients within the domain, which in turn allows extending simulations for longer time-scales.

Although in the present work the BIO_PORE model was calibrated for constructed wetlands, with few modifications it can be applied to simulate any kind of subsurface environment with microbial biofilm.

We also envisage that to accelerate the development of these powerful models the use of sophisticated computational methods (e.g. cluster computing), available in COMSOL Multiphysics™, could be of invaluable help.

CHAPTER 5

Effect of M_{cap} and M_{bio_max} on simulation outputs

This chapter is based on the article:

- Samsó, R., Blázquez, J., Agulló, N., Grau, J., Torres, R., García, J., 2014. Effect of bacteria density and accumulated inert solids on the effluent pollutant concentrations predicted by a Constructed Wetlands model. Ecological Engineering (submitted)

5.1 Introduction

Constructed Wetlands (CWs) are wastewater treatment systems usually applied for communities of less than 2000PE. This technology provides comparable treatment efficiencies with significantly lower energy and maintenance requirements than conventional technologies (García et al., 2010; Puigagut et al., 2007).

However, and due to the diversity and complexity of the physic-chemical and biological processes occurring within CWs, their functioning is far less well understood than that of activated sludge systems. To bridge this knowledge gap, several mathematical models have been developed in recent years to simulate CWs functioning (Meyer et al., 2014; Samsó et al., 2014b).

The BIO_PORE model is one of such models and was developed in COMSOL Multiphysics™, a commercial finite elements (FE) simulation platform (Meyer

et al., 2014; Samsó and García, 2014a; Samsó et al., 2014b; Samsó and García, 2013a,b).

In BIO_PORE two logistic functions were added to the original formulation of CWM1, which involve two new empirical parameters M_{bio_max} and M_{cap} (Samsó and García, 2013a). These two parameters represent, respectively, the maximum microbial biomass (carrying capacity) and the maximum amount of particulate solids that can be maintained in a representative volume of granular material. The function involving M_{bio_max} has already been used in several bioclogging studies (Brovelli et al., 2009b) and adds a negative feedback term to the growth of all bacteria groups to prevent their unlimited growth in areas where substrates concentrations are high. On the other hand, the expression involving parameter M_{cap} also adds a negative feedback term to the growth equations, but in this case it decreases the growth rate of bacteria due to the progressive accumulation of inert solids in the pore space of the granular media (Samsó and García, 2014a). Our previous studies proved the importance of these two functions in order to obtain realistic bacteria concentrations within the granular media (Samsó and García, 2014a; Samsó and García, 2013a). As bacterial communities play a major role on the treatment of wastewater in CWs, these two functions also improved the model predictions regarding effluent pollutant concentrations.

However, in these previous studies a sensitivity analysis of parameters M_{bio_max} and M_{cap} was not carried out and so their effect on the model output could not be evaluated. A parameter with high sensitivity is one for which small changes in its value produce large variation in a certain output of the model. On the contrary, low sensitivity parameters are those which do not affect model outputs even for large changes on their value. In this context, the main objective of the current chapter was to evaluate the sensitivity of M_{bio_max} and M_{cap} on the effluent pollutant concentrations of COD and ammonia and ammonium nitrogen predicted by the model. To that end, the BIO_PORE model was used with the same domain, parameter values and initial and boundary conditions than in Chapter 4 in which the model was calibrated (Samsó and García, 2013a). Due to the large computational cost associated with solving the model for a simulated period of an entire year of operation of a wetland (up to 16 hours for dense finite elements (FE) meshes with a current desktop computer), and due to the large number of simulations needed for the current and for further studies, a previous mesh optimization procedure was carried out. The objective of this part of the study was to find the FE mesh which would provide the best compromise between numerical solutions accuracy and computational cost.

The two empirical parameters discussed in this chapter are essential to obtain realistic bacteria concentrations when simulating CWs and this study shows how they affect the effluent pollutant concentrations predicted by the BIO_PORE model. In this chapter we also exploited the batch and parallel computation functionalities of COMSOL Multiphysics™ on a high-end multi-processor computer which is easily

justified by the large number of simulations performed.

5.2 Methods

The local parameter sensitivity analysis and the mesh optimization procedure were performed using the exact same domain, parameter values and boundary and initial conditions as in Chapter 4.

All simulations performed in this study were run for the entire first year of operation of a pilot wetland.

5.2.1 Mesh Optimization

After a previous detailed study with simplified versions of the model (progressively increasing the number of functional bacterial groups)(results not shown), 5 triangular meshes of different elements densities (Table 5.1) were chosen to perform the mesh optimization of the complete model (with all bacteria groups of CWM1). Among those meshes, $M_{0.1}$ was the coarsest, $M_{0.025}$ the most dense and $M_{BIO-PORE}$ was the one used in Chapter 4. $M_{BIO-PORE}$ was the only mesh with a predefined numbers of elements at boundaries 3 (20 elements), 4 (550 elements) and 5 (7 elements), which were reckoned as the most critical ones numerically (large concentration gradients).

Table 5.1: Meshes used in the mesh optimization procedure.

Mesh	**Maximum element size (m)**	**Number of elements**
$M_{0.1}$	0.1	1860
$M_{0.04}$	0.04	11446
$M_{BIO-PORE}$	0.05 [a]	19851
$M_{0.03}$	0.03	20064
$M_{0.025}$	0.025	28884

[a]Note that $M_{BIO-PORE}$ was built with a maximum element size of 0.05 m but fixing the number of elements at boundaries 3 (20 elements), 4 (550 elements) and 5 (7 elements), and its total number of elements is very similar to that of $M_{0.03}$.

Simulated effluent concentrations of COD (sum of S_F, S_A, S_I, X_{Sm} and X_{Im}) and S_{NH}, as well as the simulation time were recorded for all different meshes. Although the simulated effluent concentrations of the rest of model components could have also been studied, only COD and S_{NH} were used for the sake of brevity and because these are the two most widely used water quality indicators. The Sum of Squared Errors (SSE) for the effluent COD and S_{NH} curves for all different meshes were calculated using the coarser mesh ($M_{0.1}$) as a reference, to showcase the progressive accuracy gains with increasing mesh densities. The optimal mesh corresponds to

that after which any further increments on the number of elements does not produce notable improvements on the numerical accuracy of the solution (SSE remains fairly constant). Moreover, for evident practical reasons, the optimal mesh is also that with the shortest computational cost/time.

5.2.2 Parameter sensitivity

The sensitivity of M_{bio_max} and M_{cap} was studied by giving three different values to each of the two parameters (Table 5.2) and running a different simulation for each different pair (9 simulations in total) (Table 5.3).

Table 5.2: Values for M_{cap} and M_{bio_max}.

Value	$M_{cap}(kgVS \cdot m^{-3})$	$M_{bio\_max}(kgVS \cdot m^{-3})$
Minimum	5	0.1
Intermediate	10	0.3
Maximum	15	0.5

Table 5.3: Combinations of M_{cap} and M_{bio_max} values for the different simulations carried out for the local sensitivity analysis.

Parameter	$M_{cap}(kgVS \cdot m^{-3})$	$M_{bio\_max}(kgVS \cdot m^{-3})$
S_1	15	0.5
S_2	15	0.3
S_3	15	0.1
S_4	10	0.5
S_5	10	0.3
S_6	10	0.1
S_7	5	0.5
S_8	5	0.3
S_9	5	0.1

The reason for selection the values of Table 5.2 are discussed later in the text. Notice that the range of variability of M_{cap} was smaller than that of M_{bio_max}. In the first case, the highest value of M_{cap} was 3 times the smallest, whereas for M_{bio_max} the highest was 5 times the smallest.

The sensitivity of the two parameters was determined qualitatively by comparing the effluent concentrations of COD among them with the 9 different parameter pairs. The same is done for the simulated effluent concentrations of S_{NH}. A qualitative comparison was made between the effluent concentrations of COD and S_{NH} obtained with each parameter pair.

The mesh used to execute all these processes was the optimum mesh obtained in the previous step (Section 5.2.1).

5.2.3 Launching simulations and hardware specifications

In this chapter two different computers were used. For the mesh optimization procedure, a desktop PC was used. This computer features an Intel® Xenon® E5-1620 processor with 4 cores (8 threads) running at a frequency of 3600GHz and 16 GB of RAM memory. The Linux kernel and COMSOL Multiphysics™ versions installed on this computer were 3.2.0-56 and v4.3b, respectively.

On the other hand, for the sensitivity analysis the cluster functionalities of COMSOL Multiphysics™ were used to run several simulations in parallel on a high-end multi-processor computer. This computer consisted of 4 CPUs *AMD Opteron™ 6140* with 8 cores each (2.6 GHz), a total of 64 GB of RAM memory and run Linux Kernel 2.6.38. The COMSOL Multiphysics™ version installed in this machine was v4.2a. Since this machine was shared with other researchers, only 3 parallel simulations (using 4 CPU cores each) were launched at a time (see Figure 5.1). Therefore only 12 cores, out of the 32 available, were utilized. A bash script was used to automatically launch each different batch of 3 parallel simulations without any intervention.

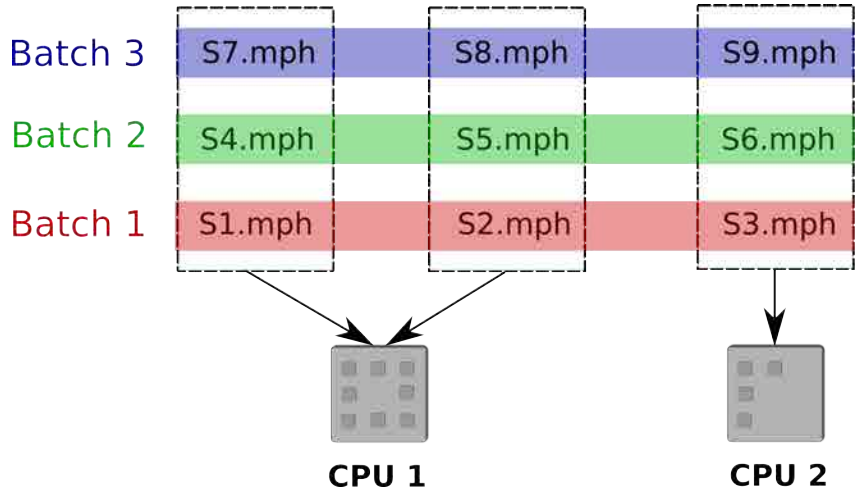

Figure 5.1: CPU and processor utilisation in the high-end multi-processor computer during the sensitivity analysis. Model files built in COMSOL Multiphysics™ have *mph* extension. Three batches of 3 parallel simulations, each with a different $M_{cap} - M_{bio\_max}$ pair (see Table 5.3), were launched. Each simulation took up only 4 processor cores. All cores of CPU1 were used, while CPU2 was only loaded to a 50%.

5.3 Results and discussion

5.3.1 Mesh optimization

In the current study the focus was not on how well or bad simulated effluent concentrations fit experimental data, since that discussion was already made in Chapter 4, but rather on the comparison of the simulation results obtained with different meshes. However, note that the poor fitting of the simulated effluent COD and S_{NH} with experimental data at the beginning of all simulations (Figures 5.2 and 5.3), was due to the fact that initial bacteria and accumulated solids concentrations were underestimated. However, after around 70 days of simulated time, the fitting improved.

Figures 5.2 and 5.3 show that the effluent pollutant concentrations of COD and S_{NH} obtained with the different meshes (Table 5.1) are visually different in some cases.

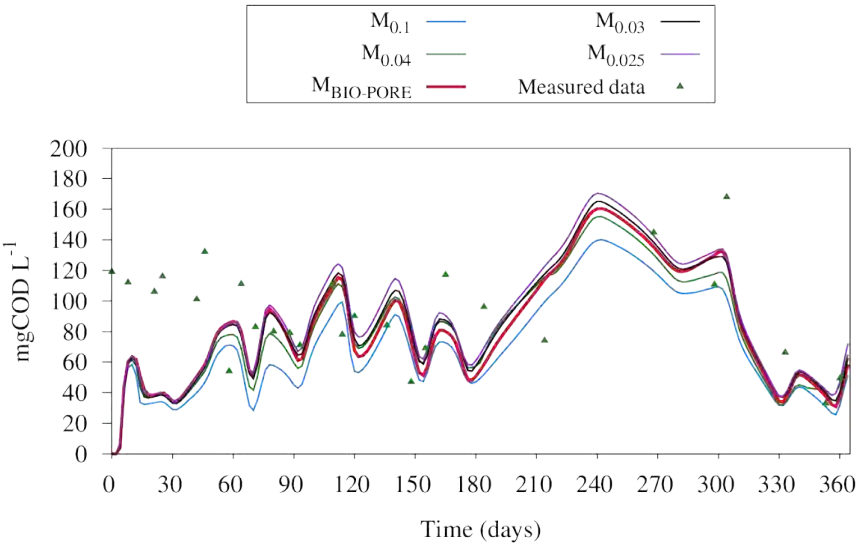

Figure 5.2: Simulated effluent COD concentrations obtained from the mesh optimization procedure with the meshes of Table 5.1.

Finer FE meshes provide more accurate numerical results. Thus in our study, mesh $M_{0.025}$, with a maximum element size of $2,5\ cm$ and a total of 28884 elements is the one giving more accurate results. Despite even better results could have been obtained by further refining the mesh, the total simulation time of $M_{0.025}$ (16 hours and 18 minutes) was already seen as too large for practical reasons. Moreover, refining the mesh to such an extent would only make sense if field data, which is given as

model input and later used to compare with simulated effluent concentrations, had been gathered in higher frequency.

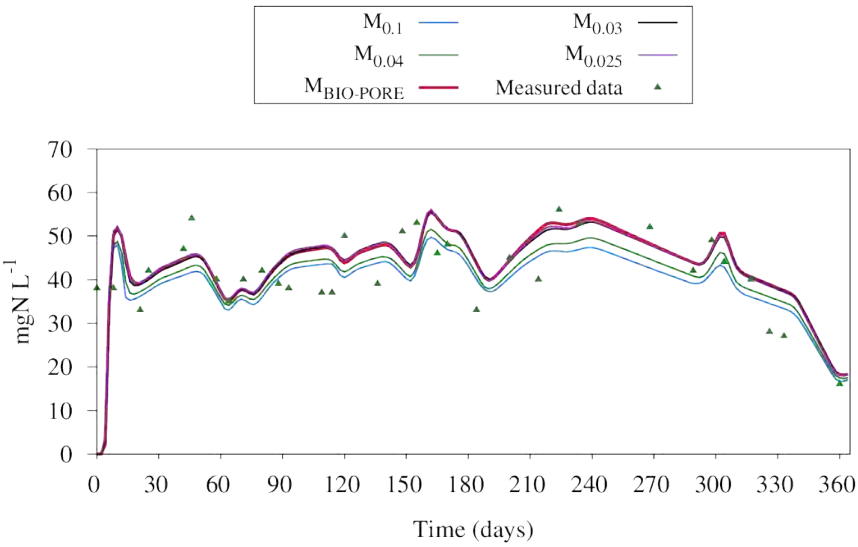

Figure 5.3: Simulated effluent S_{NH} concentrations obtained from the mesh optimization procedure with the meshes of Table 5.1.

Figure 5.3 clearly shows that almost identical results were obtained for simulated effluent S_{NH} concentrations with meshes $M_{BIO-PORE}$ and $M_{0.03}$ which account for c.a. 30% less elements than $M_{0.025}$. That is also confirmed with the tendency of the SSE for S_{NH} (Figure 5.5), which shows clear signs of stabilization already with meshes $M_{BIO-PORE}$ and $M_{0.03}$. Therefore, further mesh refinements would not improve the description of the effluent S_{NH} concentrations. In the case of COD (Figure 5.2), although the differences between the curves obtained with different meshes were higher than for S_{NH}, and the SSE still did not show signs of stabilization (Figure 5.4), the maximum difference of effluent COD concentrations obtained with meshes $M_{BIO-PORE}$ and $M_{0.025}$ was lower than 15 $mgCOD \cdot L^{-1}$, which was only around 8% the maximum effluent COD concentration simulated with mesh $M_{0.025}$. Moreover, note that the reference mesh $M_{0.1}$ was already fine (1860 elements) and thus reaching SSE stability is more difficult than if a coarser mesh had been used as a reference to calculate SSE.

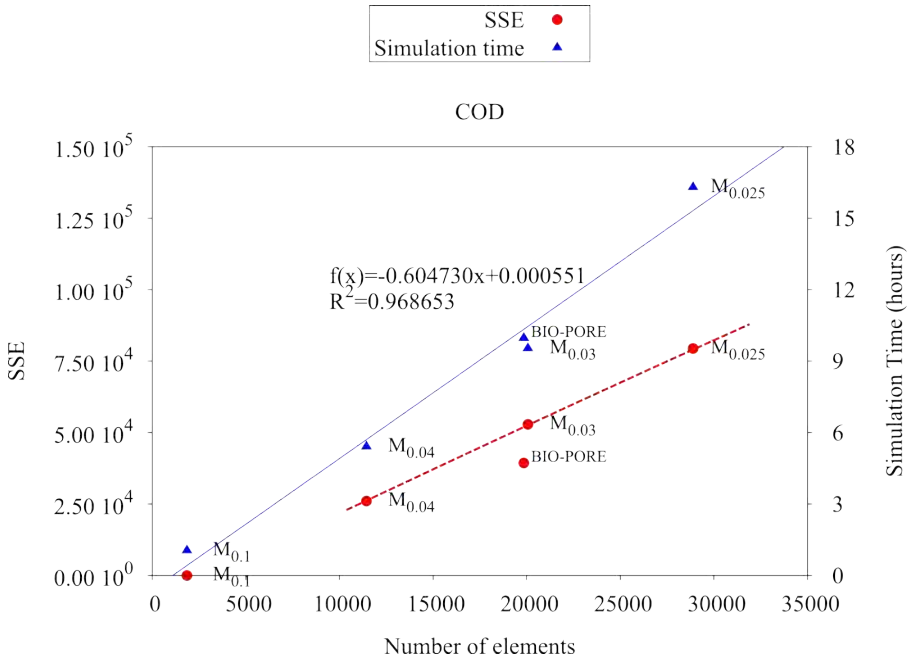

Figure 5.4: Sum of Squared Errors (SSE) (left y-axes) and simulation time (right y-axes) for the simulated effluent COD concentrations obtained with meshes of different elements density (see Table 5.2). The blue line shows the positive linear relationship ($R^2 = 0.97$) between the number of triangular elements of the mesh and the simulation time. The dotted red line was drawn to show that the SSE does not tend to a constant value with increasing number of elements. Notice that this line was drawn neglecting the SSE of $M_{BIO-PORE}$ since this mesh was built with a pre-set number of elements in specific domain boundaries. Mesh $M_{0.1}$ was also neglected, since it was the reference mesh, from which all SSE plotted in this figure were calculated.

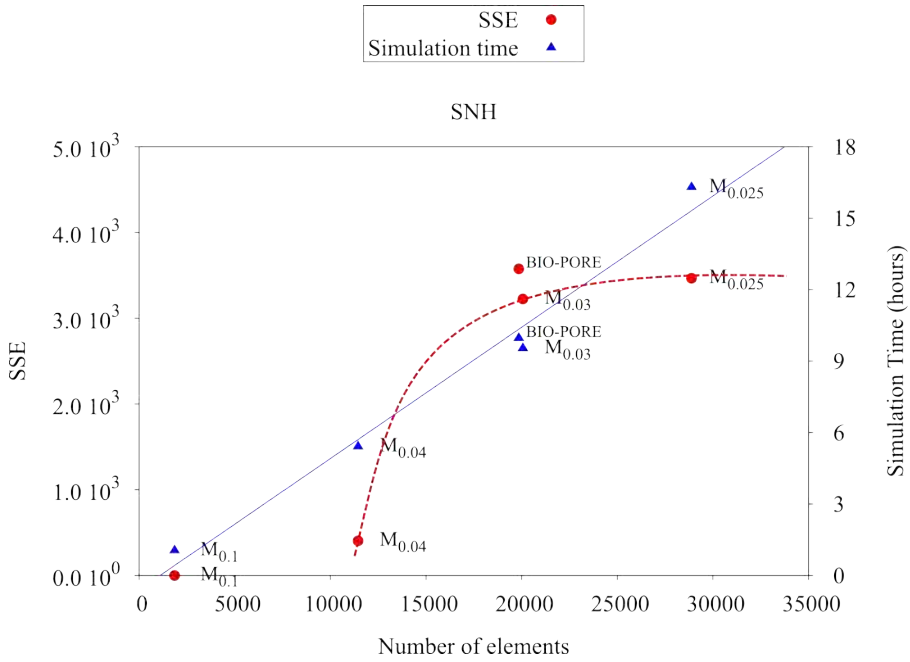

Figure 5.5: Sum of Squared Errors (SSE) (left y-axes) and simulation time (right y-axes) for the simulated effluent S_{NH} concentrations obtained with meshes of different elements density (see Table 5.2). The R^2 of the linear regression of the Simulation time is the same as in Figure 5.4, since all data shown in both figures was obtained from the same simulations (each focusing on different model outputs). The dotted red line was drawn to show that for S_{NH} the SSE tends to a constant value with increasing number of elements. As in the previous figure, the SSE of meshes $M_{BIO-PORE}$ and $M_{0.1}$ were neglected to draw this line.

Table 5.4 shows that, in general, the simulation time increased with increasing mesh densities. $M_{BIO-PORE}$ was the exception, and although it had 213 less elements than $M_{0.03}$ the former took 25 minutes more than the later to reach the final solution. The most likely reason for that is that the mesh element quality of $M_{BIO-PORE}$ was lower than that of $M_{0.03}$ and thus the solver algorithm required a few more iterations at every time step to reach a solution. In fact, $M_{BIO-PORE}$ was the one with the second largest maximum element size (0.05 cm), only after $M_{0.1}$, but in contrast it was the mesh with the highest elements densities in boundaries 3, 4 and 5, which were the ones accounting for the highest concentration gradients. The relation between number of elements and simulated time can also be observed in Figures 5.4 and 5.5, and shows that a linear relationship ($R^2 = 0.97$) exists between the two.

Table 5.4: Number of elements and simulation time for each of the meshes used for mesh optimization.

Mesh	Number of triangular elements	Simulation time (hours)
$M_{0.1}$	1860	1.04
$M_{0.04}$	11446	5.41
$M_{BIO-PORE}$	19851	9.96 [a]
$M_{0.03}$	20064	9.53
$M_{0.025}$	28884	16.30

[a]Notice that although $M_{BIO-PORE}$ had fewer elements than $M_{0.03}$ its simulation time was slightly higher. Notice as well that $M_{BIO-PORE}$ was the only one of the selected meshes with higher elements density in boundaries 3, 4 and 5 (see Figure 4.1).

According to these results, the mesh with a better compromise between numerical accuracy and simulation time was $M_{0.03}$. The results obtained with mesh $M_{BIO-PORE}$ were almost as good as those obtained with $M_{0.03}$ (see Figures 5.2, 5.3, 5.4 and 5.5), and since mesh $M_{BIO-PORE}$ had already been used successfully in Chapter 4, it was chosen as the one to be used for the sensitivity analysis.

5.3.2 Parameter sensitivity

Despite BIO_PORE includes more than 50 parameters, only the sensitivity of M_{bio_max} and M_{cap} was analysed because they are two new additions to the formulation of CWM1. Moreover, the sensitivity of the different parameters of CWM1 has already been studied in other works (Mburu et al., 2012). Note that the type of analysis carried out in this chapter is a local sensitivity analysis, which only addresses sensitivity relative to the point estimates chosen and not for the entire parameter distribution.

The function involving M_{bio_max} (function 4.7 in Chapter 4) limits the maximum concentration of bacteria that each pore of the granular media can hold (carrying capacity) by stopping the growth of bacteria once M_{bio} reaches the value of M_{bio_max}. The second function (4.8) works in the same way, but M_{cap} corresponds to the maximum amount of particulate solids (X_{Sf} and X_{If}) porosity can hold, and bacterial growth stops once $M_{X_{If}} = M_{cap}$.

The values given to parameters M_{bio_max} were chosen based on our previous experiences with the BIO_PORE model, since no literature values for these parameters exist for CWs. In fact the intermediate value of this parameter used in the current chapter was that obtained from the calibration of the model in Chapter 4, and the other two were chosen to be at a sound distance from the first. On the other hand, the amount of accumulated solids in horizontal subsurface flow CWs presents a great variability depending on the COD and TSS loading rates and on the turn-over rates. Measurements carried out by Caselles-Osorio et al. (2007) in 6 full-scale horizontal subsurface flow CWs showed that accumulated solids ranged from as low as

2.3 $kgVS \cdot m^{-2}$ up to 57.3 $kgVS \cdot m^{-2}$ (between around 6 and 162 $kgCOD \cdot m^{-3}$, considering an average wetland depth of 0.5 m and that 1 $gVS \approx 1.42\ gCOD$ (Samsó and García, 2014a)). In this study we selected the values of M_{cap} to be in the lower part of that range, since the gravel size of the pilot system was quite fine ($D_{60} = 3.5\ mm$ and $C_u = 1.7$).

Results indicate that M_{bio_max} and M_{cap} are both very sensitive parameters since they had a large impact on the simulated concentrations of COD (Figure 5.6) and S_{NH} (Figure 5.7). At the beginning of all simulations, effluent concentrations obtained with the different pairs of M_{bio_max} and M_{cap} were very similar, and it was not until around simulated day 60 that they started diverging. Figures 5.6 and 5.7 show that both for COD and S_{NH} the most sensitive parameter was M_{cap}, and the higher its value, and thus the higher the capacity of porosity to retain particulate solids (X_{If} and X_{Sf}), the lower the effluent concentrations of the two pollutants. A possible reasoning for this behaviour is that for high values of M_{cap} the amount of slowly biodegradable particulate COD (X_{Sf}) that can be reached in the granular media is much higher than that the maximum bacteria biomass present in the same location (which is limited by the value of M_{bio_max}) can biodegrade, and so they accumulate. Therefore this accumulated organic matter, which also contains a fraction of organic nitrogen, is retained within the system and does not add to the concentrations of COD and S_{NH} measured at the outlet.

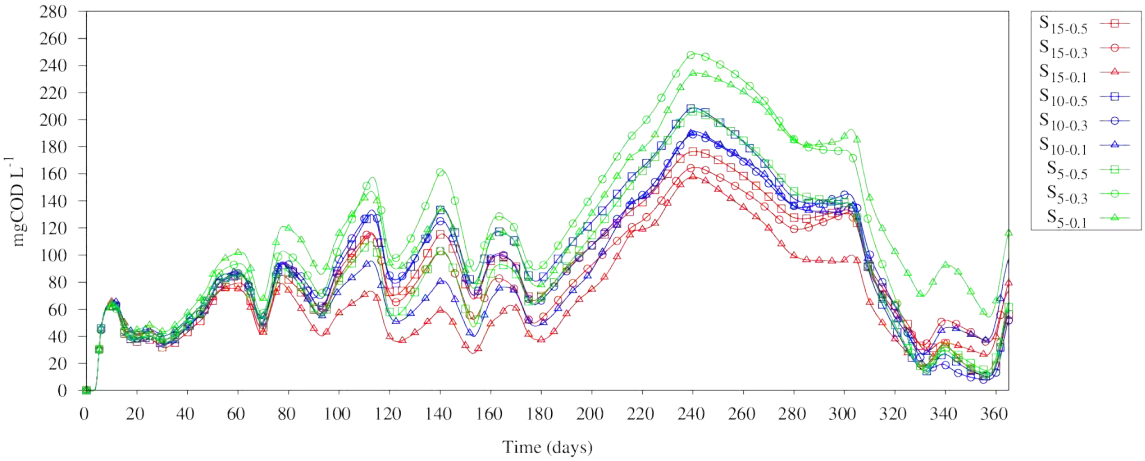

Figure 5.6: Effluent COD concentrations obtained with the combinations of M_{bio_max} and M_{cap} shown in Table 5.3.

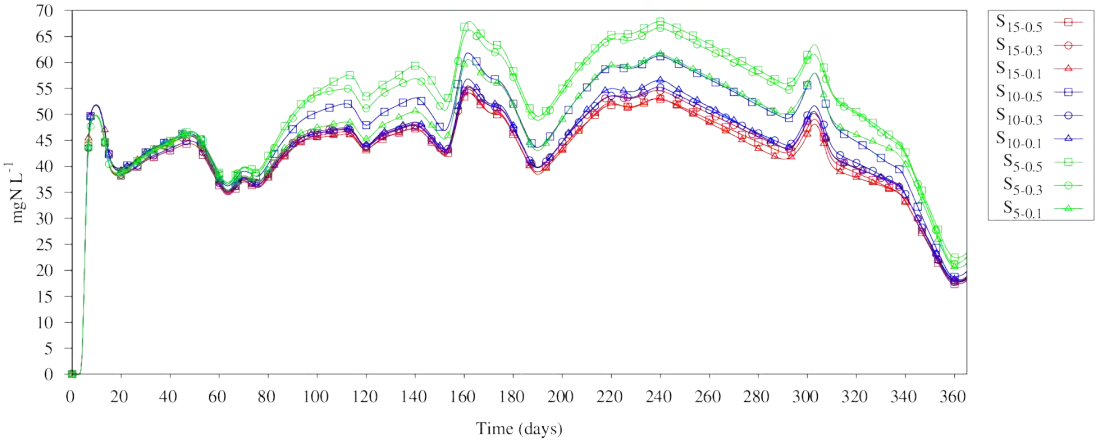

Figure 5.7: Effluent S_{NH} concentrations obtained with the combinations of M_{bio_max} and M_{cap} shown in Table 5.3.

On the other hand, although perturbations of the M_{bio_max} value produced observable changes in the effluent COD and S_{NH} concentrations, these changes were smaller than those produced by changing the value of M_{cap}. Regarding the effluent COD concentrations (Figure 5.6), for $M_{cap} = 15\ kgVS \cdot m^{-3}$ and $M_{cap} = 10\ kgVS \cdot m^{-3}$, the higher the value of M_{bio_max} the higher the effluent concentrations of COD. This can be explained by the fact that the higher the maximum concentrations of biomass in a specific point of the granular media, the larger proportion of the accumulated X_{Sf} can be hydrolysed and thus released through the outlet (in the form of S_F, S_A, S_I and S_{NH}) increasing the effluent concentrations of COD and S_{NH}. On the contrary, for $M_{cap} = 5\ kgVS \cdot m^{-3}$, the tendency is different and the effluent concentrations are higher for $M_{bio\_max} = 0.3\ kgVS \cdot m^{-3}$, intermediate for $M_{bio\_max} = 0.1\ Kg \cdot m^{-3}$ and the lowest for $M_{bio\_max} = 0.5\ KgVS \cdot m^{-3}$. Therefore no clear pattern can be extracted for M_{bio_max} when the values of M_{cap} are relatively small.

Regarding S_{NH} (Figure 5.7), for $M_{cap} = 15\ kgVS \cdot m^{-3}$, the effluent concentrations of this component are almost the same regardless of the value of M_{bio_max}. For the intermediate value of M_{cap} ($10\ kgVS \cdot m^{-3}$), $M_{bio\_max} = 0.5\ kgVS \cdot m^{-3}$ gives the highest effluent concentration, while for $M_{bio\_max} = 0.3\ kgVS \cdot m^{-3}$ and $M_{bio\_max} = 0.1\ kgVS \cdot m^{-3}$ the effluent concentrations are almost identical. For the lowest value of M_{cap} ($5\ kgVS \cdot m^{-3}$) there are also differences between the curves, but in this case $M_{bio\_max} = 0.1\ kgVS \cdot m^{-3}$ gives the lowest effluent concentrations of S_{NH} while $M_{bio\_max} = 0.5\ kgVS \cdot m^{-3}$ and $M_{bio\_max} = 0.3\ kgVS \cdot m^{-3}$ give almost the same results.

Therefore, contrarily to what happened for M_{cap}, for M_{bio_max} although some patterns can be detected for the effluent COD concentrations, there is not a clear distinguishable tendency regarding the effluent concentrations of S_{NH} obtained with

the different values of this parameter. However, the higher the value of M_{cap}, the larger the difference between the effluent concentrations obtained with the different values of M_{bio_max}.

5.4 Conclusions

In this chapter we performed a mesh optimization procedure in order to reduce the simulation time (while maintaining similar numerical accuracy) for subsequent simulations, and we also performed a local sensitivity analysis of parameters M_{cap} and M_{bio_max}.

Results of the mesh optimization procedure indicated that for homogeneous meshes, a positive linear relationship existed between the number of elements and simulated time. The best compromise between numerical accuracy and computational cost was obtained with meshes $M_{0.03}$ and $M_{BIO-PORE}$. $M_{BIO-PORE}$ was selected as the optimal mesh to carry out the sensitivity analysis.

Despite the range of values given to M_{cap} was smaller than that given to M_{bio_max}, the former parameter proved to be the most sensitive one, and the higher its value the lower the simulated effluent concentrations of COD and S_{NH} of the wetland. This was due to the fact that for larger values of M_{cap}, more slowly biodegradable solids can accumulate in a specific point, and if there is not enough bacteria to hydrolyse them, they are not released and thus the effluent concentrations of COD and S_{NH} does not increase.

On the other hand, from the values given to M_{bio_max} no clear recognisable pattern on the effluent concentrations of COD and S_{NH} could be observed.

CHAPTER 6

CWs functioning based on simulation results: a case study

This chapter is based on the article:

- Samsó, R., García, J., 2013b. Bacteria distribution and dynamics in constructed wetlands based on modelling results. Science of The Total Environment 461-462, 430440. doi:10.1016/j.scitotenv.2013.04.073

6.1 Introduction

Subsurface flow constructed wetlands (SSF CWs) are nowadays one of the most common types of eco-technologies for wastewater treatment used throughout the world. In SSF CWs three relevant elements contribute to wastewater treatment: granular medium, plants and bacterial communities. However, from these three, it is widely accepted that the activity of diverse bacterial communities growing in the form of biofilms is the most important element in pollutant transformation and removal (Ahn et al., 2007; Faulwetter et al., 2009; García et al., 2010; Iasur-Kruh et al., 2010; Krasnits et al., 2009; Ramond et al., 2012; Truu et al., 2009).

The idea that in SSF CWs coexist diverse bacterial communities with completely different metabolic requirements and functional roles (i.e. from strictly aerobes to anaerobes, from autotrophs to heterotrophs) has been progressively built through intense fundamental research on this technology. The role of bacterial communities was put into evidence when the activity of bacterial groups was inferred by measuring concentration changes of different electron acceptors (i.e. oxygen, nitrate and

sulphate) and donors (i.e. ammonia and dihydrogensulphide) in pilot wetland systems (Aguirre et al., 2005; García et al., 2004b; Huang et al., 2005). The detection of gaseous or volatile intermediate and end-products such as methane, nitrous oxide and dimethylsulfide was also an indication of the metabolic activity of different bacterial groups (García et al., 2005; Huang et al., 2005; Mander et al., 2003; Teiter and Mander, 2005). More recently, characterization of bacterial communities in SSF CWs has proliferated with the advent of molecular microbiology methods such as fluorescence in-situ hybridization and PCR-based techniques, and other advanced methods such as community-level physiological profiling (Criado and Bécares, 2005; Krasnits et al., 2009; Ramond et al., 2012; Weber and Legge, 2011). Results obtained with such studies revealed that SSF CWs account for a diversity of bacterial strains comparable to that found in natural ecosystems (Calheiros et al., 2010; Criado and Bécares, 2005; Hadwin et al., 2006; Hallberg and Johnson, 2005; Hench et al., 2004; Sims et al., 2012; Sleytr et al., 2009). However, most of these studies consist in point-in-time observations and only a few investigated temporal dynamics of bacterial communities in SSF CW (Ramond et al., 2012; Truu et al., 2009; Weber and Legge, 2011). This is probably due to the fact that such experimental studies involve complex methodologies which are generally very time and resource-consuming. Therefore, complementary techniques could help to give a wider image of the temporal evolution of microbial communities in SSF CWs. Mathematical models are one such complementary technique, with which bacteria dynamics and interrelations can be studied under different scenarios and at much lower costs.

The BIO_PORE model is a mathematical code built in the COMSOL Multiphysics™ platform that was specifically designed to simulate the behaviour of SSF CWs and incorporates the biokinetic reactions described in the Constructed Wetland Model Number 1 (CWM1)(Langergraber et al., 2009a). CWM1 has also been implemented in other simulation platforms (Langergraber and Simunek, 2012; Llorens et al., 2011a,b; Mburu et al., 2012) and the resulting codes have been used to match experimentally measured effluent pollutant concentrations, while giving little attention to the results on bacteria abundance, distribution and interrelations. Moreover, to study the temporal dynamics of bacterial groups from modelling results, long-term simulations are required and BIO_PORE is, to our knowledge, the only model able to run long-term simulations of continuously fed SSF CWs. Besides, one of the most useful features of BIO_PORE is that it allows for exploratory research, as each inhibitory/limiting term affecting the growth of the different bacteria groups can be studied individually and its relative impact on bacteria dynamics can be pinpointed.

The presence of a well-developed and stable microbial community is generally considered to be a critical factor for a good functioning of SSF CWs in terms of pollutant removal (Ramond et al., 2012; Torsvik and Ovreas, 2002; Weber and Legge, 2011; Wohl et al., 2004). Experimental studies in mesocosms suggested that bacteria community stabilization in SSF CWs is reached between 75 and 100 days (Ramond et al., 2012; Truu et al., 2009; Weber and Legge, 2011). In the present study we

demonstrate based on simulations in a pilot system with BIO_PORE model that bacteria communities reach stability, but that it is a slower process than what has generally been reported. We also study the sequence of processes that lead to bacterial stability and analyse the abundance of the different bacteria groups at different times within a 3 years period. We also analyse the distribution of bacteria communities when stability is reached.

To our knowledge, this is the first time that bacterial communities distribution and dynamics in SSF CWs are studied from modelling results. It is important to note, though, that by being this the first work of its kind on this topic we considered a simplified scenario (constant influent concentrations, flow-rates and water temperatures) which will gain in complexity once the basis are set.

6.2 Methods

6.2.1 Simulation strategy

A simulation was conducted for the pilot wetland described in Cahpter 3. Values of the hydraulic and hydrodynamic parameters utilized for the simulation are shown in Table 6.1.

Table 6.1: Values of the hydraulic and hydrodynamic parameters utilised in our simulation. These values were obtained during calibration by Samsó and García (2013a).

Parameter	Description	Value	Unit
α_L	Longitudinal dispersivity	0.05	m
α_T	Transverse dispersivity	0.005	m
K	Hydraulic conductivity	50	$m \cdot d^{-1}$

Although BIO_PORE can handle variable input data, in the present study constant values for hydraulic loading rate (HLR) (36.6 $mm \cdot d^{-1}$), water temperature (20 $°C$) and influent pollutant concentrations were used. This is of course a theoretical simplified scenario, but it was adopted to facilitate interpretation of the results. Constant values of influent concentration of the components considered in CWM1 were extracted from data averages of an experimental study carried out in the pilot wetland by García et al. (2005) (Table 6.2).

Note that in this system, the influent sulphur concentrations were higher than in average urban wastewater, since potable water in the metropolitan area of Barcelona is partially obtained from a river that drains a chalk basin. The fractioning of the influent COD was made using recommended values for primary effluents in ASMs (Henze et al., 2000). Note, however, that the recommended values for primary effluents may differ slightly from the Imhoff effluents, but they were assumed in a pragmatic approach to avoid a detailed characterisation of the influent wastewater.

Table 6.2: Constant inflow concentrations used for simulations. These values were obtained from averages of an experimental study conducted in the pilot wetland (García et al., 2005).

Componenet	Description	Inflow concentration	Unit
S_O	Dissolved oxygen	0	$mgCOD \cdot L^{-1}$
S_F	Soluble fermentable COD	39	$mgCOD \cdot L^{-1}$
S_A	Fermentation products as acetate as COD	52	$mgCOD \cdot L^{-1}$
S_I	Inert soluble COD	13	$mgCOD \cdot L^{-1}$
X_{Sm}	Aqueous slowly biodegradable particulate COD	130	$mgCOD \cdot L^{-1}$
X_{Sf}	Solid slowly biodegradable particulate COD	0	$mgCOD \cdot L^{-1}$
X_{Im}	Aqueous inert particulate COD	26	$mgCOD \cdot L^{-1}$
XI_f	Solid inert particulate COD	0	$mgCOD \cdot L^{-1}$
S_{NO} [a]	Nitrite and nitrate nitrogen	0	$mgN \cdot L^{-1}$
S_{NH}	Anmonium and ammonia nitrogen	57	$mgN \cdot L^{-1}$
S_{SO4}	Sulphate sulphur	72	$mgS \cdot L^{-1}$
S_{H2S}	Dihydrogensulphide sulphur	0	$mgS \cdot L^{-1}$

[a]Note that SNO is assumed to include all nitrite and nitrate nitrogen, since nitrite is not included as a separate model component.

Influent concentrations of bacteria were neglected because they generally are small in comparison with the concentrations found within the wetland itself Truu et al. (2009). As in Chapter 4, initial concentrations of bacteria, particulate solids and dissolved components within the wetland were all set to 0.001 $mg \cdot L^{-1}$ to simulate start-up conditions.

Constant oxygen release and nitrogen uptake rates by plant roots were taken from Samsó and García (2013a) (3 $gO_2 \cdot m^{-2}d^{-1}$ and 0.2 $gN \cdot m^{-2}d^{-1}$, respectively) and apply to the top 30 cm layer of the granular media. Passive diffusion of atmospheric oxygen into the water body is also considered in BIO_PORE (see Chapter 4).

A simulation was run to reproduce bacterial dynamics between start-up and until the 3^{rd} year of continuous operation of the wetland, which according to current knowledge should be more than sufficient time for bacteria communities to stabilize (Ramond et al., 2012; Truu et al., 2009; Weber and Legge, 2011).

6.2.2 Study of bacteria dynamics and pollutants removal efficiencies

To study the abundance of each bacterial group within the whole wetland we estimated the total concentration of their biomass. The actual biomass was obtained by integrating their concentration within the simulated longitudinal section (obtaining

$kgCOD \cdot m^{-1}$) and multiplying it by the width of the wetland (5.3 m) (obtaining $kgCOD$). Biomass was later normalised to a cubic meter of granular material by dividing it by the volume of the entire wetland.

During simulations, the different wastewater constituents were monitored inside the wetland and in the effluent to determine pollutant removal efficiencies and also inhibition effects on different bacteria groups. Specific substrates known to cause competition between different bacteria groups were also studied in detail. To determine the removal efficiencies of N, the total influent nitrogen was considered to be the sum of ammonia, nitrite and nitrate and organic nitrogen (that contained in SF, SI, XS and XI). The N contents of each COD fraction are listed in Table 6.3:

Table 6.3: Nitrogen content of the different fractions of COD.

Parameter name	**Description**	**Value**	**Source**
iN, S_F	Nitrogen content of S_F ($gN \cdot gCOD_{S_F}^{-1}$)	0.03	Langergraber et al. (2009a)
iN, S_I	Nitrogen content of S_I ($gN \cdot gCOD_{S_I}^{-1}$)	0.01	Langergraber et al. (2009a)
iN, X_S	Nitrogen content of X_S ($gN \cdot gCOD_{X_S}^{-1}$)	0.04	Langergraber et al. (2009a)
iN, X_I	Nitrogen content of X_I ($gN \cdot gCOD_{X_I}^{-1}$)	0.03	Langergraber et al. (2009a)

Therefore, with the concentrations listed in Table 6.2, the total influent N in the system can be calculated as:

$$Total\ N = S_{NH} + S_{NO} + S_F \cdot iN,S_F + S_I * iN,S_I + (X_{Sf} + X_{Sm}) \cdot iN,X_S + (X_{If} + X_{Im}) \cdot iN,X_I = 57 + 0 + 39 \cdot 0.03 + 13 \cdot 0.01 + (0+130) \cdot 0.04 + (0+26) \cdot 0.03 = 64.28 \frac{mgN}{L}$$

Note, however, that not all organic nitrogen becomes available for bacterial growth or nitrification-denitrification processes, since it has to be previously released through the degradation of the organic compound in which it is contained.

Three different indicators were utilized to determine bacterial stabilization. The first indicator considered was the stabilisation of the total amount of biomass within the wetland. The second indicator considers that bacteria stability is reached when no more major changes are observed in the effluent pollutant concentrations. Finally, the third indicator considered the stabilisation of Shannon diversity index (Shannon, 1948) (Equation 6.1).

$$H' = -\sum_i^n \left(\frac{X_i}{X_{tot}} log_2 \left(\frac{X_i}{X_{tot}} \right) \right) \tag{6.1}$$

Where n is the total number of functional bacteria groups, X_i is the biomass of functional bacteria group i and X_{tot} is the sum of the biomass of all groups. The distribution of bacteria was studied after bacterial stabilisation, since before that, it

was seen to change very rapidly. Bacterial distribution was studied by representing the concentration of the different bacteria groups on the 2D domain.

6.3 Results

Sections 6.3.1 and 6.3.2 present the results for the entire 3 years of operation, while Section 6.3.3 focuses only on the results obtained after bacteria stabilised. In Section 6.3.1 we present the evolution of the total biomass of the different bacteria groups. Only partial attention was given to bacterial distribution in this section. In Section 6.3.2 the pollutant removal efficiencies obtained with the model are presented. The first part of Section 6.3.3 presents the results obtained with the three indicators of bacterial stabilisation. In the second part we present bacterial distribution when stability is achieved.

6.3.1 Overall bacteria dynamics

At the very beginning of operation (first 15 days) the presence and concentration of dissolved oxygen (S_O) was the main factor affecting bacterial dynamics within the wetland. Figure 6.1 represents S_O concentrations within the wetland at days 3, 10 and 15, while in Figure 6.2, the value of $\left(\frac{K_{SOFB}}{K_{SOFB}+S_O}\right)$ in Equation 6.2 is represented in the same days. Equation 6.2 describes the growth rate of fermenting bacteria (X_{FB}) ($mgCOD \cdot L^{-1}d^{-1}$) and $\left(\frac{K_{SOFB}}{K_{SOFB}+S_O}\right)$ describes the inhibiting effect of dissolved oxygen (S_O) on such rate. Note that for the sake of brevity the inhibition of oxygen is only shown for X_{FB}, since its effects on the other anaerobic bacteria groups are almost identical.

$$\frac{dX_{FB}}{dt}=\mu_{FB}\left(\frac{S_F}{K_{SFFB}+S_F}\right)\left(\frac{K_{H2SFB}}{K_{H2SFB}+S_{H2S}}\right)\left(\frac{K_{SOFB}}{K_{SOFB}+S_O}\right)\left(\frac{K_{NOFB}}{K_{NOFB}+S_{NO}}\right)\left(\frac{S_{NH}}{K_{NHFB}+S_{NH}}\right)X_{FB}-bX_{FB} \tag{6.2}$$

Values close to zero for $\left(\frac{K_{SOFB}}{K_{SOFB}+S_O}\right)$ indicate complete inhibition of X_{FB} growth $\left(\frac{dX_{FB}}{dt}=-bX_{FB}\right)$ resulting from high oxygen concentrations, while values close to 1 indicate insignificant inhibition effects.

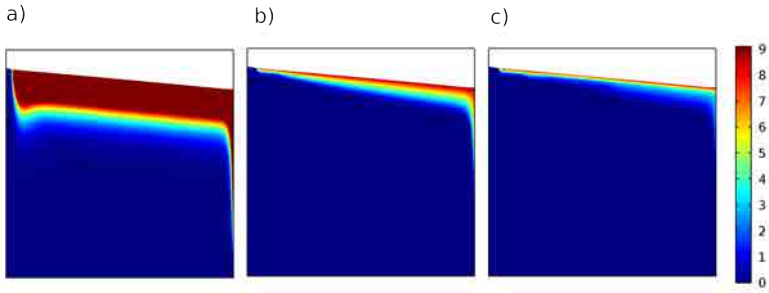

Figure 6.1: Oxygen concentration within the wetland ($mgO_2 \cdot L^{-1}$) after a) 3, b) 10 and c) 15 days of operation. The key at the right indicates S_O concentration. Note that the images are longitudinal cross sections of the wetland which have been deformed to fit a reasonable size. The x-axis of each image represents the longitudinal direction of the wetland (from 0 to 10.3 m) and the y-axis the depth of the wetland (from 0 to 0.7 m). Also note that the coloured areas of each image correspond to wetted areas, while the white areas correspond to areas without water. Note that water level decreases from inlet to outlet.

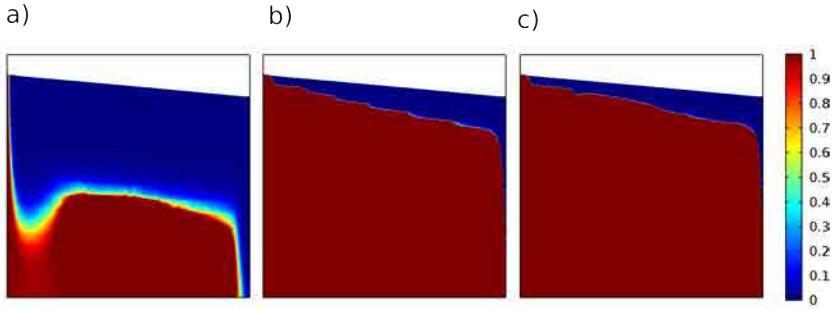

Figure 6.2: Representation of the values of the inhibition term of fermenting bacteria (X_{FB}) due to the presence of dissolved oxygen (S_O) after a) 3, b) 10 and c) 15 days of operation. This is a representation of the highlighted term in Equation 6.2. Values close to 1 indicate that S_O is not inhibiting the growth of this bacteria group, while values close to 0 indicate 100% inhibition. The key at the right indicates S_O concentration in $mgO_2 \cdot L^{-1}$. Note that the images are longitudinal cross sections of the wetland which have been deformed to fit a reasonable size. The x-axis of each image represents the longitudinal direction of the wetland (from 0 to 10.3 m) and the y-axis the depth of the wetland (from 0 to 0.7 m). Also note that the coloured areas of each image correspond to wetted areas, while the white areas correspond to areas without water.

At day 3, dissolved oxygen (S_O) was very widespread within the wetland (Figure 6.1a), favouring the growth of heterotrophic bacteria (X_H), which became the most abundant and widely distributed group at that time (Figures 6.3 and 6.4). The lack of oxygen in the influent wastewater allowed fermenting bacteria (X_{FB}) reach high concentrations near the inlet section (Figure 6.3b), although their distribution was much narrower due to the presence of high S_O in further sections. After day 3, both the S_O concentration and its inhibition on anaerobic bacteria near the bottom of the wetland progressively decreased as a result of the combined effect of the consumption

by aerobic bacteria (mainly heterotrophic bacteria (X_H)) and the washout with the water flow (Figures 6.3 and 6.4).

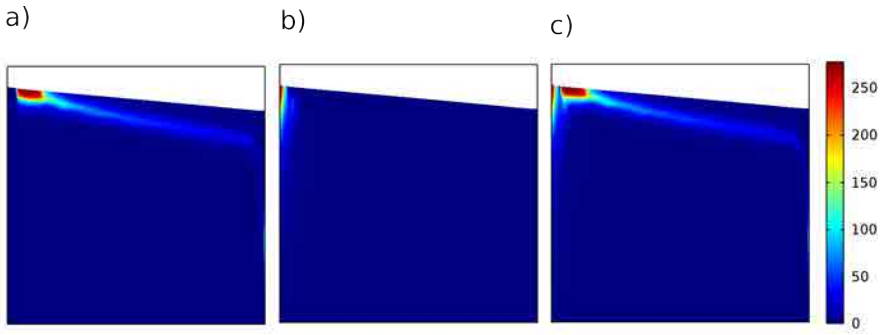

Figure 6.3: Distribution of a) Heterotrophic (X_H), b) Fermenting (X_{FB}) and c) all bacteria groups together (X_H, X_A, X_{FB}, X_{AMB}, X_{ASRB} and X_{SOB}) are shown after 10 days of operation. The key at the right indicates bacteria concentration in $mgCOD \cdot L^{-1}$. Note that the images are longitudinal cross sections of the wetland which have been deformed to fit a reasonable size. The x-axis of each image represents the longitudinal direction of the wetland (from 0 to 10.3 m) and the y-axis the depth of the wetland (from 0 to 0.7 m). Also note that the coloured areas of each image correspond to wetted areas, while the white areas correspond to areas without water. Note that water level decreases from inlet to outlet.

After this initial stage nitrifying bacteria (X_A) reached their maximum biomass around day 20 (Figure 6.4a). Subsequently, around the 80^{th} day of operation fermenting bacteria (X_{FB}) biomass exceeded that of heterotrophic bacteria (X_H) for the first time. This fact was followed by a progressive decrease of X_H biomass, and after day 110 the biomass of sulphate reducing bacteria (X_{ASRB}) was already higher. At this stage X_{ASRB} produced sufficient dihydrogensulphide (S_{H2S}) to allow the growth of sulphide oxidising bacteria (X_{SOB}), but also to inhibit the growth of other bacteria groups such as methanogenic bacteria (X_{AMB}). Sulphate reducing bacteria (X_{ASRB}) overcome fermenting bacteria (X_{FB}) as the dominant group at c.a. day 280, and remained so until the end of the 3 years. Methanogenic bacteria (X_{AMB}) were the slowest group to develop and only reached their maximum concentrations after around 2 years of operation.

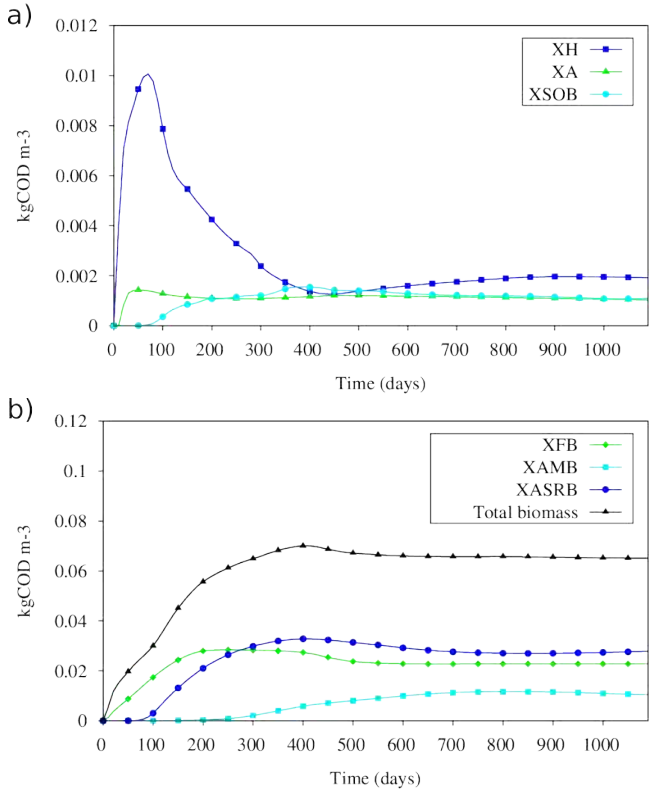

Figure 6.4: Changes in the average concentration of a) heterotrophic (X_H), nitrifiying (X_A) and sulfide oxidising (X_{SOB}) bacteria and b) fermenting (X_{FB}), sulphate reducing (X_{ASRB}) and methanogenic (X_{AMB}) bacteria ($kgCOD \cdot m^{-3}$) within the entire wetland through 3 years of operation. Total biomass ($X_H + X_A + X_{FB} + X_{AMB} + X_{ASRB} + X_{SOB}$) is also represented in image b). The separation of bacteria groups in two graphs is made to facilitate visualisation of the results. Note that y-axis scales of the two captions are different.

According to these results, the wetland was dominated by anaerobic bacteria (X_{FB}, X_{AMB} and X_{ASRB}) ($56 - 95\%$) for the majority of the time (from c.a. day 80), while aerobic groups (X_H, X_A and X_{SOB}) were found at much lower proportions ($5 - 44\%$).

6.3.2 Pollutant removal efficiencies

The system achieved its maximum COD removal efficiency (94%) after c.a. 400 days, and remained higher than 90% until the end of the three years period (Figure 6.5a). From around day 80, all nitrified ammonium nitrogen was completely denitrified (Figure 6.5b), and the average removal of total nitrogen from then and until the end of the three years was $20 - 30\%$. Bacterial assimilation was responsible for $4 - 10\%$ of the removed total N and nitrification-denitrification processes accounted

for $20 - 30\%$ (Figure 6.6). The rest of the total N removed from inlet to outlet corresponds to accumulated organic nitrogen (manly in the form of X_{If}) (results not shown). Note that most of the effluent nitrogen was in the form of ammonium and ammonia (S_{NH}). Sulphur was not removed within the system. However, a significant amount of the influent sulphate (S_{SO4}) was reduced to sulphide (S_{H2S}), and the opposite process also took place. From c.a. day 110 and until the end of the simulated period, the effluent concentrations of S_{H2S} exceeded that of S_{SO4} (Figure 6.5c), indicating intense sulphate reducing activity.

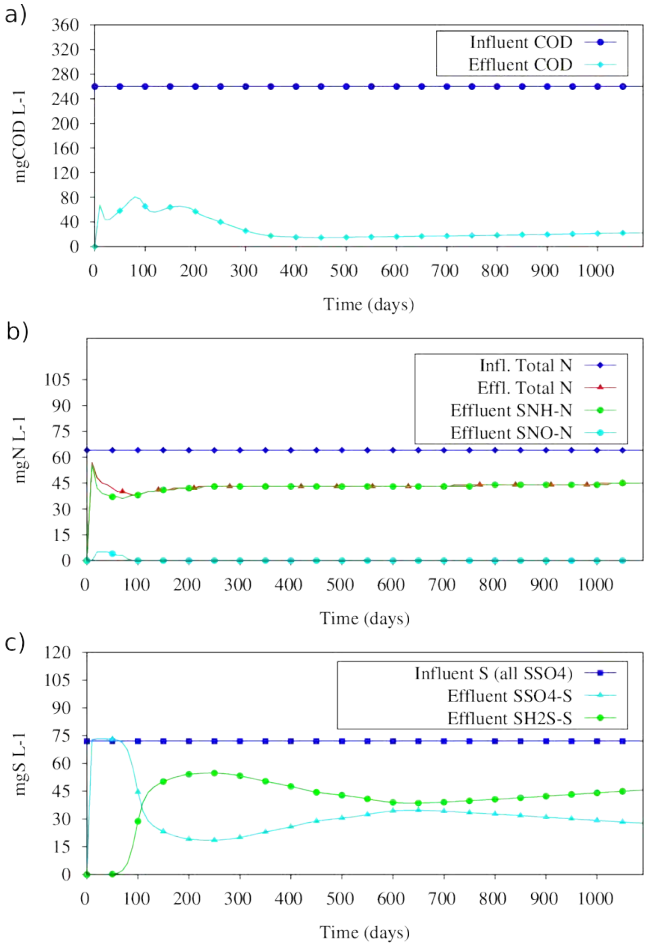

Figure 6.5: Changes in effluent concentrations of a) total COD ($mgCOD \cdot L^{-1}$), b) total, ammonium and ammonia (S_{NH}) and nitrite and nitrate (S_{NO}) nitrogen ($mgN \cdot L^{-1}$) and c) sulphate (S_{SO4}) and dihydrogensulphide (S_{H2S}) sulphur ($mgS \cdot L^{-1}$). Influent concentrations of total COD, total N and S are also represented for comparison. Note that total N includes S_{NH}, S_{NO} and organic nitrogen.

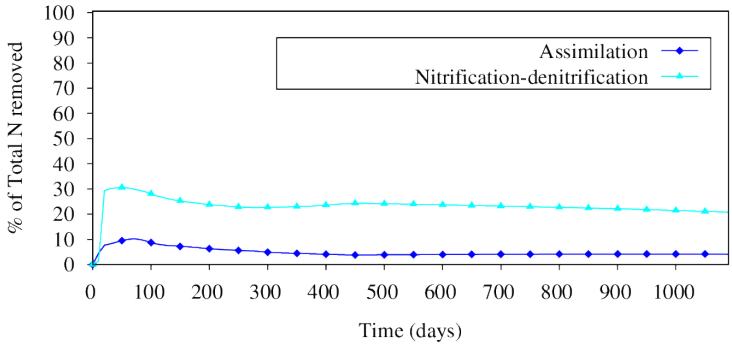

Figure 6.6: Percentage of the total N removed by bacterial assimilation and by nitrification-denitrification processes through the 3 years period. Note that the percentage was referred to the amount of total nitrogen removed and not to the influent total nitrogen.

6.3.3 Bacterial stability

Indicators of bacterial stability

Bacterial stabilisation was studied using three different indicators. The first indicator was the total bacterial biomass, which stabilised after c.a. 400 days (Figure 6.4). At that time, progressive increase in methanogenic bacteria (X_{AMB}) biomass was compensated with an equivalent decrease of sulphate reducing bacteria (X_{ASRB}) biomass, while the total biomass remained almost constant.

The second indicator of stability was the stabilisation of the effluent pollutant concentrations. In the case of total COD, its concentration reached almost constant values after c.a. 400 days (Figure 6.5a). After that the accumulated variation of the effluent COD until the end of the 3 years period was smaller than 8 $mgCOD \cdot L^{-1}$. On the other hand, total nitrogen effluent concentrations reached a steady-state from day c.a. 250. After that time effluent concentrations of this component increased slightly until the end of the 3 years period (accumulated change of 2 $mgN \cdot L^{-1}$) (Figure 6.5b). Finally, effluent concentrations of sulphate (S_{SO4}) and dihydrogensulphide (S_{H2S}) did not stabilise at all, although the accumulated changes in their respective effluent concentrations were lower than 15 $mgS \cdot L^{-1}$ after c.a. day 240 (Figure 6.5c).

Shannon diversity index was the third indicator of stability. Figure 6.7 shows that the diversity at day 0 was the highest, as all bacteria groups were in the same proportions (0.001 $mgCOD \cdot L^{-1}$). From then, the value of the diversity index decreased, reaching its minimum after c.a. 10 days, coinciding with the explosive growth of heterotrophic bacteria (X_H) and fermenting bacteria (X_{FB}), while the

biomass of the other groups remained negligible. After that, the diversity increased and it was only after c.a. 700 days that it reached its higher and stable values.

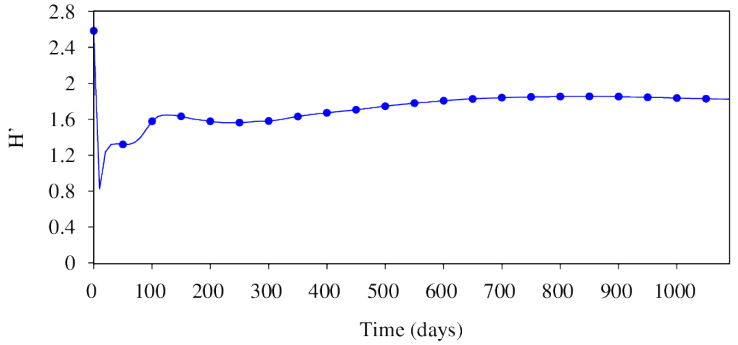

Figure 6.7: Changes in Shannon diversity index (H').

Bacterial distribution after stabilisation

In this section we present the results of bacteria distribution after 580 days (Figure 6.8), which falls in the period when bacterial stability is reached according to the results of the different indicators shown above (between 400 and 700 days). This results show a clear separation between the areas occupied by aerobic bacteria (X_H, X_A and X_{SOB}) and those occupied by anaerobic bacteria (X_{FB}, X_{AMB} and X_{ASRB}). The absence of bacteria in the inlet section observed after 580 days was due to the high concentration of accumulated inert solids, which occupied the porosity in this area and prevented further bacteria growth (Figure 6.9). Fermenting bacteria (X_{FB}) were located the closest to the inlet and occupied the entire depth of the wetland. In the aerobic layer, heterotrophic bacteria (X_H) achieved its highest concentrations also close to the inlet but further to the outlet than fermenting bacteria (X_{FB}). Nitrifying bacteria (X_A) grew just behind heterotrophic bacteria (X_H), in the areas where there was not enough COD to sustain X_H growth and hence with dissolved oxygen (S_O) availability. Due to the strong competence for oxygen with heterotrophic (X_H) and nitrifying (X_A) bacteria, to the low concentration of S_{H2S} in the aerobic layer (Figure 6.11), sulphide oxidising bacteria (X_{SOB}) grew mainly in anoxic conditions (Figure 6.10), benefiting from the nitrate (S_{NO}) produced by nitrifying bacteria (X_A), and for that reason grew mostly after the main location of X_A (Figures 6.8c and 6.10). In the anaerobic zone and from inlet to outlet, sulphate reducing bacteria (X_{ASRB}) grew just after fermenting bacteria (X_{FB}) and followed by methanogenic bacteria (X_{AMB}). X_{ASRB} and X_{AMB} also showed both vertical and longitudinal gradients, with decreasing bacteria concentrations from inlet to outlet and from the bottom to the surface of the wetland. Although the active bacteria zone in our system was very narrow, especially in the anaerobic region, note that bacteria biomass was detected in the whole wetland (results not shown).

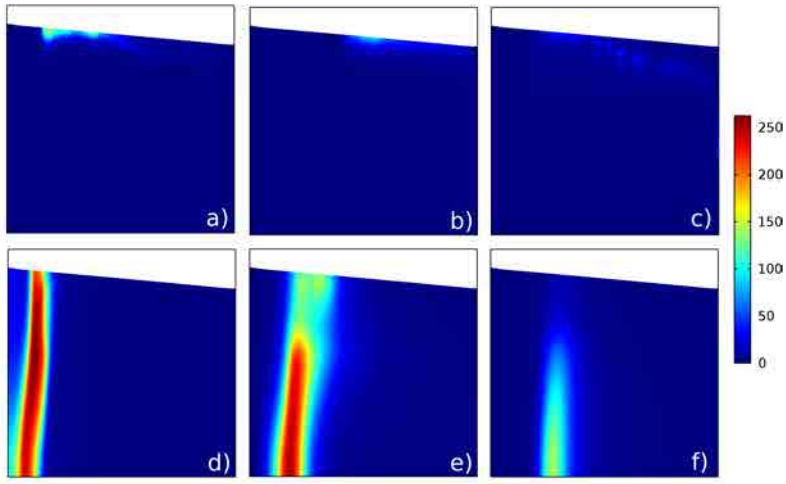

Figure 6.8: Distribution of a) heterotrophic (X_H), b) nitrifiying (X_A), c) sulphide oxidizing (X_{SOB}), d) fermenting (X_{FB}), e) sulphate reducing (X_{ASRB}) and f) methanogenic (X_{AMB}) bacteria after 580 days of operation. The key at the right indicates bacteria concentration in $mgCOD \cdot L^{-1}$. Note that the images are longitudinal cross sections of the wetland which have been deformed to fit a reasonable size. The x-axis of each image represents the longitudinal direction of the wetland (from 0 to 10.3 m) and the y-axis the depth of the wetland (from 0 to 0.7 m). Also note that the coloured areas of each image correspond to wetted areas, while the white areas correspond to areas without water. Note that water level decreases from inlet to outlet.

Despite the three indicators of stability and the total biomass of each bacteria group remained almost constant after bacteria stability, Figure 6.9 shows that the location of the active bacteria zone kept varying. This resulted from the negative effect of accumulated inert solids on the growth of bacteria. Indeed, although the biomass and distribution of all bacteria groups remained constant, the progressive advance of accumulated inert solids from inlet to outlet pushed the active bacteria in the same direction with time.

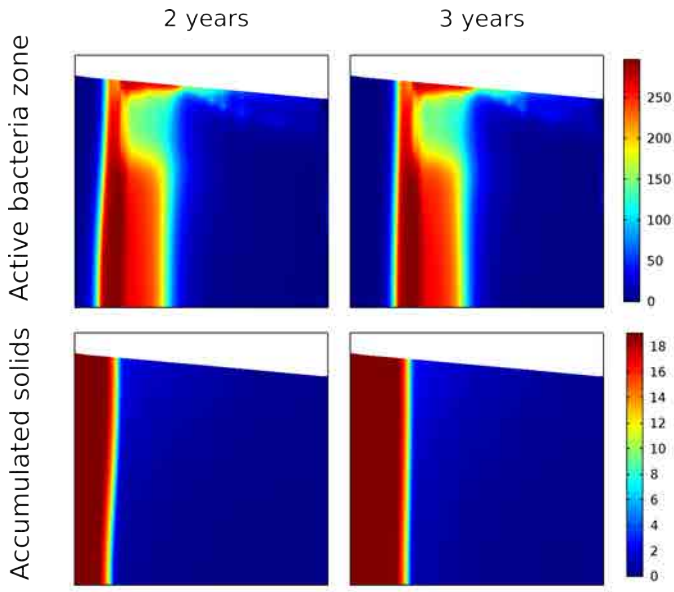

Figure 6.9: Active bacteria zone and accumulated solids concentrations after 2 and 3 years.

6.4 Discussion

6.4.1 Overall bacteria dynamics

The high energy yields of aerobic bacteria (Faulwetter et al., 2009; Mitsch and Gosselink, 2000) combined with the high availability of dissolved oxygen (S_O) at the very beginning of operation made heterotrophic bacteria (X_H) the most abundant and widely distributed bacteria group at that time (Figures 6.3 and 6.4). Fermenting bacteria (X_{FB}) were also present near the inlet section, since the concentration of S_O in the influent wastewater is usually very small (Tyroller et al., 2010) and in our simulation it was set to zero. This result, together with the intense oxygen inhibition on the initial development of anaerobic bacteria (Figure 6.2) had not been previously reported.

Heterotrophic, nitrifying and sulphide oxidising bacteria (X_H, X_A and X_{SOB}) compete for available oxygen in SSF CWs (Faulwetter et al., 2009; Nogueira et al., 2002; Okabe et al., 1996; Schramm et al., 1996; Wu et al., 2013). As the specific growth rate of heterotrophic bacteria (X_H) is higher than that of nitrifying bacteria (X_A), the latter group was only able to grow once COD concentrations near the wetlands surface were already low (low X_H biomass and high S_O concentrations). Moreover, the low biomass of X_A obtained in our simulation (between 1 and 2% of the total biomass from day 400) is in agreement with the results by Krasnits et al. (2009), who found nitrifying bacteria to account for $1 - 3\%$ of the total biomass.

Kalin and Caetano Chaves (2003) and Wiessner et al. (2005) attributed less effective and more variable sulphate removal rates in new SSF CWs to either insufficient time for sulphate reducing bacteria establishment or acclimatization. In the present study this delay was related to the low acetate (S_A) concentrations in the influent wastewater, which only increased after enough fermenting bacteria (X_{FB}) biomass was present (after around 50 days). Sulphate reducing bacteria (X_{ASRB}) and methanogenic bacteria (X_{AMB}) are known to compete for available carbon (S_A in BIO_PORE) at similar redox levels (Faulwetter et al., 2009; Huang et al., 2005). Previous studies suggest that when these two bacteria groups grow together and the COD/sulphate ratio (expressed as COD:S) is lower than 1.5, sulphate reducing bacteria are able to outcompete methanogenic bacteria. When the ratio is greater than 6, X_{AMB} predominate over X_{ASRB} (Stein et al., 2007). In the scenario assumed in the present study this ratio was 3.6 (between 1.5 and 6) and the two bacteria groups coexisted, although X_{ASRB} grew significantly faster and accounted for higher biomass than X_{AMB} (46% of the total microbial count after 580 days). However, it has to be noted that sulphate and dihydrogensulphide sulphur concentrations within the wetland may be slightly higher than in reality since the main sulphur removal mechanisms (precipitation, adsorption, volatilisation and plant uptake (Wu et al., 2013)) were not considered. Therefore sulphate reducing and sulphide oxidising bacteria biomasses may have been slightly overestimated. Such intense sulphate reducing activity produced high dihydrogensulphide (S_{H2S}) concentrations within the system that allowed a sustained growth of sulphide reducing bacteria (X_{SOB}) from c.a. day 50. However at that time nitrifying bacteria (X_A) had already reached their maximum concentration and were consuming most of the available dissolved oxygen (S_O). Therefore the growth of X_{SOB} was slower, as it took place mainly using nitrate (S_{NO}) as electron acceptor (anoxic growth) (Figure 6.10).

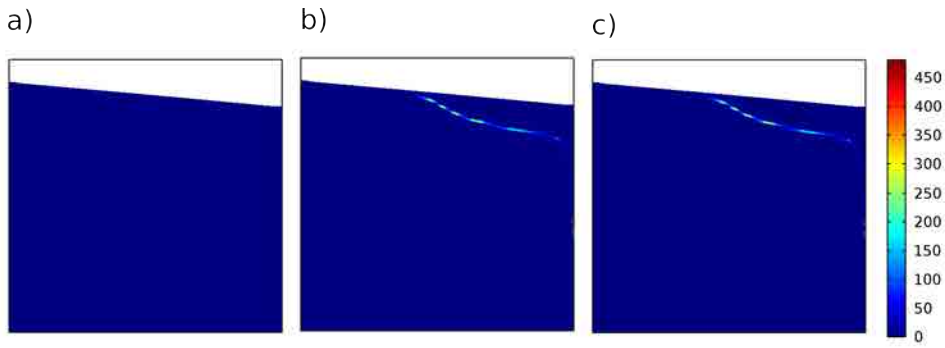

Figure 6.10: Denitrification rate ($mgS_{NO} \cdot L^{-1}d^{-1}$) by a) heterotrophic ($X_H$), b) sulphide oxidising (X_{SOB}) and c) X_H and X_{SOB} together.

Another consequence of the high dihydrogensulphide (S_{H2S}) concentrations observed within the system was their toxicity to some bacteria groups, especially those growing in the anaerobic layer (Figure 6.11). Indeed, high concentrations of S_{H2S} are

known to cause severe deterioration and pose a serious threat to wetlands ecosystems and their microbial communities (Wu et al., 2013). This effect combined with the competence for COD (S_A) with sulphate reducing bacteria (X_{ASRB}) may have also contributed to the delay observed in the growth of methanogenic bacteria (X_{AMB}) (Figure 6.3b).

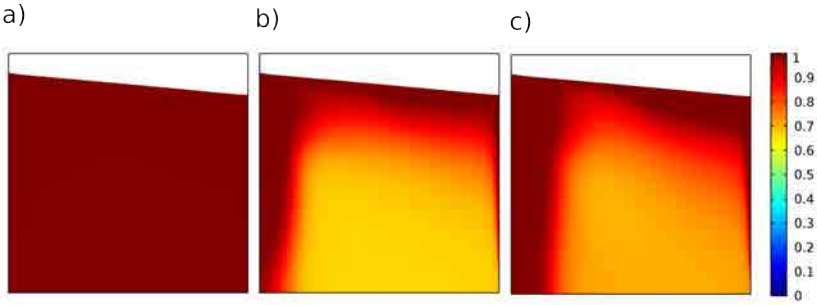

Figure 6.11: Representation of the inhibition term of hydrogen sulphide (S_{H2S}) on all bacteria groups at a) 50, b) 240 and c) 580 days after starting operation. Unitless. This is a representation of the term $K_{SH2S}/(K_{SH2S} + S_{H2S})$ which multiplies the maximum growth rate of each bacteria group. Values close to 1 indicate that sulphide is not inhibiting the growth of bacteria group X, while values close to zero indicate 100% inhibition. Note that the images are longitudinal cross sections of the wetland which have been deformed to fit a reasonable size. The x-axis of each image represents the longitudinal direction of the wetland (from 0 to 10.3 m) and the y-axis the depth of the wetland (from 0 to 0.7 m). Also note that the coloured areas of each image correspond to wetted areas, while the white areas correspond to areas without water. Note that water level decreases from inlet to outlet.

6.4.2 Pollutant removal efficiencies

The low effluent COD concentrations observed in the present study (Figure 6.5a) are attributed to the high water temperature used in our simulation (20 $°C$), which boosted microbial activity (Truu et al., 2009), and to the intense sulphate reduction observed. It is well known that sulphate reduction can contribute significantly to the removal of organic matter in SSF CWs (Aguirre et al., 2005; García et al., 2005, 2004b; Wu et al., 2013). In fact, García et al. (2004b) estimated the removal of organic matter by sulphate reduction to be between 47% and 79% in the same pilot wetland assumed in the present study. In another work, Baptista et al. (2003) attributed 25% of the carbon removal to the activity of sulphate reducing bacteria (X_{ASRB}). However, in our simulations both sulphate reducing bacteria (X_{ASRB}) and sulphide oxidising bacteria (X_{SOB}) might have been slightly overestimated by not considering all processes related to the sulphur cycle. This can also be observed with the high percentage of sulphate reduced within the wetland (between 51 and 72% of the total influent S_{SO4} from day c.a. 220). In comparison, Krasnits et al. (2009) measured a 40% removal of sulphate, although in their case the proportion

of sulphate reducing bacteria was also smaller ($21 - 30\%$ against 46% in the current work).

In our simulation accumulation was the main removal mechanism for N, followed by nitrification and bacterial assimilation. The fact that all nitrified nitrogen (S_{NO}) was used as electron acceptor and hence removed (Figure 6.5b) is also in agreement with the large decrease in nitrate observed in most horizontal SSF CWs, indicating that denitrification is an important process in these systems (Faulwetter et al., 2009; Kadlec, 2005; Vymazal, 2007). Another relevant result from this study was that sulphide oxidising bacteria (X_{SOB}) was the group that most significantly contributed to denitrification (Figure 6.10), and therefore autotrophic denitrification was more important than heterotrophic denitrification.

6.4.3 Bacterial stability

Indicators of bacterial stability

Experimental evidences indicate that extended periods of time are required for microbial communities in SSF CWs to stabilise, although the basis used to indicate community stability is not always consistent (Ramond et al., 2012; Truu et al., 2009; Weber and Legge, 2011). In the available studies it is considered that bacterial stability is reached when the number of strains stops changing. However, if only the number of strains is taken into account, we can think that the system has reached bacterial stability, while the relative biomass of every bacterial strain may still be changing. For this reason, in the present study bacterial stability was not only studied by observing the behaviour of the total biomass and the effluent pollutant concentrations, but also taking into account the changes on the proportions of each bacterial group through time. To that end, Shannon diversity index was used, which is a function commonly used in population ecology and incorporates both the abundance and evenness of the species present in a unified parameter.

Combining the information provided by the three indicators, it is apparent that bacteria stabilisation in our wetland occurred between c.a. 400 and 700 days after starting operation. This was, despite the biomass of all bacteria groups, the effluent pollutant concentrations and Shannon index were not perfectly stable at that time. These results differ from the available experimental studies, according to which bacteria stability is reached between 75 and 100 days (Ramond et al., 2012; Truu et al., 2009; Weber and Legge, 2011). These differences can be mainly explained by the different criterion utilised to define bacterial stability. Another plausible explanation is related to the composition of the influent wastewater. Indeed, 50% of the COD in our wastewater was particulate, and thus required a previous hydrolysis to become available to all bacterial groups, hence delaying the overall bacteria development. This fact combined with the low percentage of acetate (S_A, 20%) in the influent

and the high toxicity resulting from intense sulphate reduction (high dihydrogen sulphide (S_{H2S}) concentrations) (Figure 6.11), delayed the growth of methanogenic bacteria (X_{AMB}) and sulphate reducing bacteria (X_{ASRB}), and therefore the global stability.

Bacterial distribution after stabilisation

In our simulation aerobic bacteria groups (X_H, X_A and X_{SOB}) were dominant near the surface of the wetland (Figures 6.8a, b and c) while anaerobic bacteria grew in deeper sections (Figures 6.8d, e and f). This is consistent with the generally accepted idea that S_O concentrations tend to increase towards the outlet and decrease towards the bottom of the wetland (Allen et al., 2002; García et al., 2003; Headley et al., 2005; Wang et al., 2012); thus the potential of microbial processes depending on oxygen tend to be more pronounced in the upper strata and near the outlet of the wetland, while low oxygen conditions favour anaerobic processes (Kern, 2003; Nurk et al., 2005; Truu et al., 2009).

In the aerobic layer, heterotrophic bacteria (X_H) were dominant close to the inlet owing to the high COD availability. The highest concentrations of nitrifying bacteria (X_A) were measured from the centre to the outlet of the wetland. Similarly, Nurk et al. (2005) observed higher nitrifying bacteria biomass near the outlet of a wetland. The fact that in our simulations sulphate reducing bacteria (X_{SOB}) were seen to grow near the outlet, and essentially under anoxic conditions (Figures 6.8c and 6.10b) is of particular importance since only a few studies address the activity of this bacteria group in treatment wetlands (Faulwetter et al., 2009).

Regarding anaerobic bacteria, the lack of S_O in the influent wastewater made fermenting bacteria (X_{FB}) the dominant bacteria group close to the inlet and at all depths (Figure 6.8d). Sulphate reducing (X_{ASRB}) and methanogenic (X_{AMB}) bacteria grew in the anaerobic zone and just after X_{FB} (Figures 6.8e and 6.8f), as they degrade a product of fermentation (acetate, S_A).

The narrow bacteria distribution obtained in our simulations can be attributed to the presence of accumulated inert solids (Figure 6.9) and to the toxicity effects of S_{H2S} (Figure 6.11), which hindered bacteria growth near the inlet section and after the location of X_{ASRB} respectively.

Figure 6.9 illustrates that the driving force behind the displacement of the active zone after bacterial stabilisation was the accumulation of inert solids. Nguyen (2000) found that more than 90% of the OM accumulated in a SSF CWs receiving farm dairy wastewater over a 5-year period was composed of inert OM fractions. These solids not only limit substrates availability but also reduce the available space for bacteria to grow (Samsó and García, 2013a). Our simulation results show that accumulated solids from the influent wastewater were higher near the inlet as a combined effect

of physical filtration and bacteria decay (Figure 6.9). This phenomenon is already well documented in literature (Caselles-Osorio et al., 2007; Nguyen, 2000). The displacement of the active zone resulting from solids accumulation has not been documented in any previous studies, and should therefore be studied in more detail in further experimental works.

6.5 Conclusions

In this chapter, simulation results for a period of 3 years with BIO_PORE model (Samsó and García, 2013a) were presented to study bacteria dynamics and distribution in the pilot CW.

At the start-up period heterotrophic bacteria (X_H) were the first group to develop and colonize the system. After day 80 and until the end of the 3 years anaerobic bacteria groups dominated the system, being sulphate reducing bacteria (X_{ASRB}) the most abundant group in terms of overall biomass ($47 - 79\%$) for most of the time. The high sulphate reducing activity within the wetland caused toxicity by dihydrogensulphide (S_{H2S}) and delayed the growth of methanogenic bacteria (X_{AMB}). Nitrifying bacteria (X_A) accounted for $1-2\%$ of the total biomass while sulphide oxidising bacteria (X_{SOB}) grew mainly under anoxic conditions and were responsible for the complete denitrification observed in the wetland (autotrophic denitrification).

Bacterial stability was achieved between 400 and 700 days after starting operation. This time to stability is longer than the $75 - 100$ days reported by previous experimental works, although the criteria for bacterial stabilisation is different from the ones used in this work. After bacteria stability X_H and X_A occupied the first few centimetres near the wetlands surface, where oxygen concentrations were higher while X_{FB}, X_{AMB} and X_{ASRB} grew on the rest of the wetland and thus had a much wider vertical distribution. X_{SOB} grew in a very restricted area near the outlet of the bed in which high S_{H2S} and S_{NO} concentrations coexisted.

The driving force behind the displacement of bacteria after stability was the progressive advance of accumulated inert particulate solids (X_{If}) towards the outlet of the wetland, which pushed the active bacteria zone in the same direction.

The results of this study coupled with previous field results will give new insights and perspectives on wetland functioning. This chapter is just a stepping stone towards the end goal of establishing a general conceptual framework of the functioning of constructed wetlands based on modelling results.

CHAPTER 7

The cartridge theory

This chapter is based on the article:

- Samsó, R., García, J., 2014a. The Cartridge Theory: a description of the functioning of horizontal subsurface flow constructed wetlands for wastewater treatment, based on modelling results. Science of The Total Environment 473-474, 651658. doi:10.1016/j.scitotenv.2013.12.070.

7.1 Introduction

Subsurface flow constructed wetlands (SSF CWs) are complex reactors in which different physical, chemical and biochemical reactions take place simultaneously. Nowadays the available knowledge on this technology is mostly empirical and very case-specific and for this reason it is very difficult to elucidate which are the most fundamental functioning patterns of these systems. In fact, there is still not a clear overall understanding of the interrelations of all processes taking place within these systems (Kumar and Zhao, 2011; Langergraber, 2007). In our opinion, understanding the basics of the internal functioning of wetlands is a crucial step towards making this technology more efficient, predictable and reliable in the forthcoming years. It will also help us clearly identify and define what we can expect from this technology and decide whether it is the best option in every specific case.

Since the application of numerical models to SSF CWs, they have been seen as a potential tool to brighten the "black box" to which these systems have usually been assimilated. Although most of the available models include equations to simulate a large proportion of the processes that take place within SSF CWs (Langergraber and Simunek, 2012; Llorens et al., 2011a,b; Mburu et al., 2012; Ojeda et al., 2008; Rousseau et al., 2005), so far most efforts have been put on matching measured effluent pollutant concentrations and, in general, less attention has been given to describing the internal dynamics of the wetlands. Acknowledging this fact, the BIO_PORE model was developed with the main aim of improving the understanding of SSF CWs' internal functioning, and more specifically on the interrelations between bacterial communities and accumulated solids in the long-term.

In this chapter we introduce what we named *The Cartridge Theory* for horizontal subsurface flow constructed wetlands (HSSF CWs), which is a description of their functioning based on the interaction between accumulated solids (leading to clogging) and bacterial populations. This theory intends to be as generic as possible, and for this reason it presents a simplified and thus ideal perspective of how wetlands function. Generally speaking, this theory assimilates the progressive clogging of HSSF CWs granular media to the consumption of a generic cartridge and was developed from a combination of our practical knowledge on CWs, and from the deep understanding of the main treatment processes gained during the development and application of the BIO_PORE model (Samsó and García, 2013a,b).

Since the presented theory is mostly based on simulation results obtained with BIO_PORE model, in this chapter we first justify the changes applied to the original formulation of CWM1 so that the resulting growth of bacterial communities is consistent with an existing and widely accepted population dynamics model (Verhulst, 1838). We do that by individually studying the evolution of the biomass of a single functional bacterial group (fermenting bacteria) in a specific point near the inlet section of a HSSF CW. This study brings up a discussion of how bacterial communities interact with each other and how they depend on the environmental conditions (e.g. accumulated solids, available space and substrates), which leads us to the final theory for horizontal subsurface-flow constructed wetlands functioning, detailed at the end of the chapter.

We expect that the current work will not only contribute to improve the way the dynamics of bacterial communities are described with current mathematical models for CWs, but will also provide a tool (the Cartridge Theory) to explain the most basic functioning patterns of HSSF CWs.

7.2 Methods

7.2.1 Pilot system used for simulations

Simulations were run for the pilot wetland presented in Chapter 3. Average measured inflow pollutant concentrations, which were used to feed the model, are given later in the text (See Table 7.1). Notice that although measured effluent pollutant concentrations are available for this system, they are not utilized in the current chapter, since the comparison of measured data and simulation results was already carried out in Chapter 4.

7.2.2 Simulation strategy

Three individual simulations ($S1$, $S2$ and $S3$) were run using incremental versions of the same equation to represent the period comprised between the start-up and the third year of operation of the pilot system. Despite a 3 year period was simulated, the time-scale of the figures presented in the results section was cropped to emphasize only the relevant data. Initial concentrations of all functional bacteria groups within the wetland were set to very low values ($0.001\ mgCOD \cdot L^{-1}$) for all three simulations to represent start-up conditions. Constant values for hydraulic loading rate ($36.6\ mm \cdot d^{-1}$), water temperature ($20°C$) and influent pollutant concentrations were used to facilitate interpretation of the model output. Influent pollutant concentrations were extracted from data averages of an experimental study carried out in the pilot wetland by García et al. (2005). The fractioning of the influent COD was made using recommended values for primary effluents in ASMs (Henze et al., 2000) (Table 7.1), which is a common practice for all models based on its formulation, since otherwise a very detailed characterisation of the influent wastewater is required. Note that in this system, the influent sulphur concentrations were higher than in average urban wastewaters, since potable water in the metropolitan area of Barcelona is partially obtained from a river that drains a chalk basin (Samsó and García, 2013b).

Plant oxygen release ($3\ gO_2 \cdot m^{-2}d^{-1}$) and S_{NH} and S_{NO} uptake ($0.2\ gN \cdot m^{-2}d^{-1}$ each) were considered to take place only on the top 30 cm of the granular media after the mixing zone. Plant effects on the hydrodynamics of the wetland were not considered in the current version of the model (Samsó and García, 2013a). Likewise, all sorts of stochastic processes known to take place in wetlands (e.g. preferential flow-paths, granular media and plant distribution heterogeneities, bacteria and solids washout) were not considered.

Table 7.1: Influent concentrations of the different wastewater components considered in CWM1 in the pilot wetland used for simulations.

Componenet	Description	Influent concentration	Unit
S_O	Dissolved oxygen	0	$mgCOD \cdot L^{-1}$
S_F	Soluble fermentable COD	39	$mgCOD \cdot L^{-1}$
S_A	Fermentation products as acetate as COD	52	$mgCOD \cdot L^{-1}$
SI	Inert soluble COD	13	$mgCOD \cdot L^{-1}$
X_{Sm}	Aqueous slowly biodegradable particulate COD	130	$mgCOD \cdot L^{-1}$
X_{Sf}	Solid slowly biodegradable particulate COD	0	$mgCOD \cdot L^{-1}$
X_{Im}	Aqueous inert particulate COD	26	$mgCOD \cdot L^{-1}$
X_{If}	Solid inert particulate COD	0	$mgCOD \cdot L^{-1}$
S_{NO}	Nitrite and nitrate nitrogen	0	$mgN \cdot L^{-1}$
S_{NH}	Anmonium and ammonia nitrogen	57	$mgN \cdot L^{-1}$
S_{SO4}	Sulphate sulphur	72	$mgS \cdot L^{-1}$
S_{H2S}	Sihydrogensulphide sulphur	0	$mgS \cdot L^{-1}$

7.3 Results and discussion

7.3.1 Modelling bacterial growth in constructed wetlands

In this section we demonstrate that the bacteria growth obtained using the original formulation of CWM1 does not satisfy the main principles of population ecology. In addition, we include two simple modifications to the original formulation which makes the BIO_PORE model comply with the stated principles. For the sake of brevity, only the growth equation of one functional bacteria group (Equations 7.1 to 7.4) is analysed. Fermenting bacteria was selected for that matter, since in a previous work this functional bacteria group was seen to exhibit the highest growth-rate close to the inlet section (Samsó and García, 2013b), and thus very short simulation times are required to exemplify the limitations of CWM1. All results in this section correspond to a point located near the inlet and near the water surface of the pilot wetland ($x = 0\ m$, $y = 0.6\ m$) (Figure 7.1), where most of the substrate concentrations are persistently very high.

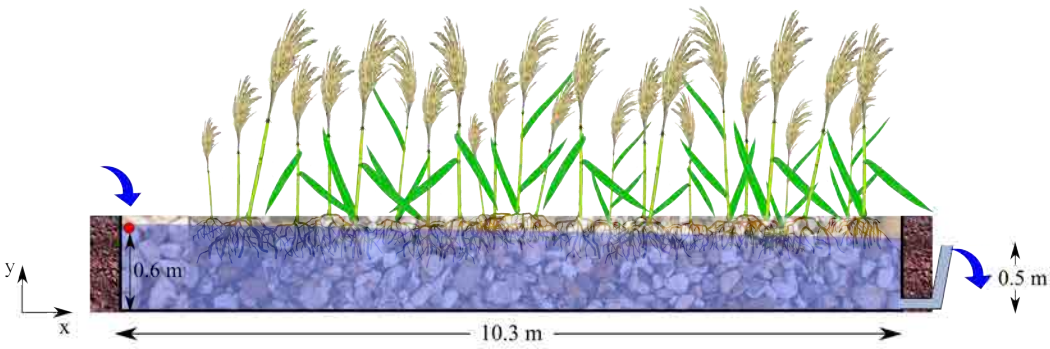

Figure 7.1: Longitudinal section of the pilot wetland. The blue arrows indicate the influent and effluent of the wetland. Note that the hydraulic head decreases towards the outlet. The red dot indicates the point where the parameters shown in Figures 7.2 to 7.7 were measured.

The concentration of fermenting bacteria (X_{FB}, in $mgCOD \cdot L^{-1}$) through time at the point near the inlet indicated in Figure 7.1 using CWM1s original formulation is obtained by solving Equation 7.1:

$$\frac{\partial X_{FB}}{\partial t} = \mu_{FB}\left(\frac{S_F}{K_{S_{FB}}+S_F}\right)\left(\frac{K_{H2SFB}}{K_{H2SFB}+S_{H2S}}\right)\left(\frac{K_{OFB}}{K_{OFB}+S_O}\right)\left(\frac{K_{NOFB}}{K_{NOFB}+S_{NO}}\right)\left(\frac{S_{NH}}{K_{NHFB}+S_{NH}}\right) - b_{FB}X_{FB} \tag{7.1}$$

The definition of the parameters, their values and units is given in Table 7.2.

Table 7.2: Values of the constant parameters of the equations describing the growth of fermenting bacteria (Equations 7.1 to 7.4). For a complete list of all parameters of CWM1 the reader is referred to Langergraber et al. (2009a) and Samsó and García (2013a,b).

Parameter	Description	Value	Unit
μ_{FB}	Specific growth-rate	3	d^{-1}
b_{FB}	Rate constant for lysis	0.02	d^{-1}
X_{FB_0}	Initial concentration	0.001	$mgCOD \cdot L^{-1}$
K_{SFB}	Saturation coefficient for S_F	28	$mgCOD \cdot L^{-1}$
K_{H2SFB}	Inhibition coefficient for S_{H2S}	140	$mgS \cdot L^{-1}$
K_{OFB}	Inhibition coefficient for S_O	0.2	$mgO_2 \cdot L^{-1}$
K_{NOFB}	Inhibition coefficient for S_{NO}	0.5	$mgN \cdot L^{-1}$
K_{NHFB}	Saturation coefficient for S_{NH}	0.01	$mgN \cdot L^{-1}$

Equation 7.1 is a first-order linear ordinary differential equation, the analytical solution of which is:

$$X_{FB}(t) = X_{FB_0} \cdot e^{\left(\mu_{FB}\left(\frac{S_F}{K_{S_{FB}}+S_F}\right)\left(\frac{K_{H2SFB}}{K_{H2SFB}+S_{H2S}}\right)\left(\frac{K_{OFB}}{K_{OFB}+S_O}\right)\left(\frac{K_{NOFB}}{K_{NOFB}+S_{NO}}\right)\left(\frac{S_{NH}}{K_{NHFB}+S_{NH}}\right) - b_{FB}\right)t} \tag{7.2}$$

Therefore, with CWM1s original formulation the growth of bacteria follows an exponential tendency (Equation 7.2), which in the population ecology discipline is known as Malthusian or exponential growth. In a situation where substrates concentrations are not limiting, such as in the inlet section of continuously fed CWs, Equation 7.2 predicts very high bacterial densities after very short time-frames. However, Malthusian growth is only realistic when the density of organisms is relatively low, since for high bacterial densities the competition for space and resources hinders the production of new bacterial cells (Stanescu and Chen-Charpentier, 2009).

Simulation S1: Bacterial growth with CWM1s original formulation

A first run of the BIO_PORE model (simulation $S1$) with the original formulation of CWM1 (as in Equation 7.1) confirms that after around 25 days of operation fermenting bacteria concentrations near the inlet (point indicated in Figure 7.1) are already very high and unrealistic (in the order of magnitude of hundreds of grams of COD per litre) (Figure 7.2). These bacterial hot spots develop even with average values of the product of the Monod switching functions (around 0.6). Notice that this product can range from 0 (substrates scarcity and/or high concentration of inhibitors) to 1 (high substrates availability and/or low concentration of inhibitors).

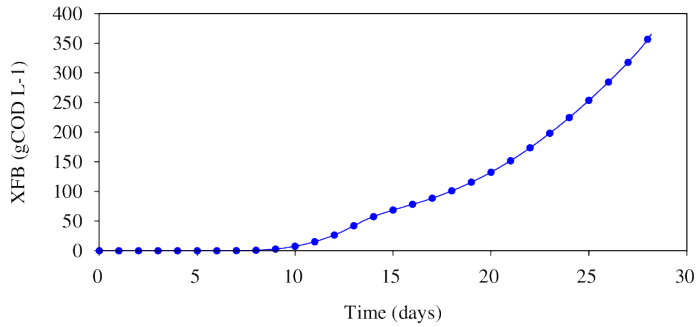

Figure 7.2: Fermenting bacteria concentrations (X_{FB}) (in $gCOD \cdot L^{-1}$) over time obtained from simulation $S1$ at the point indicated in Figure 7.1. Note that $S1$ was run considering start-up conditions and for this reason the concentration of bacteria was very low at the beginning. Note that simulation $S1$ was stopped before day 30 since the big gradients of bacteria concentration generated before that time prevented convergence of numerical solutions.

Simulation S2: Effect of increasing bacterial densities on bacterial growth

To prevent limitless bacterial growth and the formation of bacteria hot spots near the inlet section, we included a linear function of the total bacterial density (M_{bio}) on the growth rate expression of each bacteria group. This function, which was proposed by *Pierre Franois Verhulst* back in the XIXth century (Verhulst, 1838) and

has later been used in several bioclogging studies (Brovelli et al., 2009b), adds a negative feed-back on the growth rate since its value decreases with increasing total bacterial density. Equation 7.3 represents the growth rate expression of fermenting bacteria (as in Equation 7.1) with the inclusion of the negative feed-back term.

$$\frac{\partial X_{FB}}{\partial t} = \mu_{FB}\left(1-\frac{M_{bio}}{M_{biomax}}\right)\left(\frac{S_F}{K_{S_{FB}}+S_F}\right)\left(\frac{K_{H2SFB}}{K_{H2SFB}+S_{H2S}}\right)\left(\frac{K_{OFB}}{K_{OFB}+S_O}\right)\left(\frac{K_{NOFB}}{K_{NOFB}+S_{NO}}\right)\left(\frac{S_{NH}}{K_{NHFB}+S_{NH}}\right) - b_{FB}X_{FB} \tag{7.3}$$

Where, M_{bio} ($kgVS \cdot m^{-3}$ of granular material) is the sum of to the biomass concentration of all bacterial groups (heterotrophic, nitrifying, fermenting, acetotrophic methanogenic, acetotrophic sulphate reducing and sulphyde oxidyising bacteria). M_{bio_max} ($kgVS \cdot m^{-3}$ of granular material) is the carrying capacity of the environment, whichis a constant value that corresponds to the maximum concentration of bacteria that can be attained in a specific volume of granular material. In fact, this is an empirical value, which is usually smaller than porositys capacity (Brovelli et al., 2009b), and needs to be found for every specific wetland.

Figure 7.3 was obtained from a new simulation ($S2$) following the same procedure as for $S1$ but with the inclusion of the negative feed-back term to the growth expression (as in Equation 7.3). This simulation was carried out considering $M_{bio\_max} = 0.093\ kgVS \cdot m^{-3}$ of granular material ($300 mgCOD \cdot L^{-1}$ of water, considering a porosity of 0.4 and assuming $1\ gVS = 1.42\ g$ suspended COD (Wanner et al., 2006)). The value of M_{bio_max} was obtained during calibration of BIO_PORE model, which was conducted for the same pilot wetland (Samsó and García, 2013a). With the inclusion of the negative feed-back term fermenting bacteria growth follows a logistic curve (Stanescu and Chen-Charpentier, 2009) (Figure 7.3). The exponential phase is stopped after around 15 days, when total bacterial biomass in the studied point reaches the carrying capacity of the system ($M_{bio} = M_{bio\_max}$) and thus $\left(1-\frac{M_{bio}}{M_{bio\_max}}\right)$ turns 0 (Figure 7.4). Figure 7.3 also shows that fermenting bacteria concentrations become constant after the total bacterial biomass reaches the carrying capacity of the system.

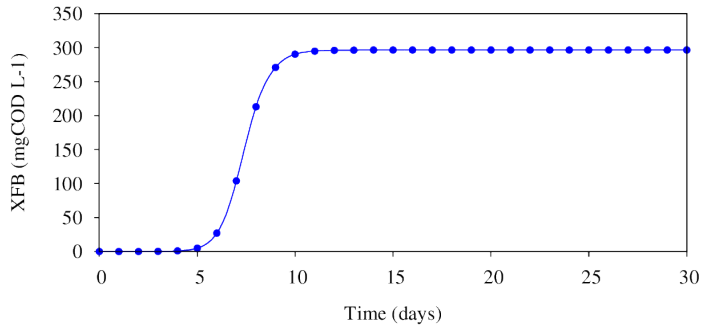

Figure 7.3: Fermenting bacteria concentrations (X_{FB}) over time obtained from simulation $S2$ (including the negative feed-back term $\left(1 - \frac{M_{bio}}{M_{bio\_max}}\right)$ to the growth expression of all bacteria groups) at the point indicated in Figure 7.1. Note that $S2$ was run considering start-up conditions and for this reason the concentration of bacteria was very low at the beginning. Also note that fermenting bacteria was the most abundant functional bacterial group near the inlet section ($M_{bio} \simeq M_{X_{FB}}$).

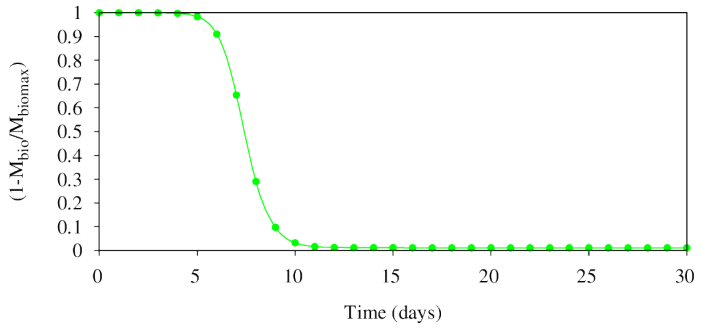

Figure 7.4: Value of the negative feed-back term $\left(1 - \frac{M_{bio}}{M_{bio\_max}}\right)$ over time obtained in $S2$ at the point indicated in Figure 7.1. Note that this value can range from 0 to 1.

Simulation S3: Effect of inert organic solids accumulation on bacterial growth

Both wastewater and dead bacteria cells contain an inert fraction which is refractory (not biodegradable or very slowly biodegradable) and accumulates in the granular media, causing its progressive clogging (García et al., 2010; Hua et al., 2013; Knowles et al., 2011; Nguyen, 2000). In CWM1, the soluble and particulate inert fractions of wastewater are represented with the variables S_I and X_I respectively (both in $mgCOD \cdot L^{-1}$). Likewise, CWM1 defines that all bacteria cells contain a 10% of inert solids in the form of X_I (see parameter $f_{BM,X_I} = 0.1 \frac{gCOD_{X_I}}{gCOD_{biomass}}$ in Langergraber et al. (2009a)).

Notice, as well, that inorganic solids coming with the influent wastewater or arising from reactions with the filter media are not considered in BIO_PORE. Also,

although particulate biodegradable solids (X_S in CWM1) can occupy pore space and contribute to clogging, in this work they are considered not to cause any effect on bacterial communities since the volume occupied by this type of solids can be replaced by new bacteria cells (Samsó and García, 2013a).

The porosity reduction caused by the progressive accumulation of inert solids, which results in decreasing available space and substrates, must translate into decreasing bacteria concentrations with time. Figure 7.3 shows that this behaviour cannot be reproduced with Equation 7.3. Therefore, to account for the impact that accumulated inert solids have on the development of bacterial communities a second negative feed-back function was added to Equation 7.3:

$$\frac{\partial X_{FB}}{\partial t} = \mu_{FB}\left(1-\frac{M_{bio}}{M_{biomax}}\right)\left(1-\frac{M_{X_{If}}}{M_{cap}}\right)\left(\frac{S_F}{K_{S_{FB}}+S_F}\right)\left(\frac{K_{H2SFB}}{K_{H2SFB}+S_{H2S}}\right)\left(\frac{K_{OFB}}{K_{OFB}+S_O}\right)\left(\frac{K_{NOFB}}{K_{NOFB}+S_{NO}}\right)\left(\frac{S_{NH}}{K_{NHFB}+S_{NH}}\right)-b_{FB}X_{FB} \tag{7.4}$$

Where, $M_{X_{If}}$ ($kgVS \cdot m^{-3}$ of granular material) and M_{cap} ($kgVS \cdot m^{-3}$ of granular material) are, respectively, the actual mass of inert solids and the maximum mass of solids that fit a cubic meter of granular media. Note that biodegradable solids are not included in this new logistic function as they can be degraded and the released space can be subsequently occupied by new bacterial cells (Samsó and García, 2013a).

Figure 7.5 shows fermenting bacteria concentrations over time obtained from simulation $S3$, in which the growth of all bacteria groups is described using Equation 7.4. Simulations were run considering $M_{bio\_max} = 0.093\ kgVS \cdot m^{-3}$ of granular media ($= 300\ mgCOD \cdot L^{-1}$ of water) and $M_{cap} = 6\ kgVS \cdot m^{-3}$ of granular media ($= 19.35\ gCOD \cdot L^{-1}$ of water, considering a porosity of 0.4 and $1\ gVS = 1.42\ g$ suspended COD (Wanner et al., 2006). Note that all these values were obtained by Samsó and García (2013a) during calibration.

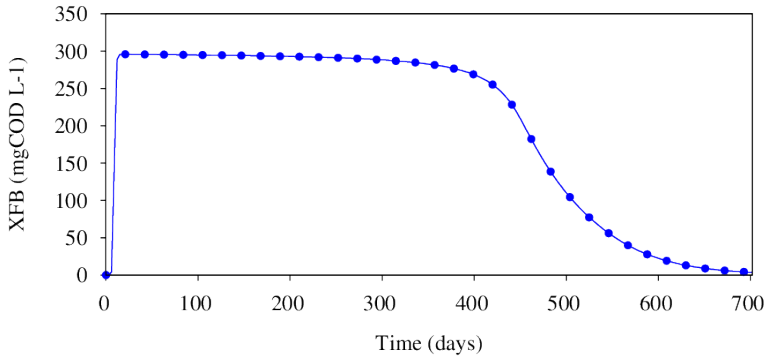

Figure 7.5: Fermenting bacteria concentrations (X_{FB}) over time obtained from simulation $S3$ (including the negative feed-back terms $\left(1 - \frac{M_{bio}}{M_{bio\_max}}\right)$ and $\left(1 - \frac{M_{X_{If}}}{M_{cap}}\right)$ to the growth expression of all bacteria groups) at the point indicated in Figure 7.1. Note that $S3$ was run considering start-up conditions and for this reason the concentration of bacteria was very low at the beginning. Also note that fermenting bacteria was the most abundant functional bacterial group near the inlet section ($M_{bio} \simeq M_{X_{FB}}$). The time-frame represented in this figure is longer than in the previous ones to depict the entire bacteria cycle.

In simulation $S3$, the initial stages of the growth of fermenting bacteria (Figure 7.5) coincide with those of simulation $S2$ (Figure 7.3): the rapid bacterial growth near the inlet section of the wetland turns the negative feed-back term $\left(1 - \frac{M_{bio}}{M_{bio\_max}}\right)$ to almost zero before day 15 (line with circles in Figure 7.6) and no net bacteria growth is observed after then. However, in this case fermenting bacteria concentrations start decreasing shortly after reaching the systems carrying capacity (M_{bio_max}) due to the increasing concentrations of accumulated inert solids ($M_{X_{If}}$) (Figure 7.7), which progressively diminish the value of the negative feed-back term $\left(1 - \frac{M_{X_{If}}}{M_{cap}}\right)$ (line with squares in Figure 7.6). After around 450 days, inert accumulated solids reach the value of M_{cap} and subsequently, the concentration of fermenting bacteria decreases more rapidly until it becomes negligible (around day 700), since dead bacterial cells are not anymore replaced with new ones. That is even when the value of the negative feed-back term $\left(1 - \frac{M_{bio}}{M_{bio\_max}}\right)$ increases again resulting from decreasing bacterial concentrations (M_{bio}) (Figure 7.6).

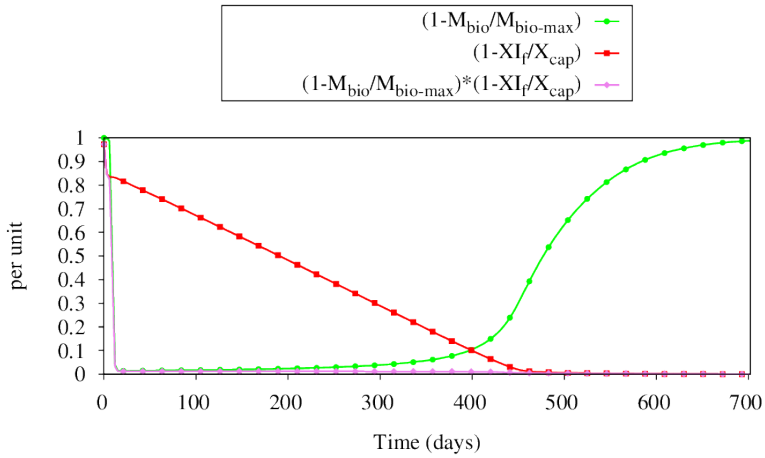

Figure 7.6: Values of the negative feed-back terms $\left(1 - \frac{M_{bio}}{M_{bio\_max}}\right)$ and $\left(1 - \frac{M_{X_{If}}}{M_{cap}}\right)$ and their product over time obtained from simulation $S3$ at the point indicated in Figure 7.1. Note that the values of these functions range from 0 to 1.

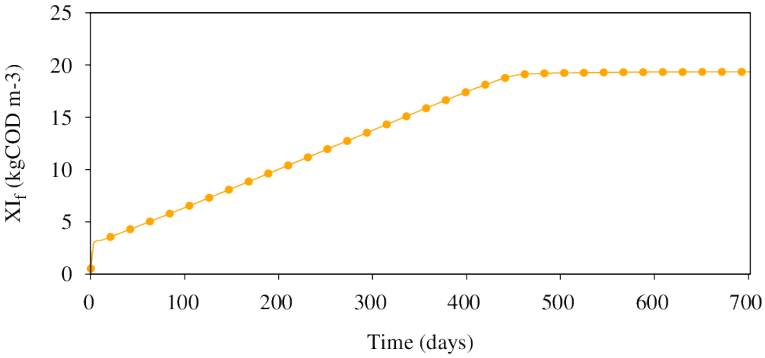

Figure 7.7: Concentration of inert solids (X_{If}, $kgCOD \cdot m^{-3}$ of water) over time obtained for simulation $S3$ in the point indicated in Figure 7.1.

7.3.2 Simulation results on bacteria distribution and solids accumulation pattern in HSSF CWs

In this section bacterial communities and inert solids concentrations obtained from simulation $S3$ are shown for the whole longitudinal section of the wetland. Figure 7.8 shows that bacteria communities after 1, 2 and 3 years of operation are distributed in a rather narrow strip in the direction of the flow, occupying approximately a third of the beds length. This is an intrinsic feature of HSSF CWs, which behave as as non-ideal plug-flow reactors in which both substrates and bacterial concentrations are much higher near the inlet section and progressively lower towards the outlet (García et al., 2010; Vacca et al., 2005). In our model, the extent of the active bacteria zone,

which is the area of the wetland where most pollutants are transformed/removed (warmer colours in Figure 7.8, depends on the value of M_{bio_max}; the higher the value of this parameter, the narrower the resulting bacteria distribution.

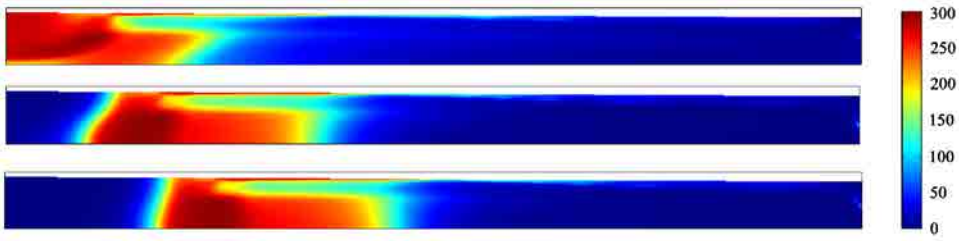

Figure 7.8: Distribution of bacteria (sum of the 6 functional groups considered in CWM1 after 1 (top), 2 (center) and 3 (bottom) years of operation of the pilot wetland obtained from simulation $S3$. The key at the right indicates bacteria concentration in $mgCOD \cdot L^{-1}$. The x-axis of each image represents the longitudinal direction of the bed (from 0 to 10.3 m) and the y-axis the depth of the bed (from 0 to 0.7 m). Also note that the coloured areas of each image correspond to wetted areas, while the white areas correspond to areas without water. Despite it is not noticeable with this colour legend, bacteria concentrations were present on the whole longitudinal section.

On the other hand, Figure 7.9 shows that inert solids coming from the influent wastewater and from dead bacteria cells initially accumulate near the inlet and progress towards the outlet with time. This accumulation pattern is responsible for the progressive displacement of the active bacteria zone observed in Figure 7.8 and is a direct consequence of the inclusion of the second negative feed-back term $\left(1 - \frac{M_{X_{If}}}{M_{cap}}\right)$, which dictates that no further bacteria growth can take place when porosity is already full with inert solids. As with M_{bio_max}, the value of M_{cap} does have a direct impact on the rate at which accumulated inert solids progress towards the outlet and hence on the bacteria displacement rate and on the predicted life-span of the wetland.

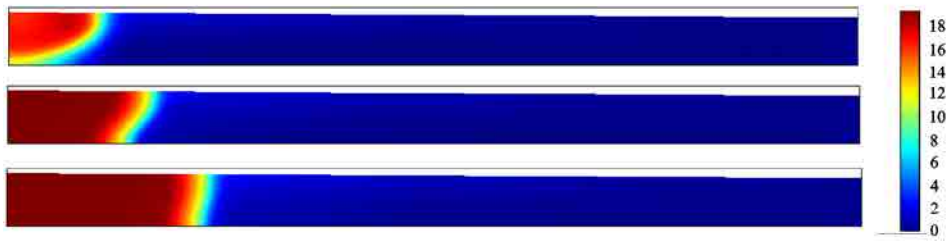

Figure 7.9: Distribution of accumulated inert solids after 1 (top), 2 (center) and 3 (bottom) years of operation of the pilot wetland obtained from simulation $S3$. The key at the right indicates inert solids concentration in $kgCOD \cdot m^{-3}$ of granular material. The x-axis of each image represents the longitudinal direction of the bed (from 0 to 10.3 m) and the y-axis the depth of the bed (from 0 to 0.7 m). Also note that the coloured areas of each image correspond to wetted areas, while the white areas correspond to areas without water.

7.4 The Cartridge Theory

The Cartridge Theory is a description of the functioning of HSSF CWs based on the interactions between bacterial communities and accumulated inert solids. This theory derives from simulation results obtained with BIO_PORE model in the current (simulation $S3$) and in Chapter 6.

The Theory states that a close interrelation exists between bacterial communities and accumulated inert solids produced from bacteria dye-off and those contained in the influent wastewater, which defines the most basic functioning patterns of all HSSF CWs. The progressive accumulation of inert solids from inlet to outlet with time causes the displacement of the active bacteria zone (area of the wetland where most pollutants transformations and degradation take place) in the same direction (Figure 7.10). This implies that wetlands have a limited life-span which corresponds to the time when bacterial communities are pushed as much towards the outlet (due to the presence of inert solids) that their biomass is not anymore sufficient to remove the desirable proportion of the influent pollutants. Note, however, that in this work the BIO_PORE model has been used to propose a reasonable theory in accordance to the current state of the art of constructed wetlands and not to make accurate predictions of the life-span of the pilot wetland. Moreover, the simulation results presented in this work correspond to a particular case, since depending on factors such as the type of municipal wastewater (primary or secondary effluents), hydraulic loading rate and method of influent distribution the rate at which clogging develops may vary (Knowles et al., 2011).

However, the functioning of our pilot wetland as described by the BIO_PORE model is in agreement with observations in field scale systems, in which although a

portion of the wetland was clogged, the systems still produced effluents of acceptable quality (Knowles et al., 2011)

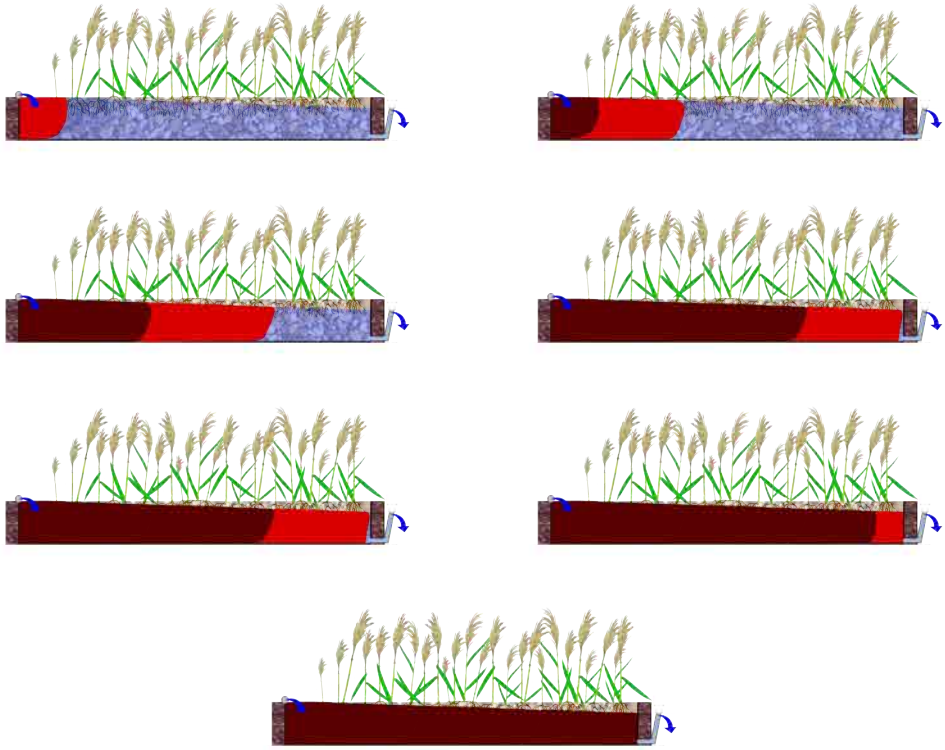

Figure 7.10: Graphical explanation of *The Cartridge Theory*. The images show the progressive accumulation of inert solids (represented in brown) and the subsequent displacement of the active bacteria zone (represented in red) from the beginning of operation and until the hypothetical complete failure of the wetland (from left to right and from top to bottom). Note that stochastic processes such as surface-flow have not been considered.

Moreover, the solids accumulation pattern described by *The Cartridge Theory* is also in agreement with reports of many authors who describe the existence of a horizontal gradient in solids accumulation from inlet to outlet (Caselles-Osorio et al., 2007; García et al., 2005; Kadlec and Watson, 1993; Nivala et al., 2012; Pedescoll et al., 2013; Tanner et al., 1998; Tanner and Sukias, 1995). Likewise, Nguyen (2000) found that up to 90% of the particulate organic matter accumulated in a pilot system treating dairy wastewater was composed of recalcitrant fractions, confirming that the accumulated solids that result in clogging of the granular media are mostly of inert nature. The narrow bacterial distribution obtained with the model is also consistent with reports of greater biofilm development at the inlet region of wetlands (García et al., 2007; Ragusa et al., 2004; Tietz et al., 2007), which the authors relate to the higher concentration of organic matter in the wastewater in this area. However the

displacement of the active bacteria zone in the direction of the flow predicted by the model has not been previously reported and should therefore be subject of further investigations.

7.5 Limitations of The Cartridge Theory

Since *The Cartridge Theory* is based on simulation results with BIO_PORE model, its limitations are inherited from the own model limitations. This model was calibrated in a previous study for effluent pollutant concentrations (Samsó and García, 2013a) but the results obtained in the current work are not validated due to the scarcity of published experimental or simulated data on bacterial distribution and solids accumulation (and their interaction) in HSSF CWs. We hope that the progressive advance of the microbiological techniques applied in CWs will soon allow verifying the results obtained with the model.

The first limitation of the theory results from the fact that CWM1 is a deterministic model, whereas HSSF CWs are known to account for a great deal of randomness; hence this theory provides an ideal description of the functioning of HSSF CWs. However, it is worth noting that in the current study all sorts of stochastic processes were deliberately ignored to provide the most general and case-insensitive theory possible. For instance, the washout of bacteria and solids is a known process that occurs in porous media for peak flow-rates (Rittmann, 1982). This phenomenon can be simulated with BIO_PORE model (Samsó and García, 2013a) but in the current study all simulations were run considering normal flow conditions to avoid any interferences of this phenomenon on the results. Moreover, BIO_PORE is a macroscopic model, and thus heterogeneities on the biofilm structure cannot be simulated.

Possibly the most important limitation of the theory rises from the fact that the changes in the hydrodynamic properties of the granular media caused by bacterial growth (Weber et al., 2011), belowground plant biomass (Knowles et al., 2011; Rousseau et al., 2005; Samsó and García, 2013a) and solids accumulation (Pedescoll et al., 2013) cannot be simulated with the current version of the model. Therefore, heterogeneous distributions of bacteria and solids caused by preferential flow-paths and from the development of overland flow (Nivala et al., 2012) are not described with *The Cartridge Theory*.

Another limitation of the model is that the widespread of bacterial communities within the granular media and the velocity at which accumulated solids progress towards the outlet depend on the values given to M_{bio_max} and M_{cap}. The value of these two parameters must be obtained for every wetland, since they will take different values depending on, for instance, the granular media properties. In this study the values of M_{bio_max} and M_{cap} where taken from calibration results in the same pilot wetland (Samsó and García, 2013a).

Moreover, a future improvement to the model formulation could correspond to making the value of the carrying capacity of the system (M_{bio_max}) dependent on the concentration of inert solids, rather than using two separate logistic functions (as in the current work). However the results obtained with this new formulation would certainly be very similar to those obtained with the current one, since the value of M_{cap} is much greater than that of M_{bio_max} and thus the effect of inert solids on bacterial communities is only apparent once the total biomass has already reached the value of M_{bio_max}.

Finally, in this work water temperature was considered constant. Although temperature does have an effect on bacterial communities, it is only noticeable on the rate of the processes and on the performance of pollutants removal, which are not subjects of discussion of the current work. However, by considering variable temperatures, the rate of clogging by inert solids obtained with the model would not change significantly, since inert solids are not degraded, and the amount of solids produced by bacterial processes in comparison to those entering the system through the inflow is very small. Moreover, in real cases it is likely that the changes of temperature on a particular CW produce intra-annual variations, which are less evident in the long term.

7.6 Conclusions

In this chapter we presented a theory on the general functioning of HSSF CWs based on the interaction between bacterial communities and accumulated solids (clogging) which was derived from simulation results with BIO_PORE model.

The theory assimilates the granular media of HSSF CWs to a generic cartridge which is consumed (clogged) with inert solids from inlet to outlet with time. The reduction of porosity caused by the accumulation of solids causes the displacement of bacterial communities, which are progressively pushed towards the outlet. According to this, the failure of a CW occurs when the active bacteria zone is located as close to the outlet section that its total biomass is not sufficient to degrade an acceptable proportion of the influent pollutants.

Although *The Cartridge Theory* may be considered as an oversimplification of the real complexity of HSSF CWs, this is the first time an integrated description of the functioning these systems is made based on modelling results and represents an important step towards the complete understanding of the functioning of these systems. This is also the first time the effect of accumulated inert solids on the development of bacterial communities is described.

CHAPTER 8

Modelling bioclogging and overland flow in CWs

This chapter is based on the article:

- Samsó, R., Forquet, N., Molle, P., García, J., 2014. Modeling bioclogging effects on the hydrodynamics of Constructed Wetlands and the subsequent overland-flow (in preparation).

8.1 Introduction

Constructed Wetlands (CWs) are a wastewater treatment technology designed to mimic and intensify the pollutants removal potential of natural wetlands. Like most subsurface environments, the granular material of these systems is prone to clogging (Knowles et al., 2011). This phenomena is responsible for severe changes in the hydrodynamic properties of the granular media i.e. the reduction of both porosity and hydraulic conductivity lead in many cases the proliferation of overland flow (Knowles et al., 2010; Nivala et al., 2012; Pedescoll et al., 2009; Soleimani et al., 2009). Mechanisms responsible of clogging in CWs include biofilm growth, chemical precipitation, filtration and plant roots development (Knowles et al., 2011; Suliman et al., 2006). After several years of clogging development, this phenomena can cause the complete failure of CWs. Accordingly, clogging is generally referred to as the main operational problem of CWs (Knowles et al., 2011; Pedescoll et al., 2011).

Experimental study of clogging is made difficult by the number of involved parameters and their non-linear cross-influence, the ability to observe non-destructively

and by the typical duration of the processes (it may take many years for a filter to be completely clogged). Numerical modelling may then be an interesting tool as it allows to observe the outcome of complex conceptual models in various experimental conditions (Oberkampf and Trucano, 2002) and to test their validity and how they enable a better understanding of the involved processes.

So far, modelling of biological clogging (bioclogging) has been the target of many studies in different disciplines, e.g. soil remediation (Seki et al., 2006), groundwater recharge (Greskowiak et al., 2005) and Aquifer Thermal Energy Storage (Bonte et al., 2013). Modelling of bioclogging requires to couple the flow and transport processes to biofilm growth and subsequent modification of the hydraulic properties. Biofilm growth can be modelled at different scales (Soleimani et al., 2009): microcolony models, biofilm models and macroscopic models. The biofilm models are the most commonly used. Similarly, hydraulic properties changes can be modelled using Thullner (2010): empirical laws derived from column experiments, conceptual models, and pore network models at the macroscopic scale. Furthermore, most attempts to simulate bioclogging have been made in saturated conditions, while only a few have focused on unsaturated conditions (Mostafa and Van Geel, 2007).

In the field of CWs, few attempts have also been made to simulate bioclogging (Hua et al., 2013; Knowles et al., 2011; Rousseau et al., 2005) using complex biokinetic models. Brovelli et al. (2009b) compared the performances of three bioclogging models derived from the three different approaches mentioned above to experimental data under saturated conditions and concluded that models were unable to reproduce long-term clogging evolution. Giraldi et al. (2009, 2010) developed a model (FITOVERT) for VF CWs that includes a bioclogging model. The latter uses an empirical law to modify the saturated hydraulic conductivity according to the biomass concentration but does not modify the unsaturated flow properties.

However there is still little experience on this field and none of them have been able to predict clogging development in the long-term operation of CWs (Nivala et al., 2012). Furthermore, in horizontal subsurface flow Constructed Wetlands (HSSF CWs) both saturated and unsaturated sites exist, and when severe clogging occurs, surface flow also develops. Therefore, to simulate bioclogging and its effects on the hydraulic and hydrodynamic functioning of CWs using numerical models, flow under these three conditions must be considered. Therefore, more research is needed to be able to simulate clogging in CWs.

In this study we compared simulation results obtained with two numerical models based on the BIO_PORE model: one accounting for the changes on the hydrodynamic properties of the granular media (by including a conceptual bioclogging model) and the other one neglecting them. Special attention was dedicated to study how the bioclogging model influences the flow distribution, the biomass development and the treatment performances.

The BIO_PORE model was built in the COMSOL Multiphysics™ simulation environment and was conceived as a tool to simulate the widest possible range of physical and biochemical processes involved in the treatment of wastewater in CWs, as well as the flux of water (Samsó and García, 2013a,b; Samsó and García, 2014a; Samsó et al., 2014b; Meyer et al., 2014). However, and despite bacterial growth and filtration processes were included, the BIO_PORE model was not suited to simulate the effects of clogging on the hydraulics and hydrodynamics of CWs.

In this work we aim to present a standalone model to simulate saturated and unsaturated subsurface flow, bioclogging produced by a single bacterial group using the conceptual model of Rosenzweig et al. (2009) and the subsequent surface flow.

At the end of the paper a discussion is made about the limitations of the current model and on research needs and possible model improvements.

8.2 Methods

8.2.1 Governing equations

The equations used to describe the hydrodynamics, solute transport, bacterial growth and bioclogging are detailed in the following sections.

Hydrodynamics

The Richards equation (Richards, 1931) is used to described variably saturated porous media flow, assuming that air remains at atmospheric pressure and that flow velocity can be estimated using the Darcy-Buckingham equation (no creeping flow) (Eq. 8.1):

$$\sigma(h)\frac{\partial h}{\partial t} - \nabla.(K(h)\nabla h) = s_s \tag{8.1}$$

Where h $[L]$ is the hydraulic head, t $[T]$ is time, $\sigma(h)$ $[L^{-1}]$ is the specific volumetric storability, $K(h)$ $[LT^{-1}]$ is the hydraulic conductivity and s_s $[LT^{-1}]$ represents the contribution of sources and sinks.

The initial (biofilm-free) soil water retention curve is obtained from Eq. 8.2 (van Genuchten, 1980):

$$\theta(h) = \theta_r + S_e(h)(\theta_s - \theta_r) \tag{8.2}$$

Where $\theta(h)$ is the volumetric water content. θ_s (-) and θ_r (-) represent, respectively, the saturated and residual liquid volume fractions and

$$S_e(h) = \frac{1}{[1 + (\alpha h)^n]^l} \tag{8.3}$$

is the effective water saturation. α, n and $l = 1 - \frac{1}{n}$ are van Genuchten fitting parameters.

In this work the Richards equation was chosen to describe both subsurface and overland flow. This choice was primarily driven by the will to keep the same governing equation over the entire flow domain. By doing so, we implicitly assumed that there is no local nor convective acceleration of the overland flow and that the viscosity effects can be estimated by a Darcy-like expression. The implications of these assumptions will be discussed later in the chapter (Section 8.4).

The van Genuchten parameters of the Richards equation for the overland flow lack any physical meaning and were selected with the sole purpose of assimilating flow in porous media to overland flow. The same occurs for its saturated hydraulic conductivity ($K_{sat_{RL}}$), which was set to very high values to reduce flow resistance, and for θ_r and θ_s, which were defined as 1 and 0, respectively, so that all pore volume is considered as water only.

Solute Transport

The fate and transport of solutes is described with Eq. 8.4:

$$\frac{\partial}{\partial t}(\theta C_k) + \nabla \cdot [-\theta D \nabla C_k + u C_k] = s_{C_k} + r_{C_k} \tag{8.4}$$

$k = 1, \ldots, n$

Where n is the total number of transported species C_k $[ML^{-1}]$, θ (-) is the liquid volume fraction, D $[L^2T^{-1}]$ is the hydrodynamic dispersion tensor, u is the specific discharge $[LT^{-1}]$, s_{C_k} $[ML^{-3}T^{-1}]$ represents the source/sink term of C_k per unit time and r_{C_k} $[ML^{-3}T^{-1}]$ denotes the reaction rate of C_k.

Bacterial Growth

For the sake of simplicity, only one bacterial group (X) was considered in the current work. The growth of this hypothetical bacteria only requires the availability of one substrate (C) and is described using the following Monod equation (Monod, 1949)(Eq. 8.5).

$$\frac{\partial X}{\partial t} = \mu_X \left(1 - \frac{X}{\rho_X \left(\theta_s - \theta_r\right)}\right) \left(\frac{C}{K_{X,C} + C}\right) X - k_X X \tag{8.5}$$

Where, X and C have units of $mgCOD \cdot L^{-1}$, μ_X and k_X (both in d^{-1}) are the maximum growth rate and decay rate of X, respectively. ρ_X is the density of X ($kg \cdot m^{-3}$) and θ_s (-) and θ_r (-) represent the saturated and residual liquid volume fractions of the porous material, respectively. Finally, $K_{X,C}$ ($mg \cdot L^{-1}$) represents the half saturation coefficient of C for X.

The logistic term $\left(1 - \frac{X}{\rho_X (\theta_s - \theta_r)}\right)$ was added to Eq.8.5 to prevent unlimited growth of X in areas with persistently high C concentrations (inlet section) (Samsó and García, 2013a,b).

X growth occurs at the expenses of substrate C consumption at a rate defined by the following expression:

$$\frac{\partial C}{\partial t} = -\frac{1}{Y_{X,C}} \mu_X \left(1 - \frac{X}{\rho_X \left(\theta_s - \theta_r\right)}\right) \left(\frac{C}{K_{X,C} + C}\right) X \tag{8.6}$$

Where $Y_{X,C}$ ($mgCOD_X \cdot mgCOD_C{}^{-1}$) is the yield coefficient for bacteria X. Eq. 8.6 corresponds to the reaction term r_C in Eq. 8.4.

Bioclogging

Based on the capillary model (Mualem, 1976), which is a simplistic conceptual representation of soil capabilities to retain and conduct water, we estimate the equivalent pore size distribution of the bacteria-free WB using Eqs. 8.7 and 8.8 (Rosenzweig et al., 2009).

$$r_f = -\frac{2\sigma \cos\beta}{\gamma h} \tag{8.7}$$

$$N_{f,i} = \frac{\Delta\theta}{\pi r_{f,i}^2} \tag{8.8}$$

Where r_f is the effective radius of the largest water-filled capillary for every pressure head value, and $N_{f,i}$ (Eq. 8.8) is the density number of the capillaries of radius $r_{f,i}$ (Rosenzweig et al., 2009). Following the notation utilized by Rosenzweig et al. (2009), sub-index f indicates biofilm-free conditions. σ is the water surface tension ($0.072N \cdot m^{-1}$ for distilled water at 20 °C), γ is water's specific weight and β $(-)$ is the water contact angle within the tube walls, which is usually set to 0 (Rosenzweig et al., 2009). θ is the initial (biofilm-free) water content for every pressure head value, obtained with van Genuchten model (Eq. 8.2) and $\Delta\theta$ are increments of the water content between two consecutive pore radii.

Rosenzweig et al. (2009) suggests that the biofilm can be modelled as a continuous layer covering the pore walls, thus decreasing the radii of pores. The new pore radii distribution in the presence of biofilm can be calculated with Eqs. 8.9 and 8.10:

$$r_{b,i} = r_{f,i}\sqrt{1 - S_{em}(h)} \tag{8.9}$$

$$N_{b,i} = N_{f,i} \tag{8.10}$$

Where $S_{em}(h) = \frac{\theta_m}{\theta_s - \theta_r}$ is the specific saturation of bacteria. $\theta_m = \frac{V_m}{V_{total}}$ (-) is the volume fraction of the soil occupied by bacteria (Mostafa and Van Geel, 2007; Weill et al., 2009) and V_{total} and V_m (both in $[L^3]$) are, respectively, a representative volume of granular material and the actual volume of biomass in that representative volume. V_m is obtained by multiplying bacteria concentrations (X $(mgCOD \cdot L^{-1})$) by the density of biomass.

The updated water content in the presence of biofilm is obtained with Eq. 8.11 (Rosenzweig et al., 2009):

$$\theta_{w,j} = \theta_r + \pi \sum_{i=1}^{j} N_{b,i} r_{b,i}^2 \tag{8.11}$$

The value of $\theta_{w,j}$ ranges from θ_r to $\theta_r - \theta_m$. In Eq. 8.11, $j = 1 : M$ corresponds to the index of the capillary groups.

The water content ($\theta_{w,j}$) is then used to calculate the new effective water saturation ($S_{ew,j}$) as follows:

$$S_{ew,j}(h) = \frac{\theta_{w,j} - \theta_r}{\theta_s - \theta_r} \tag{8.12}$$

Finally, the relative unsaturated hydraulic conductivity (with respect to the initial one) in the presence of biofilm (k_b) is calculated using the following expression (Rosenzweig et al., 2009):

$$k_b(\theta_{w,j}) = \frac{\sum_{i=1}^{j} N_{b,i} r_{b,i}^4}{\sum_{i=1}^{M} N_{f,i} r_{f,i}^4} \tag{8.13}$$

and thus the updated value of $K(h)$ in Eq. 8.1 in areas where bioclogging occurs is obtained with:

$$K(h) = k_b(h) K_{sat} \tag{8.14}$$

whereas in areas where bioclogging does not take place, the hydraulic conductivity remains the same as in the initial conditions and is obtained with:

$$K(h) = k_r(h) K_{sat} \tag{8.15}$$

Where,

$$k_r(h) = S_e(h)^l [1 - (1 - S_e(h)^{\frac{1}{l}})^l]^2 \tag{8.16}$$

is the biofilm-free relative hydraulic conductivity and $S_e(h)$ is obtained from Eq. 8.3.

8.2.2 Hardware and Software

All simulations were run on a computer cluster running Linux kernel 2.6.18-238 and the Portable Batch System (PBS) job scheduler. The cluster had a total of 14 nodes, 10 of *Type1* and 4 of *Type2*. The main features of *Type1* and *Type2* nodes are detailed in Table 8.1.

Table 8.1: Features of Type1 and Type2 cluster nodes.

	Type1 nodes	**Type2 nodes**
Number of nodes of this type	10	4
Number of processor cores	2*4	2*6
Frequency of processors	2.66 GHz	2.66 GHz
RAM memory	32 GB	48 GB

The COMSOL Multiphysics™ and MATLAB® versions installed in the cluster were v4.3b and R2013a, respectively.

8.2.3 Model Implementation

All model equations were implemented using the COMSOL Multiphysics™ interface, except for the equations used to calculate the volumetric water content ($\theta_{w,j}$) and the relative hydraulic conductivity in the presence of biofilm (k_b) (Eqs. 8.11 and 8.13), that were implemented in MATLAB®. The exchange of data between COMSOL Multiphysics™ and MATLAB® is made at each numerical iteration using the *Livelink for MATLAB®* COMSOL Multiphysics™ module (Figure 8.1).

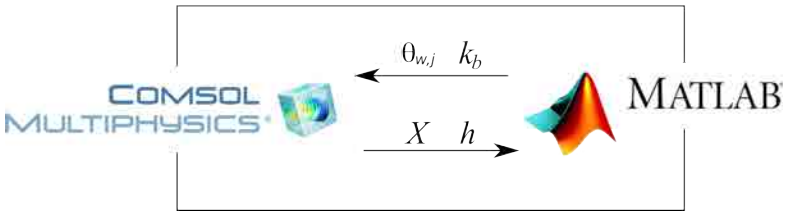

Figure 8.1: Parameter exchange between COMSOL Multiphysics™ and MATLAB®.

In the following lines, the MATLAB® code used to calculate k_b and $\theta_{w,j}$ is presented:

```
1
2  function k_b = relcond(alpha,thetam,thetas,thetar,sigma,gamma,m,n,p)
3
4  %function k_b calculates the relative hydraulic conductivity in the ...
       presence of biofilm. It imports the following 2D matrices from ...
       COMSOL Multiphysics:
5
6  %alpha, n, m =van Genuchten parameters
7  %thetas and thetar = saturated and residual water volume fraction
8  %sigma and gamma = water surface tension and specific weight
9  %thetam = volume fraction of soil occupied by bacteria
10 %p = pressure head
11
12 %defining the vector of capillary head values
13     pr=-logspace(4,-4,100)';
14
15 %create 3D matrices for all data imported from COMSOL with ...
       dimensions (size(p,1),size(p,2),size(pr,1)).
```

```
16
17 %3D matrix for the capillary head pressure
18     pr_3D(1,1,:)=pr;
19     pr_3D=repmat(pr_3D, [size(p,1) size(p,2) 1]);
20     p_3D=repmat(p, [1 1 size(pr,1)]);
21
22 %3D matrices for van Genuchten parameters and soil properties ...
       imported from COMSOL
23     alpha_3D=repmat(alpha, [1 1 size(pr,1)]);
24     n_3D=repmat(n, [1 1 size(pr,1)]);
25     m_3D=repmat(m, [1 1 size(pr,1)]);
26     thetar_3D=repmat(thetar, [1 1 size(pr,1)]);
27     thetas_3D=repmat(thetas, [1 1 size(pr,1)]);
28     thetam_3D=repmat(thetam, [1 1 size(pr,1)]);
29     gamma_3D=repmat(gamma, [1 1 size(pr,1)]);
30     sigma_3D=repmat(sigma, [1 1 size(pr,1)]);
31
32
33 %Calculating the distribution of the Specific saturation without ...
       biofilm for each pressure (3D matrix)
34
35     Se = ones(size(p,1),size(p,2),size(pr,1))./...
36     (ones(size(p,1),size(p,2),size(pr,1))+...
37     (abs(alpha_3D.*pr_3D./gamma_3D)).^n_3D).^m_3D;
38
39 %Calculating the distribution of the water content without biofilm ...
       of every pore for each pressure (3D matrix)
40
41     W_cont = thetar_3D+Se.*(thetas_3D-thetar_3D);
42
43 %Calculating the pore radii distribution at every node for each ...
       pressure (3D matrix)
44
45     rf = -2*sigma_3D./pr_3D;
46     Nf=zeros(size(p,1),size(p,2),size(pr,1));
47
48   for k=1:size(pr,1)-1
49
50         Nf(:,:,k+1) = ...
               (W_cont(:,:,k+1)-W_cont(:,:,k))./(pi*rf(:,:,k+1).^2);
51   end
52
53
54 %Calculating the specific saturation of bacteria
55
56     Sem=thetam_3D./(thetas_3D-thetar_3D);
57
58 %Updating the pore radii distribution in the presence of biofilm ...
       using model R3 of \citep{Rosenzweig2009}
59     Nb=Nf;
60     rb=rf.*sqrt(ones(size(p,1),size(p,2),size(pr,1))-Sem);
61
62 %diff matrix calculates the difference between the real pressure ...
```

```
    and that of the capillary model (3D matrix)

    diff=abs(pr_3D-p_3D);

%preallocation

    k_b=zeros(size(p,1),size(p,2));


%with the following loop the z indices of the minimum value of each ...
    column of the diff matrix are obtained and then the sum of ...
    Nb*rb^2 up to the value of the index is calculated.

    for i=1:size(p,1)
            for j=1:size(p,2)

                locn=find(diff(i,j,:)==(min(diff(i,j,:))));
                k_b(i,j)=sum(Nb(i,j,1:locn).*rb(i,j,1:locn).^4)./...
                sum(Nf(i,j,1:end).*rf(i,j,1:end).^4);

        end
    end

end
```

```
function W_contb = ...
    watcont(alpha,thetam,thetas,thetar,sigma,gamma,m,n,p)

%function W_contb calculates the water content in the presence of ...
    biofilm. It imports the following 2D matrices from COMSOL ...
    Multiphysics:

%alpha, n, m =van Genuchten parameters
%thetas and thetar = saturated and residual water volume fraction
%sigma and gamma = water surface tension and specific weight
%thetam = volume fraction of soil occupied by bacteria
%p = pressure head

%defining the vector of capillary head values
    pr=-logspace(4,-4,100)';

%create 3D matrices for all data imported from COMSOL with ...
    dimensions (size(p,1),size(p,2),size(pr,1)).

%3D matrix for the capillary head pressure
    pr_3D(1,1,:)=pr;
    pr_3D=repmat(pr_3D, [size(p,1) size(p,2) 1]);
    p_3D=repmat(p, [1 1 size(pr,1)]);

%3D matrices for van Genuchten parameters and soil properties ...
    imported from COMSOL
```

```
22      alpha_3D=repmat(alpha, [1 1 size(pr,1)]);
23      n_3D=repmat(n, [1 1 size(pr,1)]);
24      m_3D=repmat(m, [1 1 size(pr,1)]);
25      thetar_3D=repmat(thetar, [1 1 size(pr,1)]);
26      thetas_3D=repmat(thetas, [1 1 size(pr,1)]);
27      thetam_3D=repmat(thetam, [1 1 size(pr,1)]);
28      gamma_3D=repmat(gamma, [1 1 size(pr,1)]);
29      sigma_3D=repmat(sigma, [1 1 size(pr,1)]);
30
31
32  %Calculating the distribution of the Specific saturation without ...
        biofilm for each pressure (3D matrix)
33
34      Se = ones(size(p,1),size(p,2),size(pr,1))./...
35      (ones(size(p,1),size(p,2),size(pr,1))+...
36      (abs(alpha_3D.*pr_3D./gamma_3D)).^n_3D).^m_3D;
37
38  %Calculating the distribution of the water content without biofilm ...
        of every pore for each pressure (3D matrix)
39
40      W_cont = thetar_3D+Se.*(thetas_3D-thetar_3D);
41
42  %Calculating the pore radii distribution at every node for each ...
        pressure (3D matrix)
43
44      rf = -2*sigma_3D./pr_3D;
45      Nf=zeros(size(p,1),size(p,2),size(pr,1));
46
47    for k=1:size(pr,1)-1
48
49          Nf(:,:,k+1) = ...
                (W_cont(:,:,k+1)-W_cont(:,:,k))./(pi*rf(:,:,k+1).^2);
50    end
51
52
53  %Calculating the specific saturation of bacteria
54
55      Sem=thetam_3D./(thetas_3D-thetar_3D);
56
57  %Updating the pore radii distribution in the presence of biofilm ...
        using model R3 of \citep{Rosenzweig2009}
58      Nb=Nf;
59      rb=rf.*sqrt(ones(size(p,1),size(p,2),size(pr,1))-Sem);
60
61  %diff matrix calculates the difference between the real pressure ...
        and that of the capillary model (3D matrix)
62
63      diff=abs(pr_3D-p_3D);
64
65  %preallocation
66
67      M=zeros(size(p,1),size(p,2));
68
```

```
%with the following loop the z indices of the minimum value of each ...
    column of the diff matrix are obtained and then the sum of ...
    Nb*rb^2 up to the value of the index is calculated.

    for i=1:size(p,1)
            for j=1:size(p,2)
                locn=find(diff(i,j,:)==(min(diff(i,j,:))));
                M(i,j)=sum(Nb(i,j,1:locn).*rb(i,j,1:locn).^2);
            end
    end

%The water content in the presence of biofilm is then calculated as:

    W_contb=thetar+pi*M;

end
```

8.2.4 Geometrical description

Three 2D sub-domains were defined for the current model, representing a longitudinal section of a generic CW: two belowground sub-domains, representing the mixing zone (MZ) and the body of the wetland (WB), respectively, and a runoff (RL) layer on top of the previous two (Figure 8.2).

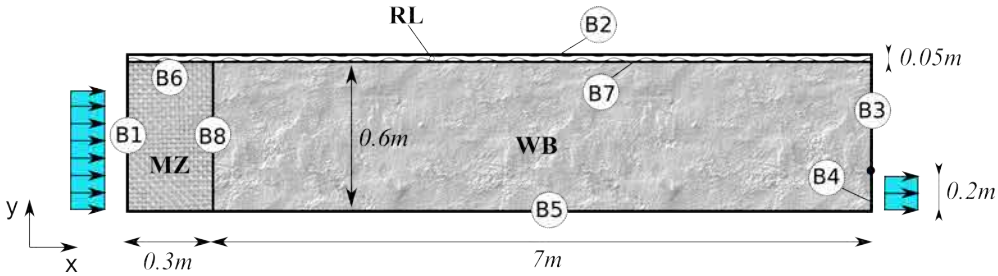

Figure 8.2: Schematic representation of the model domain, including the mixing zone (MZ), the body of the wetland (WB) and the runoff layer (RL). Notice that the y-axes is exaggerated so that the image fits a reasonable size.

8.2.5 Meshing

A triangular mesh was built automatically with COMSOL Multiphysics™ using the advancing front algorithm and by setting the specific parameter values for each sub-domain. The resulting mesh, consisting of a total of 31457 elements, has higher elements density in the RL and lower density in the belowground sub-domains (MZ and WB). Note that a predefined number of 350 triangular elements was set in

boundary $B4$ so that the mass of water would be preserved from inlet to outlet. In Table 8.2 all mesh parameters are described in detail.

Table 8.2: Mesh characteristics.

	Mixing zone and Wetland body [a]	**Runoff layer**
Maximum element size	0.07 m	0.012 m
Minimum element size	0.0014 m	$9.75 \cdot 10^{-5}$ m
Maximum element growth rate	1.25	1.08
Resolution of curvature	0.3	0.25
Resolution in narrow regions	1	4
Total Number of triangular elements	31457	

[a] A predefined number of 350 triangular elements was set at boundary $B4$ of the domain (see Figure 8.2) to avoid water mass losses from inlet to outlet.

8.2.6 Model features and Input parameters

Biokinetic parameters used in Eqs. 8.5 and 8.6 are shown in Table 8.3.

Table 8.3: Values of the biokinetic parameters of Eqs.8.3 and 8.4

Parameter	**Value**	**Unit**	**Description**
μ_X	3	d^{-1}	Maximum growth rate of X
k_X	0.1	d^{-1}	Decay rate of bacteria X
$K_{X,C}$	0.025	$Kg \cdot m^{-3}$	Saturation coefficient of X for C
ρ_X	1	$Kg \cdot m^{-3}$	Density of bacteria X
$Y_{X,C}$	0.1	$KgX \cdot KgC^{-1}$	Yield coefficient for bacteria X

Bacterial growth is assumed to take place only in the belowground sub-domains (MZ and WB), and the changes in the hydrodynamics of the granular media caused by bacterial growth are only considered in the WB sub-domain. That is because the granular media of the MZ is generally coarser than that of the WB, and thus the impact of bacterial growth on the hydrodynamic properties of the former is much smaller than that on the latter. Therefore the water retention curves of all sub-domains are calculated using the van Genuchten parameters shown in Table 8.4, but only in the WB it is updated over time using the capillary model (Eqs. 8.9 to 8.16).

Table 8.4: Values of the hydrodynamic parameters of the wetland body (WB), the mixing zone (MZ) and the runoff layer (RL).

	Values			
Parameter	**WB**	**MZ**	**RL**	**Unit**
α	14.5	14	150	m^{-1}
n	2.6	2.5	2.6	-
m	$1-\frac{1}{n}$		1	-
θ_s	0.43	0.4	1	-
θ_r	0.01	0	0	-
K_{sat}	100	300	2000	$m \cdot d^{-1}$
α_L	0.01		0	m
α_T	0.001		0	m
D	$1 \cdot 10^{-9}$		$1 \cdot 10^{-9}$	$m^2 \cdot d^{-1}$

8.2.7 Boundary and Initial Conditions

For the Richards equation (Eq. 8.1), a flow-rate of 1 $m \cdot s^{-1}$ (Neumann) was imposed in boundary $B1$ and a pressure head of 0.5 m (Dirichlet) at boundary $B4$. We set the initial pressure heads to be at hydrostatic equilibrium. For any node of elevation y, the initial pressure head equals $(0.5 - y)$ m, and the origin of coordinates is located at the top left corner of the domain.

For the transport equation (Eq. 8.2) a flux of 450 $mgC \cdot L^{-1}$ was imposed at boundary $B1$ (Cauchy) and an outflow boundary condition was applied at boundary $B4$ (Neumann). The initial concentration of C was set to 10 $mg \cdot L^{-1}$ for the belowground sub-domains and 0 $mg \cdot L^{-1}$ on the RL.

The rest of boundaries were defined as no-flow boundaries. Also note that both the flow-rate and the flux of C imposed at boundary $B1$ were limited to nodes below $y = 0.5$ m to avoid unwanted diffusion of C in the RL.

The initial concentrations of bacteria X were set to 1 $mg \cdot L^{-1}$ in the belowground sub-domains to recreate start-up conditions, and 0 $mg \cdot L^{-1}$ on the RL.

8.2.8 Numerical experiment

To showcase the importance of including bioclogging in CWs models two separate simulations were run, one considering bioclogging effects on the hydrodynamics of the granular media of the WB and another one neglecting them. Notice that it was assumed that the gravel in the MZ is sufficiently coarse so that bioclogging effects can be safely neglected.

A visual comparison of the bacteria distribution obtained with the two simulations is made by plotting the bacteria concentrations within the 2D domain. This

qualitative comparison is complemented with a quantitative comparison of four different outputs of the two simulations: (i) the center of mass of bacteria, (ii) the percentage of pore volume occupied within the WB, (iii) the effluent concentration of C and (iv) the proportion of flow circulating on the RL and through the WB.

The coordinates of the center of mass of bacteria (x_{CM}, y_{CM}) in the WB over time are obtained with Eqs. 8.17 and 8.18 (French et al., 2001):

$$x_{CM}(t) = \frac{\iint X(t)x \; dxdy}{\iint X(t) \; dxdy} \tag{8.17}$$

$$y_{CM}(t) = \frac{\iint X(t)y \; dxdy}{\iint X(t) \; dxdy} \tag{8.18}$$

Where x and y are the Cartesian coordinates of the WB.

The percentage of pore space occupied by bacteria is obtained with Eq. 8.19:

$$\%\text{ occupied } = \frac{\text{Pore Volume occupied}}{\text{Total Pore Volume}} \cdot 100 = \frac{\frac{\iint X \; dxdy \cdot W_{WB}}{\rho_X}}{(\theta_s - \theta_r) \cdot L_{WB} \cdot W_{WB} \cdot D_{WB}} \cdot 100 \tag{8.19}$$

Where L_{WB}, W_{WB} and D_{WB} (all in m) are the length, width and depth of the wetland body, respectively.

The effluent concentrations of C over time are obtained by averaging its value on boundary $B4$ of the domain.

Finally, the proportion of flow passing through the RL is obtained by integrating the vertical component of the flow velocity vector (v_y) over boundary $B6$, while the flow passing through the WB is calculated by integrating the horizontal component of the flow velocity vector (v_x) over boundary $B8$.

8.3 Results

8.3.1 Qualitative comparison

Overall, very different bacterial distributions and flow patterns were obtained by including bioclogging effects on the hydrodynamics of the granular media as compared to the case where bioclogging effects were neglected (Figures 8.3 and 8.4). In fact, until day 5 bacteria grew mainly in the mixing zone (MZ) and close to the inlet section for the two cases (Figure 8.3a), and only after that moment bacteria dynamics started to diverge.

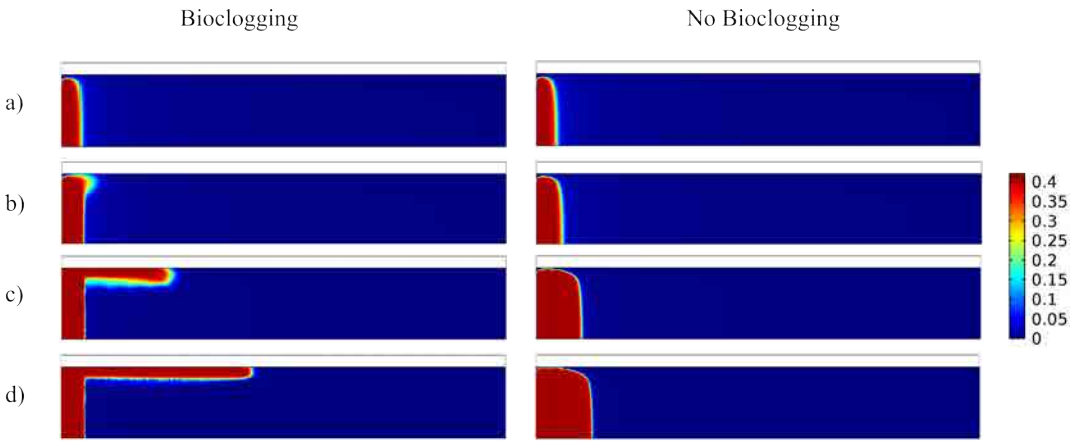

Figure 8.3: Concentration of bacteria X (in $kgCOD \cdot m^{-3}$) within the domain with and without the effects of bioclogging after a)5, b)6.5, c)15 and d)30 days. Note that in comparison to the gravel of the WB, that of the MZ is usually coarser, and for that reason in this work bioclogging effects on the hydrodynamics of the MZ were neglected.

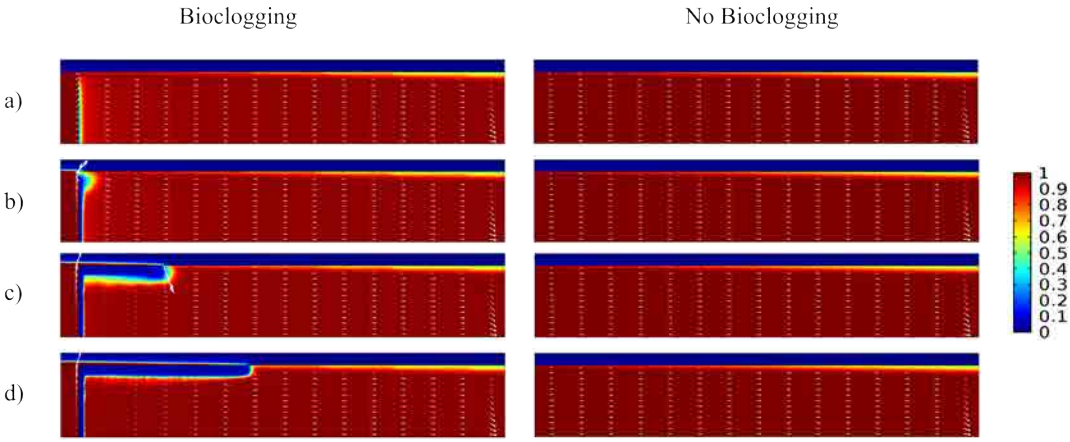

Figure 8.4: Specific saturation of water (S_e) (-) within the domain with and without the effects of bioclogging after a)5, b) 6.5, c) 15 and d) 30 days. The arrows indicate the direction of the velocity vector at every loacation within the domain. Notice that for images b, c and d for the Bioclogging case, the value of S_e in the RL, just above the area where bacteria grows is equal to 1, indicating the existence of overland flow.

The elongated bacteria distribution near the surface of the wetland when bioclogging effects were considered (images on the left in Figure 8.3) resulted from the succession of the following facts: around day 5 the biomass in the mixing zone (MZ) reached the carrying capacity of the granular media ($X \cdot \rho_X^{-1} = \theta_s - \theta_r$) and its net growth stopped (results not shown), even though there was still substrate (C) left to biodegrade. This remaining C was transported towards the WB by advection and resulted in the growth of bacteria in that region (Figure 8.3b), which decreased

its hydraulic conductivity and the flow velocity over time. As a result, the water level within the MZ progressively increased until around day 6, when water started to circulate on the runnof layer RL (Figures 8.4b,c and d). When the runoff water reached the surface of the WB (domain boundary $B7$) it infiltrated again, resulting in new bacteria growth in that region. Subsequently, the hydraulic conductivity near the surface of the WB decreased and instead of infiltrating, overland water continued to circulate on the runoff layer (RL) until the conductivity underneath was sufficient to infiltrate again.

On the other hand, in the numerical experiment neglecting clogging effects, water circulated continually through the same pathways within the subsurface domains and no overland flow developed (right images in Figures 8.3 and 8.4). In this case, bacterial concentrations progressed from inlet to outlet, occupying the entire depth of the bed.

8.3.2 Quantitative comparison

Proportion of overland and subsurface flow

Until the 6^{th} day all flow circulated through the subsurface domains (MZ and WB) (Figure 8.5). After that moment, and as seen in previous figures, an increasing proportion of flow started to circulate on the RL (Figure 8.2). Despite the existence of a bacteria barrier in the WB close to boundary with the MZ (Figure 8.3b, c and d), the continuous death and regrowth of bacteria allowed a 20% of the total inflow to continue to circulate within the subsurface domains.

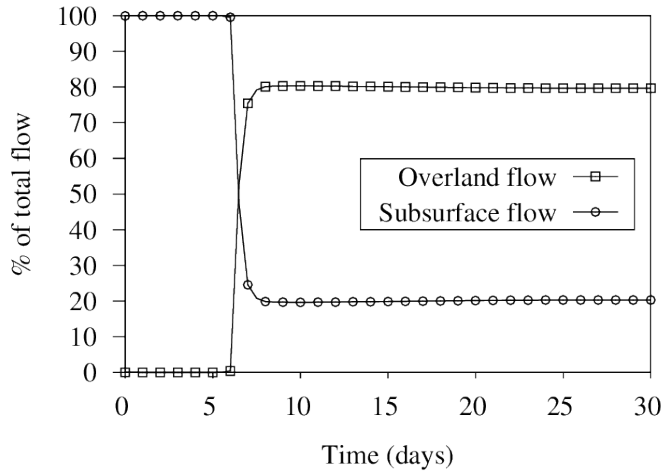

Figure 8.5: Proportion of overland and subsurface flow obtained with bioclogging (Eq. 8.19). Notice that without bioclogging, all the flow circulates in the subsurface domains.

Center of masses of bacteria

The same initial concentration of bacteria X was set for the MZ and the WB. Accordingly, at the beginning of the two simulations the center of mass of bacteria was located at the geometrical center of the two subsurface domains ($x_{CM} = 3.65\ m$, $y_{CM} = 0.3\ m$) (Figure 8.6). Shortly after, and for the two experimental cases the value of x_{CM} started to decrease following the progressive accumulation of bacteria biomass near the inlet, where C concentrations were the highest. On the other hand y_{CM}'s slight initial decrease was due to the fact that inflow concentrations of C entered the system through boundary $B1$ but only for $y < 0.5\ m$.

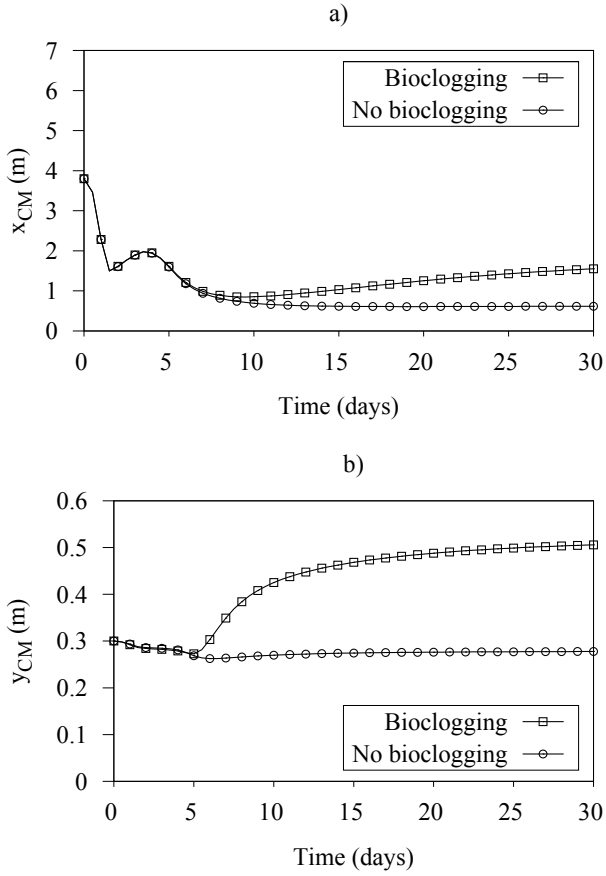

Figure 8.6: Evolution of coordinate x (a) and y (b) of the center of mass of bacteria X in the WB with and without bioclogging (Eqs. 8.17 and 8.18).

From day 5, and when no bioclogging effects were considered, x_{CM} and y_{CM} remained almost constant until the end of the simulated period. On the contrary, for the bioclogging case, both y_{CM} and x_{CM} increased since bacteria grew closer to

the surface and towards the outlet section following the infiltration of the overland flow.

Porosity occupation

Very similar percentages of bacteria porosity occupation were obtained for the two cases. In both of them, pore spaces progressively filled up with time, reaching a 10% occupation after 30 days (Figure 8.7).

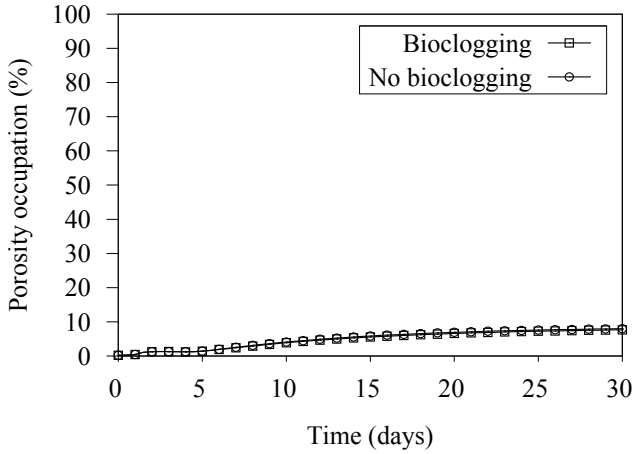

Figure 8.7: Proportion of the WB occupied by bacteria over time with and without bioclogging (Eq. 8.19).

Effluent C concentration

Finally, Figure 8.8 shows that the effluent concentrations obtained with and without bioclogging effects followed the exact same trend; there was a peak concentration at around day 4, corresponding to the first flush of C entering the system, and after the peak, all inflow C was already degraded by X. The peak concentration was due to the fact that bacterial biomass at the beginning of the simulation was still small, and thus it could not yet biodegrade all inflow C.

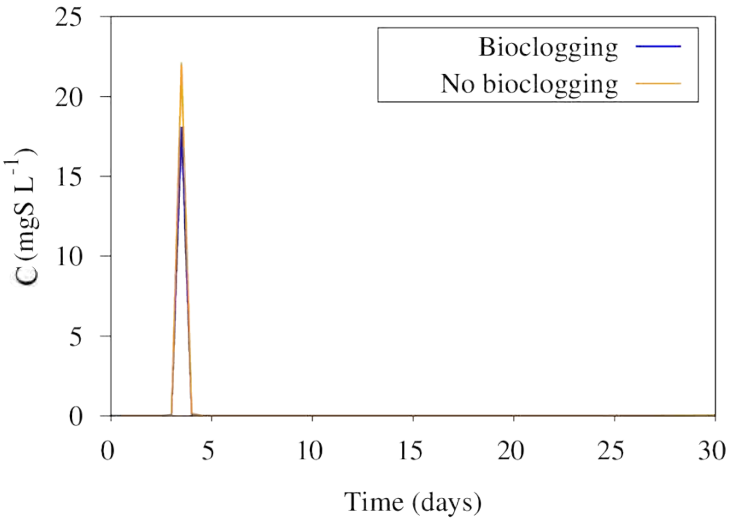

Figure 8.8: Effluent concentrations of C over time obtained with and without bioclogging effects on the granular media.

8.4 Discussion

8.4.1 Model equations

The mathematical modelling of the hydraulics of HSSF CWs requires equations to describe variably saturated subsurface flow and overland flow. In hydrology, the interaction between surface and subsurface flow is usually simulated by coupling any form of the Richards equation for the subsurface variably saturated flow with the Saint-Venant equations (or any of its approximations i.e. the shallow water equations) for the surface flow (Furman, 2008). The coupling of these two different types of equations has been subject of intensive research since the late 60's and several models have been developed over the years for that purpose (Panday and Huyakorn, 2004; Kollet and Maxwell, 2006).

Weill et al. (2009) indicates that in the inertia approximation of Saint-Venant equations, runoff flow-rate is proportional to the runoff hydraulic gradient, which implies that runoff can be simulated as a flow in a porous medium with particular properties. Therefore, with a few assumptions, and accepting a certain degree of error in the flow and transport balances, the Richards equation was used in the current chapter to simulate both subsurface flow and overland flow. These assumptions were in essence the same than those used for the shallow water equations: low flow-rates and shallow water depths. In contrast, although in vertical flow CWs ponding also occurs, the surface water remains mostly in hydrostatic conditions and thus a

changing hydraulic head boundary condition is sufficient to simulate this phenomena (Forquet et al., 2009; Giraldi et al., 2010).

Regarding bacterial growth, according to literature, there are three alternative approaches to simulate it: the continuous biofilm, the discrete microcolonies and the macroscopic approaches. The first two approaches consider either continuous biofilms or patchy colonies, and in reality bacteria in porous media is found as a combination of the two (Clement et al., 1996). In this chapter we used a macroscopic model, which considers only spatially averaged biomass concentrations and thus is more realistic than other alternatives and makes no assumptions about the microscopic biomass distribution (Kildsgaard and Engesgaard, 2001). Moreover, this approach is the most commonly reported in literature and it is also appropriate for practical reasons, since in experimental studies data for microbes is reported as average concentrations (Clement et al., 1996).

In this chapter we used one of the 3 models of Rosenzweig et al. (2009) to translate biomass growth into hydraulic conductivity reduction of the porous media. These models are based on those proposed by Mostafa and Van Geel (2007) and expand by considering the change in biofilm pore-size distribution and its effect on the entire hydraulic conductivity function. In this chapter we used model R3 of Rosenzweig et al. (2009), which involves that all pores are filled by bacteria in the same proportion, regardless of their size. Model R3 was selected for its simplicity, although it is not clear that it may be the best choice, since there is evidence that under unsaturated conditions the small pores clog first, reducing the relative permeability and causing the water flow to shift to the larger pores (Soleimani et al., 2009). Despite some extra work would be required, models R1 and R2 could also be implemented in the presented model.

In a very similar study, Soleimani et al. (2009) used the conceptual model by Mostafa and Van Geel (2007) to relate the relative permeability term for unsaturated flow to the microbial growth in biofilters (septic beds). The aims of that study were, on one hand, to evaluate the properties of the granular media that produce faster clogging, and on the other hand to observe the effects of progressive clogging on a septic bed. In their study, microbial growth was dependent only on one substrate and it was also described with a single Monod equation, although it did not include the carrying capacity function to limit the growth. The accuracy of their biological clogging model was tested by comparing its results with the one-dimensional reactive transport experiment presented in Taylor and Jaffé (1990a) and Taylor et al. (1990b) and the one-dimensional unsaturated clogging experiment by Spychala and Blazejewski (2004). Their results showed good agreement with the experimental data and model simulation presented in Taylor and Jaffé (1990a) and Taylor et al. (1990b), but on the contrary, the model was not able to reproduce the reduction of effluent flow rate obtained by Spychala and Blazejewski (2004). However, the main difference with our study was that in their case they considered a vertical flow biofilter, and so

they did not require the inclusion of overland flow and transport equations.

8.4.2 Assumptions and limitations

The model used in this chapter is an oversimplification of all processes occurring in real CWs since it only considers one bacterial group (X) and one substrate (C). Likewise, clogging in CWs is attributed to several factors e.g. plant roots, solids accumulation, bacterial growth (Knowles et al., 2011), and in this chapter only the clogging caused by bacteria was simulated. Moreover dead cells coming from bacteria decay, which are known to accumulate in the granular media over time (Samsó and García, 2014a; Weintraub et al., 2002), were not considered in the model and do not cause any clogging effects. Temperature effects on bacteria growth were not included either, and according to Samsó and García (2013a) the inclusion of temperature in the bacterial growth expressions was essential to match effluent pollutant concentrations of a pilot HSSF CW in the long-term with the BIO_PORE model.

Another assumption made in this chapter consisted in neglecting bioclogging effects on the hydrodynamics of the MZ. This approach was necessary, since in our numerical experimental setup the inflow water entered the system through a lateral wall of the MZ and so if bacteria were to fill the whole porous media in that region, pore velocities would become very high, which would certainly result in numerical issues. A similar approach was adopted by Soleimani et al. (2009) who neglected clogging effects on the top row of elements of their 2D domain to avoid reaching high water depths on the surface of the domain.

In this chapter we also assumed that neither bacterial growth nor substrates degradation take place in the RL. In CWs operated under average conditions, although bioclogging might occur in several regions, overland flow infiltrates rapidly once the clogged area is surpassed and the changes in bacteria concentrations during their transport in contact with the atmosphere are most certainly negligible in comparison to those occurring in the interstitial pore space.

Finally, as a result of the assumptions required to use the Richards equation for overland flow, mentioned in the previous section, the presented model can only be used for low flow-rates and surface water depths. Moreover, the inlet section (boundary $B1$) had to be set only in the nodes below $y = 0.5$ because the RL domain was defined as a fully saturated porous media ($S_e = 1$) and thus diffusion in that sub-domain may take place even when there is no advective flow of water on it.

8.4.3 Model results

Results of the numerical experiment carried out in this chapter clearly demonstrate the importance of considering bioclogging effects in the hydrodynamics of the porous media when simulating the general functioning of HSSF CWs. They also show that for a complete and sound description of the functioning of these systems, overland flow needs to be simulated.

The rapid bacterial growth and porosity occupation observed in this chapter were due to the fact that all model parameters were chosen so that the simulation time required to obtain relevant results would be shortened. Thus, high values of inflow C concentration, Yield coefficient (Y) and maximum specific growth rate (μ_X) and low values for decay rate (k_X), saturation coefficient ($K_{X,C}$) and initial saturated hydraulic conductivity (K_{sat}) were selected. On the other hand, a conservative value for the inflow rate was used so that the hypothesis of slow flow velocities and shallow water depth for the overland flow are fulfilled.

The extent of the spatial distribution reached by bacteria within the domain in the two cases depends mostly on the flow-rate, the inflow concentration of C, the value of the carrying capacity of the granular media ($\theta_s - \theta_r$) and the density of bacteria. The higher the inflow concentration of C and the flow-rate, the wider the bacteria distribution. On the contrary, the larger the value of $\theta_s - \theta_r$, the narrower the bacterial distribution. Moreover, the widespread of bacterial communities when considering bioclogging also depends on the relative proportion of overland and sub-surface flows. In contrast, most of the other parameters considered in this model only affected the velocity at which clogging developed.

Although the difference between the bacterial distribution and the flow pattern obtained from the two simulations increased over time, the effluent concentrations and the percentage of porosity occupied was the same for the two cases. Based on these results, one could argue that bioclogging does not have an effect neither on the treatment performance of CWs nor on its lifespan. However, it has to be noted that, for practical reasons, very short time frames were simulated in the current chapter. Thus, if longer time-scales were simulated the predicted lifespan of the wetland would certainly be compromised. As a matter of fact, everything seems to indicate that following the trend observed in Figure 8.3 if bacteria were to reach to outlet section, the wetland would start to work with vertical flow. It has to be noted as well that when all the components and processes described by the BIO_PORE are combined with the formulation presented in this chapter, the results will certainly differ.

Despite the differences in the numerical experiment setup, the bacteria dynamics obtained in this chapter when considering bioclogging effects on the granular media (Figure 8.3) were very similar to those obtained by Soleimani et al. (2009). In their work, and among other things, they used their model in a 2D domain, representing a vertical flow biofilter (septic bed), to evaluate its progressive clogging. Indeed,

the first areas to clog where those near the inlet pipe, and then water was forced to move horizontally within the domain in order to find sufficiently high hydraulic conductivities underneath to infiltrate.

8.4.4 Further research needs and model improvements

Although the objective of the current chapter was not to obtain accurate predictions of bioclogging in CWs, validation of the model should be provided. Moreover, a sensitivity analysis would help to identify the sensitivity of the model output to prescribed perturbations on the values of the in input parameters. Among the parameters used in the current model, those affecting bacterial growth rates (Table 8.3) as well as the saturated hydraulic conductivity of the WB (K_{sat}) would be of great interest.

As mentioned in previous sections, future works could also be dedicated on one hand, to improve the mathematical description of overland flow and transport, and on the other hand to implement models R1 and R2 from Rosenzweig et al. (2009) since, as detailed in previous sections, they are supposed to provide more accurate results than model R3.

Additionally, the formulation for bioclogging presented in this chapter could be added to the BIO_PORE model (Samsó and García, 2013a), and the resulting model would certainly become the most capable one developed so far for HSSF CWs. Moreover the results obtained with that hypothetical work could be used to update, if necessary, the description of the most basic functioning patterns of HSSF CWs made by the Cartridge Theory (Samsó and García, 2014a).

8.5 Conclusions

In this chapter we presented a standalone model built on COMSOL Multiphysics™ to simulate bioclogging and surface/subsurface flow interactions in horizontal subsurface flow Constructed Wetlands (CWs). A numerical experiment was also carried out to showcase the importance of including a bioclogging model in order to obtain a sound description of the functioning of these systems. The numerical experiment consisted in comparing several model outputs for two different simulations: one considering clogging effects on the hydrodynamics of the granular media and the other one neglecting them.

Very different bacteria distributions and flow patterns were obtained from the two simulations. When considering bioclogging, overland flow started to take place after 5 days of simulated time. The existence of overland flow also resulted in an elongated shape of bacterial communities near the surface of the bed. This elongated

shape was also the responsible of the observed drift of the center of masses of bacteria towards the top of the central section of the subsurface subdomains. On the other hand, both the percentage of porosity occupied by bacteria and the effluent pollutant concentrations obtained for the two simulations were almost identical. This fact was attributed to the short simulated time considered in this chapter.

Also, the few processes considered in the current chapter do not allow to describe the intrinsic complexity of real CWs. In order to approximate the simulated results to the real functioning of wetlands, the formulation presented in this chapter should be combined with more robust models for CWs already available such as the BIO_PORE model.

Further research on this model should include a parametric sensitivity analysis in order to stablish the relative impact of each model parameter on the different model outputs.

CHAPTER 9

Discussion

In this chapter we aim to link and extend all the knowledge generated during the development of this work and to share some of the lessons learned and the experience gained.

Section 9.1 is dedicated to explain which are the main difficulties that need to be overcome when simulating CWs. This discussion is made by comparing CWs technology and models with activated sludge systems and the well known ASM model series (Henze et al., 2000).

Section 9.2 is dedicated to putting together the different equations that have been presented all along this work and that make up the complete and final formulation of the BIO_PORE model. CWM1's Petersen matrices are also updated with the innovations introduced in this work. This section also helps as a reference for further versions of BIO_PORE as well as to set a starting point for the development of CWs models in other simulation platforms or codes.

Later, in Section 9.3 we make a three-way comparison of the BIO_PORE model with the most capable models for CWs available to date (those presented in Section 1.3.1). This is done so that any researcher aiming to take up an existing model for CWs to further develop it or simply build a new model from scratch, can easily pinpoint the main advantages and disadvantages of each of the available models or simulation platforms.

In Section 9.4 we list all the essential processes that models developed at current state of the art should include.

To close the discussion, in section 9.5 a global overview of the past and present of CWs models is made. This overview leads to a suggestion of what we should aim at with the models developed from now onwards. This section does not aim at giving specific details or to forecast the future, but rather on providing certain hints of what the author of this thesis believes the discipline of CW models is likely to move towards in coming years.

The different sections of the current chapter also intend to highlight that the BIO_PORE model is far from being the final solution to simulate CWs, and that there is still a lot of work to be done to make it more capable and reliable.

9.1 The complexity of modelling CWs

Since the inception of CWs, their functioning and performance have usually been compared to those of other biological wastewater treatment technologies, and most commonly to activated sludge systems. Such is the case that the biokinetic models used to describe bacterial growth and pollutants removal in CWs are based on the formulation of the activated sludge model series (ASMs).

In fact, it is very true that similar biological processes take place within both activated sludge systems and CWs, but it is as much true that their general functioning is markedly different. In the following lines, a comparison of these two technologies is made in several aspects, to see how the models used for activated sludge and CWs differ from each other, and why simulating CWs presents, in our opinion, more challenges than simulating activated sludge systems.

Activated sludge systems are, in many cases, completely stirred tank reactors (CSTR) and, as such, one can consider them to have complete mixing of the liquor. Therefore, the concentrations of all components are homogeneous within the reactor and if the structure of the flocks is neglected, the simulation of these systems becomes relatively simple, since most of the reactions can be simulated with ordinary differential equations (ODE). This fact also reduces considerably the simulation time, since a 0D domain is sufficient to simulate their general behaviour. In contrast, in CWs there is flux of water, which is similar to that of a plug flow reactor (PFR), in which pollutants, accumulated solids and bacterial concentrations decrease from inlet to outlet (García et al., 2010; Truu et al., 2009). Moreover, reactive-transport equations are required to simulate the transport and attachment and detachment of both particulate and dissolved components through the porous media. This inevitably requires the use of 1D domains and also the use of partial differential equations (PDEs) instead of ODEs. However, and mainly due to the dissolved oxygen distribution within the media (Allen et al., 2002; García et al., 2003; Headley et al., 2005; Wang et al., 2012), there also exist gradients of bacteria, solids and substrates in the vertical direction, which makes the use of 2D domains a necessity. Moreover,

CWs are very stochastic, meaning that there exist a number of random phenomena that can modify the functioning of these systems (e.g. clogging, preferential flow-paths, below ground plant roots distribution, granular media heterogeneities, plant litter deposition, evapotranspiration...). For this reason, for a complete description of their functioning 3D domains should be considered.

Another significant difference that set the modelling of these two technologies apart is the characteristics of the biomass. In activated sludge systems the biomass is generally found in suspended cultures, while in CWs biomass is found also in suspension but predominantly in the form of biofilms. Moreover, and as detailed in previous chapters, the growth of bacteria within the porous media of CWs is not only limited by the availability of substrates but also by space.

In this Thesis we have demonstrated that the use of Monod expressions in CWs leads to exponential bacterial growth (Chapter 7). This does not occur when simulating activated sludge systems for two main reasons:

- in activated sludge systems the mixing of the inflow immediately dilutes pollutants,thus lowering their concentrations within the reactor.
- in activated sludge systems the excess of biomass and inert solids is controlled by purging; when simulating activated sludge systems the continuous purging keeps bacterial concentrations within a desired range.

On the contrary, in continuously fed CWs the pollutant concentrations near the inlet section are permanently the highest. Therefore, when using Monod expressions as described in the ASMs, the growth of bacteria rapidly becomes exponential in these regions. This is worsened by the fact that in in CWs no external physical control is exerted on bacterial populations and thus their growth is conditioned only by their environmental conditions. Therefore if growth limitations are not applied, bacterial concentrations become unrealistically high, preventing the convergence of numerical solutions and rendering misleading results (Samsó and García, 2014a).

Another difficulty of simulating CWs as compared to activated sludge systems is the fact that the later are operated under relatively controlled conditions (e.g. biomass concentration, oxygen concentration), while the former operate at the mercy of the environment. Therefore, identifying the impact of each parameter on the performance of CWs is a very difficult task. The same applies for the calibration of CWs models.

Clogging due to accumulated solids and bacterial biomass is another process associated to the transport in porous media that does not occur in activated sludge systems. In general, simulating clogging requires the use of sophisticated mathematical expressions which are very non-linear.

Finally, activated sludge systems are mostly aerobic (except in the inner layers of the flocks) and thus only aerobic/anoxic processes have to be simulated. On the

contrary, in CWs aerobic, anoxic and anaerobic microsites exist, and for a complete description of their functioning the processes occurring under these three conditions must be simulated. This adds to the complexity of the model by increasing the number of dependent variables.

9.2 Complete formulation of the BIO_PORE model

In Chapter 4 the mathematical model BIO_PORE was presented, and in the successive chapters only the boundary and initial conditions were modified according to the specific needs, while maintaining its original formulation. However, in Chapter 8 a new model was presented to simulate the effects of bioclogging in CWs, which also updates the hydrodynamic description used by the BIO_PORE model. Therefore, the main aim of the current section is to present the formulation resulting from including the equations of Chapter 8 in the BIO_PORE model. Once the formulation presented in this section is implemented in COMSOL Multiphysics™ and MATLAB®, the BIO_PORE model, a part from its current capabilities, will also be able to simulate clogging due to accumulated solids and bacteria biomass (biomat) as well as overland flow and transport.

9.2.1 Hydrodynamics

As seen in previous chapters, the flow of water in CWs occurs in three different conditions: saturated and unsaturated subsurface flow and overland flow. In the final formulation, and according to the assumptions made in Chapter 8, the Richards equation (Equation 9.1) is used to describe both variably saturated subsurface flow and overland flow:

$$\sigma(h)\frac{\partial h}{\partial t} - \nabla.(K(h)\nabla h) = s_s \tag{9.1}$$

where h $[L]$ is the hydraulic head, t $[T]$ is time, $\sigma(h)$ $[L^{-1}]$ is the specific volumetric storability, $K(h)$ $[LT^{-1}]$ is the hydraulic conductivity and s_s $[LT^{-1}]$ represents the contribution of sources and sinks.

The soil water retention curve in the absence of biomat for both surface and subsurface environments is obtained with Equation 9.2 (van Genuchten, 1980):

$$\theta(h) = \theta_r + S_e(h)(\theta_s - \theta_r) \tag{9.2}$$

Where $\theta(h)$ is the volumetric water content. θ_s (-) and θ_r (-) represent, respectively, the saturated and residual liquid volume fractions and

$$S_e(h) = \frac{1}{[1 + (\alpha h)^n]^l} \tag{9.3}$$

is the effective water saturation. α, n and $l = 1 - \frac{1}{n}$ are van Genuchten fitting parameters.

Note that, the van Genuchten parameters of the Richards equation for the overland flow lack any physical meaning and were selected with the sole purpose of assimilating flow in porous media to overland flow (see Chapter 8 for details). The same occurs for its saturated hydraulic conductivity and for the saturated and residual liquid volume fractions.

9.2.2 Transport of aqueous and solid phase components

The fate and transport of aqueous phase components is described with Equation 9.4:

$$\frac{\partial}{\partial t}(\theta C_k) + \nabla \cdot [-\theta D \nabla C_k + q C_k] = r_{C_k} - r_{att} + r_{det} + s_{C_k} \tag{9.4}$$

$k = 1, \ldots, n$

Where n is the total number of aqueous phase components (dissolved and particulate) and C_k $[ML^{-3}]$ is the aqueous phase concentration of the k^{th} species. θ (-) represents the liquid volume fraction, D $[L^2T^{-1}]$ is the hydrodynamic dispersion tensor and q corresponds to the specific discharge $[LT^{-1}]$. r_{C_k} $[ML^{-3}T^{-1}]$ is the reaction rate of the k^{th} species in the aqueous phase and r_{att} $[ML^{-3}T^{-1}]$ and r_{det} $[ML^{-3}T^{-1}]$ are attachment and detachment rates, respectively. s_{C_k} $[ML^{-3}T^{-1}]$ is the source/sink term, which represents external sources or sinks of species C_k.

Note that in the surface environment, dispersion (α_L and α_T), attachment (r_{att}) and detachment (r_{det}) are neglected since those processes only occur within the porous media. It is also assumed that water spends short periods of time in the surface environment and thus the reaction rate (r_{C_k}) can be neglected.

On the other hand, the fate and transport of the solid phase (immobile) components in the subsurface environment is described using Equation 9.5 (Clement et al., 1998):

$$\frac{d\check{C}_l}{dt} = r_{\check{C}_l} + r_{att} - r_{det} \tag{9.5}$$

Where $l = 1, 2, ..n$ and n is the total number of solid phase species (particulate only), $\check{C}_l$ $[ML^{-3}]$ is the concentration of the l^{th} species and $r_{\check{C}_l}[ML^{-3}T^{-1}]$ is the reaction rate of the l^{th} species on the solid phase.

The rate of attachment of particulate components in the aqueous phase is described with Equation 9.6:

$$r_{att} = \lambda_{att} C_k \tag{9.6}$$

while the rate of detachment of particulate components in the solid phase is obtained from Equation 9.7:

$$r_{dett} = \lambda_{dett} \check{C}_l \tag{9.7}$$

Where λ_{att} $[T^{-1}]$ and λ_{det} $[T^{-1}]$ are first-order attachment and detachment coefficients, respectively.

9.2.3 Bacterial growth

CWM1 formulation considers the most common functional bacterial groups found in CWs for wastewater treatment: heterotrophic (X_H), nitrifying (X_A), fermenting (X_{FB}), acetotrophic methanogenic (X_{AMB}), acetotrophic sulphate reducing (X_{ASRB}) and sulphyde oxidising (X_{SOB}) bacteria.

In CWM1 all process rates are defined with a Monod expression, and the growth rate of each bacteria group is only limited or inhibited by the presence or absence of the different substrates (see Table 1.2). As detailed in Chapter 7 this formulation leads to unlimited bacteria growth. The addition of the logistic functions of Equation 9.8 to the original formulation of CWM1 helps preventing unlimited and unrealistic growth of bacteria.

$$f_{GL} = \left(1 - \frac{M_{bio}}{M_{bio\_max}}\right)\left(1 - \frac{M_{X_{If}}}{M_{cap}}\right) \tag{9.8}$$

In Equation 9.8, the parenthesis on the left represents biofilm's self-exerted growth limitation due to diffusion-controlled transport of substrates through its exterior boundary (Wanner et al., 2006), while the parenthesis on the right represents the growth limitation exerted by the reduction of porosity as a consequence of inert solids (X_{If}) accumulation. M_{bio} $(= M_{X_H} + M_{X_A} + M_{X_{FB}} + M_{X_{AMB}} + M_{X_{ASRB}} + M_{X_{SOB}})$ $[M]$ is the sum of the total microbial biomass present in a representative volume of granular material and M_{bio_max} $[M]$ is an empirical parameter representing the maximum mass of active microbial biomass that can be maintained in the same volume (carrying capacity). $M_{X_{If}}$ $[M]$ is the actual mass of immobile X_I and M_{cap} is the maximum concentration of particulate solids that can fit a representative volume of

granular material. Biodegradable particulate organic matter (X_S) is considered not to hinder the growth of bacteria, as they can feed on it and replace the occupied volume with new cells.

The rates of all processes of CWM1 (ρ_j) after including parameter f_{GL} (Equation 9.8) are shown in Table 9.1.

Table 9.1: Processes rates in $mg \cdot l^{-1}d^{-1}$ (adapted from Langergraber et al. (2009a)).

j	**Process**	**Process rate** ρ_j
1	Hydrolysis X_{Sf}	$k_h \left[\frac{\frac{X_{Sf}}{X_H+X_{FB}}}{K_X\left(\frac{X_{Sf}}{X_H+X_{FB}}\right)} \right] (X_H+\eta_h X_{FB})$
2	Aerobic growth of X_H on S_F	$\mu_H \cdot f_{GL}\left(\frac{S_F}{K_{S_F}+S_F}\right)\left(\frac{S_F}{S_F+S_A}\right)\left(\frac{S_O}{K_{OH}+S_O}\right)\left(\frac{S_{NH}}{K_{NHH}+S_{NH}}\right)\left(\frac{K_{H2SH}}{K_{H2SH}+S_{H2S}}\right)X_H$
3	Anoxic growth of X_H on S_F	$\eta_g \cdot \mu_H \cdot f_{GL}\left(\frac{S_F}{K_{S_F}+S_F}\right)\left(\frac{S_F}{S_F+S_A}\right)\left(\frac{K_{OH}}{K_{OH}+S_O}\right)\left(\frac{S_{NO}}{K_{NOH}+S_{NO}}\right)\left(\frac{S_{NH}}{K_{NHH}+S_{NH}}\right)\left(\frac{K_{H2SH}}{K_{H2SH}+S_{H2S}}\right)X_H$
4	Aerobic growth of X_H on S_A	$\mu_H \cdot f_{GL}\left(\frac{S_A}{K_{S_A}+S_A}\right)\left(\frac{S_A}{S_F+S_A}\right)\left(\frac{S_O}{K_{OH}+S_O}\right)\left(\frac{S_{NH}}{K_{NHH}+S_{NH}}\right)\left(\frac{K_{H2SH}}{K_{H2SH}+S_{H2S}}\right)X_H$
5	Anoxic growth of X_H on S_A	$\eta_g \cdot \mu_H \cdot f_{GL}\left(\frac{S_A}{K_{S_A}+S_A}\right)\left(\frac{S_A}{S_F+S_A}\right)\left(\frac{K_{OH}}{K_{OH}+S_O}\right)\left(\frac{S_{NO}}{K_{NOH}+S_{NO}}\right)\left(\frac{S_{NH}}{K_{NHH}+S_{NH}}\right)\left(\frac{K_{H2SH}}{K_{H2SH}+S_{H2S}}\right)X_H$
6	Lysis of X_H	$b_X X_H$
7	Aerobic growth of X_A on S_{NH}	$\mu_A \cdot f_{GL}\left(\frac{S_{NH}}{K_{NHA}+S_{NH}}\right)\left(\frac{S_O}{K_{OA}+S_O}\right)\left(\frac{K_{H2SA}}{K_{H2SA}+S_{H2S}}\right)X_A$
8	Lysis of X_A	$b_A X_A$
9	Growth of X_{FB}	$\mu_{FB} \cdot f_{GL}\left(\frac{S_F}{K_{S_{FB}}+S_F}\right)\left(\frac{K_{H2SFB}}{K_{H2SFB}+S_{H2S}}\right)\left(\frac{K_{OFB}}{K_{OFB}+S_O}\right)\left(\frac{K_{NOFB}}{K_{NOFB}+S_{NO}}\right)\left(\frac{S_{NH}}{K_{NHFB}+S_{NH}}\right)X_{FB}$
10	Lysis of X_{FB}	$b_{FB} X_{FB}$
11	Growth of X_{AMB}	$\mu_{AMB} \cdot f_{GL}\left(\frac{S_A}{K_{SAMB}+S_A}\right)\left(\frac{K_{H2SAMB}}{K_{H2SAMB}+S_{H2S}}\right)\left(\frac{K_{OAMB}}{K_{OAMB}+S_O}\right)\left(\frac{K_{NOAMB}}{K_{NOAMB}+S_{NO}}\right)\left(\frac{S_{NH}}{K_{NHAMB}+S_{NH}}\right)X_{AMB}$
12	Lysis of X_{AMB}	$b_{AMB} X_{AMB}$
13	Growth of X_{ASRB}	$\mu_{ASRB} \cdot f_{GL}\left(\frac{S_A}{K_{SAASRB}+S_A}\right)\left(\frac{S_{SO4}}{K_{SO4ASRB}+S_{SO4}}\right)\left(\frac{K_{H2SASRB}}{K_{H2SASRB}+S_{H2S}}\right)\left(\frac{K_{OASRB}}{K_{OASRB}+S_O}\right)\left(\frac{K_{NOASRB}}{K_{NOASRB}+S_{NO}}\right)\left(\frac{S_{NH}}{K_{NHASRB}+S_{NH}}\right)X_{ASRB}$
14	Lysis of X_{XASRB}	$b_{ASRB} X_{ASRB}$
15	Aerobic growth of X_{SOB} on S_{H2S}	$\mu_{SOB} \cdot f_{GL}\left(\frac{S_{H2S}}{K_{SSOB}+S_{H2S}}\right)\left(\frac{S_O}{K_{OSOB}+S_O}\right)\left(\frac{S_{NH}}{K_{NHSOB}+S_{NH}}\right)X_{SOB}$
16	Anoxic growth of X_{SOB} on S_{H2S}	$\eta_{SOB} \cdot \mu_{SOB} \cdot f_{GL}\left(\frac{S_{H2S}}{K_{SSOB}+S_{H2S}}\right)\left(\frac{S_{NO}}{K_{NOSOB}+S_{NO}}\right)\left(\frac{K_{OSOB}}{K_{OSOB}+S_O}\right)\left(\frac{S_{NH}}{K_{NHSOB}+S_{NH}}\right)X_{SOB}$
17	Lysis of X_{SOB}	$b_{SOB} X_{SOB}$

9.2.4 Substrates degradation/transformation rates

The rate at which the different substrates are degraded/transformed (r_i) is obtained with equation 9.9.

$$r_i = \sum_{j=1}^{R} v_{i,j} \cdot \rho_j \tag{9.9}$$

where $i = 1, \ldots, N$ and N is the number of components. $j = 1, \ldots, R$ and R is the number of processes. $v_{i,j}$ is the stoichiometric factor for component i and process j from Table 9.1 and ρ_j is the reaction rate of process j as described in Table 9.2.

Note that r_i corresponds to r_{C_k} in Equation 9.4 for aqueous phase components and to $r_{\check{C}_l}$ in Equation 9.5 for solid phase components. Also note that the original stoichiometric matrix of CWM1 (Table 1.1) has been updated to consider the division of X_S (in X_{Sf} and X_{Sm}) and X_I (in X_{If} and X_{Im}) required to simulate attachment and detachment of these components (see Section 9.2.2). The new stoichiometric matrix is presented in Tables 9.2 and 9.3. Note that the stoichiometric matrix has been divided in two to fit the page size.

Table 9.2: Stoichiometric matrix of CWM1 (adapted from Langergraber et al. (2009a)).

	i	1	2	3	4	5	6	7	8	9	10	11	12	...
	Process component	S_O	S_F	S_A	S_I	S_{NH}	S_{NO}	S_{SO4}	S_{H2S}	X_{Sf}	X_{If}	X_{Sm}	X_{Im}	
j	*expressed as*	O_2	COD	COD	COD	N	N	S	S	COD	COD	COD	COD	
1	Hydrolysis		$1-f_{Hyd,SI}$		$f_{Hyd,SI}$	$v_{5,1}$								
2	Aerobic growth of X_H on S_F	$1-\frac{1}{Y_H}$	$\frac{-1}{Y_H}$			$v_{5,2}$								
3	Anoxic growth of X_H on S_F		$\frac{-1}{Y_H}$			$v_{5,3}$	$\frac{-1-Y_H}{2.86 \cdot Y_H}$							
4	Aerobic growth of X_H on S_A	$1-\frac{1}{Y_H}$		$-\frac{1}{Y_H}$		$v_{5,4}$								
5	Anoxic growth of X_H on S_A			$-\frac{1}{Y_H}$		$v_{5,5}$	$-\frac{1-Y_H}{2.86 \cdot Y_H}$							
6	Lysis of X_H		$f_{BM,SF}$			$v_{5,6}$				$v_{9,Lysis}$	$f_{BM,XI}$			
7	Aerobic growth of X_A on S_{NH}	$-\frac{4.57-Y_A}{Y_A}$				$v_{5,7}$								
8	Lysis of X_A		$f_{BM,SF}$			$v_{5,8}$				$v_{9,Lysis}$	$f_{BM,XI}$			
9	Growth of X_{FB}		$\frac{-1}{Y_{FB}}$	$\frac{1-Y_{FB}}{Y_{FB}}$		$v_{5,9}$								
10	Lysis of X_{FB}		$f_{BM,SF}$			$v_{5,10}$				$v_{9,Lysis}$	$f_{BM,XI}$			
11	Growth of X_{AMB}			$\frac{-1}{Y_{AMB}}$		$v_{5,11}$								
12	Lysis of X_{AMB}		$f_{BM,SF}$			$v_{5,12}$				$v_{9,Lysis}$	$f_{BM,XI}$			
13	Growth of X_{ASRB}			$\frac{-1}{Y_{ASRB}}$		$v_{5,13}$		$-\frac{1-Y_{ASRB}}{2 \cdot Y_{ASRB}}$	$\frac{1-Y_{ASRB}}{2 \cdot Y_{ASRB}}$					
14	Lysis of X_{XASRB}		$f_{BM,SF}$			$v_{5,14}$				$v_{9,Lysis}$	$f_{BM,XI}$			
15	Aerobic growth of X_{SOB} on S_{H2S}	$-\frac{2-Y_{SOB}}{Y_{SOB}}$				$v_{5,15}$		$\frac{-1-Y_{SOB}}{0.875-Y_{SOB}}$	$\frac{1}{Y_{SOB}}$					
16	Anoxic growth of X_{SOB} on S_{H2S}					$v_{5,16}$	$\frac{-1-Y_{SOB}}{0.875-Y_{SOB}}$	$\frac{1}{Y_{SOB}}$	$\frac{-1}{Y_{SOB}}$					
17	Lysis of X_{SOB}		$f_{BM,SF}$			$v_{5,17}$				$v_{9,Lysis}$	$f_{BM,XI}$			

$v_{9,Lysis} = 1 - f_{BM,SF} - f_{BM,XI}$

Table 9.3: Stoichiometric matrix of CWM1 (adapted from Langergraber et al. (2009a)).

	i	...	13	14	15	16	17	18
	Process component		X_H	X_A	X_{FB}	X_{AMB}	X_{ASRB}	X_{SOB}
j	*expressed as*		COD	COD	COD	COD	COD	COD
1	Hydrolysis							
2	Aerobic growth of X_H on S_F		1					
3	Anoxic growth of X_H on S_F		1					
4	Aerobic growth of X_H on S_A		1					
5	Anoxic growth of X_H on S_A		1					
6	Lysis of X_H		−1					
7	Aerobic growth of X_A on S_{NH}			1				
8	Lysis of X_A			−1				
9	Growth of X_{FB}				1			
10	Lysis of X_{FB}				−1			
11	Growth of X_{AMB}					1		
12	Lysis of X_{AMB}					−1		
13	Growth of X_{ASRB}						1	
14	Lysis of X_{XASRB}						−1	
15	Aerobic growth of X_{SOB} on S_{H2S}							1
16	Anoxic growth of X_{SOB} on S_{H2S}							1
17	Lysis of X_{SOB}							−1

$v_{9,Lysis} = 1 - f_{BM,SF} - f_{BM,XI}$

9.2.5 Clogging

Based on the capillary model (Mualem, 1976), the pore size distribution of the areas free of bacteria and particulate solids (biomat) is estimated using Equations 9.10 and 9.11 (Rosenzweig et al., 2009).

$$r_f = -\frac{2\sigma \cos\beta}{\gamma h} \tag{9.10}$$

$$N_{f,i} = \frac{\Delta\theta}{\pi r_{f,i}^2} \tag{9.11}$$

Where r_f is the effective radius of the largest water-filled capillary for every pressure head value, and $N_{f,i}$ is the density number of the capillaries of radius $r_{f,i}$ (Rosenzweig et al., 2009). Following the notation utilized by Rosenzweig et al. (2009), sub-index f indicates biomat-free conditions. σ is the water surface tension ($0.072 N \cdot m^{-1}$ for distilled water at 20 °C), γ is water's specific weight and β $(-)$ is the water contact angle within the tube walls, which is usually set to 0 (Rosenzweig et al., 2009). θ is the initial (biomat-free) water content for every pressure head value, obtained with van Genuchten model (Equation 9.2) and $\Delta\theta$ are increments of the water content between two consecutive pore radii.

The new pore size distribution in the presence of biomat is calculated with Equations 9.12 and 9.13:

$$r_{b,i} = r_{f,i}\sqrt{1 - S_{em}(h)} \tag{9.12}$$

$$N_{b,i} = N_{f,i} \tag{9.13}$$

Where $S_{em}(h) = \frac{\theta_m}{\theta_s - \theta_r}$ is the specific saturation of biomat. $\theta_m = \frac{V_m}{V_{total}}$ (-) is the volume fraction of the soil occupied by bacteria (Mostafa and Van Geel, 2007; Weill et al., 2009) and V_{total} and V_m (both in $[L^3]$) are, respectively, a representative volume of granular material and the actual volume of biomat in that representative volume. V_m is obtained by summing the concentration of each functional bacterial group ($X_H + X_A + X_{FB} + X_{AMB} + X_{ASRB} + X_{SOB}$ (all in $mgCOD \cdot L^{-1}$)) and the concentration of accumulated particulate solids (X_{Sf} and X_{If} (in $mgCOD \cdot L^{-1}$)) and multiplying it by the density of the biomat (ρ_{biomat}).

The updated water content in the presence of biomat is obtained with Eq. 9.14 (Rosenzweig et al., 2009):

$$\theta_{w,j} = \theta_r + \pi \sum_{i=1}^{j} N_{b,i} r_{b,i}^2 \tag{9.14}$$

The value of $\theta_{w,j}$ ranges from θ_r to $\theta_r - \theta_m$. In Equation 9.14, $j = 1 : M$ corresponds to the index of the capillary groups.

The water content ($\theta_{w,j}$) is then used to calculate the new effective water saturation ($S_{ew,j}$) as follows:

$$S_{ew,j}(h) = \frac{\theta_{w,j} - \theta_r}{\theta_s - \theta_r} \tag{9.15}$$

Finally, the relative unsaturated hydraulic conductivity (with respect to the initial one) in the presence of biomat (k_b) is calculated using the following expression (Rosenzweig et al., 2009):

$$k_b(\theta_{w,j}) = \frac{\sum_{i=1}^{j} N_{b,i} r_{b,i}^4}{\sum_{i=1}^{M} N_{f,i} r_{f,i}^4} \tag{9.16}$$

and thus the updated value of $K(h)$ in Eq. 9.1 in areas where clogging occurs is obtained with:

$$K(h) = k_b(h) K_{sat} \tag{9.17}$$

whereas in areas where clogging does not take place, the hydraulic conductivity remains the same as in the initial conditions and is obtained with:

$$K(h) = k_r(h) K_{sat} \tag{9.18}$$

Where,

$$k_r(h) = S_e(h)^l [1 - (1 - S_e(h)^{\frac{1}{l}})^l]^2 \tag{9.19}$$

is the biomat-free relative hydraulic conductivity and $S_e(h)$ is obtained from Equation 9.3.

9.3 Comparison of available CWs models

In the first part of the present section we contextualise what was achieved with the current work by comparing BIO_PORE's main features with those of the other models presented in Chapter 1. Those models are *FITOVERT*, *HYDRUS-2D-CW2D/CWM1*, *AQUASIM-CWM1*, *CWM1-RETRASO* and *PHWAT*. Then all these models are also compared to find advantages and disadvantages of each one of them in terms of the licensing and the expected evolution of the codes in the future.

9.3.1 Richness of features

The most relevant aspect of *FITOVERT* (Giraldi et al., 2009, 2010) is that it is able to simulate the effects of bacterial growth and solids accumulation on the hydraulic properties of the granular media. It is also able to handle bed surface ponding by adapting the hydraulic boundary conditions. This model was specifically designed to simulate VF CWs only, and it includes a dedicated graphical user interface (GUI). It is the only of the reviewed models using neither CW2D nor CWM1, although its biokinetic model is also based on the ASM formulation. This model was only calibrated for the hydraulics and hydrodynamics, while the biokinetic model lacks calibration. To our knowledge, only the two publications cited above are available on the application of *FITOVERT*.

As for *FITOVERT*, the main advantage of *HYDRUS-2D-CW2D/CWM1* models (Langergraber, 2005; Langergraber and Simunek, 2012), is that they include a dedicated GUI to simulate CWs. This fact has ended in a good adoption of these models among the scientific community which has given place to several scientific publications (Korkusuz et al., 2007; Langergraber, 2007, 2005). Another advantage is that HYDRUS-2D can use different biokinetic models depending on whether a VF (CW2D) or a HF (CWM1) CW is to be simulated. However, the model has only been applied and calibrated for short simulation time-frames, since bacterial growth is not limited and hence the high bacterial concentrations reached after a short simulation time prevents model convergence (Samsó and García, 2013a). Another unresolved issue of this model is its inability to simulate the transport and retention of particulate components and thus clogging (Langergraber and Simunek, 2012).

On the other hand, the main advantage of *PHWAT* (Brovelli et al., 2009a,b,c, 2007) is that it includes a large number of physical-chemical and biological processes. Its modularity is also a positive point, since it facilitates the task of adding or removing features. It is also one of the few available models for CWs able to simulate bioclogging together with biomass attachment-detachment processes, and also considers growth limitations for biomass. Although bacteria distribution obtained with *PHWAT* was qualitatively compared with results obtained with other models for the same experimental setup, this model could only match measured permeability decrease for the initial 28 days out of a 283 days long experiment (Brovelli et al., 2009a). Another weak point of *PHWAT* for CWs is that little information about model equations is given in the few publications available and so the work is difficult to reproduce.

The most relevant feature of *AQUASIM-CWM1* (Mburu et al., 2012) is the inclusion of a sophisticated model for plant-related processes. On the other hand, the main drawback of this model resides in the fact that it uses the mixed reactor compartment hydraulics description. For this reason the model cannot be used to simulate full-scale systems. Also, this model does not consider clogging nor bacterial

growth limitations and thus it can neither be used to simulate continuously fed CWs.

CWM1-RETRASO (Llorens et al., 2011a,b) is a powerful model in terms of biogeochemical reactions. Nevertheless its main disadvantage resides in the fact that bacterial communities are not static, but travel with the flow. The same happens with particulate solids.

Finally, the most notable feature of the *BIO_PORE* model is that it considers growth limitations for bacterial communities. These growth limitations were key to obtain realistic bacterial growth rates and distributions and also to avoid numerical problems (non converging solutions). The modifications to the CWM1 formulation presented in sections 9.2.3 and 9.2.4 also allowed the simulation of the transport and attachment and detachment of particulate solids. The previous two factors were essential to simulate the behaviour of CWs for mid to long-term scenarios (Samsó and García, 2013a,b). Moreover, this model was satisfactorily calibrated with experimentally measured effluent concentrations of COD and ammonium and ammonia nitrogen for a period of 1 year. BIO_PORE includes a bioclogging model (presented in Chapter 8), which was combined with the original formulation of the BIO_PORE model (Chapter 4) in Section 9.2 of the current chapter. The complete model adds to the original capabilities of the BIO_PORE model the possibility to simulate the reduction of the hydraulic conductivity caused by the accumulation of particulate solids and bacterial biomass. It also makes it possible to simulate overland flow caused by severe clogging conditions. However, the final version of the BIO_PORE model has not yet been implemented in COMSOL Multiphysics™.

9.3.2 Licensing

Among the platforms used to build the models that are being compared, HYDRUS is the only one offering a compiled package/module specific for CWs simulations which can be acquired at a price. The rest of the models reviewed are implementations of different sets of mathematical expressions describing biokinetic reactions and other physical-chemical processes into multi-purpose simulation platforms.

Despite having a GUI is a clear benefit for potential users, not having access to the code may represent a limitation for a model that is currently under development and that is meant to be used for academic purposes. That is the case of *HYDRUS-CW2D/CWM1*, which is a closed-source piece of software, and thus any modifications to the code can only be applied by their developers.

One of the advantages of the implementation of *AQUASIM-CWM1* is that the AQUASIM platform itself can be downloaded free of charge (although it is not open source), and so the distribution of the implementation of the CWM1 made by Mburu et al. (2012) only depends on the author's willingness to share it. Likewise, the

equations describing the different physical-chemical and biological processes are easily customizable.

On the other hand, BIO_PORE model is built combining COMSOL Multiphysics™ and MATLAB® code. This simulation environment is very versatile and it is widely used around the world in many disciplines, although it is expensive and closed-source. Despite the latter inconveniences, the implementation of CWM1 and other equations on this platform can be shared and modified in a way similar as for *AQUASIM-CWM1*, as long as COMSOL Multiphysics™ and MATLAB® licenses are available. The same applies for *FITOVERT*, but in this case, the user only requires a MATLAB® license.

RetrasoCodebright (RCB) (Saaltink et al., 2004) can be downloaded free of charge, although its source code is not available. So the model of Llorens et al. (2011a,b) was built on top using the available functionalities of the software, much in the way of *BIO_PORE*, *AQUASIM-CWM1* and *FITOVERT*. However RCB lacks a graphical user interface, and the biokinetic model and other equations need to be implemented using text files, which makes it significantly less versatile and intuitive to the user.

PHWAT is a modular piece of software developed in FORTRAN 90 and C programming languages and the author makes it available for free for non-commercial use. Brovelli et al. (2007, 2009a,b,c) developed specific modules to simulate CWs, although no reference is made about their availability.

9.3.3 Code evolution

HYDRUS-CWM1/CW2D is by far the platform with the most adopters, and the one that has produced more publications, and thus it should be the one with the most chances of evolving the fastest. However, in our opinion, the fact that only the authors can modify the code is delaying its evolution.

To our knowledge, the last publication using *FITOVERT* is that of Giraldi et al. (2010), which seems to indicate that its development has been discontinued. The same happens for publications on CWs modelling using *PHWAT* platform.

Provided AQUASIM can be acquired free of charge, everything indicates that *AQUASIM-CWM1* could increase adoption if a more sophisticated description of wetland hydraulics and hydrodynamics were used.

On the other hand, a recent paper by Mburu et al. (2013) has continued the use of *CWM1-RETRASO*, although the code has not evolved since Llorens et al. (2011a,b) and so fixed biomass cannot be simulated yet. However, Llorens et al. (2013) introduced new reactions related to arsenic retention in CWs (precipitation, adsorption, uptake and accumulation in plants) in RCB's code.

Finally, *BIO_PORE* model is receiving increasing attention, since it is the only one able to simulate the functioning of continuously fed CWs in the long-term. Moreover, the fact that it will soon be able to simulate clogging may also raise interest in academic circles. Also, we expect that the ease of use and potential of combining COMSOL Multiphysics™ and MATLAB® may result in a fast evolution of the code.

9.4 Must-have processes in CW models

From this work it should be clear that for a complete and sound description of CWs functioning, at least the following essential phenomena and processes need to be included in the future generations of the scientific mechanistic models:

- A complete hydraulic description (variably saturated subsurface flow and surface flow and ponding).
- Transport of dissolved, particulate and gaseous components.
- Filtration, sedimentation, precipitation, volatilization, dissolution, adsorption and desorption and physical re-aeration.
- Bacterial processes
  - Growth and decay (suspended and in the form of biofilms).
  - Attachment and detachment.
  - Influence of substrates concentration, available space, diffusion limitations, temperature, pH and redox potential on bacterial growth.
  - Hydrolysis of both slowly biodegradable and inert organic fractions.
- Plant processes
  - Above and belowground growth.
  - Decay/senescence.
  - Nutrients uptake oxygen release through the rhizosphere.
  - Carbon exudates.
  - Evapotranspiration.
- Clogging by accumulate solids, biomass and extracellular polymeric substances (EPS), precipitates, plant roots and plant litter and its effects on the hydraulics and hydrodynamics of the granular media.

The ability to perform long-term simulations, though not being a process nor a phenomenon, is already reckoned as an essential feature of the next generations of CWs models.

9.5 Past, present and future of CWs modelling

At first (nineties) the idea was to develop simple models that could be used to improve design, based on first order decay expressions and neglecting the real processes leading to pollutants removal (Kadlec, 2000). However, wetlands are very complex systems that interact with the environment and the experience using these models demonstrated that they were not sufficient to reproduce the enormous variability observed in their performance in different environments and for different wastewater compositions (Kadlec, 2000).

Therefore, these initial ideas and models were later substituted with the use of more sophisticated models, which intend to describe the widest possible range of the internal processes taking place within wetlands with deterministic mathematical expressions.

However, the expectations around these models has progressively decreased due to their complexity (for the untrained users) and their inability to generate consistent results for long-term scenarios, which hinders their use by designers, operators and the scientific community (Samsó and García, 2013a). In fact, so far these models have only been used to match effluent pollutant concentrations for short periods of time, while paying little or no attention to the internal processes (Samsó and García, 2014a).

A new trend has been growing in recent times, which accepts the embrionary stage of these models to be used for design, and rather it recognizes their great potential in terms of improving the understanding of CWs functioning. The current tendency is thus to increase even more the complexity and the number of processes that these models consider and to try to produce long-term simulations and to focus not only on matching effluent pollutant concentrations but also on understanding the internal processes (scientific purposes).

In parallel to the development of these complex models, a separate branch has started developing models of lower complexity, which aim to provide an easy-to-use tool that can be used by designers and operators without requiring much understanding of the internal processes of CWs (Meyer, 2011).

Figure 9.1 shows the evolution of the complexity of numerical models for CWs since the early nineties until today. A prediction of the future of CWs models is also presented.

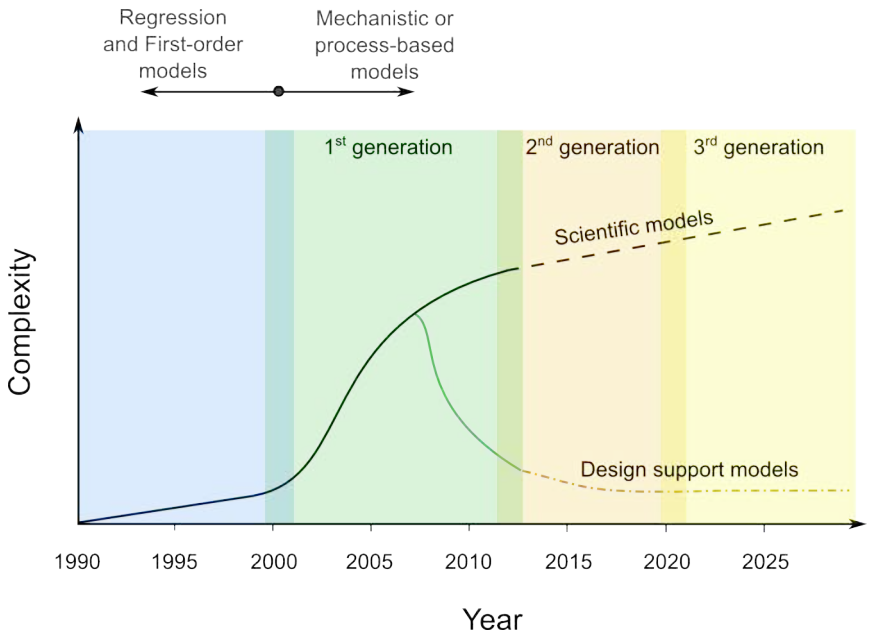

Figure 9.1: Evolution of the complexity of the scientific models and those used to support the design of CWs models over the years. The likely evolution of these models in the near future is represented with dotted lines.

In the following lines, a brief description of the different stages shown in Figure 9.1 is made.

9.5.1 1st generation models

After around 20 years of CWs models development, the current (1st generation) scientific models are able to confidently simulate saturated or variably saturated subsurface flow (horizontal or vertical), transport of dissolved and particulate pollutants and the temperature and substrates dependent growth and decay of different bacterial groups at the macro-scale. Most models are also able to describe other relevant processes such as sorption, evapotranspiration and plant nutrients uptake and oxygen release. At the current stage, these models can be used to direct research, to explain experimental results and to increase the understanding of the internal functioning of CWs.

On the other hand, the 1st generation of models for design purposes are still under heavy development. The first stage of their development consisted on cutting down the number of processes so as to only consider those with the biggest impact on the functioning and application of CWs. A good example of that is the model *RSF_Sim*, developed to simulate the treatment of combined sewer overflows with CWs (Meyer, 2011; Meyer et al., 2014).

9.5.2 2nd generation models

Possibly the most easily achievable and most significant evolution of the current scientific models for CWs will come from the development of sophisticated clogging models, which will include the pore space and subsequent hydraulic conductivity reduction caused by the accumulation of solids (organic and inorganic) and by bacterial growth. To that end, the first step will be to improve the description of the transport of particulate components (attachment and detachment). Furthermore, to make a comprehensive description of the whole clogging processes, the subsurface-flow equations (Darcy/Richards equations) will need to be coupled to surface-flow equations (e.g. shallow water equations or Saint-Venant equations) to represent surface-flow and ponding. To this regard, the model developed in the current work is steadily progressing in that direction. These clogging models will need to be calibrated and validated first with experimental data coming from lab-scale experiments (due to the lack of experimental data in real cases) and later for full-scale systems.

It is already well accepted that bacterial communities play a major role in the functioning of CWs (Faulwetter et al., 2009; Samsó and García, 2013a,b) and thus better models for CWs will necessary come from more advanced biokinetic models. CWM1 and CW2D are both based on the initial versions of ASM models, which have received continuous upgrades over the years. On the contrary, neither CWM1 nor CW2D has received any modifications since their inception. Moreover, having two different biokinetic models for CWs only makes sense in terms of saving computational power (fewer dependent variables), since the biokinetic processes are mostly the same (in different proportions) in all subsurface-flow CWs. However, with the ever increasing computational power, having fewer dependent variables is ever less of an advantage. In fact a unified biokinetic model would reduce model divergence and by joining all efforts on a unique and common platform, faster development could be achieved.

We also envisage that future models will incorporate chemical equilibrium equations for several key components as well as the inclusion of pH and redox potential (Rolle et al., 2008) as controlling factors of the growth of the different functional bacterial groups.

Regarding the second generation of CWs models for design purposes, they will result from a progressive reduction of the number of considered processes, and from extensive validation with experimental data. The main idea can be found in a shift away from a process description towards a treatment effect description. The biggest challenge will be the definition of limits for the extrapolation of performance assumptions. This will only be achieved by creating a freely available database of experimental data from a wide range of systems, especially from those showing malfunctioning. In this way a strong link between researchers and industrial partners is

essential, because the stakeholders of interest in design support models are also the stakeholders of the required database (Samsó et al., 2014b).

9.5.3 3rd generation models

The third generation of mechanistic models will come from a better description of biofilm structure and processes through micro-scale models and possibly with the inclusion of more sophisticated above and belowground plant models. However, it is expected that the stochastic nature of plant roots distribution will delay the inclusion of this phenomenon on the clogging description.

The evolution of mathematical models has to go side by side with progresses through experimental studies and fundamental research (empirical evidence). The scientific community can keep increasing the complexity of the models in a parallel to the increasing knowledge. The limit of complexity that these models can achieve will likely come from our difficulties to understand and justify their outputs.

On the other hand, a third generation of design support models will have already been validated in many different scenarios. These models could incorporate optimization modules that should give the optimum wetland configuration and dimensioning for specific cases based only on small sets of monitoring data from the corresponding locations. An easy-to-use GUI should be available for engineers in daily practice. Risks can be seen in inadequate applications, since a model can only support, but not replace engineering (Samsó et al., 2014b).

CHAPTER 10

Conclusions

In this PhD, a mathematical model was developed to simulate the main physic-chemical and biological processes taking place within Horizontal Subsurface Flow Constructed Wetlands (HSSF CWs). This model includes two empirical parameters that improve the description of biomass growth defined by the biokinetic model Constructed Wetlands Model number 1 (CWM1). The model was calibrated with experimental data from an entire year of operation of a pilot HSSF CW and a sensitivity analysis was performed to evaluate the effects of the newly introduced empirical parameters on the outputs of the model. A mesh optimization study was also carried out to limit computational cost. The model was later utilized on a case study to increase the understanding of the internal functioning of these systems, paying special attention to the dynamics of bacterial communities and their interaction with inert accumulated solids. A theoretical background to describe the most basic functioning patterns of HSSF CWs was derived from simulation results. Finally, a mathematical formulation was proposed to describe the effects of bioclogging in the hydrodynamics of these systems.

The conclusions have been separated in the 4 main blocks in which this Thesis is divided to facilitate the identification of each conclusion with the starting objectives.

The BIO_PORE model

- The BIO_PORE is a mathematical model for HSSF CWs built in COMSOL Multiphysics™, which uses the finite elements method to obtain approximate solutions to the model equations. It includes equations to describe saturated/unsaturated flow and transport of aqueous and solid phase pollutants through porous media. The pollutants and bacteria considered are those included in the biokinetic model Constructed Wetlands Model number 1, which also describes the rates of all processes involved. All model parameters are made temperature dependent and the uptake of nutrients and oxygen release by plant roots are also included. The BIO_PORE model is also able to simulate filtration and retention of solid phase (particulate) components.
- The BIO_PORE was able to reproduce the hydraulic and hydrodynamic behaviour of a pilot constructed wetland. Moreover, a reasonable good fit was achieved between the effluent COD and ammonia and ammonium nitrogen (S_{NH}) predicted by the model and those measured in the experimental plant during its entire first year of operation. Simulation results also showed that by considering measured water temperatures, experimental data could be better matched. On the other hand, the inclusion of plant roots oxygen release and nutrients uptake did not cause significant differences in the results.
- Parameter M_{cap} $[M]$ corresponds to the mass of accumulated slowly biodegradable (X_{Sf}) and inert (X_{If}) solids that can be reached in a representative volume of granular material. M_{bio_max} $[M]$ is the carrying capacity of the system, which is the maximum amount of biomass that can be sustained within the representative volume before competition for substrates and space start to affect bacterial growth.
- Parameter M_{bio_max} is essential to prevent simulated unlimited bacterial growth in the areas of wetlands where substrates concentrations are persistently high. That is the case of the inlet section of continuously fed constructed wetlands. By preventing the unlimited growth of bacteria, simulated time can be set as desired and it is not limited by convergence issues resulting from large bacterial gradients. Parameter M_{cap} takes into account the necessary effect of accumulated solids on bacterial communities.
- Parameter M_{cap} dictates the rate of displacement of bacterial communities towards the outlet section over time predicted by the model. On the other hand M_{bio_max} influences the extent of the spatial distribution of bacterial communities within the wetland.
- Small perturbations on the values of M_{cap} and M_{bio_max} produce important changes in the effluent pollutant concentrations predicted by the model. The

higher the value of M_{cap} the lower the simulated effluent pollutant concentrations. On the other hand, and although very different results are obtained for different values of M_{bio_max}, no clear recognisable pattern on the effluent pollutant concentrations can be observed.

Case study of a HSSF CW

- Aerobic bacteria dominated the wetland during the beginning of operation due to their faster specific growth rate and to the highly oxygenated initial conditions. Shortly after the initial period (around 80 days) anaerobic bacteria groups became dominant. Sulphate reducing bacteria (X_{ASRB}) became the most abundant group ($47 - 79\%$ of total biomass).
- Toxicity caused by dihydrogen sulphide (S_{H2S}) was an important parameter affecting the general functioning of the wetland, since it delayed the growth of methanogenic bacteria (X_{AMB}) and hence the overall bacterial stability.
- Bacterial stability as predicted by our model was achieved between 400 and 700 days after start-up of the wetland. This time to stability is longer than the $75 - 100$ days reported by previous experimental works. This fact was attributed to the high toxicity by S_{H2S} within the simulated wetland.
- The active bacteria zone was located in a narrow strip of the constructed wetland (approximately a third of its length), which progressed towards the outlet over time. Aerobic bacteria occupied the first few centimetres near the wetland's surface while anaerobic bacteria grew just underneath, thus having a much wider vertical distribution. Sulphide oxidising bacteria grew mainly under anoxic conditions in a very restricted area near the outlet and was responsible for practically all S_{NO} removed within the wetland.

The Cartridge Theory

- *The Cartridge Theory* describes the general functioning of HSSF CWs based on the interaction between bacterial communities and accumulated solids (clogging) and was derived from simulation results with BIO_PORE model.
- The theory assimilates the granular media of HSSF CWs to a generic cartridge which is consumed (clogged) with inert solids from inlet to outlet with time.
- The failure of a wetland as described by *The Cartridge Theory* occurs when the active bacteria zone is located as close to the outlet section that its total biomass is not sufficient to degrade an acceptable proportion of the inflow pollutants.

- Although *The Cartridge Theory* may be considered as an oversimplification of the real complexity of HSSF CWs, this is the first time that an integrated description of the functioning of these systems is made based on modelling results and represents an important step towards the complete understanding of the functioning of these systems.

Integrated simulation of bioclogging in HSSF CWS

- In this part of the work we presented a standalone model built on COMSOL Multiphysics™ to simulate bioclogging and surface/subsurface flow interactions in HSSF CWs.
- A numerical experiment was carried out, which consisted on comparing different model outputs from two separate simulations: one considering the effects of bioclogging in the hydrodynamics of the granular media and the other one neglecting them.
- Very different bacteria distributions and flow patterns were obtained from the two simulations. On the contrary, the effluent concentrations and the percentage of total porosity occupation were almost identical for the two cases.
- The formulation presented in this work needs to be merged to that of the the BIO_PORE model in order to have a complete description of the functioning of HSSF CWs.
- Further research on this model should include a parametric sensitivity analysis in order to stablish the relative impact of each model parameter on the different model outputs.

Bibliography

Aguirre, P., Ojeda, E., García, J., Barragán, J., Mujeriego, R., 2005. Effect of water depth on the removal of organic matter in horizontal subsurface flow constructed wetlands. Journal of environmental science and health 40, 1457–1466.

Ahn, C., Gillevet, P., Sikaroodi, M., 2007. Molecular characterization of microbial communities in treatment microcosm wetlands as influenced by macrophytes and phosphorus loading. Ecological Indicators 7, 852–863. doi:10.1016/j.ecolind.2006.10.004.

Akratos, C., Papaspyros, J., Tsihrintzis, V., 2008. An artificial neural network model and design equations for BOD and COD removal prediction in horizontal subsurface flow constructed wetlands. Chemical Engineering Journal 143, 96–110. doi:10.1016/j.cej.2007.12.029.

Akratos, C.S., Papaspyros, J.N.E., Tsihrintzis, V.a., 2009. Total nitrogen and ammonia removal prediction in horizontal subsurface flow constructed wetlands: use of artificial neural networks and development of a design equation. Bioresource technology 100, 586–96. doi:10.1016/j.biortech.2008.06.071.

Alburquerque, C., 2013. Report of the Special Rapporteur on the human right to safe drinking water and sanitation. Technical Report July. United Nations General Assembly.

Allen, W.C., Hook, P.B., Biederman, J.A., Stein, O.R., 2002. Temperature and Wetland Plant Species Effects on Wastewater Treatment and Root Zone Oxidation. Journal of Environmental Quality 31. doi:10.2134/jeq2002.1010.

Álvarez, J., Ruíz, I., Soto, M., 2008. Anaerobic digesters as a pretreatment for constructed wetlands. Ecological Engineering 33, 54–67. doi:10.1016/j.ecoleng.2008.02.001.

Arias, L., Bertrand-Krajewski, J., Molle, P., 2014. Simplified hydraulic Model of French vertical-flow constructed wetlands. Water Science and Technology. (Submitted) .

Baptista, J., Donnelly, T., Rayne, D., Davenport, R., 2003. Microbial Mechanisms of Carbon Removal in Laboratory-scale Subsurface Flow Constructed Wetlands. Water Science and Technology 5.

Batstone, D.J., Keller, J., Angelidaki, I., Kalyuzhny, S.V., Pavlostathis, S.G., Rozzi, A., Sanders, W.T.M., Siegrist, H., Vavilin, V.A., 2002. Anaerobic digestion model No. 1 (ADM1). IWA Publishing.

Boller, M., Kavanaugh, M., 1995. Particle characteristics and headloss increase in granular media filtration. Water Research 29, 1139–1149.

Bonte, M., Van Breukelen, B.M., Stuyfzand, P.J., 2013. Environmental impacts of aquifer thermal energy storage investigated by field and laboratory experiments. Journal of Water and Climate Change 4, 77. doi:10.2166/wcc.2013.061.

Bradford, S.A., Bettahar, M., Simunek, J., van Genuchten, M.T., 2004. Straining and Attachment of Colloids in Physically Heterogeneous Porous Media. Vadose Zone Journal , 384–394.

Bresler, E., 1973. Simultaneous transport of solutes and water under transient unsaturated flow conditions. Water Resources Research 9, 975–986. doi:10.1029/WR009i004p00975.

Brix, H., Arias, C.A., 2005. The use of vertical flow constructed wetlands for on-site treatment of domestic wastewater: New Danish guidelines. Ecological Engineering 25, 491–500. doi:10.1016/j.ecoleng.2005.07.009.

Brovelli, A., Baechler, S., L., R., D.A., B., 2009a. Comprehensive process-based modelling of sand filters and subsurface flow constructed wetlands, in: Proceedings of the 3rd International symposium on wetland pollutant dynamics and control, Barcelona, Spain. p. 18.

Brovelli, A., Baechler, S., Rossi, L., G., L., D.A., B., 2007. Coupled flow and hydrogeochemical modelling for design and optimization of horizontal flow constructed wetlands, in: Proceedings of the 2nd WETPOL, Tartu, Estonia. pp. 393–395.

Brovelli, A., L., R., D.A., B., 2009c. Mechanistic understanding and prediction of bioclogging in sand filters and subsurface flow constructed wetlands, in: Proceedings of the 3rd International symposium on wetland pollutant dynamics and control, Barcelona, Spain.

Brovelli, A., Malaguerra, F., Barry, D., 2009b. Bioclogging in porous media: Model development and sensitivity to initial conditions. Environmental Modelling & Software 24, 611–626. doi:10.1016/j.envsoft.2008.10.001.

Calheiros, C.S.C., Teixeira, A., Pires, C., Franco, a.R., Duque, a.F., Crispim, L.F.C., Moura, S.C., Castro, P.M.L., 2010. Bacterial community dynamics in horizontal flow constructed wetlands with different plants for high salinity industrial wastewater polishing. Water research 44, 5032–8. doi:10.1016/j.watres.2010.07.017.

Caselles-Osorio, A., Puigagut, J., Segú, E., Vaello, N., Granés, F., García, D., García, J., 2007. Solids accumulation in six full-scale subsurface flow constructed wetlands. Water research 41, 1388–98. doi:10.1016/j.watres.2006.12.019.

Chazarenc, F., 2003. Hydrodynamics of horizontal subsurface flow constructed wetlands. Ecological Engineering 21, 165–173. doi:10.1016/j.ecoleng.2003.12.001.

Chazarenc, F., Maltais-Landry, G., Troesch, S., Comeau, Y., Brisson, J., 2007. Effect of loading rate on performance of constructed wetlands treating an anaerobic supernatant. Water Science & Technology 56, 23. doi:10.2166/wst.2007.500.

Chen-Charpentier, B., 1999. Numerical simulation of biofilm growth in porous media. Journal of Computational and Applied Mathematics 103, 55–66. doi:10.1016/S0377-0427(98)00240-4.

Clement, T., Peyton, B., Skeen, R., Jennings, D., Petersen, J., 1997. Microbial growth and transport in porous media under denitrification conditions: experiments and simulations. Journal of Contaminant Hydrology 24, 269–285. doi:10.1016/S0169-7722(96)00014-9.

Clement, T.P., Hooker, B., Skeen, R., 1996. Macroscopic Models for Predicting Changes in Saturated Porous Media Properties Caused by Microbial Growth. Ground Water 34, 8.

Clement, T.P., Sun, Y., Hooker, B., Peterser, J., 1998. Modeling Multispecies Reactive Transport in Ground Water. Groundwater Monitoring and Remediation 18, 79–92.

Cooke, A.J., Rowe, R.K., Vangulck, J., Rittmann, B.E., 2005. Application of the BioClog model for landfill leachate clogging of gravel-packed columns. Canadian Geotechnical Journal , 1600 – 1614doi:10.1139/T05-078.

Criado, C., Bécares, E., 2005. Characterization of bacterial communities of a constructed wetland in cold conditions. J Gen Appl Microbiol 51, 197–201.

Dittmer, U., Meyer, D., Langergraber, G., 2005. Simulation of a subsurface vertical flow constructed wetland for CSO treatment. Water science and technology : a journal of the International Association on Water Pollution Research 51, 225–32.

Eberl, H., Morgenroth, E., Noguera, D., Picioreanu, C., Rittmann, B., van Loosdrecht, M., Wanner, O., 2006. Mathematical modeling of biofilms. IWA Scientific and Technical Rep. 18. Technical Report. International Water Association. London, UK.

Fan, L., Reti, H., Wang, W., Lu, Z., Yang, Z., 2008. Application of computational fluid dynamic to model the hydraulic performance of subsurface flow wetlands. Journal of Environmental Sciences 20, 1415–1422. doi:10.1016/S1001-0742(08)62542-5.

Faulwetter, J.L., Gagnon, V., Sundberg, C., Chazarenc, F., Burr, M.D., Brisson, J., Camper, A.K., Stein, O.R., 2009. Microbial processes influencing performance of treatment wetlands: A review. Ecological Engineering 35, 987–1004. doi:10.1016/j.ecoleng.2008.12.030.

Forquet, N., Wanko, a., Molle, P., Mosé, R., a G Sadowski, 2009. Two-phase flow modelling for oxygen renewal estimation in vertical flow filter: luxury or necessity? Water science and technology : a journal of the International Association on Water Pollution Research 59, 2311–9. doi:10.2166/wst.2009.311.

French, H.K., Van der Zee, S.E., Leijnse, A., 2001. Transport and degradation of propyleneglycol and potassium acetate in the unsaturated zone. Journal of contaminant hydrology 49, 23–48.

Furman, A., 2008. Modeling Coupled SurfaceSubsurface Flow Processes: A Review. Vadose Zone Journal 7, 741. doi:10.2136/vzj2007.0065.

Galvão, A.F., Matos, J.S., Ferreira, F.S., Correia, F.N., 2010. Simulating flows in horizontal subsurface flow constructed wetlands operating in Portugal. Ecological Engineering 36, 596–600. doi:10.1016/j.ecoleng.2009.11.014.

García, J., Aguirre, P., Barragan, J., Mujeriego, R., Matamoros, V., Bayona, J., 2005. Effect of key design parameters on the efficiency of horizontal subsurface flow constructed wetlands. Ecological Engineering 25, 405–418. doi:10.1016/j.ecoleng.2005.06.010.

García, J., Aguirre, P., Mujeriego, R., Huang, Y., Ortiz, L., Bayona, J.M., 2004b. Initial contaminant removal performance factors in horizontal flow reed beds used for treating urban wastewater. Water research 38, 1669–78. doi:10.1016/j.watres.2004.01.011.

García, J., Capel, V., Castro, A., Ruíz, I., Soto, M., 2007. Anaerobic biodegradation tests and gas emissions from subsurface flow constructed wetlands. Bioresource technology 98, 3044–52. doi:10.1016/j.biortech.2006.10.016.

García, J., Chiva, J., Aguirre, P., Alvarez, E., Sierra, J., Mujeriego, R., 2004a. Hydraulic behaviour of horizontal subsurface flow constructed wetlands with different aspect ratio and granular medium size. Ecological Engineering 23, 177–187. doi:10.1016/j.ecoleng.2004.09.002.

García, J., Mujeriego, R., Obis, J.M., Bou, J., 2001. Wastewater treatment for small communities in Catalonia (Mediterranean region). Water Policy 3, 341–350.

García, J., Ojeda, E., Sales, E., Chico, F., Píriz, T., Aguirre, P., Mujeriego, R., 2003. Spatial variations of temperature, redox potential, and contaminants in horizontal flow reed beds. Ecological Engineering 21, 129–142. doi:10.1016/j.ecoleng.2003.10.001.

García, J., Rousseau, D.P.L., Morató, J., Lesage, E., Matamoros, V., Bayona, J.M., 2010. Contaminant Removal Processes in Subsurface-Flow Constructed Wetlands: A Review. Critical Reviews in Environmental Science and Technology 40, 561–661. doi:10.1080/10643380802471076.

Garriga Riu, J., 2013. *El Punt Avui*, 21 December 2013. Fer caixa amb les aigües residuals. Available: http://www.elpuntavui.cat/noticia/article/4-economia/18-economia/702707-fer-caixa-amb-les-aiguees-residuals.html [Last accessed: 13 February 2013].

van Genuchten, M.T., 1980. A Closed-form Equation for Predicting the Hydraulic Conductivity of Unsaturated Soils. doi:doi:10.2136/sssaj1980.03615995004400050002x.

Giraldi, D., de Michieli Vitturi, M., Iannelli, R., 2010. FITOVERT: A dynamic numerical model of subsurface vertical flow constructed wetlands. Environmental Modelling & Software 25, 633–640. doi:10.1016/j.envsoft.2009.05.007.

Giraldi, D., deMichieli Vitturi, M., Zaramella, M., Marion, A., Iannelli, R., 2009. Hydrodynamics of vertical subsurface flow constructed wetlands: Tracer tests with rhodamine WT and numerical modelling. Ecological Engineering 35, 265–273. doi:10.1016/j.ecoleng.2008.06.004.

Gonzalias, A., Kuschk, P., Wiessner, a., Jank, M., Kästner, M., Köser, H., 2007. Treatment of an artificial sulphide containing wastewater in subsurface horizontal flow laboratory-scale constructed wetlands. Ecological Engineering 31, 259–268. doi:10.1016/j.ecoleng.2007.08.002.

Goulet, R., 2001. Test of the first-order removal model for metal retention in a young constructed wetland. Ecological Engineering 17, 357–371. doi:10.1016/S0925-8574(00)00137-3.

Greskowiak, J., Prommer, H., Massmann, G., Johnston, C.D., Nützmann, G., Pekdeger, A., 2005. The impact of variably saturated conditions on hydrogeochemical changes during artificial recharge of groundwater. Applied Geochemistry 20, 1409–1426. doi:10.1016/j.apgeochem.2005.03.002.

Gujer, W., Boller, M., 1990. A Mathematical Model for Rotating Biological Contactors. Water Science and Technology 22, 53–73.

Hadwin, A.K.M., Del Rio, L.F., Pinto, L.J., Painter, M., Routledge, R., Moore, M.M., 2006. Microbial communities in wetlands of the Athabasca oil sands: genetic and metabolic characterization. FEMS Microbiol Ecol 55, 68–78.

Hafner, S., Jewell, W., 2006. Predicting nitrogen and phosphorus removal in wetlands due to detritus accumulation: A simple mechanistic model. Ecological Engineering 27, 13–21. doi:10.1016/j.ecoleng.2005.09.014.

Hallberg, K.B., Johnson, D.B., 2005. Microbiology of a wetland ecosystem constructed to remediate mine drainage from a heavy metal mine. The Science of the total environment 338, 53–66. doi:10.1016/j.scitotenv.2004.09.005.

Headley, T.R., Herity, E., Davison, L., 2005. Treatment at different depths and vertical mixing within a 1-m deep horizontal subsurface-flow wetland. Ecological Engineering 25, 567–582. doi:10.1016/j.ecoleng.2005.07.012.

Hench, K., Sexstone, A.J., Bissonnette, G.K., 2004. Heterotrophic community-level physiological profiles of domestic wastewater following treatment by small constructed subsurface flow wetlands. Water Environment Research 76, 468–473.

Henrichs, M., Langergraber, G., Uhl, M., 2007. Modelling of organic matter degradation in constructed wetlands for treatment of combined sewer overflow. Science of The Total Environment 380, 196–209.

Henrichs, M., Welker, a., Uhl, M., 2009. Modelling of biofilters for ammonium reduction in combined sewer overflow. Water science and technology : a journal of the International Association on Water Pollution Research 60, 825–31. doi:10.2166/wst.2009.397.

Henze, M., on Mathematical Modelling for Design, I.W.A.T.G., of Biological Wastewater Treatment, O., 2000. Activated Sludge Models ASM1, ASM2, ASM2d and ASM3. Eighteenth century collections online, IWA Publishing.

Hijosa-Valsero, M., Sidrach-Cardona, R., Martín-Villacorta, J., Cruz Valsero-Blanco, M., Bayona, J.M., Bécares, E., 2011. Statistical modelling of organic matter and emerging pollutants removal in constructed wetlands. Bioresource Technology 102, 4981–4988.

Hornberger, G.M., Mills, A.L., Herman, J.S., 1992. Bacterial transport in porous media: Evaluation of a model using laboratory observations. Water Resources Research 28, 915–923. doi:10.1029/91WR02980.

Hua, G.F., Li, L., Zhao, Y.Q., Zhu, W., Shen, J.Q., 2013. An integrated model of substrate clogging in vertical flow constructed wetlands. Journal of environmental management 119, 67–75. doi:10.1016/j.jenvman.2013.01.023.

Huang, Y., Ortiz, L., Aguirre, P., García, J., Mujeriego, R., Bayona, J.M., 2005. Effect of design parameters in horizontal flow constructed wetland on the behaviour of volatile fatty acids and volatile alkylsulfides. Chemosphere 59, 769–77. doi:10.1016/j.chemosphere.2004.11.015.

Iasur-Kruh, L., Hadar, Y., Milstein, D., Gasith, A., Minz, D., 2010. Microbial population and activity in wetland microcosms constructed for improving treated municipal wastewater. Microbial ecology 59, 700–9. doi:10.1007/s00248-009-9611-z.

Iwasaki, I., 1937. Some notes on sand filtration. J. Am.WaterWorks Assoc. , 1591–1602.

Kadlec, R., 2000. The inadequacy of first-order treatment wetland models. Ecological Engineering 15, 105–119. doi:10.1016/S0925-8574(99)00039-7.

Kadlec, R., Watson, J., 1993. Hydraulics and solids accumulation in a gravel bed treatment wetland., in: (Ed.), M.G. (Ed.), Constructed Wetlands for Water Quality Improvement. Lewis Publishers, Boca Raton, Florida, USA, p. 656.

Kadlec, R.H., 2005. Nitrogen Farming for Pollution Control. Journal of Environmental Science and Health, Part A 40, 1307–1330. doi:10.1081/ESE-200055836.

Kadlec, R.H., Wallace, S., 2008. Treatment Wetlands, Second Edition. Taylor & Francis.

Kalin, M., Caetano Chaves, W., 2003. Acid reduction using microbiology: treating AMD effluent emerging from an abandoned mine portal. Hydrometallurgy 71, 217–225. doi:10.1016/S0304-386X(03)00159-2.

Kapellos, G.E., Alexiou, T.S., Payatakes, A.C., 2007. Hierarchical simulator of biofilm growth and dynamics in granular porous materials. Advances in Water Resources 30, 1648–1667. doi:10.1016/j.advwatres.2006.05.030.

Kern, J., 2003. Seasonal efficiency of a constructed wetland for treating dairy farm wastewater., in: Constructed wetlands for wastewater treatment in cold climates. WIT Press, Southampton, United Kingdom, pp. 197–214.

Kildsgaard, J., Engesgaard, P., 2001. Numerical analysis of biological clogging in two-dimensional sand box experiments. Journal of contaminant hydrology 50, 261–85.

Knowles, P., Dotro, G., Nivala, J., García, J., 2011. Clogging in subsurface-flow treatment wetlands: Occurrence and contributing factors. Ecological Engineering 37, 99–112. doi:10.1016/j.ecoleng.2010.08.005.

Knowles, P.R., Griffin, P., Davies, P.a., 2010. Complementary methods to investigate the development of clogging within a horizontal sub-surface flow tertiary treatment wetland. Water research 44, 320–30. doi:10.1016/j.watres.2009.09.028.

Kollet, S.J., Maxwell, R.M., 2006. Integrated surfacegroundwater flow modeling: A free-surface overland flow boundary condition in a parallel groundwater flow model. Advances in Water Resources 29, 945–958.

Korkusuz, E., Meyer, D., Langergraber, G., 2007. Cw2d simulation results of lab-scale vertical flowfilters filled with specialmedia and loaded with municipal wastewater, in: Proceedings of the 2nd WETPOL, Tartu, Estonia. pp. 448–450.

Kotti, I.P., Sylaios, G.K., Tsihrintzis, V.A., 2013. Fuzzy logic models for BOD removal prediction in free-water surface constructed wetlands. Ecological Engineering 51, 66–74.

Krasnits, E., Friedler, E., Sabbah, I., Beliavski, M., Tarre, S., Green, M., 2009. Spatial distribution of major microbial groups in a well established constructed wetland treating municipal wastewater. Ecological Engineering 35, 1085–1089. doi:10.1016/j.ecoleng.2009.03.020.

Krone-Davis, P., Watson, F., Los Huertos, M., Starner, K., 2013. Assessing pesticide reduction in constructed wetlands using a tanks-in-series model within a Bayesian framework. Ecological Engineering 57, 342–352. doi:10.1016/j.ecoleng.2013.04.053.

Kumar, J.L.G., Zhao, Y.Q., 2011. A review on numerous modeling approaches for effective, economical and ecological treatment wetlands. Journal of environmental management 92, 400–6. doi:10.1016/j.jenvman.2010.11.012.

Langergraber, G., 2001. Development of a simulation tool for subsurface flow constructed wetlands. Ph.D. thesis. Wiener Mitteilungen 169, Vienna, Austria.

Langergraber, G., 2003. Simulation of subsurface flow constructed wetlands–results and further research needs. Water science and technology : a journal of the International Association on Water Pollution Research 48, 157–66.

Langergraber, G., 2005. The role of plant uptake on the removal of organic matter and nutrients in subsurface flow constructed wetlands: a simulation study. Water science and technology : a journal of the International Association on Water Pollution Research 51, 213–23.

Langergraber, G., 2007. Simulation of the treatment performance of outdoor subsurface flow constructed wetlands in temperate climates. The Science of the total environment 380, 210–9. doi:10.1016/j.scitotenv.2006.10.030.

Langergraber, G., 2008. Modeling of Processes in Subsurface Flow Constructed Wetlands: A Review. Vadose Zone Journal 7, 830. doi:10.2136/vzj2007.0054.

Langergraber, G., 2010. Water and Nutrient Management in Natural and Constructed Wetlands, in: Vymazal, J. (Ed.), Process based models for subsurface flow constructed wetlands. Springer, Dordrecht, The Netherlands, pp. 21–36.

Langergraber, G., Giraldi, D., Mena, J., Meyer, D., Peña, M., Toscano, A., Brovelli, A., Korkusuz, E.A., 2009b. Recent developments in numerical modelling of subsurface flow constructed wetlands. The Science of the total environment 407, 3931–43. doi:10.1016/j.scitotenv.2008.07.057.

Langergraber, G., Rousseau, D.P.L., García, J., Mena, J., 2009a. CWM1: a general model to describe biokinetic processes in subsurface flow constructed wetlands. Water science and technology : a journal of the International Association on Water Pollution Research 59, 1687–1697. doi:10.2166/wst.2009.131.

Langergraber, G., Simunek, J., 2012. Reactive Transport Modeling of Subsurface Flow Constructed Wetlands Using the HYDRUS Wetland Module. Vadose Zone Journal 11. doi:10.2136/vzj2011.0104.

Lee, M., Lee, K., Hyun, Y., Clement, T.P., Hamilton, D., 2006. Nitrogen transformation and transport modeling in groundwater aquifers. Ecological Modelling 192, 143–159. doi:10.1016/j.ecolmodel.2005.07.013.

Liolios, K.A., Moutsopoulos, K.N., Tsihrintzis, V.A., 2012. Modeling of flow and BOD fate in horizontal subsurface flow constructed wetlands. Chemical Engineering Journal 200, 681–693.

Llorens, E., Obradors, J., Alarcón-Herrera, M.T., Poch, M., 2013. Modelling of arsenic retention in constructed wetlands. Bioresource technology 147C, 221–227. doi:10.1016/j.biortech.2013.08.012.

Llorens, E., Saaltink, M.W., García, J., 2011b. CWM1 implementation in RetrasoCodeBright: First results using horizontal subsurface flow constructed wetland data. Chemical Engineering Journal 166, 224–232. doi:10.1016/j.cej.2010.10.065.

Llorens, E., Saaltink, M.W., Poch, M., García, J., 2011a. Bacterial transformation and biodegradation processes simulation in horizontal subsurface flow constructed wetlands using CWM1-RETRASO. Bioresource technology 102, 928–36. doi:10.1016/j.biortech.2010.09.038.

Lloyd, J., Klessa, D., Parry, D., Buck, P., Brown, N., 2004. Stimulation of microbial sulphate reduction in a constructed wetland: microbiological and geochemical analysis. Water Research 38, 1822–1830.

Mander, U., Kuusemets, V., Lõhmus, K., Mauring, T., Teiter, S., Augustin, J., 2003. Nitrous oxide, dinitrogen and methane emission in a subsurface flow constructed wetland. Water science and technology : a journal of the International Association on Water Pollution Research 48, 135–142.

Mao, X., Prommer, H., Barry, D., Langevin, C., Panteleit, B., Li, L., 2006. Three-dimensional model for multi-component reactive transport with variable density groundwater flow. Environmental Modelling & Software 21, 615–628. doi:10.1016/j.envsoft.2004.11.008.

Maurer, M., Rittmann, B.E., 2004. Modeling Intrinsic Bioremediation for Interpret Observable Biogeochemical Footprints of BTEX Biodegradation: The Need for Fermentation and Abiotic Chemical Processes. Biodegradation 15, 405–417. doi:10.1023/B:BIOD.0000044590.23221.b1.

Mayo, A., Bigambo, T., 2005. Nitrogen transformation in horizontal subsurface flow constructed wetlands I: Model development. Physics and Chemistry of the Earth, Parts A/B/C 30, 658–667. doi:10.1016/j.pce.2005.08.005.

Mburu, N., Rousseau, D.P.L., van Bruggen, J.J.a., Thumbi, G., Llorens, E., García, J., Lens, P.N.L., 2013. Reactive transport simulation in a tropical horizontal subsurface flow constructed wetland treating domestic wastewater. The Science of the total environment 449, 309–19. doi:10.1016/j.scitotenv.2013.01.069.

Mburu, N., Sánchez-Ramos, D., Rousseau, D.P., van Bruggen, J.J., Thumbi, G., Stein, O.R., Hook, P.B., Lens, P.N., 2012. Simulation of carbon, nitrogen and sulphur conversion in batch-operated experimental wetland mesocosms. Ecological Engineering 42, 304–315. doi:10.1016/j.ecoleng.2012.02.003.

Mcbride, G.B., Tanner, C.C., 2000. Modelling biofilm nitrogen transformations in constructed wetland mesocosms with fluctuating water levels. Ecological Engineering 14, 93–106.

McDonald, M., Harbaugh, A., 1988. A Modular Three-Dimensional Finite-Difference Ground-Water Flow Model.

McNevin, D., Harrison, M., King, A., David, K., Mitchell, C., 2000. Towards an integrated performance model for subsurface flow constructed wetlands. Journal of Environmental Science and Health, Part A 35, 1415–1429. doi:10.1080/10934520009377044.

Mena, J., Villasenor, J., Fernández, F., Gómez, R., De Lucas, A., 2011. Hydraulic modelling of horizontal-subsurface flow constructed wetlands: Influence of operation time and plant species. International Journal of Environmental Analytical Chemistry 91, 786–800. doi:10.1080/03067319.2010.500057.

Meyer, D., 2011. Modellierung und Simulation von Retentionsbodenfiltern zur weitergehenden Mischwasserbehandlung (Modelling and simulation of constructed wetlands for enhanced combined sewer overflow treatment). Ph.D. thesis. Institute of Urban Water Management, Technical University of Kaiserslautern. Kaiserslautern, Germany.

Meyer, D., Chazarenc, F., Claveau-Mallet, D., Dittmer, U., Forquet, N., Molle, P., Morvannou, A., Pálfy, T., Petitjean, A., Rizzo, A., Samsó, R., Scholz, M., Soric, A., Langergraber, G., 2014. Modelling constructed wetlands: scopes and aims - a review. Ecological Engineering (accepted) .

Meyer, D., Langergraber, G., Dittmer, U., 2006. Simulation of sorption processes in vertical flow constructed wetlands for cso treatment, in: Proceedings 10th International Conference on Wetland Systems for Water Pollution Control, Lisbon, Portugal.

Mitsch, W.J., Gosselink, J.G., 2000. Wetlands. 3rd ed. JohnWiley and Sons.

Mitsch, W.J., Wise, K.M., 1998. Water quality, fate of metals, and predictive model validation of a constructed wetland treating acid mine drainage. Water Research 32, 1888–1900.

Monod, J., 1949. The growth of bacterial cultures. Annual Review of Microbiology .

Mostafa, M., Van Geel, P.J., 2007. Conceptual Models and Simulations for Biological Clogging in Unsaturated Soils. Vadose Zone Journal 6, 175. doi:10.2136/vzj2006.0033.

Moutsopoulos, K.N., Poultsidis, V.G., Papaspyros, J.N., Tsihrintzis, V.a., 2011. Simulation of hydrodynamics and nitrogen transformation processes in HSF constructed wetlands and porous media using the advectiondispersion-reaction equation with linear sink-source terms. Ecological Engineering 37, 1407–1415. doi:10.1016/j.ecoleng.2011.03.034.

Mualem, Y., 1976. A new model for predicting the hydraulic conductivity of unsaturated porous media. Water Resources Research 12, 513–522. doi:10.1029/WR012i003p00513.

Nguyen, L., 2000. Organic matter composition, microbial biomass and microbial activity in gravel-bed constructed wetlands treating farm dairy wastewaters. Ecological Engineering 16, 199–221. doi:10.1016/S0925-8574(00)00044-6.

Nguyen, L., 2001. Accumulation of organic matter fractions in a gravel-bed constructed wetland. Water science and technology : a journal of the International Association on Water Pollution Research 44, 281–7.

Nivala, J., Knowles, P., Dotro, G., García, J., Wallace, S., 2012. Clogging in subsurface-flow treatment wetlands: measurement, modeling and management. Water research 46, 1625–40. doi:10.1016/j.watres.2011.12.051.

Nogueira, R., Melo, L.F., Purkhold, U., Wuertz, S., Wagner, M., 2002. Nitrifying and heterotrophic population dynamics in biofilm reactors: effects of hydraulic retention time and the presence of organic carbon. Water research 36, 469–81.

Nurk, K., Truu, J., Truu, M., Mander, U., 2005. Microbial Characteristics and Nitrogen Transformation in Planted Soil Filter for Domestic Wastewater Treatment. Journal of Environmental Science and Health Part A-toxic/hazardous Substances & Environmental Engineering 40, 1201–1214. doi:10.1081/ESE-200055659.

Oberkampf, W.L., Trucano, T.G., 2002. Verification and validation in computational fluid dynamics. Progress in Aerospace Sciences 38, 209–272. doi:10.1016/S0376-0421(02)00005-2.

Ojeda, E., Caldentey, J., Saaltink, M., García, J., 2008. Evaluation of relative importance of different microbial reactions on organic matter removal in horizontal subsurface-flow constructed wetlands using a 2D simulation model. Ecological Engineering 34, 65–75. doi:10.1016/j.ecoleng.2008.05.007.

Okabe, S., Hiratia, K., Ozawa, Y., Watanabe, Y., 1996. Spatial microbial distributions of nitrifiers and heterotrophs in mixed-population biofilms. Biotechnology and Bioengineering 50, 24–35. doi:10.1002/(SICI)1097-0290(19960405)50:1<24::AID-BIT4>3.0.CO;2-3.

Panday, S., Huyakorn, P.S., 2004. A fully coupled physically-based spatially-distributed model for evaluating surface/subsurface flow. Advances in Water Resources 27, 361–382.

Parkhurst, D., Appelo, C., 1999. User's guide to PHREEQC (version 2)–A computer program for speciation, batch-reaction, one-dimensional transport, and inverse geochemical calculations: U.S. Geological Survey Water-Resources Investigations Report 99-4259.

Parr, T., 1990. Factors affecting reed (Phragmites australis) growth in UK reed bed treatment systems, in: Constructed Wetlands in Water Pollution Control. Pergamon Press, Oxford, UK, pp. 67–76.

Pedescoll, A., Corzo, A., Alvarez, E., García, J., Puigagut, J., 2011. The effect of primary treatment and flow regime on clogging development in horizontal subsurface flow constructed wetlands: An experimental evaluation. Water research 45, 3579–89. doi:10.1016/j.watres.2011.03.049.

Pedescoll, a., Sidrach-Cardona, R., Sánchez, J.C., Carretero, J., Garfi, M., Bécares, E., 2013. Design configurations affecting flow pattern and solids accumulation in horizontal free water and subsurface flow constructed wetlands. Water research 47, 1448–58. doi:10.1016/j.watres.2012.12.010.

Pedescoll, A., Uggetti, E., Llorens, E., Granés, F., García, D., García, J., 2009. Practical method based on saturated hydraulic conductivity used to assess clogging in subsurface flow constructed wetlands. Ecological Engineering 35, 1216–1224. doi:10.1016/j.ecoleng.2009.03.016.

Peyton, B., Characklis, W.G., 1993. A statistical analysis of the effect of substrate utilization and shear stress on the kinetics of biofilm detachment. Biotechnology and Bioengineering 41, 728–735. doi:doi:10.1002/bit.260410707.

Puigagut, J., Villaseñor, J., Salas, J., Bécares, E., García, J., 2007. Subsurface-flow constructed wetlands in Spain for the sanitation of small communities: A comparative study. Ecological Engineering 30, 312–319. doi:10.1016/j.ecoleng.2007.04.005.

Ragusa, S.R., McNevin, D., Qasem, S., Mitchell, C., 2004. Indicators of biofilm development and activity in constructed wetlands microcosms. Water research 38, 2865–73. doi:10.1016/j.watres.2004.03.039.

Ramond, J.B., Welz, P.J., Cowan, D.a., Burton, S.G., 2012. Microbial community structure stability, a key parameter in monitoring the development of constructed wetland mesocosms during start-up. Research in microbiology 163, 28–35. doi:10.1016/j.resmic.2011.09.003.

Reed, S.C., Crites, R.W., Middlebrooks, E.J., 1995. Natural Systems for Waste Management and Treatment. McGraw-Hill Professional Publishing.

Reichert, P., 1998. Aquasim 2.0user manual computer program for the identification and simulation of aquatic systems.

Richards, L., 1931. Capillary conduction of liquids through porous mediums. Applied Physics 1. doi:10.1063/1.1745010.

Rittmann, B.E., 1982. The Effect of Shear-Stress on Biofilm Loss Rate. Biotechnology and Bioengineering 24, 501–506.

Rolle, M., Clement, T.P., Sethi, R., Molfetta, A.D., 2008. A kinetic approach for simulating redox-controlled fringe and core biodegradation processes in groundwater: model development and application to a landfill site in Piedmont, Italy. Hydrological Processes 4921, 4905– 4921. doi:10.1002/hyp.

Rosenzweig, R., Shavit, U., Furman, A., 2009. The Influence of Biofilm Spatial Distribution Scenarios on Hydraulic Conductivity of Unsaturated Soils. Vadose Zone Journal 8, 1080. doi:10.2136/vzj2009.0017.

Rousseau, D., Griffin, P., Vanrolleghem, P., De Pauw, N., 2005. Model Study of Short-Term Dynamics of Secondary Treatment Reed Beds at Saxby (Leicestershire, UK). Journal of Environmental Science and Health, Part A 40, 1479–1492. doi:10.1081/ESE-200055895.

Rousseau, D.P.L., Vanrolleghem, P.a., De Pauw, N., 2004. Model-based design of horizontal subsurface flow constructed treatment wetlands: a review. Water research 38, 1484–93. doi:10.1016/j.watres.2003.12.013.

Ruiz, I., Díaz, M., Crujeiras, B., García, J., Soto, M., 2010. Solids hydrolysis and accumulation in a hybrid anaerobic digester-constructed wetlands system. Ecological Engineering 36, 1007–1016. doi:10.1016/j.ecoleng.2010.04.006.

Saaltink, M.W., Batlle, F., Ayora, C., Carrera, J., Olivella, S., 2004. RETRASO, a code for modeling reactive transport in saturated and unsaturated porous media. Geol. Acta 2, 235–251.

Samsó, R., García, J., 2013a. BIO_PORE, a mathematical model to simulate biofilm growth and water quality improvement in porous media: Application and calibration for constructed wetlands. Ecological Engineering 54, 116–127. doi:10.1016/j.ecoleng.2013.01.021.

Samsó, R., García, J., 2013b. Bacteria distribution and dynamics in constructed wetlands based on modelling results. Science of The Total Environment 461-462, 430–440. doi:10.1016/j.scitotenv.2013.04.073.

Samsó, R., García, J., 2014a. The Cartridge Theory: A description of the functioning of horizontal subsurface flow constructed wetlands for wastewater treatment, based on modelling results. Science of The Total Environment 473-474, 651–658. doi:10.1016/j.scitotenv.2013.12.070.

Samsó, R., Meyer, D., García, J., 2014b. Subsurface flow constructed wetlands models: review and prospects, in: Vymazal, J. (Ed.), The Role of Natural and Constructed Wetlands in Nutrient Cycling and Retention on the Landscape. Springer, Dordrecht, The Netherlands (in press).

Schramm, A., Larsen, L.H., Revsbech, N.P., Ramsing, N.B., Amann, R., Schleifer, K.H., 1996. Structure and function of a nitrifying biofilm as determined by in situ hybridization and the use of microelectrodes. Applied and Environmental Microbiology 62, 4641–4647.

Seki, K., Thullner, M., Hanada, J., Miyazaki, T., 2006. Moderate Bioclogging Leading to Preferential Flow Paths in Biobarriers. Ground Water Monitoring & Remediation 26, 68–76. doi:10.1111/j.1745-6592.2006.00086.x.

Shannon, C.E., 1948. A mathematical theory of communication. Bell system technical journal 27.

Sharp, R.R., Cunningham, A.B., Komlos, J., Billmayer, J., 1999. Observation of thick biofilm accumulation and structure in porous media and corresponding hydrodynamic and mass transfer effects. Water Science and Technology 39, 195–201. doi:http://dx.doi.org/10.1016/S0273-1223(99)00168-7.

Sims, A., Gajaraj, S., Hu, Z., 2012. Seasonal population changes of ammonia-oxidizing organisms and their relationship to water quality in a constructed wetland. Ecological Engineering 40, 100–107. doi:10.1016/j.ecoleng.2011.12.021.

Simunek, J., Sejna, M., van Genuchten, M., 1999. The hydrus-2d software package for simulating two-dimensional movement of water, heat, and multiple salutes in variably saturated media, version 2.0. manual.

Sleytr, K., Tietz, A., Langergraber, G., Haberl, R., Sessitsch, A., 2009. Diversity of abundant bacteria in subsurface vertical flow constructed wetlands. Ecological Engineering 35, 1021–1025. doi:10.1016/j.ecoleng.2008.11.005.

Soleimani, S., Van Geel, P.J., Isgor, O.B., Mostafa, M.B., 2009. Modeling of biological clogging in unsaturated porous media. Journal of contaminant hydrology 106, 39–50. doi:10.1016/j.jconhyd.2008.12.007.

Spychala, M., Blazejewski, R., 2004. Sand filter clogging by septic tank effluent. Water Science and Technology 48, 153–159.

Stanescu, D., Chen-Charpentier, B.M., 2009. Random coefficient differential equation models for bacterial growth. Mathematical and Computer Modelling 50, 885–895. doi:10.1016/j.mcm.2009.05.017.

Stein, O., Biederman, J., Hook, P., Allen, W., 2006. Plant species and temperature effects on the k-C* first-order model for COD removal in batch-loaded SSF wetlands. Ecological Engineering 26, 100–112. doi:10.1016/j.ecoleng.2005.07.001.

Stein, O.R., Borden-Stewart, D.J., Hook, P.B., Jones, W.L., 2007. Seasonal influence on sulfate reduction and zinc sequestration in subsurface treatment wetlands. Water research 41, 3440–8. doi:10.1016/j.watres.2007.04.023.

Stewart, T., Kim, D.S., 2004. Modeling of biomass-plug development and propagation in porous media. Biochemical Engineering Journal 17, 107–119. doi:10.1016/S1369-703X(03)00146-3.

Suliman, F., French, H., Haugen, L., a.K. Sovik, 2006. Change in flow and transport patterns in horizontal subsurface flow constructed wetlands as a result of biological growth. Ecological Engineering 27, 124–133. doi:10.1016/j.ecoleng.2005.12.007.

Tanner, C., Sukias, J., Upsdell, M., 1998. Organic matter accumulation during maturation of gravel-bed constructed wetlands treating farm dairy wastewaters. Water Research 32, 3046–3054. doi:10.1016/S0043-1354(98)00078-5.

Tanner, C.C., 2001. Plants as ecosystem engineers in subsurface-flow treatment wetlands. Water science and technology : a journal of the International Association on Water Pollution Research 44, 9–17.

Tanner, C.C., Sukias, J.P., 1995. Accumulation of organic solids in gravel-bed constructed wetlands. Water Science and Technology 32, 229 – 239. doi:http://dx.doi.org/10.1016/0273-1223(95)00624-9. proceedings of the 4th International Conference on Wetland Systems for Water Pollution Control 1994.

Taylor, S.W., Jaffé, P.R., 1990a. Biofilm growth and the related changes in the physical properties of a porous medium: 1. Experimental investigation. Water Resources Research 26, 2153–2159. doi:10.1029/WR026i009p02153.

Taylor, S.W., Milly, P.C.D., Jaffé, P.R., 1990b. Biofilm growth and the related changes in the physical properties of a porous medium: 2. Permeability. Water Resources Research 26, 2161–2169. doi:10.1029/WR026i009p02161.

Teiter, S., Mander, U., 2005. Emission of N2O, N2, CH4, and CO2 from constructed wetlands for wastewater treatment and from riparian buffer zones. Ecological Engineering 25, 528–541. doi:10.1016/j.ecoleng.2005.07.011.

Thullner, M., 2009. Comparison of bioclogging effects in saturated porous media within one- and two-dimensional flow systems. Ecological Engineering 36, 176–196. doi:10.1016/j.ecoleng.2008.12.037.

Thullner, M., 2010. Comparison of bioclogging effects in saturated porous media within one- and two-dimensional flow systems. Ecological Engineering , 176–196doi:doi:10.1016/j.ecoleng.2008.12.037.

Thullner, M., Schroth, M.H., Zeyer, J., Kinzelbach, W., 2004. Modeling of a microbial growth experiment with bioclogging in a two-dimensional saturated porous media flow field. Journal of contaminant hydrology 70, 37–62. doi:10.1016/j.jconhyd.2003.08.008.

Tien, C., Turian, R.M., Pendse, H., 1979. Simulation of the dynamic behavior of deep bed filters. AIChE Journal 25, 385–395. doi:10.1002/aic.690250302.

Tietz, A., Kirschner, A., Langergraber, G., Sleytr, K., Haberl, R., 2007. Characterisation of microbial biocoenosis in vertical subsurface flow constructed wetlands. The Science of the total environment 380, 163–72. doi:10.1016/j.scitotenv.2006.11.034.

Tiwari, S.K., Park, R., Bowers, K.L., 2001. Modeling Biofilm Growth for Porous Media Applications. Mathematical and Computer Modelling .

Torsvik, V., Ovreas, L., 2002. Microbial diversity and function in soil: from genes to ecosystems. Current Opinion in Microbiology 5, 240–245.

Toscano, A., Langergraber, G., Consoli, S., Cirelli, G.L., 2009. Modelling pollutant removal in a pilot-scale two-stage subsurface flow constructed wetlands. Ecological Engineering 35, 281–289. doi:10.1016/j.ecoleng.2008.07.011.

Truu, M., Truu, J., Heinsoo, K., 2009. Changes in soil microbial community under willow coppice: The effect of irrigation with secondary-treated municipal wastewater. Ecological Engineering 35, 1011–1020. doi:10.1016/j.ecoleng.2008.08.010.

Tyroller, L., Rousseau, D.P.L., Santa, S., García, J., 2010. Application of the gas tracer method for measuring oxygen transfer rates in subsurface flow constructed wetlands. Water research 44, 4217–25. doi:10.1016/j.watres.2010.05.027.

UN-OHCH-UNHabitat-WHO, 2010. The Right to Water (Fact sheet 35). Technical Report. United Nations, Office of the High Commissioner for Human Rights , United Nations Human Settlements Programme , World Health Organization.

UNEP-UNWATER-FAOWATER, 2010. Frequently asked questions on water quality (World Water Day 2010). Technical Report. UNWATER-UNEP-FAOWATER.

United Nations, 2013. World Population Prospects. The 2012 Revision. Technical Report. Department of Economic and Social Affairs. New York.

USEPA, 2000. Constructed Wetlands Treatment of Municipal Wastewaters. September, US EPA Office of Research and Development, Washington, DC.

Vacca, G., Wand, H., Nikolausz, M., Kuschk, P., Kästner, M., 2005. Effect of plants and filter materials on bacteria removal in pilot-scale constructed wetlands. Water research 39, 1361–73. doi:10.1016/j.watres.2005.01.005.

Vera, I., García, J., Sáez, K., Moragas, L., Vidal, G., 2011. Performance evaluation of eight years experience of constructed wetland systems in Catalonia as alternative treatment for small communities. Ecological Engineering 37, 364–371. doi:10.1016/j.ecoleng.2010.11.031.

Verhulst, P., 1838. Notice sur la loi que la population suit dans son accroissement. Correspondance Mathematique et Physique , 113121.

Vymazal, J., 2005. Horizontal sub-surface flow and hybrid constructed wetlands systems for wastewater treatment. Ecological Engineering 25, 478–490. doi:10.1016/j.ecoleng.2005.07.010.

Vymazal, J., 2007. Removal of nutrients in various types of constructed wetlands. The Science of the total environment 380, 48–65. doi:10.1016/j.scitotenv.2006.09.014.

Wang, F., Liu, Y., Ma, Y., Wu, X., Yang, H., 2012. Characterization of nitrification and microbial community in a shallow moss constructed wetland at cold temperatures. Ecological Engineering 42, 124–129. doi:10.1016/j.ecoleng.2012.01.006.

Wanner, O., Eberl, H., Morgenroth, E., Noguera, D., Picioreanu, C., Rittmann, B., van Loosdrecht, M., 2006. Mathematical Modeling of Biofilms. IWA Scientific and Technical Report 18. IWA Publishing, London.

Weber, K.P., Legge, R.L., 2011. Dynamics in the bacterial community-level physiological profiles and hydrological characteristics of constructed wetland mesocosms during start-up. Ecological Engineering 37, 666–677. doi:10.1016/j.ecoleng.2010.03.016.

Weill, S., Mouche, E., Patin, J., 2009. A generalized Richards equation for surface/subsurface flow modelling. Journal of Hydrology 366, 9–20. doi:10.1016/j.jhydrol.2008.12.007.

Weintraub, L., Chen, C.W., Tsai, W., Herr, J., Goldstein, R.A., Siegrist, R., 2002. Modifications of WARMF to asses the efficacy of onsite wastewater systems on public health, in: Proceedings of the Water Environment Federation, Water Environment Federation. pp. 152–165(14). doi:10.2175/193864702784164686.

Wiessner, A., Kappelmeyer, U., Kuschk, P., Kästner, M., 2005. Sulphate reduction and the removal of carbon and ammonia in a laboratory-scale constructed wetland. Water research 39, 4643–4650.

Winter, K.J., Goetz, D., 2003. The impact of sewage composition on the soil clogging phenomena of vertical flow constructed wetlands. Water science and technology , 9–14.

Wohl, D.L., Arora, S., Gladstone, J.R., 2004. Functional Redundancy Supports Biodiversity and Ecosystem Function in a Closed and Constant Environment. Ecology 85, 1534–1540. doi:10.1890/03-3050.

Wu, S., Kuschk, P., Wiessner, A., Müller, J., a.B. Saad, R., Dong, R., 2013. Sulphur transformations in constructed wetlands for wastewater treatment: A review. Ecological Engineering doi:10.1016/j.ecoleng.2012.11.003.

Zheng, C., Wang, P., 1998. MT3DMS, a Modular Three-Dimensional Multi-Species Transport Model for Simulation of Advection, Dispersion and Chemical Reactions of Contaminants in Ground-Water Systems; Documentation and Users Guide.

Zysset, A., Stauffer, F., Dracos, T., 1994. Modeling of reactive groundwater transport governed by biodegradation. Water Resources Research 30, 2423–2434. doi:10.1029/94WR01045.

Acknowledgements

De nou, i com en cadascuna de les petites i grans fites que he anat assolint amb el pas dels anys, als primers a qui vull donar les gràcies és als meus pares, **Manel Samsó i Encarna Campà**, als quals dec ser qui sóc i tot el que tinc.

En segon lloc, gràcies a **Joan García**, l'instigador d'aquest treball i gran professional i persona. Gràcies per confiar en mi, per donar-me mil i una oportunitats, per estirar-me les orelles quan ha fet falta i per fer-me anar sempre més enllà.

De la resta de companys/es i ex-companys/es de departament, el primer agraïment és per a l'**Anna Pedescoll**, la persona que em va guiar en els meus primers passos en el camp de la recerca i sense la qual potser no m'hagués decidit a llançar-me a començar la tesi. Gràcies també a la **Cristina Ávila**, amb qui he tingut el plaer de compartir aquest trajecte, de principi a fi i la persona amb qui més somriures he compartit durant aquests anys. A l'**Enrica Uggetti**, per tants bons moments viscuts abans, durant i després, aquí, allà i qui sap a on més. A la **Raquel Gutiérrez**, la **Clara Corbella** i la **Maria Solé**, que tot i haver aparegut ja en les etapes finals d'aquest viatge, sembla que hi hagin estat sempre, per l'aire fresc i bon humor que han aportat al grup. A l'**Alessandro Solimeno**, tant en la seva faceta de tesinand com en l'actual de doctorand, per les seva voluntat d'aportar i la seva amabilitat.

Especial agraïment també al **Jaume Puigagut**, a la **Ivet Ferrer** i a l'**Anna Garfí**, per la seva amistat i per la seva proximitat i disposició a ajudar, tant en el camp professional com en el personal. A **Javier Carretero**, company fidel, per ser tant ben parit. Als tesinants que han treballat al meu costat durant tot aquest temps, i als quals espero haver ajudat tant com ells m'han ajudat a mi: **Laura Coma**, **Pau Termes**, **Felipe Valderrama**, **Alessandro Solimeno**, **Adrián Gabarró**, **Jordi Blázquez** i **Nuria Agulló**.

Gràcies a la **Carla Tenedor** i a la **Carme Fernández**, per la seva gran tasca, mai prou reconeguda, i per la seva paciència i amabilitat.

Gràcies a **Ricardo Torres** i **Joan Grau** per cedir la infraestructura del seu grup de recerca per a la realització d'aquest treball, per la seva absoulta disponibilitat i pels coneixements i l'entusiasme que m'han transmès.

Gracias a **Santiago Gassó**, **Daniel Fernández** y **Eduardo Ayesa** por sus sabios consejos y por guiar la segunda y mas productiva parte de este trabajo. Gracias también a Santiago por su labor como coordinador del programa de doctorado en Ingeniería Ambiental.

Aux collègues d'IRSTEA: merci à **Pascal Molle** pour me donner la possibilité de travailler dans son group et pour sa gentillesse et sa disponibilité et amitié. Un merci spécial à **Nicolas Forquet**, mon menteur pendant mon stage à IRSTEA. Il a été une source immense de connaissances, toujours prêt à m'aider, sa contribution a fait une grande différence dans mon travail. Merci à tous ceux qui j'ai connus, pour nombrer quelqu'un: **Alain Petitjean**, **Ania Morvanou**, **Brice Marlet**, **Claire Eme**, **Claudia Gervasi**, **Daniel Meyer**, **Daniela Damasceno**, **Luis Arias**, **Marianne Prost**, **Olivier Sauvan** et **Paul Moretti** pour sa gentillesse et pour me faire sentir chez moi à Lyon.

Gràcies a la **família**, **amics** i **coneguts** per formar part d'aquesta història amb final feliç.

Para terminar, quero agradecer a pessoa mais especial que eu já tive do meu lado, pela sua estima, por sua alegria, pelo seu suporte incondicional e por me ensinar tantas e tão diversas coisas. Sem você a vida seria sem graça. Obrigado, **Fabiana Passos**.

Gràcies a tots!

Curriculum Vitae

Roger Samsó was born in Barcelona (Catalonia) in 1984. He obtained his bachelor degree (BSc) in Geological Engineering from the Technical University of Catalonia (UPC) in 2009. His BSc dissertation consisted of an analysis of the phenomena of clogging in horizontal subsurface flow Constructed Wetlands for wastewater treatment with in-situ and ex-situ experimental procedures. He started his PhD at the UPC in March 2010.

Articles in referred journals

- Samsó, R., Forquet, N., Molle, P., García, J., 2014. Modeling bioclogging effects on the hydrodynamics of Constructed Wetlands and the subsequent overland-flow. (in preparation)
- Samsó, R., Blázquez, J., Agulló, N., Grau, J., Torres, R., García, J., 2014. Effect of bacteria density and accumulated inert solids on the effluent pollutant concentrations predicted by a Constructed Wetlands model. Ecological Engineering (submitted)
- Meyer, D., Chazarenc, F., Claveau-Mallet, D., Dittmer, U., Forquet, N., Molle, P., Morvannou, A., Pálfy, T., Petitjean, A., Rizzo, A., Samsó, R., Scholz, M., Soric, A., Langergraber, G., 2014. Modelling constructed wetlands: scopes and aims - a review. Ecological Engineering (accepted).
- Samsó, R., García, J., 2014. The Cartridge Theory: A description of the functioning of horizontal subsurface flow constructed wetlands for wastewater

treatment, based on modelling results. Science of The Total Environment 473-474, 651658. doi:10.1016/j.scitotenv.2013.12.070.

- Samsó, R., García, J., 2013. Bacteria distribution and dynamics in constructed wetlands based on modelling results. Science of The Total Environment 461-462, 430440. doi:10.1016/j.scitotenv.2013.04.073.
- Samsó, R., García, J. 2013. BIO_PORE, a mathematical model to simulate biofilm growth and water quality improvement in porous media: application and calibration for constructed wetlands. Ecological Engineering; 54:116-127.
- Pedescoll, A., Samsó, R., Romero, E., Puigagut, J., García, J. 2010. Reliability, repeatability and accuracy of the falling head method for hydraulic conductivity measurements under laboratory conditions. Ecological Engineering. doi:10.1016/j.ecoleng.2010.06.032

Articles in non-referred journals

- Samsó, R., Pedescoll, A., García, J. Buenas prácticas en el diseo de humedales construidos, derivadas del estudio de la conductividad hidráulica, para retrasar el desarrollo de la colmatación. http://www.aguasresiduales.info

Book chapters

- Samsó, R., Meyer, D., García, J., 2014. Subsurface flow constructed wetlands models: review and prospects, in: Vymazal, J. (Ed.), The Role of Natural and Constructed Wetlands in Nutrient Cycling and Retention on the Landscape. Springer, Dordrecht, The Netherlands (in press).

Conference contributions

Oral communications

- Samsó, R., *García, J.* (13-17 October 2013) The Cartridge Theory: a conceptual approach to horizontal-flow wetlands. 5th Conference on Wetland Pollutant Dynamics and Control (WETPOL). Nantes, France.
- *Samsó, R.*, García, J. (13-17 October 2013) Dynamics of bacterial communities in Constructed Wetlands from modelling results. 5th Conference on Wetland Pollutant Dynamics and Control (WETPOL). Nantes, France.

- Samsó, R., *García, J.* (17-21 may 2013). The Cartridge Theory: a conceptual approach to horizontal-flow wetlands functioning. 8th workshop nutrient cycling and retention in natural and constructed wetlands. Trebon, Czeck Republic.
- *Samsó, R.,* García, J. (25-29 November 2012). Calibration of BIO_PORE, a mechanistic model to describe constructed wetlands functioning in long-term scenarios. 13th International Conference on Wetland Systems for Water Pollution Control. IWA. Perth, Australia.
- *Samsó, R.,* García, J. (28 february 2012). Long-term simulation of wastewater treatment and bacterial distribution in constructed wetlands with COMSOL Multiphysics™and CWM1. Conferencia Panamericana en sistemas de humedales para el manejo, tratamiento y mejoramiento de la calidad del agua. Pereira, Colombia.
- *Samsó, R.,* García, J. (November 2011) Numerical modeling of biotechnologies applied to wastewater treatment. Jornades de Recerca i Innovació a l'Escola de Camins. Barcelona, Spain.
- *Pedescoll, A.,* Uggetti, E., Samsó, R., Knowles, P., García, J. (April 2011) Design criteria on clogging of subsurface flow constructed wetlands: full scale experiences. SMALLWAT 2011. Seville, Spain.
- *Samsó, R.,* Pedescoll, A. García, J. (December 2010). Criterios de diseo de humedales construidos para retrasar los efectos de la colmatación. Mesa Espaola de Tratamiento de Aguas 2010. Bilbao, Spain.
- *Samsó, R.,* Pedescoll, A., García, J. (September 2009). Clogging distribution in two Horizontal Subsurface Flow Constructed Wetlands through measurements of hydraulic conductivity. 4th International Conference on Wetland Pollutant Dynamics and Control (WETPOL). Barcelona, Spain.

Participation in R+D projects

- Safeguarding Water Resources in India with Green and Sustainable Technologies (SWINGS). Financed by the European Comission (FP7-ENVIRONMENT. Ref: 308502) Total cost: EUR 2.364.284 . Coordinators: Asociación de Investigación metalúrgica del Noreste (AIMEN). (20122015;21 research groups-subprojects) www.swingsproject.eu
- Natural water systems and treatment technologies to cope with water shortages in urbanized areas in India (NaWaTech). Financed by the European

Commission (FP7-ENVIRONMENT. Ref:308336). Total cost: 1.778.589. Coordinators: Technologie-Transfer-Zentrum (TTZ) Bremerhaven (2012 2015; 13 research groups-subprojects). www.nawatech.net

- Criterios de Diseo de Nuevas Configuraciones de Humedales Construidos, financed by the Spanish Ministry of Science and Innovation. Coordinators: Group of Environmental Engineering and Microbiology (GEMMA-UPC)(2008-2012; 4 research groups-subprojects).

Stages in foreign recognized research institutions

- Freshwater Systems, Ecology and Pollution Research Unit. Institut national de recherche en sciences et technologies pour l'environnement et l'agriculture (IRSTEA) (Lyon, France). 6 months, from June to November 2013.
- School of Environmental and Civil Engineering. The University of Sheffield (UK). 9 monhts, from September 2007 to May 2008.